NATIONAL TECHNICAL UNIVERSITY OF ATHENS
SCHOOL OF NAVAL ARCHITECTURE & MARINE ENGINEERING
DIVISION OF MARINE STRUCTURES

Random fields and Bayesian methods for the uncertainty quantification of hull girder ultimate strength and their impact on the reliability of ship structures in ultimate limit state

A thesis submitted for the degree of

Doctor of Philosophy

by

Dimitris G. Georgiadis

Supervisor: Professor M. S. Samuelides

Athens, May 2022

Advisory Committee

M. Samuelides	Professor, National Technical University of Athens (supervisor)
V. Papadopoulos	Professor, National Technical University of Athens
M. Papadrakakis	Professor, National Technical University of Athens

Examination Committee

K. Anyfantis	Assistant Professor, National Technical University of Athens
M. Samuelides	Professor, National Technical University of Athens (supervisor)
D. Straub	Professor, Technical University of Munich
V. Papadopoulos	Professor, National Technical University of Athens
M. Papadrakakis	Professor, National Technical University of Athens
N. Tsouvalis	Professor, National Technical University of Athens
N. Ventikos	Associate Professor, National Technical University of Athens

"The actual science of logic is conversant at present only with things either certain, impossible, or entirely doubtful, none of which (fortunately) we have to reason on. Therefore, the true logic for this world is the calculus of Probabilities, which takes account of the magnitude of the probability which is, or ought to be, in a reasonable man's mind.

James Clerk Maxwell (1850)

This page intentionally left blank

Acknowledgments

The present thesis is the result of intensive research work conducted during the last five years in the School of Naval Architecture & Marine Engineering (NAME) at National Technical University of Athens (NTUA). During this journey, I had the chance to learn a lot of interesting things and meet inspiring people who helped me grow personally and professionally.

First of all, I would like to express my sincere gratitude to my supervisor Prof. Manolis Samuelides who gave me the chance to undertake this thesis, the completion of which would not have been possible without his presence. Prof. Samuelides gave me the opportunity to deal with a subject that is not so mature in the field of ship structures and provided me the freedom to develop my own ideas. Throughout the years, we had a lot of interesting talks and exceptional cooperation. I feel lucky that I had him as a teacher from my early steps when I had first entered the School of NAME at NTUA and later, as a supervisor of my diploma thesis and my Ph.D.

I am also deeply thankful to the other two members of my advisory committee, Prof. Manolis Papadrakakis and Prof. Vissarion Papadopoulos from the School of Civil Engineering of NTUA. With their valuable comments, they assisted me in crucial times during this thesis, and the time they invested in our discussions is highly appreciated. I am especially grateful to Prof. Papadopoulos. His course on Stochastic Finite Element methods which I took in the early years of my Ph.D. sparked my interest in the theory of probability and its application to structural analysis, while it contributed to the selection of the topic of my Ph.D.

I feel also the need to thank Associate Prof. Konstantinos Anyfantis from the School of NAME of NTUA for the fruitful discussions and the interesting ideas we shared. Moreover, I would like to express my gratitude to Dr. Iason Papaioannou from the Technical University of Munich (TUM) who was always available to answer my questions regarding Bayesian methods. From TUM, I also want to thank Prof. Daniel Straub for motivating me on the subject of uncertainty and reliability in engineering through the organization of a relevant course that took place in Munich. Many thanks also go to Dr. Wolfgang Betz.

Special thanks are addressed to all my colleagues from NTUA and especially to my teachers at the School of NAME at NTUA who offered me the necessary background for reaching the time to defend my Ph.D. I would like also to express my appreciation to all the members of the examination committee for accepting this invitation.

Last but not least, I would like to thank my parents and my friends for their support, their unconditional love, and their encouragement for all of these years.

Dimitris G. Georgiadis
Athens, May 2022

This page intentionally left blank

Abstract

The structural reliability assessment of ships is a field of particular interest and importance. Since the 1980s where the foundations of structural reliability analysis and probabilistic-based formats for ship structural design were laid, there have been significant advancements. Nowadays, reliability analysis provides a robust tool for the development of design codes and the assessment of existing vessels. Typically, the safety level and the design of ship structures is governed by their performance in extreme or ultimate limit state. The rational treatment and quantification of the uncertainties associated with the load and resistance models is meaningful for a proper reliability analysis.

In this thesis, the focus is placed on developing new methods for the management of uncertainties associated with the hull girder ultimate strength assessment of ocean-going vessels. Broadly speaking, this topic is addressed here by: (i) introducing the tools for a better representation of input uncertain parameters, (ii) propagating the relative uncertainties through the model effectively using Monte Carlo simulation and surrogate modelling techniques (neural networks), and (iii) using observed data to reduce the uncertainties considered in the model by means of a Bayesian analysis.

Random field theory is used to describe spatial variability on geometric characteristics of hull structures. Ships are subject to manufacturing procedures and in-service deterioration processes which are generally random in space and time. A new stochastic imperfection model is introduced for the representation of the imperfect geometry of steel plates. In addition, the impact of uneven thickness distribution of stiffened plate panels on the ultimate strength calculation is investigated here for the first time.

Bayesian methods offer a formal way to combine systematically different types of information and update model predictions as soon as new observations come into light. In the context of this thesis, Bayesian techniques are developed for: (i) the reduction of uncertainties related to modelling aspects arising from the assumptions and methods of analysis used to calculate the hull girder ultimate strength of ships, and (ii) the improvement of corrosion predictions on a vessel-specific basis by incorporating the information acquired from inspections data into existing global-based corrosion models.

The impact of the aforementioned novelties on the structural reliability of oil tankers and container ships in ultimate limit state condition is finally examined. In particular, the reliability assessment and updating of an oil tanker is examined conditional on inspections data. Moreover, the reliability of two container ships at a given point in time is evaluated using the proposed modifications on the model uncertainty factor associated with hull girder ultimate strength prediction.

This page intentionally left blank

Contents

This page intentionally left blank

Nomenclature

List of Symbols

Latin characters

Symbol	Description
A	Cross-sectional area
a	Plate's length
a_{eff}	Effective plate's length
a	Lower bound of a set of plausible values
a_n	Scale parameter of Gumbel distribution
B	Overall breadth of stiffened plate panel between supporting members, e.g., girders, floors, etc.
B	Ship's breadth
b	Plate's breadth
b	Upper bound of a set of plausible values
b_f	Face plate width stiffener
b_i	Threshold levels in subset simulation
b_n	Location parameter of Gumbel distribution
C_b	Block coefficient of a ship
C_1	Annual corrosion rate
C_2	Corrosion progress (trend)
c	A constant used for the normalization of likelihood function on the BUS problem
CoV_X	Coefficient of variation of X
D_i	Intermediate domains (or events) defined in subset simulation
$\boldsymbol{d}$	A vector of m observations or measurements $\boldsymbol{d} = \{d_1, \dots, d_m\}$
d_i	A single observation or measurement

d_∞	Maximum steady corrosion depth expected after a long period of time
E	Young' s modulus
E_t	Tangent modulus beyond the elastic limit
$\mathrm{E}(X)$	Expectation value of X
$F_X(x)$	Cumulative distribution function (CDF) of X
$f_X(x)$	Probability density function (PDF) of X
$\mathcal{F}$	Failure event
G	Limit state function expressing the reliability problem in the standard normal space
g	Limit state function expressing the reliability problem in the original space
h	Limit state function expressing the BUS problem
h_w	Web height of stiffener
I	Moment of inertia
I	Indicator function
K	Total number of simulations or realizations
k	Shape parameter of Weibull distribution
k_d	A load combination factor that considers the interaction between WVBM and whipping bending moment
k_w	A load combination factor that considers the interaction between SWBM and WVBM
L	Length of a sample function
L_0	Period of the simulated stochastic field
L_{BP}	Ship's length between perpendiculars
ℓ_c	Correlation length parameter
M	Vertical bending moment
$\mathcal{M}$	Model
M_d	Whipping bending moment
M_{sw}	Still water vertical bending moment
M_{sw}^{max}	Maximum still water vertical bending moment from all loading conditions according to the loading manual of the ship

M_t	Total applied vertical bending moment
M_u	Ultimate vertical bending moment capacity
M_u^{ch}	Characteristic ultimate vertical bending moment capacity
M_{wv}	Wave-induced vertical bending moment
M_{wv}^{ch}	Characteristic wave-induced bending moment defined by the Rules
$M_{wv,ex}$	Extreme wave-induced vertical bending moment
m	Number of measurements (or observations) in a problem
m_τ	Total number of time instances $\{\tau_1, \dots, \tau_{m_\tau}\}$
m_{x}	Plate's buckling half-wave number in the x-direction
N	Total number of terms in a series expansion or a product
n_f	Number of failure points in the MCS estimate
$\Pr(A)$	Probability of the event A
P_f	Probability of failure in reliability analysis
$P_{f,c}$	Cumulative probability of failure
p_f^{MCS}	Monte Carlo estimator of the true failure probability
p_0	Target probability in SuS problem
Q	Safety margin
R	Resistance (or capacity) term in structural reliability problem
r_i	Rotation around i-axis
r_g	radius of gyration of the stiffener with the attached plate defined as: $$r_g = \sqrt{\frac{I}{A}}$$
S	Load (or demand) term in structural reliability problem
S	Sobol index
SM	Hull girder section modulus
t	Thickness
$\bar{t}$	Mean thickness
t_c	Corrosion wastage
t_n	Net thickness with 100% corrosion reduction specified by Rules

t_{n-50}	Net thickness with 50% corrosion reduction specified by Rules
$t_{as-built}$	As-built thickness
t_p	Plate thickness
t_w	Web thickness
t_f	Flange thickness
$\boldsymbol{u}$	A collection of points/locations in space $\boldsymbol{u} = (u_1, \dots, u_n)$
v	Space lag between two arbitrary points u_i and u_j
$\mathrm{Var}[X]$	Variance of X
w_0	Initial defection
$\bar{w}_0$	Mean initial defection
w_{0c}^{max}	Maximum amplitude of initial deflection for column-type shape mode
w_{0p}^{max}	Maximum amplitude of initial deflection for plate shape mode
w_{0s}^{max}	Maximum amplitude of initial deflection for stiffener sideway shape mode
$\boldsymbol{X}$	A n-dimensional random vector
$\boldsymbol{x}$	A realization (outcome) of the random vector $\boldsymbol{X}$
X	A one-dimensional random variable
x	A realization (outcome) of the random variable X
x	Spatial Cartesian x – axis
X_d	A random variable representing the uncertainty on the whipping bending moment calculation
X_m	A random variable representing the uncertainty on material properties
X_{nl}	A random variable representing the model uncertainty associated with the computation of non-linear effects in WVBM
X_r	A random variable representing the model uncertainty associated with the prediction of hull girder ultimate strength
X_{st}	Model uncertainty associated with the computation of linear result in WVBM
X_{sw}	Model uncertainty associated with the computation of SWBM
X_u	A random variable representing an equivalent model uncertainty associated with the prediction of hull girder ultimate strength

Y	A random variable representing the model output
y	A realization of the scalar variable Y
y	Spatial Cartesian y – axis
$\boldsymbol{Z}$	A vector of n independent standard normal variables
Z	A random variable in the standard normal space
$\boldsymbol{z}$	A realization of $\boldsymbol{Z}$
z	A realization of Z
z	Spatial Cartesian z – axis

Greek characters

Symbol	**Description**
$\boldsymbol{\alpha}$	Sensitivity factors associated with FORM
α	Beta distribution shape parameter
α_i	Sensitivity index for the X_i random variable
B	Beta function
β	Generalized reliability index
β_{FORM}	Reliability index computed by FORM
β	Beta distribution shape parameter
β_p	Plate's slenderness ratio defined as: $$\beta_p = \frac{b}{t}\sqrt{\frac{\sigma_y}{E}}$$
Γ	Gamma function
δ	Dirac delta function
ε	Strain
ε	Observation or measurement error
ε_y	Normalized strain
ε_t	Combined observation and model error
ζ	Parameter of the lognormal distribution
η	Parameter of the lognormal distribution

$\boldsymbol{\theta}$	Vector containing the parameters of a distribution model
θ	A single parameter of a distribution model
ϑ	Scale of fluctuation of a random field
κ	Wave number
κ_u	Cut-off wave number
λ	Scale parameter of Weibull distribution
λ_c	Column's slenderness ratio defined as: $$\lambda_c = \frac{a}{\pi r_g}\sqrt{\frac{\sigma_y}{E}}$$
μ	Parameter of the normal distribution
$\hat{\mu}$	Spatial mean value
μ_X	Mean value of variable X
ν	Poisson' s ratio
ξ	Model error
ρ	Correlation coefficient
$\hat{\rho}$	Spatial correlation coefficient
σ	Stress
σ	Parameter of the normal distribution
$\hat{\sigma}$	Spatial standard deviation
$\sigma_{\varepsilon,\mu}$	Standard error of the mean
σ_X	Standard deviation of X
σ_X^2	Variance of X
σ_y	Yield stress
σ_y^{ch}	Characteristic (nominal) value of yield strength
σ_u	Ultimate stress
τ	Time
τ_c	Coating life duration or corrosion time initiation
τ_t	Transition time between coating life duration and corrosion initiation
Φ	Standard normal (cumulative) distribution function
φ	Standard normal probability density function

χ	Curvature
Ω	Sample space
ω	An outcome of the sample space
Ω_o	Observation domain
Ω_S	Spatial domain
$\Omega_{\mathcal{F}}$	Failure domain

List of Abbreviations

Abbreviations	Description
(a)BUS	(adaptive) Bayesian Updating using Structural reliability methods
BM	Imperfection model for the description of steel plates' imperfect geometry based on the critical number of half-waves lengthwise of the plate.
BM+2	Imperfection model for the description of steel plates' imperfect geometry based on the critical number plus two half-waves lengthwise of the plate.
CDF	Cumulative distribution function
CoV	Coefficient of variation
CSR	Common Structural Rules
DoF	Degree of freedom
FEM	Finite element method
FLNG	Floating liquified natural gas unit
FPSO	Floating, production, storage and offloading unit
HH	Hungry-horse imperfection model for the description of steel plates' imperfect geometry.
IACS	International Association of Classification Societies
ISSC	International Ship Structure Committee
JSQS	Japan Shipbuilding Quality Standard
LHS	Latin Hypercube sampling
LSC	Load-end shortening (or stress-strain) curves
LSF	Limit state function
MCMC	Markov Chain Monte Carlo
MCS	Monte Carlo simulation
MLE	Maximum Likelihood estimate
MSE	Mean squared error
NLFEA	Non-linear finite element analysis
NN	Neural network

PDF	Probability density function
PSF	Partial safety factor
QoI	Quantity of interest
RF	Random Field
RV	Random Variable
SHH	Stochastic hungry-horse imperfection model for the description of steel plates' imperfect geometry (model proposed by the author)
SSC	Ship Structure Committee
SuS	Subset Simulation
SWBM	Still water (vertical) bending moment
WVBM	Wave-induced (vertical) bending moment
ULS	Ultimate limit state

This page intentionally left blank

1 Introduction

1.1 Background

The *ultimate limit state* (ULS) defines the maximum load-carrying capacity of a ship. Checking the hull girder ultimate capacity against extreme load events is one of the most important safety measures for the design and analysis of ocean-going ship structures. This fact has been acknowledged by the International Association of Classification Societies and the Common Structural Rules (IACS CSR) through the introduction of a partial safety factor (PSF) format design criterion, the derivation of which has been based on structural reliability methods.

Structural reliability allows for the probabilistic treatment of the uncertainties related to the resistance (capacity) and the loads (demand) of an engineering structure. The ultimate purpose of a reliability analysis is generally to achieve a balance between functionality and cost, while maintaining a high level of safety. Apart from contributing to the introduction of PSFs format design criteria, reliability analysis is also a prominent method to examine the performance of existing structures and make decisions, e.g., inspection planning, reinforcement/replacement of a structural member, lifetime extension of the target vessel, etc.

The focus of this thesis is on the assessment and quantification of hull girder ultimate strength in the presence of uncertainties. Marine engineers encounter various types of uncertainties associated with hull girder ultimate strength prediction. In particular, uncertainties can be classified into two broad categories: (i) input uncertain parameters and (ii) model uncertainties. Uncertainties of the first type are related to random geometric characteristics of the hull structure (e.g., thickness, weld-induced initial imperfections, residual stresses, etc.) and variations on material properties (e.g., yield strength, Young' s modulus, etc.). Such types of uncertainties are generally the result of manufacturing processes and deterioration effects. Deterministic approaches become insufficient to accommodate the inherent randomness of such properties and their description often dictates the use of more advanced quantification techniques to characterize their spatial (temporal) uncertain characteristics over space (time). The framework of random fields (processes) is then needed to achieve this task.

On the other hand, model uncertainties arise in our attempt to replicate the behavior of the real system. As any model is – more or less – uncertain on its prediction, the development of a model that would accurately compute the hull girder ultimate strength is a challenging task. A basic limitation that magnifies the significance of the problem is the absence of real-life results. As the comparative and trustworthy term is not always clear and defined enough to obtain information about the approximation in hull girder ultimate strength calculations, subjective knowledge from experts in conjunction with advanced numerical model predictions are often needed, see ISSC (2012).

1.2 Motivation

Uncertainty reflects our imprecise state of knowledge of the universe and expresses our level of confidence, see Lindley (1975). One can reduce uncertainties by an increase in knowledge, that is, by learning. Uncertainty quantification and reduction can be mathematically expressed using the *theory of probability*. In engineering, measured or observed data, becoming available during the lifetime of a structure, can be used to reduce the uncertainties related to a model and/or its parameters. In doing so, background knowledge is updated with new information – usually of limited amount – leading thus to an improved prediction of the system's performance. Bayesian framework provides an effective tool to formalize the above procedure and quantify the effect of information through probabilistic terms.

Bayesian inference techniques have been extensively used in different engineering disciplines, including bridges, see e.g., Enright and Frangopol (1999), Strauss et al. (2008), Ma et al. (2013), floating structures, see e.g., Garbatov and Soares (2002), Vasconcelos de Farias and Netto (2012), and geotechnical applications, see e.g., Papaioannou and Straub (2017). In the above studies, the effect of new information is quantified through probabilistic terms and used to update the model parameters and the subsequent reliability of the system. In the field of ship structures, Okasha et al. (2010) and Zhu and Frangopol (2013) evaluated the reliability of a vessel after performing a Bayesian updating on the wave-induced bending moment. In terms of resistance, Garbatov and Soares (2002) used inspection data to update the distribution models of crack initiation and the subsequent fatigue reliability of ship structural components. In the context of reliability in ULS, the application of Bayesian methods as a tool to manage the uncertainties associated with basic resistance parameters can be meaningful. For instance, the probabilistic description and reduction of uncertainties related to the corrosion and the resistance model itself is an open research area for application of Bayesian approaches.

Corrosion is a time-dependent deterioration process that has a significant impact on the integrity and reliability of the ship's hull girder. However, existing corrosion models used in the framework of reliability usually provide poor quality predictive capabilities and are associated with high statistical uncertainties, since they are constructed by pooling data from various sources. The need for more sophisticated corrosion prediction models sufficient for reliability analyses purposes has been stressed by Melchers (2003).

The management of uncertainties associated with the resistance model itself can be also addressed using Bayesian techniques. Particularly, the limited amount of available data along with the need for combining different sources of information (e.g., subjective knowledge from experts and advanced finite element models) in order to improve our simplified analytical models motivates the establishment of a Bayesian framework capable of updating the model uncertainty factor associated with hull girder ultimate strength prediction. As a robust methodology for the quantification of model uncertainty factor is still missing from the literature, the establishment of such a procedure on a ship-type dependent basis would be of important practical use. An urgent need to develop practical methods to evaluate the hull

girder ultimate strength of container ships with consideration of the effect of lateral loads has been reported by ClassNK (2014) after the shipwreck of “MOL Comfort” in the Indian Ocean in June 2013.

1.3 Scope of the Thesis

The general subject of this thesis is the development of innovative methods for an improved assessment and updating of hull girder ultimate strength and reliability of ship structures. This objective is mainly achieved by managing the uncertainties associated with model parameters (model inputs) as well the model itself. From the first perspective, the advancements concern the development of a new model for the spatial random representation of the imperfect geometry of weld-induced steel plates and the introduction of a Bayesian approach to update the corrosion predictions of a target ship using inspections data. From the perspective of model, the emphasis has been placed on the refinement of model uncertainties through the combination of information from: (i) the analytical incremental-iterative method of IACS CSR based on Smith (1977) method, (ii) high-fidelity non-linear finite element analysis (NLFEA), and (iii) subjective judgment from experts. To achieve this task, an appropriate Bayesian updating scheme is developed. The impact of the aforementioned developments is investigated on: (i) the reliability assessment and updating of an oil tanker conditional on inspections data, and (ii) the reliability assessment of two container ships at a given point in time.

In particular, the thesis presents procedures for an improved modelling and uncertainty reduction of the following aspects:

- *Spatial description of random geometric characteristics of steel plates*

In ship structures, geometric characteristics of steel plates, such as thickness and imperfections, are characterized by an inherent randomness in space. The framework of stochastic FEM can efficiently accommodate the spatial randomness of such quantities through the use of random fields. Uncertainty from the input is then propagating through the FE model and the impact on the stochastic response of the system is evaluated. In the present thesis, the effect of stochastic geometric imperfections on the ultimate strength of plates and hull girders is investigated. Moreover, the validity of uniform thickness reduction in the formulation of the analytical stress-strain relations or load-end shortening curves (LSC) prescribed in IACS CSR Smith’s model is examined by simulating the actual non-uniform pattern of thickness on a representative stiffened plate element and assessing its impact on the ultimate strength.

- *Updated predictions of corrosion trends on a vessel-specific basis*

During the past decades, ship-type dependent empirical corrosion models have been developed based on corrosion data sets from the global fleet. Constructing models by collecting data from various sources – usually from ships with different characteristics and operational profile –

often leads to poor quality mean predictions and high statistical uncertainties of model parameters. Such models are generally insufficient for reliability analysis purposes where a much higher level of sophistication is needed. During a ship's operation, new information regarding the hull structure condition is acquired from inspection surveys in the form of ultrasonic-thickness (UT) measurements report. This information can and should be utilized to update the corrosion predictions of the target vessel and reduce the relevant model uncertainties. In this thesis, the framework of Bayesian analysis is used to effectively update prior model predictions based on actual measurements acquired from subsequent inspections.

- *Determination and quantification of model uncertainties*

Different models for the computation of hull girder ultimate strength of ships have been developed throughout the past years. Among the most prominent ones are: (i) the analytical progressive collapse analysis of IACS CSR Smith's method and (ii) the NLFEA method. The quantification of model uncertainties is generally a challenging task since real-life measurements are not available. In this thesis, a Bayesian approach is established to estimate the parameters of the model uncertainty factor for container ships and oil tankers with a consistent and systematic manner. In this context, experts' opinion from literature sources and advanced NLFEA results are combined in order to refine the uncertainty in IACS CSR Smith's model prediction and define a ship-type dependent model uncertainty factor.

Overall, the above investigation provides knowledge and information to address the following questions:

- IACS CSR Smith's method assumes a uniform thickness reduction of structural members when evaluating the structural behavior of a stiffened plate element through the load-end shortening curves (LSC). Does this practice lead to reliable results for ultimate strength prediction or should the effect of non-uniform thickness wastage should be considered?

- Thickness measurements of the hull structure are acquired during inspections during a ship's lifetime. How this form of information can be exploited to update existing knowledge and improve future corrosion predictions on a target vessel?

- Are the common deterministic imperfection models capable of capturing the imperfect geometry of real steel plates? Is it possible to develop a stochastic imperfection model that will approximate better the inherent randomness of weld-induced steel plates' geometry in space? What would be the impact of such a stochastic imperfection model on the ultimate strength of hull girders?

- How the various sources of available information, i.e., subjective information from experts and objective information from advanced FE models, can be combined effectively to refine the model uncertainty associated with hull girder ultimate strength

prediction using the analytical IACS CSR Smith's model? How this methodology can be applied to account for the specific characteristics of different ship types?

- What is the effect of thickness measurements collected from subsequent inspections on the reliability updating of an oil tanker in ULS? How the reliability (failure probability) of container ships is updated if a more refined strength model uncertainty factor is used?

1.4 Thesis layout

The thesis consists of the following eight chapters:

Chapter 1 introduces the background, motivation, objectives and organization of this thesis.

Chapter 2 reviews the main sources of uncertainties and their treatment in the context of hull girder ultimate strength assessment. Broadly speaking, uncertainties are categorized into geometric, material and model uncertainties. Common literature approaches used for the quantification of all sources are presented. Particular focus is placed on model and geometric uncertainties, which are the main subject of this thesis.

Chapter 3 presents the basic mathematical background of random fields theory. The context of this chapter is oriented in the numerical applications introduced in Chapter 4.

Chapter 4 describes the spatial randomness of initial geometric imperfections and non-uniform thickness on steel plates of ships through the use of random fields. A new stochastic imperfection model is introduced, and its impact on the ultimate strength of plates and hull girders is examined. Furthermore, the effect of non-uniform thickness representation on the structural behavior of a stiffened panel is investigated and compared with the IACS CSR LSC uniform thickness reduction approach.

Chapter 5 presents the fundamental theory of Bayesian analysis for engineering applications. Bayes' rule is extended to address the updating of continuous random variables. Common methods for the appropriate probabilistic modelling of the *prior* and the *likelihood* – which are two of the basic components of Bayes' rule – as well computational strategies for the solution of the Bayesian updating problem are provided. The context of this chapter is essential for the numerical investigations that follow in Chapter 6.

Chapter 6 constitutes the core of the thesis. This chapter introduces a novel methodology for the updating of the probabilistic-based hull girder ultimate strength. This is accomplished through the solution of two problems. In the first problem, a Bayesian approach is applied for determining the hull girder model uncertainty on a ship-type dependent basis. Investigations are focused on oil tankers and container ships. In the second problem, Bayesian techniques are used to learn and update the parameters of a time-dependent empirical-based corrosion model in light of available data from inspections. A numerical investigation is presented for a specific vessel.

Chapter 7 investigates the impact of the novelties developed in the previous chapter on the reliability of ship structures in ultimate limit state. The basic reliability problem and the time-dependent reliability framework for deteriorating ship structures are analyzed. Then, two numerical applications follow. In the first application, the reliability updating of an oil tanker conditional on inspections data takes place. Results from Chapter 6 regarding the updating of corrosion model are used for this purpose. In the second application, the reliability of two container ships using the proposed strength model uncertainty factor from Chapter 6 is investigated and compared with common literature approaches.

Chapter 8 provides a summary of the work and lists the originalities of this thesis. Future research directions are also presented.

A layout of the thesis is illustrated in Figure 1.1.

In Appendix A, a brief overview of the basic notions of probability theory are presented. Appendix B formally defines the concept of random variable and presents the numerical descriptors of continuous random variables. In Appendix C, some common probability distributions for the representation of continuous random variables are introduced. In Appendix D, an outline of the Monte Carlo simulation (MCS) method is presented. Appendix E outlines the fundamentals of feed-forward neural networks. Appendix F presents a phenomenon that is present in container ships and bulk carriers known as the double bottom effect. The remaining appendices present results of this thesis.

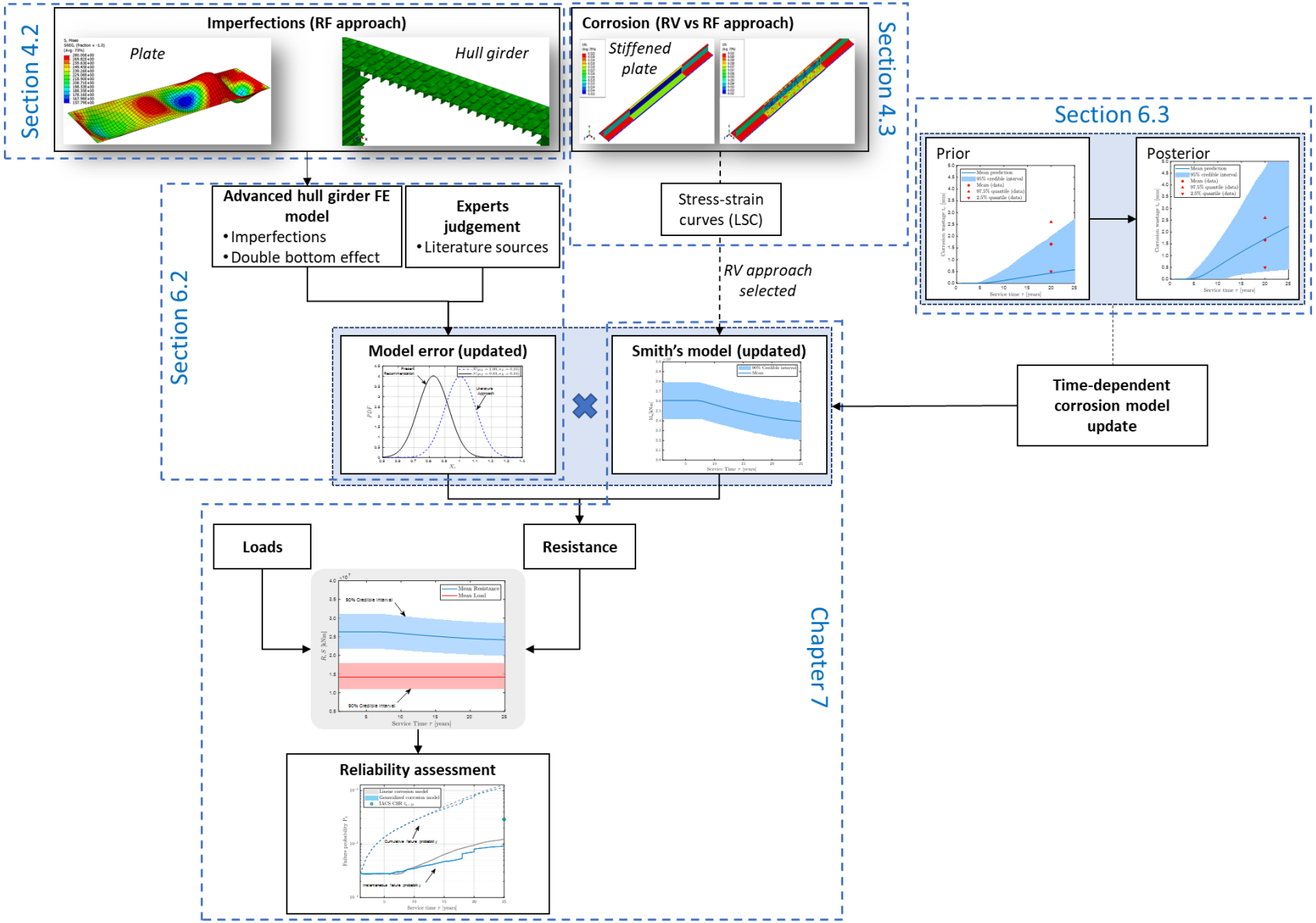

Figure 1.1. Graphical overview of the thesis.

This page intentionally left blank

2 A review on hull girder ultimate strength assessment

2.1 Introduction

This chapter reviews state-of-the-art work related to the probabilistic modelling of resistance in terms of structural reliability analysis of ship structures in ultimate limit state. The basic question that is addressed here is: "*Which* are the uncertainties that govern the probabilistic-based hull girder ultimate strength assessment and *how* are these quantified in the framework of reliability analysis?"

The chapter begins with summarizing the most commonly used computational methods for the prediction of ultimate strength of hull girders (Section 2.2). The various sources of uncertainties associated with hull girder ultimate strength assessment are briefly analyzed in Section 2.3. This section answers to the first part of the basic question stated above. The second part of the question is covered in Section 2.4. Particularly, an overview regarding the strategy for a probabilistic-based ultimate strength assessment within the framework of reliability in ULS is given in Section 2.4.1. In the remaining sections of this chapter, we present the most common practices used by researchers to treat some of the most fundamental sources of uncertainties related to the probabilistic modelling of hull girder ultimate strength, that is: (i) model uncertainty (Section 2.4.2), (ii) material characteristics (Section 2.4.3), (iii) initial geometric imperfections (Section 2.4.4) and (iv) corrosion (Section 2.4.5).

2.2 Computational methods for the hull girder ultimate strength assessment

Ships are to be designed to withstand the extreme environmental loads anticipated during their design life. The assessment of *hull girder ultimate strength* involves the computation of the maximum load-carrying capacity under longitudinal bending moment. Buckling and yielding failure mechanisms are to be considered for the determination of hull girder ultimate strength. An accurate and efficient method for evaluating the ultimate hull girder strength is thus of great practical importance.

During the past decades, useful analytical, numerical and experimental methods have been developed to assess the hull girder ultimate strength of ships[1]. Analytical methods generally involve closed-form expressions and the progressive collapse analysis method proposed by Smith (1977). Numerical methods consist of the NLFEA method and the idealized structural unit

[1] Experiments on real ships' hull collapse date back to the 1930s and the World War II. Since then, experimental efforts have been limited to reduced scale testing of box girders and ship hull models, see ISSC (2018).

method (ISUM). A brief description of the most commonly used methods is given below. For a more elaborated review, the reader is referred to Yao (2003) and ISSC (2018).

Closed-form methods involve the development of simple theoretical and empirical formulas that explicitly evaluate the hull girder ultimate strength. Such formulations have been based on a presumed stress distribution field over the hull cross-section at collapse, taking into account plasticity and buckling. Caldwell (1965) first determined the longitudinal bending strength using this method on a simplified geometry of a cross-section. Since then, several improvements, both in the assumed stress state and in the form used to express the ultimate strength, have been performed, see ISSC (2018).

Smith's model is the prescribed procedure of IACS CSR used for the evaluation of hull girder ultimate strength. Smith's method is considered superior than closed-form methods since it takes into account the strength reduction (load shedding) of each structural member after attaining its ultimate strength locally. The neglection of this phenomenon can greatly affect the ultimate strength of the whole cross-section, see ISSC (2000). Smith's method is based on an incremental-iterative algorithm and requires the division of the hull girder transverse section into a set of independent elements (stiffeners with attached plating). An important feature of the method is the identification and computation of failure mechanisms for the individual elements, expressed through the so-called load-end shortening curves (LSC) (or average stress-strain $\sigma - \varepsilon$ relationship). For a detailed presentation of the algorithm and the basic assumptions behind this method, the reader is referred to IACS (2019).

NLFEA method is an advanced tool to perform a hull girder collapse analysis – considering both material and geometric non-linearities – in a digital environment. The continuous advance of computer capabilities in conjunction with the robust finite element techniques have made this method very popular in the last years. Although NLFEA still remains time-consuming, and requires significant human effort and experience, it is an advanced tool to represent influential parameters of the problem, while at the same time, alleviates serious simplifications and weaknesses of Smith's method.

2.3 Uncertainties on the prediction of hull girder ultimate strength

The assessment of hull girder ultimate strength is governed by various types of uncertainties, the presence of which restricts the construction of an absolutely safe ship structure. In general, uncertainties can be classified into: (i) input uncertain parameters and (ii) model uncertainties (see Section 1.1). In turn, input uncertainties can be further distinguished into random geometric and material properties. An alternative categorization of input uncertain parameters, according to ISSC (2012), is their distinction between physical aspects and deterioration effects. Based on this, an overview of the main sources of uncertainties related to hull girder ultimate strength prediction is presented below and illustrated in Figure 2.1.

2.3.1 Physical aspects

Physical aspects are mainly referred to material properties' variation, geometric random characteristics and fabrication-related procedures. Inherent variability of material properties of steel plates, such as, yield strength and Young's modulus, as well geometric random characteristics, such as cross-sectional thickness of elements, are prominent sources of uncertainty that highly affect the overall strength of a vessel. Additional sources of uncertainty arise from manufacturing processes during the construction stage. Fabrication-related processes result in the development of initial geometric imperfections, residual stresses, misalignments, etc. Imperfections are characterized by a significant degree of uncertainty in terms of their magnitude and spatial variation. Although quality control methods have been improved throughout the years, these types of uncertainties are still present and may severely affect the prediction of hull girder collapse.

2.3.2 Deterioration effects

Deterioration (or ageing) effects are associated with physical processes and phenomena which take place during operation, and degrade the condition of the hull structure over time. Such phenomena include corrosion, fatigue cracks and dents' formulation. Of particular interest in the longitudinal hull girder ultimate strength and the subsequent reliability assessment is the description of uniform (or general) corrosion, see e.g., Hørte et al. (2007). A detailed description of this subject is given later in Section 2.4.5. Fatigue cracks can reduce the load carrying capacity of ship hull structural elements and eventually decrease the overall hull girder capacity. However, studies dealing with the effect of crack initiation and propagation in the context of hull girder ultimate strength and reliability are quite limited, see e.g., Akpan et al. (2002), Sun and Bai (2003), Gao et al. (2012), and Babazadeh and Khedmati (2021). This can be explained in part by the fact that the amount and location of cracks are not generally known in a ship hull, and therefore, the phenomenon cannot systematically be addressed. Another important reason is that cracks are repaired as soon as they are observed. This statement holds for dents too. Dents' formulation is usually the result of impact or accidental loads, see e.g., Smith et al. (1988). As it is a very localized and vessel-specific phenomenon, the representation of dents requires the development of an advanced FE model that will be able to approximate the real ship's imperfect geometry.

2.3.3 Model uncertainties

Model uncertainty (or model error) constitutes a significant source of uncertainty in the computation of hull girder ultimate strength. In general, this type of error may be the result of simplified mathematical descriptions that are selected in favor of convenience or/and missing variables which are not included in the model because of ignorance. Depending on the type of

the employed model (analytical, numerical, experimental) different uncertainties may arise as a result of the simplifications and assumptions made. Among the various models developed throughout the years in shipping community, the IACS CSR Smith's model and the NLFEA are the most prominent approaches for the description of hull girder collapse. Uncertainties related to these two models are discussed here.

Smith's method provides a two-dimensional idealization of the cross-section of the ship. Various sources of uncertainty exist, including the implicit modelling of imperfections, the boundary conditions and the division of the cross-section into a set of independent elements[2]. The formulation of the LSC is considered as one of the most critical factors affecting the accuracy of the method, see e.g., ISSC (2000) and Yao (2003). Another limitation of the conventional Smith model is the fact that it cannot capture the effect of double bottom bending between transverse bulkheads which is particularly profound in bulk carriers and container ships[3]. This phenomenon can considerably affect the hull girder ultimate strength of the vessel, see e.g., Amlashi and Moan (2008), Tatsumi and Fujikubo (2020).

FE method provides a refined version of the real system but is subject to other sources of uncertainties mostly related to modelling aspects, such as for example the selection of the appropriate mesh, the boundary conditions, the analysis' solver, etc., see e.g., ISSC (2018). The experience and skills of the user may also play an important role on the final results. In addition, the computational and modelling effort required for a single NLFEA is higher than that of Smith's method.

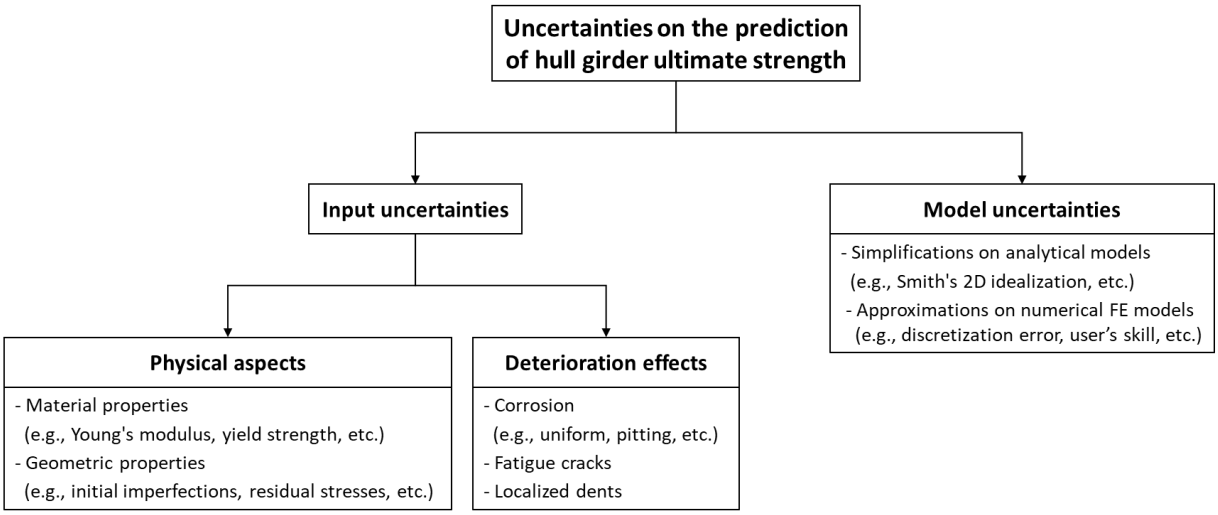

Figure 2.1. Main sources of uncertainties associated with hull girder ultimate strength assessment.

[2] Although relatively clear instructions are provided by IACS CSR upon the modelling of structural elements, differences may arise on the ultimate bending moment capacity calculation between various participants, mainly as a result of different modelling procedures, see also ISSC (2012).

[3] See Appendix F for a description of the double bottom phenomenon.

2.4 Quantification and treatment of basic types of uncertainties

2.4.1 Overview

In the framework of reliability analysis, the assessment of hull girder ultimate strength with probabilistic terms involves three basic steps:

A. The selection of a *reference model* used for the computation of capacity. Traditionally, the IACS CSR Smith's incremental-iterative algorithm is preferred as a reference model for the implementation of reliability analysis due to its computational efficiency relatively good accuracy on its predictions.

B. The probabilistic description of the *input uncertain parameters* or *basic random variables* introduced in the reference model. In the general case, uncertainties related to material characteristics (e.g., yield strength, Young's modulus) and geometric properties (e.g., corrosion) of structural elements are accounted for.

C. The selection of a distribution model to describe the *model uncertainty*, i.e., the deviation of the reference model prediction vs. real-life (true) value. This factor covers the uncertainty on the calculation model, as well other aspects that cannot be explicitly treated through the use of basic random variables, such as imperfections.

In terms of mathematical notion, the formulation of resistance (or capacity) term R in ultimate limit state is usually expressed as the product of two independent random variables, see e.g. Hørte et al. (2007):

$$R = X_r M_u \tag{2.1}$$

where, M_u denotes the hull girder ultimate strength predicted by Smith's (reference) model (A) and X_r reflects the uncertainty on the prediction model (C). The randomness on M_u derives from the uncertainty on the material and geometric characteristics (B). Common literature approaches for the determination of the distribution model of X_r are presented in Table 2.1.

An alternative formula for the representation of resistance term R is occasionally adopted in the literature. Based on this approach, the calculation of hull girder ultimate strength using IACS CSR Smith's model is performed using the minimum specified characteristic values of material properties (see Table 2.2). Therefore, a fixed value for M_u is obtained corresponding to

the characteristic value M_u^{ch}. Uncertainties related to material properties[4] are gathered into a single random variable X_m which is multiplied by the model uncertainty X_r. The resistance term R reads then:

$$R = X_r X_m M_u^{ch} \tag{2.2}$$

Usually, an *equivalent strength model uncertainty factor* X_u is established as $X_u = X_r X_m$ in order to decrease the number of random variables of the reliability problem. The statistics of X_u are obtained assuming independence between X_r and X_m. The mean value $\mathrm{E}[X_u]$ and the variance $\mathrm{Var}[X_u]$ of X_u are calculated as:

$$\mathrm{E}[X_u] = \mathrm{E}[X_r X_m] = \mathrm{E}[X_r]\mathrm{E}[X_m] = \mu_{X_r}\mu_{X_m} \tag{2.3}$$

$$\mathrm{Var}[X_u] = \sigma_{X_r}^2\mu_{X_m}^2 + \sigma_{X_m}^2\mu_{X_r}^2 + \sigma_{X_r}^2\sigma_{X_m}^2 \tag{2.4}$$

It is generally assumed that X_u follows the lognormal distribution, as a product of a normal (X_r) and lognormal distribution (X_m)[5]. The mean value and CoV of material uncertainty factor X_m for different grades of steel are listed in Table 2.2. It is stressed, however, that there is not an established procedure for the calculation of X_m when the ship is constructed by both mild and high-tensile grades of steel (which is often the case).

2.4.2 Model uncertainty

The uncertainty associated with a particular model performance is usually expressed by a single random variable X_r defined as:

$$X_r = \frac{\text{true strength (response)}}{\text{model strength (response) prediction}} \tag{2.5}$$

Typically, a Gaussian distribution model is postulated to represent model uncertainty X_r. However, for hull girder ultimate strength calculation, the statistical parameters of the respective distribution model have not met a universal acceptance. Indeed, different estimates

[4] The variability of Young's modulus is not taken into account in the specific approach, as its impact on the probabilistic-based hull girder ultimate strength calculation is considered to be limited, see e.g., Paik and Frieze (2001).

[5] However, the product of a normal distribution and a lognormal distribution does *not* give a lognormal distribution.

on mean value and standard deviation can be found in the literature. A brief historical review is outlined.

Primarily, the determination of X_r was performed empirically on the basis of experts' judgement. A degree of variability around the predicted value of a reference model was presumed. Typical values of CoV were 0.10 and 0.15, while for the mean value an unbiased estimate (unit-mean) was usually adopted, see e.g. Mansour and Hovem (1994), Soares et al. (1996) and Paik and Frieze (2001). At that time, the selection of the statistical parameters of the distribution was seen more as a "guesstimate". As soon as better information becomes available this should be considered to refine the statistics of the model, see Paik and Frieze (2001). An early effort to take into consideration additional sources of information was initiated by Frieze and Lin (1991). In their work, they estimated the parameters of X_r by combining subjective knowledge, as well, numerical and experimental results carried out on box girders.

In 2007, Hørte et al. (2007) used NLFEA predictions to calibrate X_r. A single result from the hull girder ultimate bending capacity prediction of a Suezmax tanker was adopted by a series of NLFEA conducted previously in DNV (2004). Hørte et al. (2007) used this outcome to compensate the simplifications of the Smith's method with a more sophisticated model such as FEM. In doing so, the recommended mean value of X_r shifted to a higher level (equal to 1.05), while the CoV was assumed equal to 0.10.

Up to date, most of the research studies performed under the framework of reliability analysis adopt a mean value equal to 1.00 or 1.05 and a CoV of 0.10 (in less cases equal to 0.15) for the quantification of X_r (see Table 2.1). It is stressed that this consideration is followed irrespectively on the examined type of ship. This is reflected on the numerous research studies carried out during the last two decades for tankers, see e.g., Hussein and Soares (2009), Gaspar and Soares (2013), Xu et al. (2015), Campanile et al. (2017)a, Gong and Frangopol (2020), bulk carriers, see e.g., Shu and Moan (2011)b, Campanile et al. (2016)a, Campanile et al. (2016)b, floating production and offloading units (FPSOs), see e.g., Sun and Bai (2003), Chen (2016) and container ships, see e.g., Parunov et al. (2014), Corak and Soares (2018), Shi and Gao (2021).

Table 2.1. Applied distribution models for strength mode uncertainty factor X_r. The references essentially correspond to the first studies which introduced the corresponding statistics for X_r.

Distribution	Mean	CoV	References
Normal	1.00	0.10	Paik and Frieze (2001)
Normal	1.00	0.15	Frieze and Lin (1991), Mansour and Hovem (1994)
Normal	1.05	0.10	Hørte et al. (2007)

2.4.3 Material properties

The inherent randomness associated with basic material characteristics can significantly affect the hull girder ultimate strength and the reliability of a ship structure. In general, the quantification of material properties is accomplished by means of random variables which are introduced in the resistance model R through Eq. (2.1) or Eq. (2.2).

Yield strength σ_y is the most influential parameter among other material properties, such as Young's modulus E and Poisson's ratio ν. Traditionally, a lognormal distribution is adopted to represent yield strength variability. The distribution of the yield strength is derived from its characteristic value σ_y^{ch} which represents the 5% fractile, see IMO (2006). The statistics of the distribution are listed in Table 2.2 for common types of steel grades used in the shipbuilding industry.

Young's modulus E is usually represented by a normal distribution model with mean value equal to 210 GPa and coefficient of variation equal to 0.10, see e.g., DNV (1992). Occasionally, Young's modulus is set as fixed quantity as it is considered that the impact of its variability on the results is not important, see e.g., IMO (2006). Poisson's ratio ν is also set as constant.

Usually, for a unique ship construction the same supplier of steel products is adopted. In doing so, although some degree of independence in the steel properties for different plates and stiffeners around the hull section might exist, the characteristics of the material at different locations can be assumed similar. Thus, the spatial variation of material properties around cross section is usually neglected, see e.g. Hørte et al. (2007).

Table 2.2. Properties of yield strength of steel. Characteristic values σ_y^{ch} are prescribed by IACS (2019). The distributions are given by IMO (2006).

Steel grade	Distribution	Mean	CoV	σ_y^{ch}	$\mathrm{E}[X_m] \approx \mathrm{Mean}/\sigma_y^{ch}$
Mild	Lognormal	269	0.08	235	1.14
High tensile H-32	Lognormal	348	0.06	315	1.10
High tensile H-36	Lognormal	391	0.06	355	1.10
High tensile H-40	Lognormal	426	0.06	390	1.10

2.4.4 Initial geometric imperfections

The collapse analysis of ship-type stiffened plate panels under longitudinal compression, as well the overall hull girder ultimate strength, is generally affected by initial geometric imperfections[6]. Typically, imperfections are introduced in the hull girder FE model and accommodated on the resistance model R implicitly through X_r parameter. The incorporation of initial imperfections into a FE model of a hull girder is not a trivial task, as it often needs significant human effort. Usually, the prescribed initial imperfections are assigned to the nodes of the finite elements as discrete nodal displacements. Alternatively, an eigenvalue buckling analysis on the examined stiffened panels can be carried out, see e.g., Amlashi and Moan (2008). Imperfections are usually introduced in the most vulnerable areas of midship section region, that is, areas subject to highly compressive stresses. For instance, for a ship examined in extreme hogging condition, maximum compression is developed on the bottom structure. Imperfections are then assigned on that particular region of the vessel.

As actual imperfections are rarely known, different imperfection models have been introduced to represent the imperfect geometry of a stiffened panel in a deterministic, yet practical, manner. These models aim at describing the initial deflection field by applying a presumed geometric shape and a characteristic maximum distortion magnitude. In general, the applied models are either based on more theoretical approaches trying to ensure a conservative structural behavior, or more realistic practices focusing on the approximation of the actual condition of structure. Recently, the author co-published a paper dealing with the prevailing ship-type geometric imperfection models and assessed their impact on the collapse of ship-type stiffened plated grillages, see Li et al. (2022).

2.4.4.1 Shape/mode of deflection

The initial geometric imperfection of a stiffened pated grillage is formed of three components that are linearly superimposed to generate the final imperfect geometry, i.e., (i) global column-type deflection, (ii) local stiffener sideway deflection, and (iii) local plate deflection. The prevailing initial geometric models are presented below and a schematic description is given in Figure 2.2.

[6] Imperfections generally involve initial geometric imperfections and residual stresses. Particular focus on this thesis is placed on weld-induced initial geometric imperfections. The impact of residual stresses on hull girders and stiffened panels ultimate strength prediction has been studied by e.g., Gannon et al. (2012) and Li et al. (2021).

Global column-type deflection

The column-type deflection is introduced as a half sinusoidal curve between the transverse web frames and between primary supporting members, e.g., longitudinal bulkheads. The analytical form of this deflection mode is given by Eq. (2.6) as:

$$w_{0c}(\mathrm{x},\mathrm{y}) = w_{0c}^{max}\sin\frac{\pi \mathrm{x}}{a}\sin\frac{\pi \mathrm{y}}{B} \tag{2.6}$$

where, w_{0c}^{max} is the maximum amplitude of initial deflection, a is the plate length between two adjacent transverse frames and B is the overall breadth of the entire panel between supporting members, e.g., girders and floors (see Figure 2.2).

Local stiffener sideway deflection

The initial sideway deflection mode applied on longitudinal stiffeners is represented by a half-wave between transverse web frames and a sideway deflection along the web height. The above is expressed by Eq. (2.7) as:

$$w_{0s}(\mathrm{x},\mathrm{z}) = w_{0s}^{max}\frac{\mathrm{z}}{h_w}\sin\frac{\pi \mathrm{x}}{a} \tag{2.7}$$

where, w_{0s}^{max} is the maximum amplitude of initial sideway deflection and z is the vertical position of deflection along the web height h_w. Stiffener sideway deflection may have a significant impact on the torsional buckling (tripping) of stiffeners.

Local plate deflection

The local plate deflection is described following one of the two below alternatives. The first form, which has a clearly theoretical background, is introduced based on the critical elastic buckling-mode shape of imperfection and it reads:

$$w_{0p}(\mathrm{x},\mathrm{y}) = w_{0p}^{max}\sin\frac{m_{\mathrm{x}}\pi \mathrm{x}}{a}\sin\frac{\pi \mathrm{y}}{b} \tag{2.8}$$

where, w_{0p}^{max} is the maximum amplitude of initial deflection on the plate, b is the breadth of the plate and m_{x} expresses the buckling half-wave number of the plate defined as the minimum integer satisfying the following condition:

$$\frac{a}{b} \le \sqrt{m_{\mathrm{x}}(m_{\mathrm{x}}+1)} \tag{2.9}$$

The second alternative shape is the idealized (or conventional) *hungry-horse* (HH) *or thin-horse model*. The HH model has been introduced by Ueda and Yao (1985) and is generally associated with a more realistic description of weld-induced imperfections, as it is based on full-scale measurement data of ship structures. For this model, the initial deflection pattern of a plate's geometry is expressed using the following Fourier series:

$$w_{0p}(\mathrm{x},\mathrm{y}) = \sum_{m_\mathrm{x}} A_{0m_\mathrm{x}} \sin\frac{m_\mathrm{x}\pi\mathrm{x}}{a} \sin\frac{\pi\mathrm{y}}{b} \tag{2.10}$$

where values of m_x are taken from 1 to 11. The coefficients of the deflection components A_{0m_x} for different aspect ratios a/b of plates are listed in Table 2.3.

Table 2.3. Coefficients of deflection components A_{0m_x} for the conventional HH imperfection model, see Ueda and Yao (1985).

Aspect ratio a/b	A_{01}/t	A_{03}/t	A_{05}/t	A_{07}/t	A_{09}/t	A_{11}/t
$a/b < 1.41$	1.000	0.000	0.000	0.000	0.000	0.000
$1.41 \leq a/b < 2.45$	1.200	0.240	0.034	-0.011	-0.005	0.003
$2.45 \leq a/b < 3.46$	1.241	0.333	0.124	0.035	0.000	-0.008
$3.46 \leq a/b < 4.47$	1.255	0.371	0.173	0.082	0.032	0.007
$4.47 \leq a/b < 5.48$	1.261	0.390	0.200	0.111	0.060	0.029
$5.48 \leq a/b < 6.48$	1.265	0.400	0.216	0.130	0.080	0.047

2.4.4.2 Magnitude of deflection

Once the deterministic shape of the geometric distortion is defined, the maximum amplitude of the distortion field should be specified. Different approaches are available. DNV (2013) specifies maximum permissible amplitudes for each mode of distortion profile as indicated in Table 2.4. Japan Shipbuilding Quality Standard (JSQS) has established a maximum allowable tolerance of 6 mm for all modes, see Yao and Fujikubo (2016). Smith et al. (1988) developed the following formula as a function of plate's slenderness ratio β_p and the level of imperfections' severity for the description of a plate's maximum amplitude initial distortion based on actual measurements on ship structures.

$$w_{0p}^{max} = c_p \beta_p^2 t_p \tag{2.11}$$

where,

$$c_p = \begin{cases} 0.025, & \text{for a slight level} \\ 0.1, & \text{for an average level} \\ 0.3, & \text{for a severe level} \end{cases}$$

Except otherwise specified, an average-level magnitude is commonly adopted in the above formula. It is noted that when the conventional HH mode is applied on ship grillages, it is common to express a variability on the maximum initial deflection (usually a 10% difference) between adjacent plates (see Figure 2.2). This strategy is applied in order to express the presence of asymmetric deflection component that induces the asymmetric buckling-mode deformation, and at the same time, to avoid converge issues when performing a NLFEA, see e.g., Fujikubo et al. (2005).

Table 2.4. Class tolerance of maximum imperfections amplitudes, after DNV (2013).

Deflection type	Symbol	Max amplitude
Global	w_{0c}^{max}	$a/1000$
Local – Stiffener	w_{0s}^{max}	$a/1000$
Local – Plate	w_{0p}^{max}	$b/200$

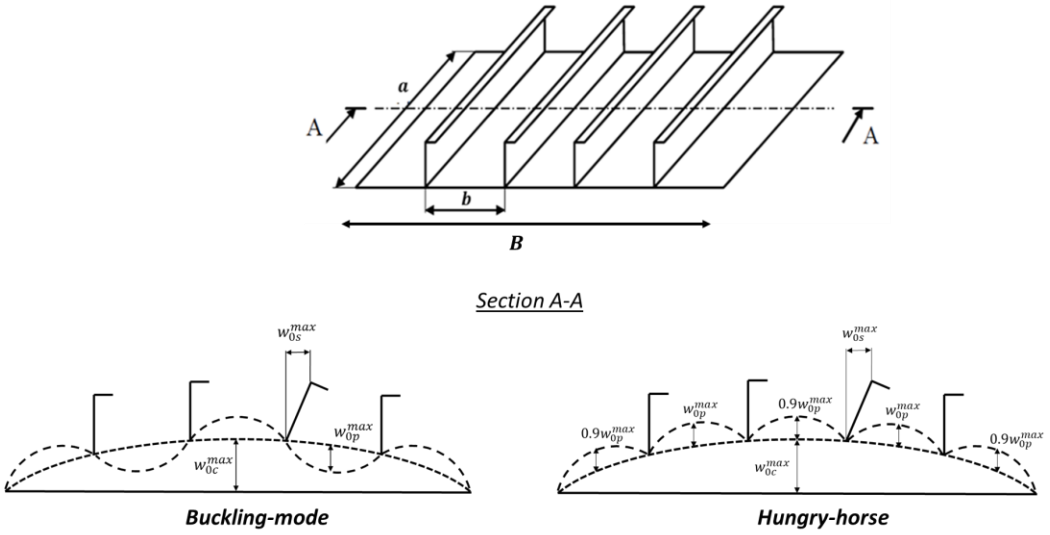

Figure 2.2. Schematic illustration of a typical initial geometric imperfection field applied on a stiffened panel. The buckling-mode (BM) and the conventional hungry-horse (HH) plate imperfection models are superimposed with a global half-wave and a local sideway stiffener deflection to generate the final imperfect geometry introduced on a FE model.

2.4.5 Corrosion

Corrosion is a deterioration process that highly affects the hull girder ultimate strength and the subsequent reliability of ship structures. Statistics for ship hull damages show that around 90% of ship failures are attributed to corrosion, including corrosion fatigue, see Emi et al. (1991). Corrosion is a complex phenomenon which is influenced by many uncertain factors, including various environmental (e.g., temperature, pH, humidity, salinity, etc.) and operational (e.g., corrosion protection system, maintenance policy, trading routes, ship cargo, etc.) aspects. A summary of the environmental factors that affect to a lesser or a greater degree the corrosion of mild and low alloy steels is given by Melchers (1999)b.

Typical corrosion mechanisms associated with steel plates of ship structures are: (i) general (or uniform), (ii) pitting and (iii) grooving corrosion, see also DNV (2020). *General corrosion* results in a uniform decrease of plate thickness which greatly affects the strength of plate elements under in-plane compression. This type of corrosion is thus of particular relevance in longitudinal strength assessment and should be always considered when studying the reliability of ships in ULS. In contrast, *pitting corrosion* leads to the formulation of localized dents with very deep holes appearing in the plate. Due to this localized effect, pitting does not affect the in-plane stress distribution of plate and generally, it is not taken into account when assessing the hull girder ultimate strength. *Grooving corrosion* may occur at stiffener connections close to a weld between the longitudinal and the deck plate. Like pitting, grooving is a more localized phenomenon that is usually not considered when assessing the overall strength of a ship.

In practice, a corrosion model should be able to represent both *temporal* and *spatial* variability. However, most of the research studies conducted so far have been focused on the temporal character of corrosion, while efforts for an efficient approach that considers the spatial dependence of corrosion growth are rare. In Section 2.4.5.1, common models used for the prediction of long-term corrosion of ship structural elements as a function of time are provided. In Section 2.4.5.2, existing methods used for the consideration of spatial dependence of corrosion at a given point in time are presented. Finally, in Section 2.4.5.3, Rule-based approaches for modelling corrosion at a given point in time are introduced.

2.4.5.1 Temporal representation of corrosion

The prediction of corrosion loss is an important task for the assessment of ship structures. Ideally, the most accurate way of approximating corrosion growth in time would be the construction of theoretical models based on the prevailing physical processes that take place on the surface of steel plates, see e.g., Melchers (1999)b. However, such models have been only partly verified for laboratory conditions. The complexity of marine environment and the interaction of the various factors influencing corrosion prevent the development of a purely theoretical model for the prediction of long-term corrosion wastage of ship structural elements.

Empirical time-dependent corrosion models are far more simple than theoretical ones as they employ only a few parameters. The parameters of these models are calibrated – mainly adopting regression techniques – based on actual corrosion data from existing ships. Corrosion data sets have been established primarily for bulk carriers, see e.g., Paik et al. (1998), Yamamoto and Ikegami (1998), Paik et al. (2003) and oil tankers, see e.g., Paik et al. (2003). Extrapolations from single hull to double hull oil tankers and FPSOs have taken place, see Paik et al. (2003), while for other types of ships, such as container ships, a corrosion data set is currently lacking. The main drawback of empirical modelling is that pooling data from various sources, covering a wide range of ship characteristics (including different operational characteristics, maintenance practices and ships' ages) usually provides poor-quality mean-value information and very high statistical uncertainties of corrosion model parameters. This fact may seem particularly problematic for reliability analysis where a much higher level of accuracy is required, see also Melchers (2003). Empirical models have become, however, an acceptable solution for marine engineers to predict future corrosion trends. In literature, two basic models are generally used: (i) Paik's model, and (ii) Soares and Garbatov model.

Paik's model

In 2002, Paik (2002) proposed a corrosion model that is divided into three main stages: (i) the durability of corrosion τ_c, (ii) the transition between coating durability and corrosion initiation τ_t, and (iii) the progress of corrosion. A schematic representation of the corrosion model process is illustrated in Figure 2.3. For the second stage, it can be pessimistically assumed that transition time is zero $\tau_c = 0$ and thus, corrosion initiates immediately after coating breakdown[7]. Mathematically, the model is expressed by the following relation:

$$t_c(\tau) = \begin{cases} C_1(\tau - \tau_c)^{C_2}, & \tau \geq \tau_c \\ 0, & \tau < \tau_c \end{cases} \tag{2.12}$$

where, t_c is the corrosion diminution of plate thickness in mm as a function of time τ, C_1 is the annual corrosion rate in $\mathrm{mm/year}$, τ_c is the coating life duration in years, and C_2 is a coefficient that determines the trend of corrosion waste over time. The following information can be used for the determination of the above model parameters.

Annual corrosion rate C_1 has been assumed to follow a Weibull distribution model. The first and second order statistics of the distribution model have been determined from thickness measurements on different locations of cross-section. Different statistics have been defined conditional on the location of element and the exposed environment of each element, see Paik et al. (2003).

[7] From the remaining of the thesis, the terms "coating life" and "corrosion initiation" are used interchangeably and are referred at the time where corrosion initiates.

Coating life duration τ_c is difficult to be identified and depends, mainly, on the type of coating system used and the relevant maintenance policy. Expected coating life duration typically lies between 5 to 10 years (with a maximum of 15 years), see e.g., Qin and Cui (2003), Moan et al. (2005). It is thus appropriate to consider the variability of coating life parameter using a random variable. Usually, a normal or a lognormal distribution is used for its representation, see e.g., Yamamoto and Ikegami (1998).

The exponent C_2 determines the trend of the corrosion progress. According to Paik (2002), one of the following three types of corrosion trends may exist (see Figure 2.3): the convex type (gradual build-up of rust layer will prevent metal from further corrosion), the concave type (likely to happen under dynamically loaded structures due to flexing exposing fresh areas to corrosion) and the linear type (rust layer are continually removed due to abrasion or wear). Typical values of C_2 are in the range [0.3 - 1.5] according to Paik (2002). However, values greater than unity are rarely used in literature, see e.g., Qin and Cui (2003), Melchers (2019).

In the context of hull girder ultimate strength and reliability assessment, Paik's model is usually employed by considering a linear corrosion progression $C_2 = 1.0$, a fixed coating life equal to $\tau_C = 7.5\,\text{years}$ and a constant but unknown corrosion rate that follows the Weibull distribution. This approach has been extensively used in the literature to evaluate the time-dependent reliability of oil tankers/FPSOs, see e.g., Akpan et al. (2002), Zhu and Frangopol (2013), Campanile et al. (2016)b and Campanile et al. (2017)a and bulk carriers, see e.g., Campanile et al. (2015) and Campanile et al. (2016)c.

Soares and Garbatov model

In 1999, Soares and Garbatov (1999) proposed a similar model which also includes no corrosion and transition between coating durability and corrosion initiation. However, they believed that the corrosion would gradually stabilize at a depth of d_∞, since corrosion products on the plate surface will prevent the corrosion process. Any disturbance, or indeed removal, of this oxide layer could lead to a re-initiation of the corrosion process. Figure 2.3 shows the corrosion wastage thickness change against time. The model proposed by Soares and Garbatov reads:

$$t_c(\tau) = \begin{cases} d_\infty \left(1 - \exp\left[\dfrac{(\tau_c - \tau)}{\tau_t}\right]\right), & \tau \geq \tau_c \\ 0, & \tau < \tau_c \end{cases} \tag{2.13}$$

where, τ_c denotes the corrosion initiation time, τ_t gives the transition time and d_∞ is the maximum steady corrosion depth expected after a long period of time.

Several data sets from oil tankers and bulk carriers have been fitted to the non-linear model. In doing so, representative/average values of these parameters can be obtained using regression analysis. Zayed et al. (2018) associated parameters' values according to the exposed

environment and defined a triplet of $\{\tau_c, \tau_t, d_\infty\}$ for each individual space. A basic limitation of the proposed model is that, in contrast with the model proposed by Paik, a full probabilistic description for all model parameters is lacking.

An extension of the Soares' model to the probabilistic regime has been recently performed by Gong and Frangopol (2020). A multiplicative error term ε_t reflecting the uncertainty of model prediction ξ and measurements' uncertainty ε has been considered as follows:

$$t_c'(\tau) = \varepsilon_t t_c(\tau) \tag{2.14}$$

where, $t_c(\tau)$ represents the average thickness loss given by Eq. (2.13). The error term ε_t has been assumed to follow a Weibull distribution with a unit mean and CoV equal to 0.50 and 1.00. This high variability is indicative of the wide scatter of corrosion growth data measured in oil tankers from over $110{,}000$ readings. Uncertainties on measurements may arise due to measurement tool inaccuracy and location errors, i.e., the fact that thickness measurements are not recorded for exactly the same locations between subsequent surveys. Location errors become meaningful when corrosion presents significant variations over the surface of a plate.

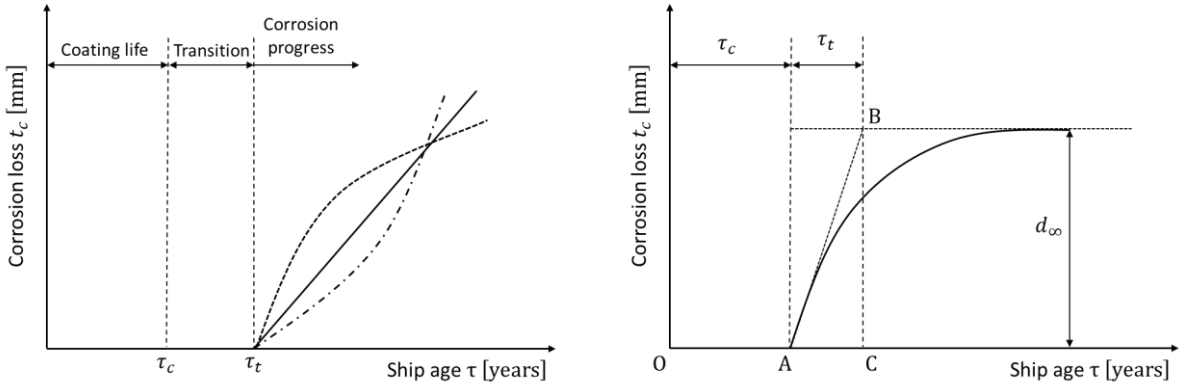

Figure 2.3. (a) The Paik and Thayamballi corrosion model, after Paik (2002), and (b) the Soares and Garbatov corrosion model, after Soares and Garbatov (1999).

2.4.5.2 Spatial representation of corrosion

The spatial dependence of corrosion needs to be considered when assessing the hull girder ultimate strength. Broadly speaking, spatial dependence of corrosion can be classified into *small-scale* and *large-scale*. The former accounts for spatial random variations of corrosion in a smaller scale, usually that of a plate. Small-scale dependence of corrosion at a given time instance is often taken into account using random fields. A more detailed description regarding

the application of random fields on plate elements and the impact on ultimate strength is presented in Section 4.3.

Large-scale dependency defines the correlation degree of corrosion penetration between elements exposed in the same or different environmental conditions around the cross-section of the hull. Corrosion growth can vary significantly between different elements around cross-section, since corrosion progress is closely related to the environment on which steel plates are exposed. Large-scale dependency is usually taken into account by assuming a *partial correlation model*, i.e., full correlation exists among corrosion growth of structural elements belonging to the same group of compartments, namely double-bottom, hopper tank, double-side and cargo oil tank, while no correlation exists for elements belonging to different categories, see e.g., Campanile et al. (2014) and Campanile et al. (2017)b.

A complete model that takes into account both large-scale and small-scale dependency has been proposed by Luque et al. (2014). The method is based on a hierarchical approach where spatial dependency is achieved by dividing the structural components of the ship into five levels, i.e., vessel, compartment, frame, structural element, plate. The dependence of corrosion in the lowest level, i.e., the plate, is modelled using a random field. Recently, Gong and Frangopol (2020) used copula theory to model the spatial dependence of corrosion growth, as well other geometric and material properties of structural elements around cross-section. This modelling approach was used to derive the time-dependent hull girder reliability of a ship structure.

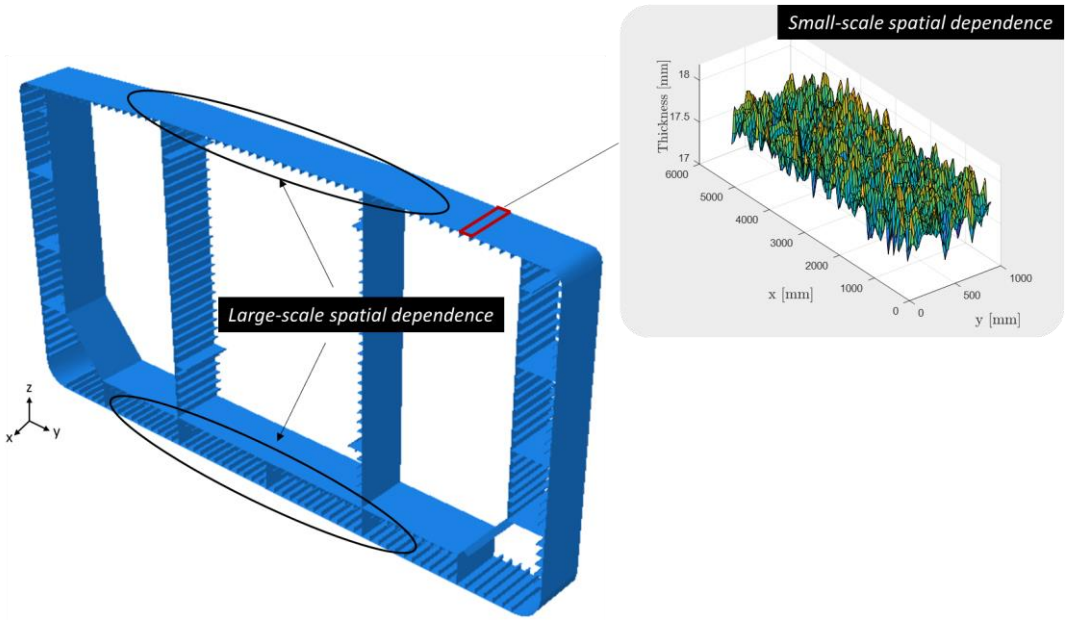

Figure 2.4. Small-scale and large-scale spatial dependency of corrosion growth at a given point in time.

2.4.5.3 Rule-based approaches for modelling corrosion

Traditionally, prescribed design values from Rules are adopted to account for corrosion wastage of ship structural elements in cases where an empirical corrosion model is not available for the examined ship type or when the interest lies on the evaluation of reliability at a given point in time, usually for 25th year of lifetime which corresponds to the design life of vessel.

According to IACS (2019), the effect of corrosion loss is accounted for using the *net scantling approach*. The net scantling approach prescribes a total corrosion addition t_n for all structural members of cross section depending on the element's type and location based on a 25-year design life[8]. For hull girder ultimate strength calculations, the *net-50 scantling approach* t_{n-50} is defined which assumes a uniform reduction of thickness by *half* of the total corrosion addition, that is:

$$t_{n-50} = t_{\text{as-built}} - 0.5t_n \tag{2.15}$$

The net-50 scantling approach has been widely adopted to account for corrosion degradation in the context of reliability on oil tankers and bulk carriers, see e.g., Parunov et al. (2007), Shu and Moan (2011)a, Xu et al. (2015), Guia et al. (2018). For container ships, the corrosion effect has been considered based on Rule-based values specified by different Classification Rules, such as Bureau Veritas (BV), see e.g., Corak and Soares (2018)), IACS URS11A, see e.g., Kim et al. (2012) or even IACS CSR for double hull oil tankers and bulk carriers, see e.g., Kim et al. (2012). Regarding FPSOs, Chen (2016) examined their reliability based on American Bureau of Shipping (ABS) Floating Production Rules and by assuming a linear decrease of thickness due to corrosion as a function of time. Finally, another practice to account for the uncertainty of corrosion at the design life is to postulate a variability around Rules nominal net-50 thicknesses, see e.g. Gaspar and Soares (2013) and Gong and Frangopol (2020).

[8] The total corrosion addition t_n has been based on historical data from oil tankers and bulk carriers, see IACS (2016). It corresponds approximately to the 95% quantile of the recorded corrosion loss empirical distribution.

3 Random fields

3.1 Introduction

The uncertainties on the input parameters of a system are generally attributed to variations on material properties (e.g., yield strength, Young's modulus, etc.), geometric characteristics (e.g., thickness, imperfections, etc.) and loads or load effects (e.g. wave loads, wave-induced bending moments). The representation of such quantities is commonly achieved through probabilistic methods. Depending on the level of sophistication which is desired and the problem at hand, different modelling approaches can be adopted.

Let us consider for example the case where the analyst is interested in simulating the uncertain character of thickness distribution over the surface of a plate for a given time instance during the service time of a ship structure. In general, the following options are available. The first, and more simple option, is to model implicitly the spatial variability of thickness using a single *random variable*. Extending this variable in the time frame – by assuming that the plate has a fixed but unknown value of thickness loss over its surface at any time – we refer to a *stochastic process*. The second option is to model a more refined version of thickness variability. This is accomplished through the use of *random fields*[9]. The extension of a random field in the time domain is usually referred as a *space-time stochastic process*.

In the above example, both approaches have their pros and cons. On the one hand, the use of a random variable approach provides simplicity, but it may insufficient to capture the variations of the actual phenomenon. On the other hand, modelling a quantity of interest (QoI) using a random field offers more realism, but increases – often significantly – the computation cost and the modelling effort. A schematic description of the above is depicted in Figure 3.1.

The fundamental theory of random fields is introduced in this chapter in a very condensed form. The definitions and basic properties of random fields are presented in Section 3.2 and Section 3.3, respectively. In Section 3.4, some popular classes and terms of random fields are analyzed, including, homogeneous RFs, Gaussian RFs, ergodicity, etc. Common methods to discretize the continuous random fields are presented in Section 3.6. Finally, in Section 3.7, we thoroughly present a popular method for generating one-dimensional (1D) and two-dimensional (2D) Gaussian homogeneous stochastic fields, i.e., the spectral representation method. The reader is referred to the books of Vanmarcke (2010), Grigoriu (2002) and Papoulis

[9] The terms "stochastic" and "random" are used interchangeably throughout this thesis. We refer to a stochastic (or random) "process" in order to define quantities that randomly vary with respect to one coordinate (or parameter), usually time. The term "field" generally denotes a generalization of a "process" and indicates that the parameter space is multi-dimensional. In this thesis, the concept of *random field* is used to describe only spatially varying random quantities.

and Pillai (2002) for a detailed view on the subjects of stochastic processes and random fields. An introduction to the basic notions of probability theory and random variables is presented in Appendix A and Appendix B.

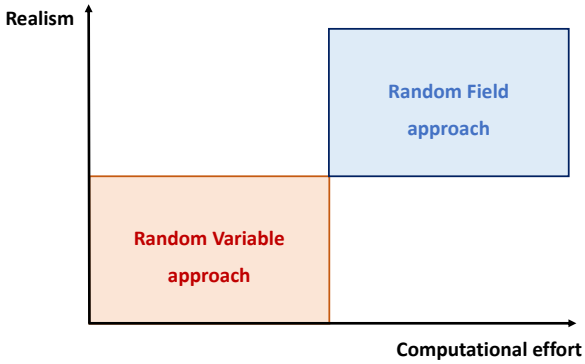

Figure 3.1. Random Variable (RV) vs. Random Field (RF) approach as a function of realism and computational effort needed for the modelling of an uncertain quantity of interest (QoI) at a given time instance.

3.2 Basic definitions

Consider[10] a set of spatial coordinates u of the spatial domain Ω_S, where $\Omega_S \subset \mathbb{R}^d$ with $d \geq 1$. A single outcome or realization of the sample space Ω is denoted by ω, such as $\omega \in \Omega$.

A *random field* $X(u;\omega)$ is defined as a collection of random variables indexed by a spatial coordinate $u \in \Omega_S$. The function $X(u;\omega)$ is a mapping from the domain $\Omega \times \Omega_S$ to the real numbers' domain $\mathbb{R}$, i.e., $\Omega \times \Omega_S \mapsto \mathbb{R}$. A *sample function* (or *realization*) $x(u;\omega)$ of $X(u;\omega)$ is defined for a *fixed* $\omega \in \Omega$. For any fixed location u_i, each $X(u_i;\omega)$ is a random variable. In the remaining chapter, the dependence of X on ω is omitted, i.e., $X(u;\omega) \equiv X(u)$.

An example of a two-dimensional (2D) random field is illustrated in Figure 3.2. Two realizations of the field, describing the thickness t variation of a 3×1 m rectangular plate, are shown. For a fixed location u_i and K realizations $(\omega_j, j = 1,2,\dots,K)$, the family of generated samples constitute a random variable $X(u_i)$.

For the complete definition of a random field, the joint distribution of the sequence of random variables $\{X(u_1), X(u_2), \dots, X(u_n)\}$ is needed.

[10] The dimensions of a physical system can be one (for 1D space), two (for 2D space) or three (for 3D space). For a space-time process four dimensions are needed in order to include the parameter of time. In a mathematical point of view, however, any $d \geq 1$ is possible.

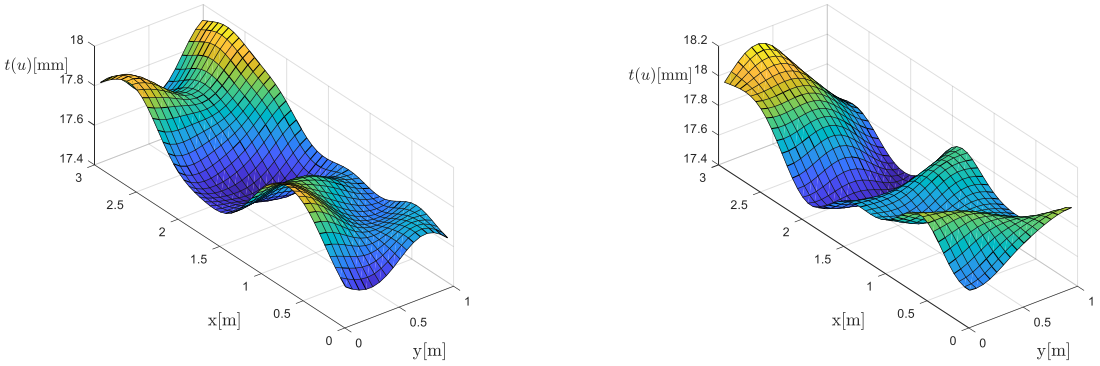

(a) (b)

Figure 3.2. Two sample functions of a two-dimensional (2D) random field representing thickness distribution on the surface of a plate.

The n-th order joint CDF of a random field $X(u)$ is the function $F_{X(u_1)\dots X(u_n)}: \Omega_S \times \mathbb{R}^n \to [0,1]$ that expresses the probability of occurrence of the event $\{X(u_1) \leq x_1 \cap \dots \cap X(u_n) \leq x_n\}$ in terms of the outcomes $\{x_1, \dots, x_n\}$ for any collection of points (locations) $\boldsymbol{u} = (u_1, \dots, u_n)$, that is:

$$F_{X(u_1)\dots X(u_n)}(x_1, \dots, x_n; u_1, \dots, u_n) = \Pr(X(u_1) \leq x_1 \cap \dots \cap X(u_n) \leq x_n) \tag{3.1}$$

The n-th order joint PDF of a random field $X(u)$ can be obtained by differentiation of the n-th order joint CDF as follows:

$$f_{X(u_1)\dots X(u_n)}(x_1, \dots, x_n; u_1, \dots, u_n) = \frac{\partial^n F_{X(u_1)\dots X(u_n)}(x_1, \dots, x_n; u_1, \dots, u_n)}{\partial x_1 \dots \partial x_n} \tag{3.2}$$

3.3 Statistics of random fields

3.3.1 First and second order moments

Let $f_X(x)$ be the PDF of random variable $X(u)$ that represents the set of samples for the ensemble at location u. The *mean value* $\mu_X(u)$ of a stochastic field X as a function of the position u is the expected value of each random variable $X(u)$, that is:

$$\mu_X(u) = \mathrm{E}[X(u)] = \int_{-\infty}^{\infty} x f_X(x) dx \tag{3.3}$$

The *variance* $\sigma_X^2(u)$ of a stochastic field X as a function of the position u is:

$$\sigma_X^2(u) = \mathrm{E}\left[\left(X(u) - \mu_X(u)\right)^2\right] = \int_{-\infty}^{\infty} \left(x - \mu_X(u)\right)^2 f_X(x)dx \tag{3.4}$$

where, $\sigma_X(u)$ is the standard deviation function of $X(u)$. Taking into account that the expectation $\mathrm{E}[\cdot]$ is a linear operator, Eq. (3.4) can take the following form:

$$\sigma_X^2(u) = \mathrm{E}[X^2(u)] - \mathrm{E}^2[X(u)] \tag{3.5}$$

3.3.2 Autocorrelation and Autocovariance functions

The *autocorrelation function* $R_{XX}(u_1, u_2)$ of a stochastic field $X(u)$ as a function of two arbitrary positions u_1, u_2 is:

$$R_{XX}(u_1, u_2) = \mathrm{E}[X(u_1)X(u_2)] = \int_{-\infty}^{\infty}\int_{-\infty}^{\infty} x_1 x_2 f_{X(u_1)X(u_2)}(x_1, x_2)dx_1 dx_2 \tag{3.6}$$

The *autocovariance function* $C_{XX}(u_1, u_2)$ of $X(u)$ is defined as:

$$\begin{aligned} C_{XX}(u_1, u_2) &= \mathrm{E}\left[\left(X(u_1) - \mu_X(u_1)\right)\left(X(u_2) - \mu_X(u_2)\right)\right] = \\ &= \int_{-\infty}^{\infty}\int_{-\infty}^{\infty} \left(x_1 - \mu_X(u_1)\right)\left(x_2 - \mu_X(u_2)\right) f_{X(u_1)X(u_2)}(x_1, x_2)dx_1 dx_2 \end{aligned} \tag{3.7}$$

After manipulations, Eq. (3.7) yields:

$$C_{XX}(u_1, u_2) = R_{XX}(u_1, u_2) - \mu_X(u_1)\mu_X(u_2) \tag{3.8}$$

In case now where $u_1 = u_2 = u$, the covariance function equals the variance of each random variable:

$$C_{XX}(u, u) = \sigma_X^2(u) \tag{3.9}$$

Also, for zero-mean stochastic fields, it is evident that $C_{XX}(u_1, u_2) \equiv R_{XX}(u_1, u_2)$.

The *autocorrelation coefficient function* $\rho_{XX}(u_1, u_2)$ is obtained if we normalize the autocovariance function with the standard deviation functions at u_1 and u_2:

$$\rho_{XX}(u_1, u_2) = \frac{C_{XX}(u_1, u_2)}{\sigma_X(u_1)\sigma_X(u_2)} \tag{3.10}$$

From the above definitions, the following properties for the second-moment functions derive:

- Symmetry:

$$R_{XX}(u_1, u_2) = R_{XX}(u_2, u_1) \tag{3.11}$$

and

$$C_{XX}(u_1, u_2) = C_{XX}(u_2, u_1) \tag{3.12}$$

- Bounded (Cauchy-Schwarz inequality):

$$R_{XX}(u_1, u_2) \leq \sqrt{R_{XX}(u_1, u_1)R_{XX}(u_2, u_2)} \tag{3.13}$$

and

$$C_{XX}(u_1, u_2) \leq \sigma_X(u_1)\sigma_X(u_2) \tag{3.14}$$

From Eq. (3.14), it is also proved that:

$$\rho_{XX}(u_1, u_2) \leq 1 \tag{3.15}$$

- Non-negative definiteness:

$$\sum_{i=1}^{n}\sum_{j=1}^{n} q_i q_j R_{XX}(u_i, u_j) \geq 0 \tag{3.16}$$

where, the coefficients $\{q_1, \dots, q_n\} \in \mathbb{R} - \{0\}$ and may be replaced by some function $q(\boldsymbol{u})$, for which it holds that:

$$\int_u \int_{u'} q(\boldsymbol{u}) q(\boldsymbol{u}') R_{XX}(\boldsymbol{u}, \boldsymbol{u}')\, d\boldsymbol{u} d\boldsymbol{u}' \geq 0 \tag{3.17}$$

3.4 Classes of random fields

There are several key attributes that may characterize a random field - homogeneity, isotropy, ergodicity, Gaussianity - and can facilitate the probabilistic modelling of the analyst. In the following section, the *strict* and *weak* definitions of these properties are presented. In practice, however, random fields that are assumed to possess these properties to any degree often do so in a limited (or *weak*) sense, not in the strict sense.

3.4.1 Homogeneous random fields

A random field is called *homogeneous in the strict sense* or *strictly homogeneous* if all the joint PDFs remain the same when shifted in space. Mathematically this is expressed as:

$$f_{X(u_1)\dots X(u_n)}(x_1,\dots,x_n;u_1,\dots,u_n) = f_{X(u_1+v)\dots X(u_n+v)}(x_1,\dots,x_n;u_1+v,\dots,u_n+v) \tag{3.18}$$

The above definition implies that the marginal PDF $f_{X(u)}(x,u)$ is invariant in u and the second order PDF $f_{X(u_1)X(u_2)}(x_1,u_1;x_2,u_2)$ is a function of the difference in locations, i.e., $v = u_1 - u_2$:

$$f_{X(u)}(x,u) = f_{X(u)}(x) \tag{3.19}$$

and:

$$f_{X(u_1)X(u_2)}(x_1,x_2;u_1,u_2) = f_{X(u_1)X(u_2)}(x_1,x_2;v) \tag{3.20}$$

Therefore, the mean and variance functions are constants and the autocorrelation, autocovariance and autocorrelation coefficient functions can be expressed as a function of space lag v, that is:

$$\mu_X(u) \to \mu_X \tag{3.21}$$

$$\sigma_X^2(u) \to \sigma_X^2 \tag{3.22}$$

$$R_{XX}(u_1,u_2) \to R_{XX}(u_1-u_2) = R_{XX}(v) \tag{3.23}$$

$$C_{XX}(u_1,u_2) \to C_{XX}(u_1-u_2) = C_{XX}(v) \tag{3.24}$$

$$\rho_{XX}(u_1, u_2) \rightarrow \rho_{XX}(u_1 - u_2) = \rho_{XX}(v) \tag{3.25}$$

The definition of Eq. (3.18) is quite restrictive and rarely met in real-life. Usually, the assumption of *wide-sense homogeneity* or *weak homogeneity* is made.

A random field is called *weakly homogeneous* if the n-th order PDF of a random field $X(u)$ is invariant to a location shift only up to a second degree, i.e., $n = 1$ and $n = 2$. In other words, a random field is said to be *weakly homogeneous*, if its mean function is constant, i.e., Eq. (3.22) holds, and *one* of its second moment functions, i.e., Eq. (3.23) - (3.25), can be expressed in terms of space lag v.

The second-moment functions of a homogeneous random field are *even* functions, i.e., symmetric with respect to the origin $v = 0$, e.g.,

$$R_{XX}(v) = R_{XX}(-v) \tag{3.26}$$

Moreover, for homogeneous fields, the bounds of $R_{XX}(v)$ and $C_{XX}(v)$ read:

$$|R_{XX}(v)| \leq R_{XX}(0) = \mathrm{E}[X^2(u)] \tag{3.27}$$

and

$$|C_{XX}(v)| \leq \sigma_X^2 \tag{3.28}$$

3.4.1.1 Correlation models for homogeneous random fields

Several models describing the form of an autocorrelation functions for homogeneous fields have been proposed in the literature, see e.g., Abrahamsen (1997). Here, we focus on some common one-dimensional correlation models, such as the triangular, the exponential and the square exponential (or Gaussian) model:

(A) Triangular:

$$\rho_{XX}(v) = \begin{cases} 1 - \dfrac{|v|}{\ell_{c,A}}, & 0 \leq |v| \leq \ell_A \\ 0, & |v| \geq \ell_A \end{cases} \tag{3.29}$$

(B) Exponential:

$$\rho_{XX}(v) = \exp\left[-\frac{|v|}{\ell_{c,B}}\right], \quad |v| \geq 0 \tag{3.30}$$

(C) Square exponential:

$$\rho_{XX}(v) = \exp\left[-\left(\frac{|v|}{\ell_{c,C}}\right)^2\right], \quad |v| \geq 0 \tag{3.31}$$

It is easy to verify that the conditions of symmetry, bounded and positive semi-definite functions hold for the above autocorrelation coefficient functions. The parameters $\ell_{c,A}$, $\ell_{c,B}$, $\ell_{c,C}$ are the *correlation lengths* of the respective correlation models. In general, a small correlation length $(\ell_c \to 0)$ indicates fully uncorrelated samples with high fluctuations in the sample functions. Conversely, large correlation lengths correspond to strongly dependent fields with a smooth shape of sample functions. In the limit, where $\ell_c \to \infty$, a random field can be modelled with a single random variable instead.

A common measure to express the degree of variability, independent of the adopted model, is the *scale of fluctuation* ϑ, defined as the integral of correlation function:

$$\vartheta = 2\int_0^\infty \rho_{XX}(v)dv = \int_{-\infty}^\infty \rho_{XX}(v)dv \tag{3.32}$$

For the above three autocorrelation models the scale of fluctuation reads: (A) $\vartheta_A = \ell_{c,A}$, (B) $\vartheta_B = 2\ell_{c,B}$ and (C) $\vartheta_C = \sqrt{\pi}\ell_{c,C}$. Figure 3.3 shows plots of the above one-dimensional correlation models using $\vartheta = 5$. In the same figure, the square exponential autocorrelation is plotted for different values of scale of fluctuation.

3.4.1.2 Isotropic correlation structure

A random field is called *isotropic* if the joint probability density functions remain the same when the constellation of location parameters is rotated in the parameter space. In other words, for an isotropic random field, the covariance function depends only on the distance v between the points $\boldsymbol{u} = (u_1, \ldots, u_n)$ and $\boldsymbol{u}' = (u_1', \ldots, u_n')$:

$$v = |\boldsymbol{v}| = |\boldsymbol{u} - \boldsymbol{u}'| = \sqrt{|{v_1}^2 + {v_2}^2 + \cdots + {v_n}^2|} \tag{3.33}$$

3.4.1.3 Fully separable correlation structure

An autocorrelation function is said to be *fully separable* if it can be expressed as a product of the autocorrelation functions of one-dimensional fields. For example, in the case of a 2D random field, it holds that:

$$R_{XX}(\boldsymbol{v}) = \sigma_X^2 \rho_{XX}(v_1)\rho_{XX}(v_2) \tag{3.34}$$

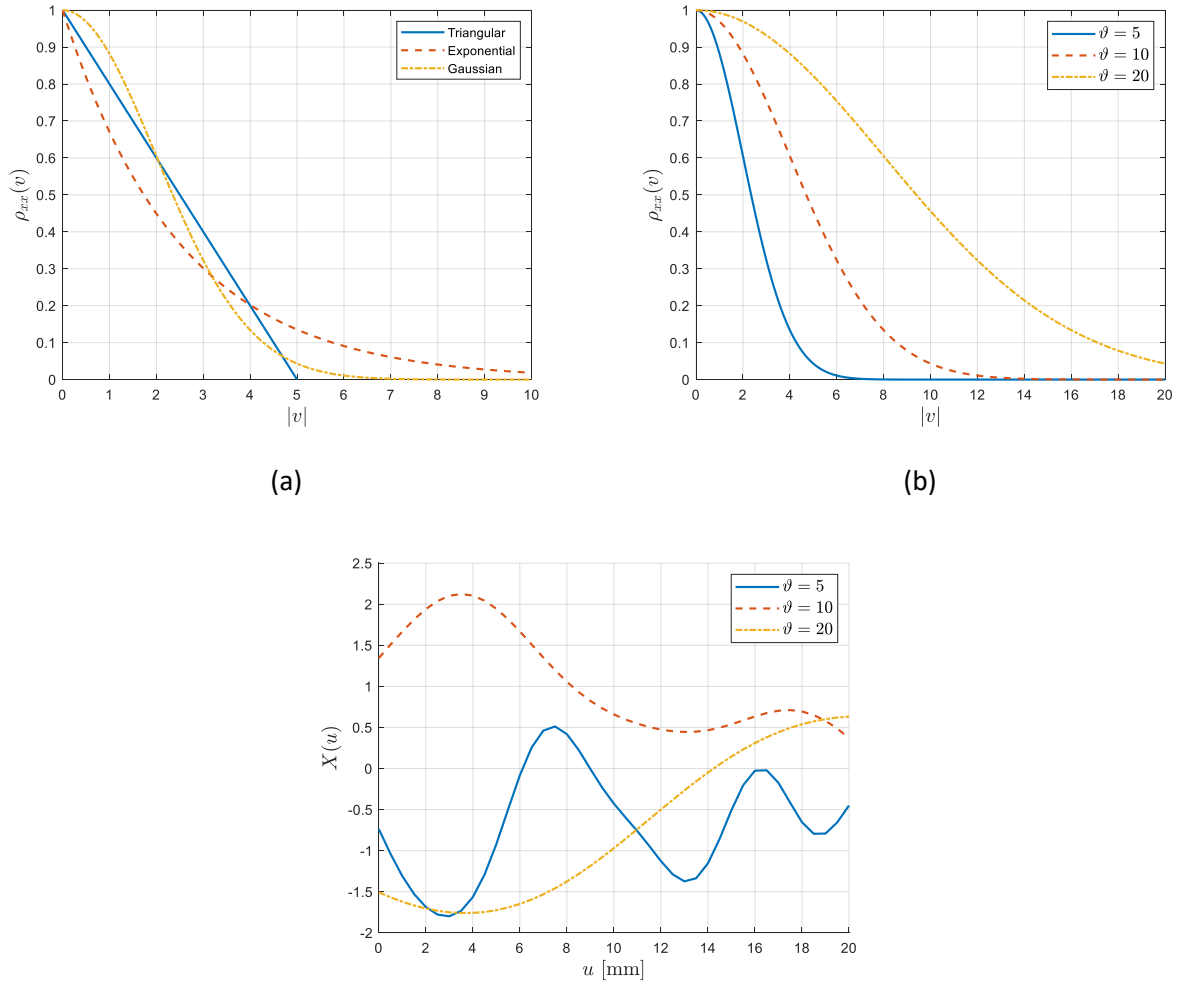

Figure 3.3. (a) Different types of autocorrelation functions for scale of fluctuation $\vartheta = 5$, (b) Gaussian type autocorrelation functions for various scale of fluctuations ϑ, and (c) three sample functions with different scales of fluctuation generated with a Gaussian type autocorrelation function.

3.4.2 Ergodic random fields

Ergodicity is a feature of a random field with exceptional practical importance. Loosely speaking, a random field is called *ergodic* if all information about its joint probability distributions (and all their statistical parameters) can be obtained *from a single sample function* of the random field.

Consider the case where a number of K realizations of a stochastic field is available. For the total set of sample realizations, the *ensemble average* for a given location u is defined as the average of the entire population of sample realizations, that is:

$$\mathrm{E}[X(u)] = \frac{X_1(u) + X_1(u) + \cdots + X_K(u)}{K} \tag{3.35}$$

In reality, one usually has only a limited number of sample functions or a long, single observation of one sample function. The question that is posed here is whether the statistical averages of the random field can be determined from a single sample function. The answer to this question is yes, and comes from the definition of ergodicity.

Practically, to determine if a field is ergodic, the following two weaker ergodicity conditions must be satisfied:

- Ergodicity of the *mean*:

$$\mu = \mathrm{E}[X(u)] = \lim_{L\to\infty} \frac{1}{L} \int_0^L X(u)dx \tag{3.36}$$

where, L is the length of the sample function. The right term denotes the *spatial* average of a sample function. Necessary and sufficient conditions for $X(u)$ to be ergodic in the *mean* are:

1. $\mathrm{E}[X(u)] = \text{constant}$
2. $X(u)$ and $X(u+v)$ must become independent as v reaches infinity.

- Ergodicity of the *autocorrelation*:

$$R_{XX}(v) = \mathrm{E}[X(u)X(u+v)] = \lim_{L\to\infty} \frac{1}{2L} \int_0^L X(u)X(u+v)dx \tag{3.37}$$

The right term denotes the *spatial* autocorrelation function of a sample function. Necessary and sufficient conditions for $X(u)$ to be ergodic in the *autocorrelation* are:

1. $\mathrm{E}[X(u)X(u+v)]$ is a function of v only

2. $\lim_{u\to\infty} R_{XX}(v) = 0$

Note that if a field is ergodic, it is also homogeneous, but the reverse does not necessarily holds.

3.4.3 Gaussian random fields

A random field can be interpreted as a sequence of random variables $\{X(u_1), \dots, X(u_n)\}$ corresponding to a set of points $\boldsymbol{u} = (u_1, \dots, u_n) \in \Omega_S$. A random field $X(u)$ is called *Gaussian* if each of these random variables is Gaussian. In the case where the field is also homogeneous, the Gaussian field can be completely defined by its mean value $\mu_X(u)$ and its autocovariance function $C_{XX}(v)$.

The marginal PDF of a Gaussian random field is given by:

$$f_{X(u)}(x;u) = \frac{1}{\sigma_X(u)\sqrt{2\pi}} \exp\left[-\frac{1}{2}\left(\frac{x-\mu_X(u)}{\sigma_X(u)}\right)^2\right] \tag{3.38}$$

The standardized (zero mean and unit standard deviation) Gaussian random field $Z(u)$ is obtained using the following transformation:

$$Z(u) = \frac{X(u)-\mu_X(u)}{\sigma_X(u)} \tag{3.39}$$

An important property is that under *linear* transformations, Gaussian random fields remain Gaussian, that is, if $X(u)$ is a Gaussian random field, it holds that:

$$Y(u) = a(u)X(u) + b(u) \tag{3.40}$$

where, a and b are deterministic functions of u. The generated Gaussian random field $Y(u)$ has the following mean and autocovariance functions:

$$\mu_Y(u) = a(u)\mu_Y(u) + b(u) \tag{3.41}$$

and

$$C_{YY}(u_1,u_2) = a(u_1)a(u_2)C_{XX}(u_1,u_2) \tag{3.42}$$

3.4.4 Non-Gaussian random fields

In nature, most of the uncertain quantities appearing in engineering systems are *non-Gaussian*, e.g., material, geometric properties, wave loads. In order to fully characterize a non-Gaussian random field, the corresponding joint PDF of the random variables $\{X(u_1), X(u_2), \dots, X(u_n)\}$ is needed, which, in practice, is not possible to be known. Usually, the available information is: i) the marginal distribution $F_{X(u)}(x, u)$ and ii) the autocorrelation coefficient function $\rho_{XX}(u_1, u_2)$. In such cases, we can model the joint distributions of the random variables $\{X(u_1), X(u_2), \dots, X(u_n)\}$ using the *Nataf model*, see Der Kiureghian and Liu (1986). This is achieved by defining the random field $X(u)$ as a marginal transformation of an equivalent Gaussian field $\mathrm{Z}(u)$ with zero mean, unit variance and autocorrelation coefficient function $\rho_{ZZ}(u_1, u_2)$. Then, $X(u)$ can be defined by the following transformation:

$$X(u) = F_{X(u)}^{-1}\big[\Phi\big(Z(u)\big)\big] \tag{3.43}$$

where, Φ is the standard Gaussian cumulative distribution function. The transformation $F_{X(u)}^{-1}[\Phi(\cdot)]$ is a *memory-less translation* since the value of $X(u)$ at an arbitrary point u depends on the value of $Z(u)$ at the same point only. The resulting non-Gaussian field $X(u)$ is called a *transation field*, see Grigoriu (1998).

The autocorrelation coefficient function $\rho_{XX}(u_1, u_2)$ differs slightly from $\rho_{ZZ}(u_1, u_2)$. The following integral equation is solved iteratively for $\rho_{ZZ}(u_1, u_2)$ in order to determine the desired $\rho_{XX}(u_1, u_2)$:

$$\rho_{XX}(u_1, u_2) = \int_{-\infty}^{\infty}\int_{-\infty}^{\infty}\left(\frac{x(u_1) - \mu_X(u_1)}{\sigma_X(u_1)}\right)\left(\frac{x(u_2) - \mu_X(u_2)}{\sigma_X(u_2)}\right)\varphi[u_1, u_2, \rho_{ZZ}(u_1, u_2)]du_1du_2 \tag{3.44}$$

where, $\mu_X(u)$, $\sigma_X(u)$ and $\rho_{XX}(u_1, u_2)$ are the mean, standard deviation and autocorrelation coefficient function of $X(u)$ and $\varphi(\cdot)$ is the standard normal PDF.

3.5 Power Spectral density function

Fourier analysis is particular useful for the description of a stochastic field as the properties of the field in the space domain can be expressed simpler into the wave number domain κ. Of particular importance is the Fourier transformation of the autocorrelation function $R_{XX}(v)$ of a homogeneous field which gives the so-called *power spectral density function* or *power spectrum* $S_{XX}(\kappa)$:

$$S_{XX}(\kappa) = \frac{1}{2\pi}\int_{-\infty}^{\infty} R_{XX}(v)\, cos(\kappa v) dv \tag{3.45}$$

$$R_{XX}(v) = \int_{-\infty}^{\infty} S_{XX}(\kappa)\, cos(\kappa v) d\kappa \tag{3.46}$$

The two above equations are known as *Wiener-Khintchine Fourier transform* pair. Since $R_{XX}(v) = R_{XX}(-v)$, it follows from Eq. (3.45) that the function $S_{XX}(\kappa)$ is an *even* function, i.e., symmetric about $\kappa = 0$:

$$S_{XX}(\kappa) = S_{XX}(-\kappa) \tag{3.47}$$

Setting $v = 0$ in Eq. (3.46) it yields that:

$$R_{XX}(0) = \mathrm{E}[X^2(u)] = \int_{-\infty}^{\infty} S_{XX}(\kappa)\, d\kappa \tag{3.48}$$

For a zero-mean homogeneous random field, it holds that $\sigma_X^2(u) = \mathrm{E}[X^2(u)]$ and thus, Eq. (3.48) becomes:

$$\sigma_X^2 = \int_{-\infty}^{\infty} S_{XX}(\kappa)\, d\kappa \tag{3.49}$$

Eq. (3.49) helps one to understand the physical meaning of power spectrum: The power spectrum $S_{XX}(\kappa)$ of a stochastic field $X(u)$ describes how its variance σ_X^2 is distributed over the wave number domain κ.

3.6 Discretization of random fields

By definition, a random field is a collection of an *infinite* set of random variables indexed in space. However, this definition is only of theoretical and conceptual value. For computational purposes, a random field has to be expressed using a *finite* number of random variables $\{X_1, X_2, \dots, X_n\}$. The discretization of the random field $X(\cdot)$ into its approximation $\hat{X}(\cdot)$ is thus needed in practice. An overview of common discretization methods can be found in Sudret and Der Kiureghian (2000). Broadly speaking, discretization techniques can be classified into three main categories:

1. *Point discretization methods*, where the random variables X_i are simply the values of the stochastic field at specific points of the system domain. The main representatives of this category are the *midpoint*, the *nodal point* and the *integration point* method.

2. *Average-type discretization methods*, where the random variables X_i are represented as (weighted) integrals of $X(u)$ over a specific domain. The *local average* and the *weighted integral* methods are the main representative of this class.

3. *Series expansion methods*, where the stochastic field is represented as a truncated finite series of random variables and deterministic shape functions. Typical techniques of this class include the *spectral representation method*, the *KL expansion* and the *EOLE* method.

It is out of the scope of this thesis to present in detail each of the above methods. The focus has been placed only on the spectral representation method which is the preferred method for the numerical investigations of Chapter 4.

3.7 Spectral representation method

The spectral representation method has been introduced by Shinozuka and Deodatis (1991) for the simulation of one-dimensional (1D) and by Shinozuka and Deodatis (1996) for simulation of multi-dimensional (nD) Gaussian homogeneous stochastic fields. In this thesis, applications span the 1D and 2D field (see Chapter 4). The main steps used for the generation of 1D and 2D fields are presented in the remaining section.

3.7.1 1D Gaussian random field

In the general case, the spectral representation method expands the stochastic field $X(u)$ as a sum of trigonometric functions (cosine series) with random phase angles and amplitudes. In most applications, the approach of having deterministic amplitudes and random phase angles is usually adopted, as one can lead to sample functions that are ergodic in their mean value and autocorrelation function**,** see Stefanou (2009). A single (i) sample function $\hat{X}(u)$ of the stochastic field $X(u)$ can be generated according to Eq. (3.50) as[11]:

[11] Alternatively, Eq. (3.50) can be written without the $\sqrt{2}$ term, see Stefanou (2009):

$$\hat{X}^{(i)}(u) = \sum_{n=0}^{N-1} A_n cos\left(\kappa_n u + \varphi_n^{(i)}\right)$$

$$\hat{X}^{(i)}(u) = \sqrt{2}\sum_{n=0}^{N-1} A_n cos\left(\kappa_n u + \varphi_n^{(i)}\right) \tag{3.50}$$

where,

- $A_n = \sqrt{2S_{XX}(\kappa_n)\Delta\kappa}$, for $n = 0,1, \dots, N-1$
- $\kappa_n = n\Delta\kappa$
- $\Delta\kappa = \frac{\kappa_u}{N}$
- $A_o = 0$ or $S_{XX}(\kappa_o = 0) = 0$ (enforced condition)

In Eq. (3.50) the amplitudes A_n are deterministic and depend only on the prescribed power spectrum S_{XX} of the stochastic field. The term $\varphi_n^{(i)}$ expresses random phase angles following the uniform probability distribution in the range $[0, 2\pi]$. Under the last enforced condition, it can be shown that the simulated stochastic field $\hat{X}(u)$ is periodic with period L_o:

$$L_o = \frac{2\pi}{\Delta\kappa} \tag{3.51}$$

The parameter κ_u is a cut-off wave number defining the active region of the power spectral density function S_{XX} of the stochastic field. For the determination of κ_u the following equation is used:

$$\int_0^{\kappa_u} S_{XX}(\kappa)\, d\kappa = (1-\psi)\int_0^{\infty} S_{XX}(\kappa)\, d\kappa \tag{3.52}$$

where, η denotes a very small number, e.g., $\psi = 0.01, 0.001$.

The following points are noted:

- Eq. (3.50) is asymptotically Gaussian as $N \to \infty$ because of the Central Limit theorem.
- The enforced condition is necessary to guarantee ergodicity, namely, that the *spatial* average and the *spatial* autocorrelation function of any sample function $\hat{X}^{(i)}(u)$ are identical to the corresponding targets.

A comparative study between the two formulas has been implemented by Grigoriu (1993).

- The step du separating the generated values of $\hat{X}^{(i)}(u)$ in the space domain must satisfy the following condition in order to avoid *aliasing* according to the sampling theorem, see Bracewell (1965):

$$du \leq \frac{\pi}{\kappa_u} \tag{3.53}$$

3.7.2 2D Gaussian random field

For the case of a two-dimensional (2D) random field, a single sample function is generated according to Eq. (3.54) as:

$$\begin{aligned}\hat{X}^{(i)}(u_{\mathrm{x}}, u_{\mathrm{y}}) = \sum_{n_1=0}^{N_1-1}\sum_{n_2=0}^{N_2-1}\Big[&A^{(1)}_{n_1n_2} cos\Big(\kappa_{1n_1}u_{\mathrm{x}} + \kappa_{2n_2}u_{\mathrm{y}} + \varphi^{(1)(i)}_{n_1n_2}\Big)\\ &+ A^{(2)}_{n_1n_2} cos\Big(\kappa_{1n_1}u_{\mathrm{x}} - \kappa_{2n_2}u_{\mathrm{y}} + \varphi^{(2)(i)}_{n_1n_2}\Big)\Big]\end{aligned} \tag{3.54}$$

where, $\varphi^{(j)(i)}_{n_1n_2}$, $j = 1{,}2$ represent the realization of the (i) simulation of the independent random phase angles uniformly distributed in the range $[0,\ 2\pi]$. The terms $A^{(1)}_{n_1n_2}, A^{(2)}_{n_1n_2}$ are defined as:

- $A^{(1)}_{n_1n_2} = \sqrt{2S_{XX}(\kappa_{1n_1}, \kappa_{2n_2})\Delta\kappa_1\Delta\kappa_2}$
- $A^{(2)}_{n_1n_2} = \sqrt{2S_{XX}(\kappa_{1n_1}, -\kappa_{2n_2})\Delta\kappa_1\Delta\kappa_2}$

where,

- $\kappa_{1n_1} = n_1\Delta\kappa_1,\ \kappa_{2n_2} = n_2\Delta\kappa_2$
- $\Delta\kappa_1 = \frac{\kappa_{u_{\mathrm{x}}}}{N_1},\ \Delta\kappa_2 = \frac{\kappa_{u_{\mathrm{y}}}}{N_2}$
- $\mathrm{A}^{(1)}_{0n_2} = \mathrm{A}^{(1)}_{n_10} = 0,\ \mathrm{A}^{(2)}_{0n_2} = \mathrm{A}^{(2)}_{n_10} = 0$ (enforced condition)

  for $n_1 = 0{,}1, \dots, N_1 - 1$ and $n_2 = 0{,}1, \dots, N_2 - 1$

The term N_j with $j = 1, 2$ represent the number of intervals in which the wave number axes κ_1 and κ_2 are subdivided and κ_{ju} are the upper cut-off wave numbers corresponding to the u_x and u_y axes in the space domain. This implies that the power spectral density function $S_{XX}(\kappa_1, \kappa_2)$ is assumed to be zero outside the region defined by:

$$-\kappa_{1u} \leq \kappa_1 \leq \kappa_{1u} \text{ and } -\kappa_{2u} \leq \kappa_2 \leq \kappa_{2u} \tag{3.55}$$

The criterion of Eq. (3.52) is usually used to determine the values of κ_{1u} and κ_{2u}.

Under the last enforced condition, the simulated random field $X(u_\mathrm{x}, u_\mathrm{y})$ given by Eq. (3.54) is periodic along the x and y axes with periods:

$$\begin{aligned} L_{\mathrm{x}0} &= \frac{2\pi}{\Delta\kappa_1} \\ L_{\mathrm{y}0} &= \frac{2\pi}{\Delta\kappa_2} \end{aligned} \tag{3.56}$$

Finally, similar to Eq. (3.53), the steps du_x and du_y of the generated sample functions must satisfy the following requirements:

$$\begin{aligned} du_\mathrm{x} &\leq \frac{\pi}{\kappa_{u_\mathrm{x}}} \\ du_\mathrm{y} &\leq \frac{\pi}{\kappa_{u_\mathrm{y}}} \end{aligned} \tag{3.57}$$

This page intentionally left blank

4 Spatial probabilistic modelling of steel plates' geometric characteristics

4.1 Introduction

Geometric characteristics of steel plates, such as thickness and imperfections, are vulnerable to variations in space, usually as a result of manufacturing processes and deterioration effects occurring during the service of ships. The spatial inherent randomness of such geometric quantities motivates the use of random fields for their explicit representation.

The main subject of this chapter is to assess the impact of the spatial uncertain character of thickness and initial imperfections on the ultimate strength of basic ship structural elements, i.e., plates, stiffened plates and hull girders. An appropriate FE model is constructed to replicate the physical system's behavior. In particular, the framework of *stochastic finite element method* (SFEM)[12], which is an extension of the classical finite element method into the probabilistic space, is used in order to assess probabilistically the structural behavior of the examined model. Spectral representation method is used to model the spatial uncertain randomness of initial imperfections and thickness. Then, Monte Carlo simulation (MCS) technique is employed to propagate the input uncertainties through the system and evaluate the ultimate strength of the model using statistical terms. In this context, a large number of samples is generated from the input parameter space and an equivalent number of FE model calls is implemented to obtain the output statistics. Neural networks are used to replace time-consuming model evaluations and accelerate the process when needed.

The structure of this chapter is organized as follows. In Section 4.2, a new stochastic imperfection model is introduced aiming at representing the actual random pattern of steel plates' imperfect geometry. The impact of stochastic initial imperfections on the ultimate strength of plates and hull girders is investigated. In Section 4.3, a two-dimensional non-uniform thickness random field is generated on the surface of a representative stiffened panel and its impact on the ultimate strength is examined. The chapter ends with discussing the utility of the findings on the course of this thesis, including its connection with the remaining part of this thesis.

The chapter presents some original work published previously in Georgiadis and Samuelides (2021)a and Georgiadis and Samuelides (2021)b.

[12] The reader is referred to the work of Stefanou (2009) for a detailed state-of-the-art upon the subject of SFEM.

4.2 The effect of stochastic geometric imperfections on the ultimate strength of plates and hull girders

4.2.1 Background

The existence of a model that is able to capture the imperfect geometry of a steel plate in ship structures is of vital importance for an engineer. An accurate description of initial imperfections can lead to a safe and reliable design, while on the other hand, significant deviations from the true geometry may result in an over/under-estimation of the true structural behavior. This fact has drawn the attention of many researchers and engineers in the past.

Smith et al. (1988) suggested a plate model that has the shape of a combined global cylindrical-shaped half-wave distortion caused by weld-induced wrap-up at the plate edges (well-known as the "hungry-horse" shape) and local wavelength components, mainly due to dents caused by point loads and accidental impacts received in service or during fabrication. They illustrated a typical initial distortion profile of such a description like the one depicted in Figure 4.1.

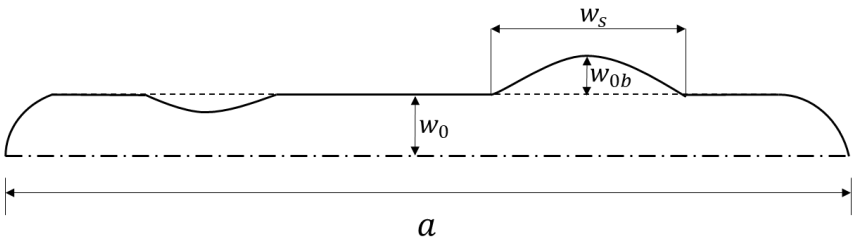

Figure 4.1. Typical profile of initial deflection along plate's length first proposed by Smith et al. (1988).

Smith et al. (1988) also highlighted the fact that the most significant form of initial deformation in such plates is a periodic or isolated distortion of amplitude w_{0b} with half-wavelength w_s equal to or somewhat less than the plate width ($w_s < b$). They also mentioned that in long rectangular plates, the overall distortion w_0 has relatively little influence on the compressive strength and may actually increase plate strength by inhibiting formation of the preferred buckling mode.

During the same period, Ueda and Yao (1985) carried out extensive measurements on the deck panels of a bulk carrier and a car carrier. In their research, they focused mainly on the shape of initial deflections rather than the maximum amplitudes developed. Similar to Smith et al. (1988), it is certified that in the majority of the examined panels, the dominant mode of initial imperfections well-suited to the HH model. A demonstration of this geometry is given in Figure 4.2 where measured geometric distortions along the length of 9 plates are illustrated. It is also apparent that local random fluctuations along the length do exist, something that confirms the remarks drawn by Smith et al. (1988) regarding the development of local dents.

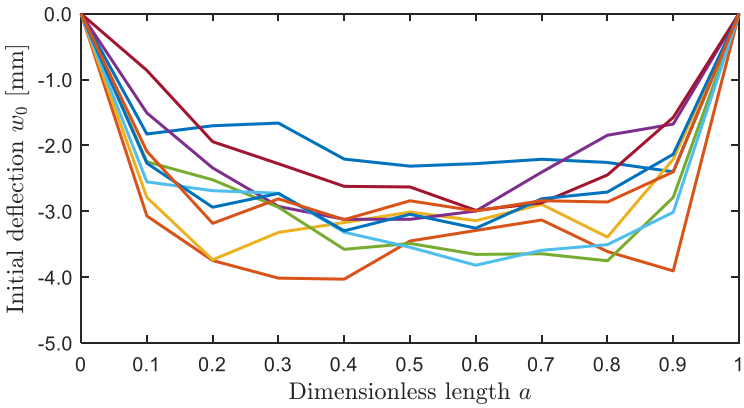

Figure 4.2. Actual measured deflections across the length of 9 deck panels on a car carrier, after Ueda and Yao (1985).

4.2.2 Development of new stochastic imperfection model

The recommended stochastic imperfection model in this thesis aims to simulate with realism the randomly distributed imperfection patterns located on a ship's plate as those illustrated in Figure 4.1 and Figure 4.2. The proposed model effectively combines the HH model by preserving the global dominant mode of imperfection, while simultaneously expressing the local pattern of imperfections along the length of the plates with a 1D Gaussian homogeneous random field. A typical portrait of the suggested model is illustrated in Figure 4.3.

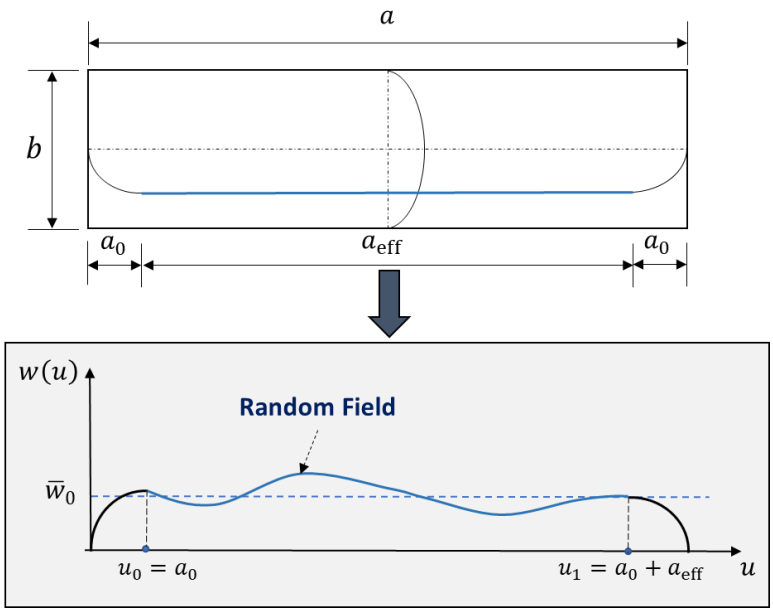

Figure 4.3. Schematic description of the proposed stochastic hungry-horse (SHH) imperfection model using a 1D homogeneous random field.

The random field is introduced on the effective length a_{eff} of the plate whose longitudinal extent is determined by the aspect ratio a/b of the plate. The concepts of *homogeneity* and *normality* are documented using actual data in Section 4.2.2.2. The one-dimensional pattern of initial imperfections $w_{\text{eff}}(u)$ along the effective length of the plate, as this described graphically in Figure 4.3, can be rationally represented using Eq. (4.1):

$$w_{\text{eff}}(u) = \overline{w}_0 + \hat{X}(u) \tag{4.1}$$

where, $\overline{w}_0$ is the mean amplitude of the imperfection and $\hat{X}(u)$ is a zero-mean Gaussian homogeneous stochastic field. The full description of the initial deflection $w(u)$ along the longitudinal path on the centerline of the plate is obtained as follows:

$$w_0(u) = \begin{cases} w_{\text{eff}}(u = u_0)\left|\sin\dfrac{\pi u}{2a_0}\right|, & \text{for } 0 \le u < u_0 \\ w_{\text{eff}}(u), & \text{for } u_0 \le u \le u_1 \\ w_{\text{eff}}(u = u_1)\left|\sin\dfrac{\pi(u - a_{\text{eff}})}{2a_0}\right|, & \text{for } u_1 < u \le a \end{cases} \tag{4.2}$$

where, $u_0 = a_0$ and $u_1 = a_0 + a_{\text{eff}}$. Finally, the entire two-dimensional deflection pattern is portrayed when considering the preserved one-half sinusoidal over the plate's breadth direction too.

In the present study, the statistical properties of the stochastic field $\hat{X}(u)$ are based on available data. Sample functions (realizations) of the stochastic field can be generated with properties equivalent to the measured ones using the spectral representation method. The theoretical background of the method was described in Section 3.7.

4.2.2.1 Autocorrelation function

The target power spectral density function $S_{XX}(\kappa)$ has been selected based on available measurements (see Section 4.2.2.3). The corresponding autocorrelation function $R_{XX}(v)$ is given by the following form:

$$R_{XX}(v) = \sigma_X^2 \rho_{XX}(v) = \sigma_X^2 \frac{\ell_c^4(\ell_c^2 - 3|v|^2)}{(\ell_c^2 + |v|^2)^3} \tag{4.3}$$

where, $|v| = |u_1 - u_2|$ expresses the relative distance (lag) between two positions, σ_X denotes the standard deviation of the stochastic field and ℓ_c is the correlation length parameter of the field. The present autocorrelation model, which has been also used at the study of Shinozuka and Deodatis (1991), is a valid one, since it is easy to show that is symmetric, bounded and

semi-definite function. Using the Fourier transformation (Eq. (3.45)), the analytical form of the power spectral density function reads:

$$S_{XX}(\kappa) = \frac{\sigma_X^2}{4} \ell_c^3 \kappa^2 \exp[-\ell_c|\kappa|] \tag{4.4}$$

The standard deviation of the stochastic field is a measure of the amplitude of imperfections, whereas the correlation length influences the shape of imperfections along the effective length of the plate. Available literature sources are used to define the mean value $\overline{w}_0$ and standard deviation σ_X parameters. This issue will be discussed thoroughly in Section 4.2.4.3.

4.2.2.2 Discussion upon the normality and homogeneity concepts

The spectral representation method generates Gaussian homogeneous random fields with a given correlation structure. This requires that the assumption of homogeneity is valid and a Gaussian probability density function fits the data of imperfections.

A weakly homogeneous random field requires that the mean function of the stochastic field is constant and the autocorrelation can be expressed as a function of the space lag (see Section 3.4.1). It is verified from the available data that the mean value of stochastic deflections does not substantially vary between plates which possess the same characteristics (aspect ratio, breadth-to-thickness ratio and slenderness ratio). In fact, the ensemble average has been obtained at different locations and the standard error of the mean $\sigma_{\varepsilon,\mu}$ has been computed as:

$$\sigma_{\varepsilon,\mu} = \frac{\sigma_m}{\sqrt{m}} \tag{4.5}$$

where, σ_m is the standard deviation of the ensemble average at all measured positions and m is the total number of measurements at the positions where the ensemble average has been computed. The above formula has been applied for two different groups of plate panels with the same characteristics leading to values equal to $\sigma_{\varepsilon,\mu} = 0.011$ and $\sigma_{\varepsilon,\mu} = 0.020$. The estimated standard errors can be characterized small enough to rationally assume that the mean function is constant over the random field.

As it will be seen in the next section, the autocorrelation may be rationally considered as a function of space lag since the spatial autocorrelation function for most of individual plate panels is of similar form. In addition, and based on intuition, no evidence to prove that deflections along the centerline of the effective length of plates are dependent on specific locations exists.

The concept of *normality* has been verified by the statistical processing of 9 deck plate panels with similar characteristics. The actual measurements along their effective length have been

depicted in Figure 4.2, while the corresponding histogram and the probability plot are presented in Figure 4.4. A normal distribution fits well the observed data. In addition, a Kolmogorov-Smirnov test has been carried out which also substantiates that the assumption of normality of the initial imperfections is justified. It is also verified that normality is maintained for plate panels possessing the same characteristics and belonging on the same vessel.

The robustness of the spectral representation method is verified in terms of Gaussianity. A number of 100 sample functions is generated using the preassigned first and second order statistics of the respective data. The PDF of the samples generated by the spectral representation method is illustrated also in Figure 4.4. It is demonstrated that the PDFs of the data and the generated samples show a very good agreement on the first two statistical moments.

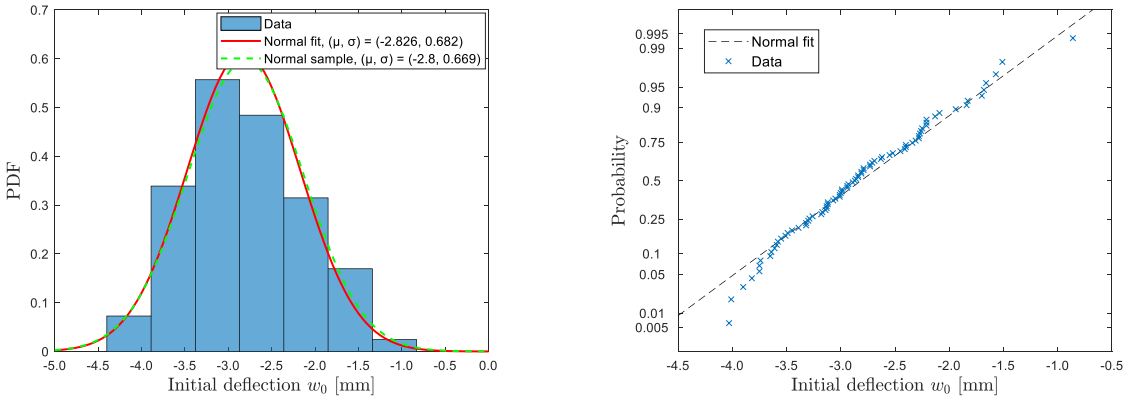

(a) (b)

Figure 4.4. Verification of normality against actual data from initial imperfections. (a) Normalized histogram of initial deflections with a fitted normal distribution, and (b) probability plot of actual data.

4.2.2.3 Discussion upon the autocorrelation function form

The correlation structure adopted for the spectral representation method is validated against measurements from Ueda and Yao (1985). Due to the fact that the data of initial imperfections provides much more comprehensive information about the imperfections of an individual plate panel, it seems to be more reasonable to estimate the autocorrelation function form over the sample, and not over the ensemble. This approach of course requires that the stochastic field of imperfections is ergodic in the mean and in the autocorrelation function. It is considered reasonable though to estimate the autocorrelation function over the sample, if no significant variation is observed. This assumption could be verified by the data. To ensure that the whole ensemble is represented by the autocorrelation form obtained from the individual samples, these characteristics have been averaged over the ensemble.

The spatial autocorrelation coefficient $\hat{\rho}_y(v)$ of the actual deflections d among two different locations u_i and $u_i + v$ along the effective length is calculated using the following formula:

$$\hat{\rho}_d(v) = \frac{1}{m-1}\sum_{i=1}^{m}\frac{\left(d_{u_i} - \hat{\mu}\right)\left(d_{u_i+v} - \hat{\mu}\right)}{\hat{\sigma}^2} \tag{4.6}$$

where, m is the total number of measurements for a given lag and $\hat{\mu}, \hat{\sigma}$ express the spatial average value and standard deviation for each individual plate panel, respectively.

The total number of plate panels has been initially considered for statistical processing. Among them, a few outliers have been excluded from the procedure resulting in 28 plate panels in total. Figure 4.5 presents the final (spatial) autocorrelation functions in the form of cloud data points along with a fitted polynomial curve. The autocorrelation coefficient, $\rho_{XX}(v)$, of Eq. with $\ell_c/a_{\text{eff}} = 0.415$ has been selected which minimizes the root mean square error between the polynomial fit and the proposed autocorrelation model. It is also shown that not significant variations between the autocorrelation form of individual samples exists, a clue that confirms the assumption of homogeneity.

The ℓ_c parameter can be expressed as a ratio of the total length a of the plate given that $a = 2a_0 + a_{\text{eff}}$. Finally, the following relation can be used to establish the correlation length parameter as a ratio of the length:

$$\frac{\ell_c}{a} = \begin{cases} 0.208, & \text{for } 1.41 \le a/b < 2.45 \\ 0.277, & \text{for } 2.45 \le a/b < 3.46 \\ 0.311, & \text{for } 3.46 \le a/b < 4.47 \\ 0.332, & \text{for } 4.47 \le a/b < 5.66 \end{cases} \tag{4.7}$$

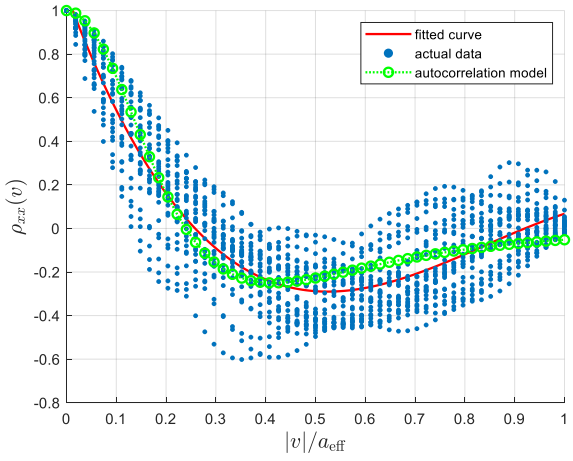

Figure 4.5. Verification of the selected auto-correlation function (Eq. (4.3)) with actual data. The auto-correlation coefficient is shown as a function of the non-dimensional distance along the effective length of plate panels.

4.2.3 Numerical investigation on plates

The performance of the proposed stochastic model is first tested against available test results presented by Ueda and Yao (1985). Actual measurements from initial deflections on several plates are used to validate the stochastic model in terms of strength prediction and accuracy of capturing the real collapse mode. This study aims to establish the recommended model as a rational one, in order for the designer/engineer to be able to use it from a probabilistic perspective, for example, to assess the reliability of the structure at hand, accounting for the uncertainties associated with the imperfect geometry of steel plates in ship structures.

The present section is formulated as follows. First, a validation test is performed for the case of a plate panel from a car carrier which was tested by Ueda and Yao (1985) in terms of ultimate strength prediction and collapse mode behavior using the actual measured initial imperfections. The same case study is now repeated using the ABAQUS finite element software in order to verify the existing results and validate our FE model. In the second stage, 15 plate panels have been considered to investigate the performance of the idealized/conventional HH imperfection model in relation to the actual initial deflections. Some important conclusions are extracted from this analysis. In the third and final stage, the proposed stochastic imperfection model is tested upon selected cases and its performance is evaluated and compared with the two common imperfection models, namely, (i) the idealized HH imperfection model, and (ii) the sinusoidal buckling-mode imperfection model. Valuable findings are drawn from this study, before proceeding with the probabilistic assessment of the hull-girder ultimate strength.

4.2.3.1 Validation test

A validation test is firstly performed to guarantee that the adopted FE model predicts accurately the ultimate strength of a plate under uniform compression. An elastoplastic large deflection analysis is performed on the plate panel no. 6 of the car carrier using the actual deflections. The initial actual deflection pattern $w_{0p}(\mathrm{x},\mathrm{y})$ of plate's geometry is expressed using Eq. (2.10), where the coefficients of the deflection components $A_{0m_{\mathrm{x}}}$ are obtained from Ueda and Yao (1985) for each plate. A schematic description of the problem at hand is presented in Figure 4.6. The length (a), breadth (b), thickness (t), yield stress (σ_y), Young's modulus (E) and Poisson's ratio (ν) are illustrated on the same figure. The pre-assigned values of w_{0p} are inserted into the FE model as initial nodal displacements. The plate is assumed as simply supported along all the edges. All edges are assumed to remain straight while subjected to in-plane movements.

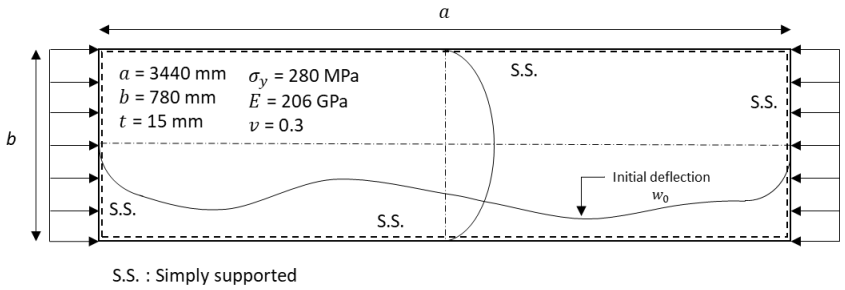

Figure 4.6. Geometric and material characteristics of the car carrier plate panel no. 6, after Ueda and Yao (1985).

The plate panel is modelled in ABAQUS software. Shell quadratic four-node elements with reduced integration points (S4R) are used for the mesh discretization. A mesh size of 50mm with aspect ratio close to unity has been verified to give stable results. The resulted axial stress for each increment is obtained by dividing the reaction axial force by the sectional area of the plate at the short edge. A static Newton-Raphson solver has been used for the non-linear analysis. The material model is assumed as elastic-perfectly plastic.

The resulted normalized axial stress-strain curve is presented in Figure 4.7a. The normalization of stress is performed with respect to the yield strength, σ_y and that of strain with the yield strain, ε_y. The maximum predicted strength is achieved for $\sigma_x/\sigma_y = 0.836$ which is in very good agreement with the corresponding prediction of Ueda and Yao (1985). In addition, the collapse mode, as illustrated in Figure 4.7b is identical with the one presented in the same paper. Overall, the verification of the FE model has been successfully accomplished.

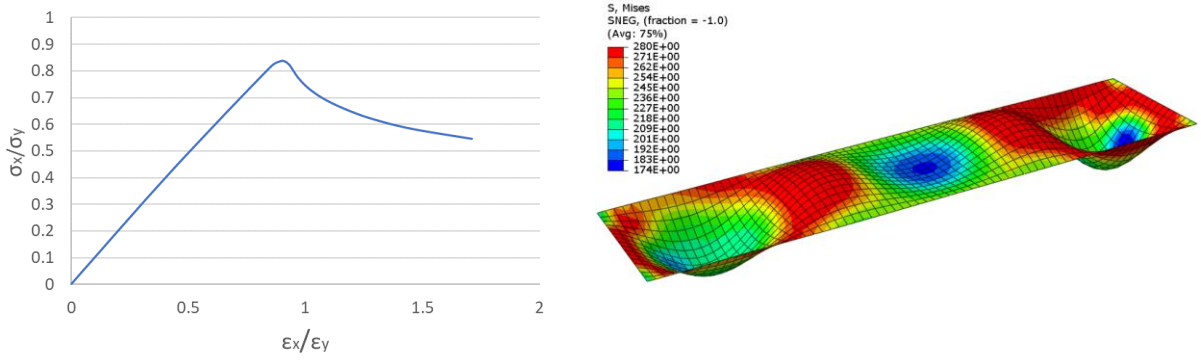

(a) (b)

Figure 4.7. (a) Average stress-strain curve and, (b) collapse mode for plate panel no. 6 of the car carrier.

4.2.3.2 Performance of the idealized HH imperfection model

A total of 15 plate panels have been employed from the study of Ueda and Yao (1985) to examine the performance of the idealized HH imperfection model for a variety of actual initial imperfections. Nine (9) of the plates belong to a bulk carrier and six (6) to a car carrier. The examined plate panels possess the following geometric characteristics:

- $a \times b \times t_p = 2800 \times 800 \times 15 \text{ mm} \quad (a/b = 3.5, b/t_p = 53, \beta_p = 2.0)$
- $a \times b \times t_p = 2800 \times 800 \times 19 \text{ mm} \quad (a/b = 3.5, b/t_p = 42, \beta_p = 1.6)$
- $a \times b \times t_p = 2100 \times 800 \times 15 \text{ mm} \quad (a/b = 2.6, b/t_p = 42, \beta_p = 1.6)$
- $a \times b \times t_p = 3440 \times 780 \times 15 \text{ mm} \quad (a/b = 4.4, b/t_p = 52, \beta_p = 1.9)$

where, β_p is the slenderness ratio. The simulations were performed for plates with medium thicknesses ranging from $t_p = 15$ mm to $t_p = 19$ mm which are usually met in oil tankers. The material characteristics for all plate panels are the ones presented in Figure 4.6. The coefficients of deflection components for the idealized HH model are obtained from Table 2.3.

The results from the NLFEA are presented in Table 4.1 in terms of ultimate to yield strength ratio, σ_u/σ_y. The average spatial deflection $\overline{w_0}$ and the individual standard deviation σ_X for each plate panel are also listed as a ratio of thickness. Although the idealized HH model gives good predictions for many of the examined plates, there are some cases where it fails to predict the ultimate strength with an emphatic way, since this deviation may reach to an overestimation of the true ultimate strength by about $7 - 8\%$. A deeper insight into this issue is given by isolating two plate panels and examining their structural behavior for the actual and idealized deflection pattern.

The case of plate panels no. 18 of the bulk carrier and no. 4 of the car carrier have been selected to investigate the effect of idealized HH model application on the structural behavior of the plate. The initial deflections are depicted in Figure 4.8a and Figure 4.9a. The idealized HH shape makes use of the average initial deflection of each individual plate panel. The behavior of the structure in terms of average stress-strain results is also presented in Figure 4.8 and Figure 4.9, along with the collapse mode of the plate when applying the average and the actual deflection pattern.

The idealized HH imperfection model seems to behave rather well when deviations of initial deflection from the average level of magnitude are relatively small along the effective length of the plate panel. As shown in Figure 4.8, the initial fluctuations around the mean value have a negligible impact on the collapse mode shape, which is highly controlled by the deflection at the end edges. This behavior of collapse has been also verified by the findings of Ueda and Yao (1985).

Table 4.1. Ultimate strength prediction for actual and idealized shape of initial deflections.

Plate panels	Actual σ_u/σ_y	Idealized HH σ_u/σ_y	Deviation (%)	$\bar{w}_0/t_p$	σ_X/t_p
Bulk carrier panel no. 13	0.878	0.904	3.03	-0.140	0.018
Bulk carrier panel no. 14	0.829	0.871	5.09	-0.241	0.021
Bulk carrier panel no. 15	0.867	0.879	1.40	-0.214	0.016
Bulk carrier panel no. 16	0.992	0.979	-1.32	-0.137	0.027
Bulk carrier panel no. 17	0.980	0.964	-1.66	-0.174	0.024
Bulk carrier panel no. 18	0.974	0.964	-1.04	-0.173	0.022
Bulk carrier panel no. 19	0.992	0.980	-1.25	-0.134	0.018
Bulk carrier panel no. 20	0.978	0.971	-0.66	-0.156	0.011
Bulk carrier panel no. 21	0.971	0.973	0.23	-0.155	0.006
Car carrier panel no. 1	0.875	0.868	-0.78	-0.319	0.022
Car carrier panel no. 2	0.865	0.872	0.87	-0.300	0.042
Car carrier panel no. 3	0.822	0.884	7.51	-0.248	0.047
Car carrier panel no. 4	0.843	0.896	6.32	-0.196	0.127
Car carrier panel no. 5	0.844	0.878	4.03	-0.273	0.036
Car carrier panel no. 6	0.836	0.871	4.24	-0.305	0.033

On the other hand, the behavior of the idealized HH imperfection model is not equally good in cases where fluctuations around the average deflection path are more pronounced, as in the case of plate panel no. 4 (see Figure 4.9a). The presence of highly peaked deflections is associated with the existence of localized dents in the structure, as discussed also in Section 4.2.1. Moreover, it is more likely that localized dents are present on higher values of aspect ratios a/b. It seems from the present results that local dents in long rectangular plates may significantly reduce the resulted ultimate strength by altering the collapse mode. This can be observed from the collapse mode and the resulted maximum strength of plate panel no. 4. In reality, the presence of one or more localized dents can trigger buckling to occur more rapidly, while simultaneously, a stable deflection mode is developed from an early stage during the progressive collapse. This may accelerate the plastification and greatly affects the resulting ultimate strength.

Last but not least, it is remarked that the conventional HH imperfection model representation underestimates the effect of any localized short wave-length distortions, e.g., dents, and for that reason can be considered unsatisfactory, see e.g., Dow and Smith (1984) and Smith et al. (1988). The Fourier series representation used by Ueda and Yao (1985) to express the imperfect

geometry may conceal that information, i.e., the presence of localized short wave-length distortions. If so, the idealized HH model will deviate even more from reality.

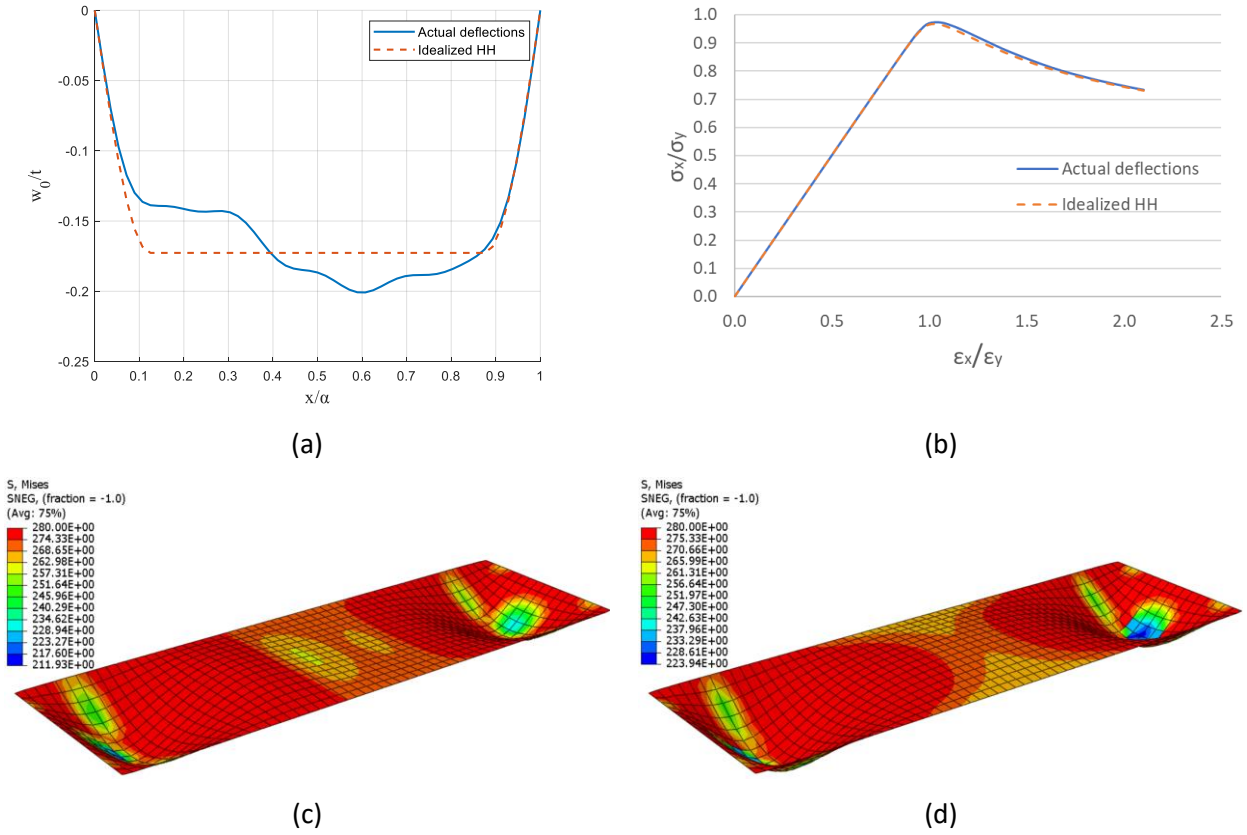

Figure 4.8. Panel no. 18 of bulk carrier. (a) Initial deflection path, (b) resulted stress-strain relationship, (c) Von Mises contour plot for actual initial deflections at collapse and (d) Von Mises contour plot for idealized HH initial deflections at collapse. A very good agreement is observed between the conventional HH model and reality.

4.2.3.3 Performance of the proposed stochastic imperfection model against common imperfection models

The recommended stochastic imperfection model is now tested against actual data. The performance of the new model is compared with the probabilistic behavior of the idealized HH and the theoretical buckling-mode common imperfection models which are employed for various amplitudes of initial deflections. The geometric and material characteristics of the car carrier panels, as those presented in Figure 4.6, are considered for the present analysis.

With respect to the proposed stochastic imperfection model, Gaussian homogeneous sample functions are generated according to the target mean value, standard deviation and the established autocorrelation model. The assigned first and second order statistics come from the statistical processing of the measured initial deflections based on the six examined panels. For

the idealized HH model, the definition of the maximum initial deflection w_{0p}^{max} is needed. This is selected to vary uniformly between the minimum (lower bound) and the maximum value (upper bound) of the average initial deflections, as obtained from Table 4.1 for the examined plate panels.

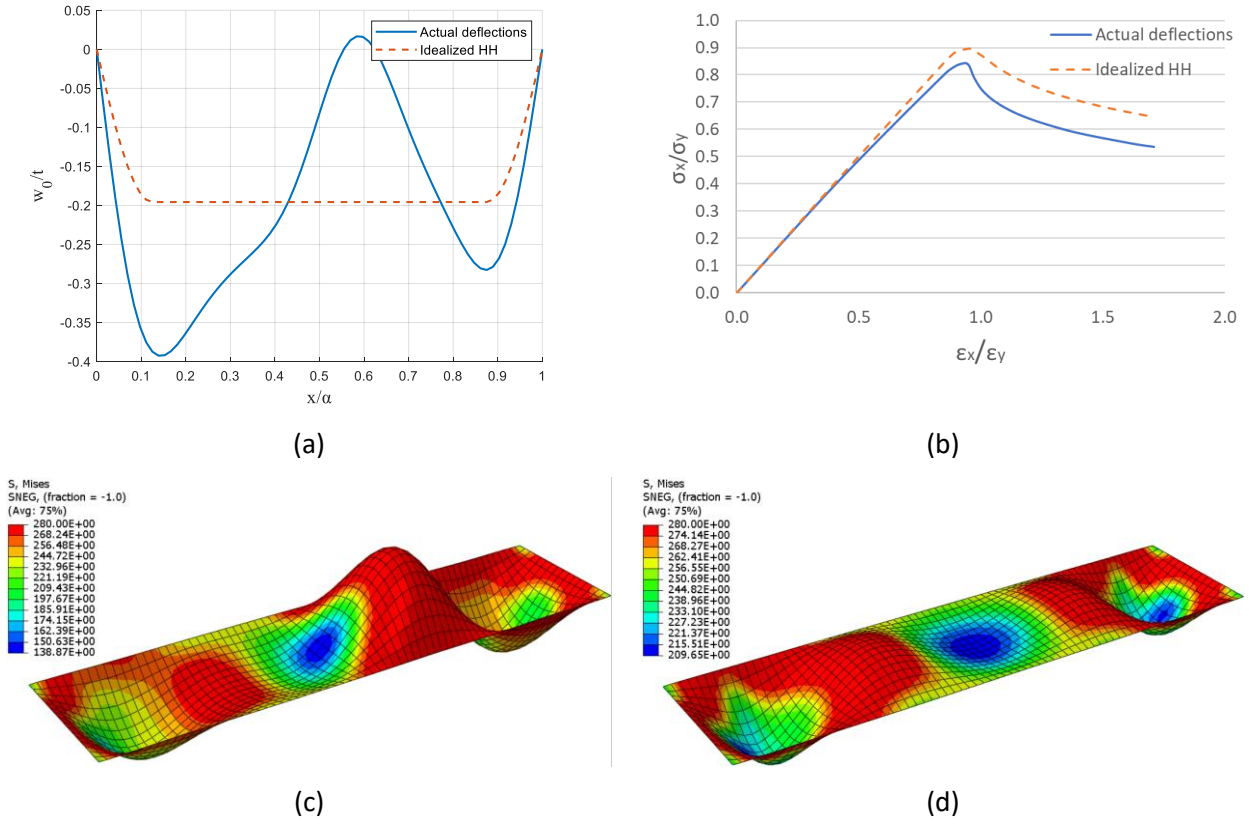

Figure 4.9. Panel no. 4 of car carrier. (a) Initial deflection path, (b) resulted stress-strain relationship, (c) Von Mises contour plot for actual initial deflections at collapse and (d) Von Mises contour plot for idealized HH initial deflections at collapse. An important deviation is observed between the conventional HH model and reality.

The buckling-mode sinusoidal imperfection model with four (referred as "BM") and six (referred as "BM+2") half-waves is also tested. The number of four half-waves corresponds to the elastic buckling mode. In addition, six half-waves have been also tested since – according to the suggestion of Ueda and Yao (1985) – the critical mode on the ultimate strength prediction of thin plates is usually higher by one or two modes than the elastic buckling one. The definition of the maximum amplitude of initial deflection is based on recommendations from literature. As a lower limit, Smith's formula (Eq. (2.11)) for a slight level of imperfections is used, while as an upper limit, the maximum allowable initial deflection of 6 mm recommended by (JSQS) is applied (see Section 2.4.4). Summarizing, the prescribed distributions with the associated parameters for the three stochastic imperfection models are presented in Table 4.2.

Table 4.2. Prescribed distributions for the selection of input initial deflections.

Imperfection model	**Distribution**	$\bar{w}_0/t_p$	σ_X/t_p	w_{0p}^{max}/t_p **(lower limit)**	w_{0p}^{max}/t_p **(upper limit)**
SHH	Gaussian	-0.274	0.073	-	-
HH	Uniform	-	-	-0.196	-0.319
BM	Uniform	-	-	0.092	0.400

A number of $K = 100$ simulations has been used for each imperfection model. The predicted minimum and maximum values, together with the 25% quartile, 50% quartile (median) and 75% quartile, of ultimate strength sample values are estimated for the three models and displayed graphically in Figure 4.10. The actual predicted values of the six plate panels, as those listed in Table 4.1, are also illustrated.

From the results of Figure 4.10 it seems that the stochastic HH model performs better than the common imperfection models. The proposed SHH model predicts all of the actual scenarios while offering a reasonable conservatism on its estimations. On the other hand, the idealized HH model overestimates the actual predicted strength in most of the cases. The more theoretical buckling-mode imperfection models gives too conservative predictions of the true ultimate strength. The efficiency and robustness of the proposed stochastic HH model lies on the fact that it can adjust the magnitude and initial shape of deflections through the selection of three parameters, i.e., the mean value, the standard deviation and the autocorrelation form. This makes the model more flexible upon capturing a variety of plausible outcomes of plates' imperfect geometries.

In Figure 4.11, the collapse mode of panel no. 3 of the car carrier is depicted for the true imperfections and a randomly selected sample function of the stochastic field. It is shown that an excellent agreement between the two collapse modes exists, something that is also captured from the stress-strain diagram of Figure 4.11c.

The average coefficients of deflection components for the generated sample functions have been also derived and presented in Table 4.3. These coefficients account for the entire length of the plate panel a and depict the average characteristics of all panels. It is observed that the coefficients of odd terms are higher than those of even terms. This behavior is quite reasonable indicating a relatively symmetric shape of deflection with respect to the midspan of the plate. This finding is in symphony with the observations made by Ueda and Yao (1985) for the same data source.

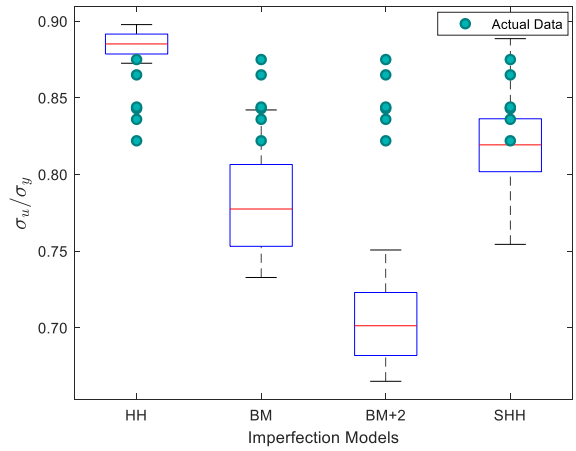

Figure 4.10. Ultimate strength predictions of the three imperfection models; the conventional HH model, the theoretical BM model with four half-waves, the theoretical BM with six half-waves (BM+2) and the proposed stochastic HH (SHH) imperfection model against actual predictions.

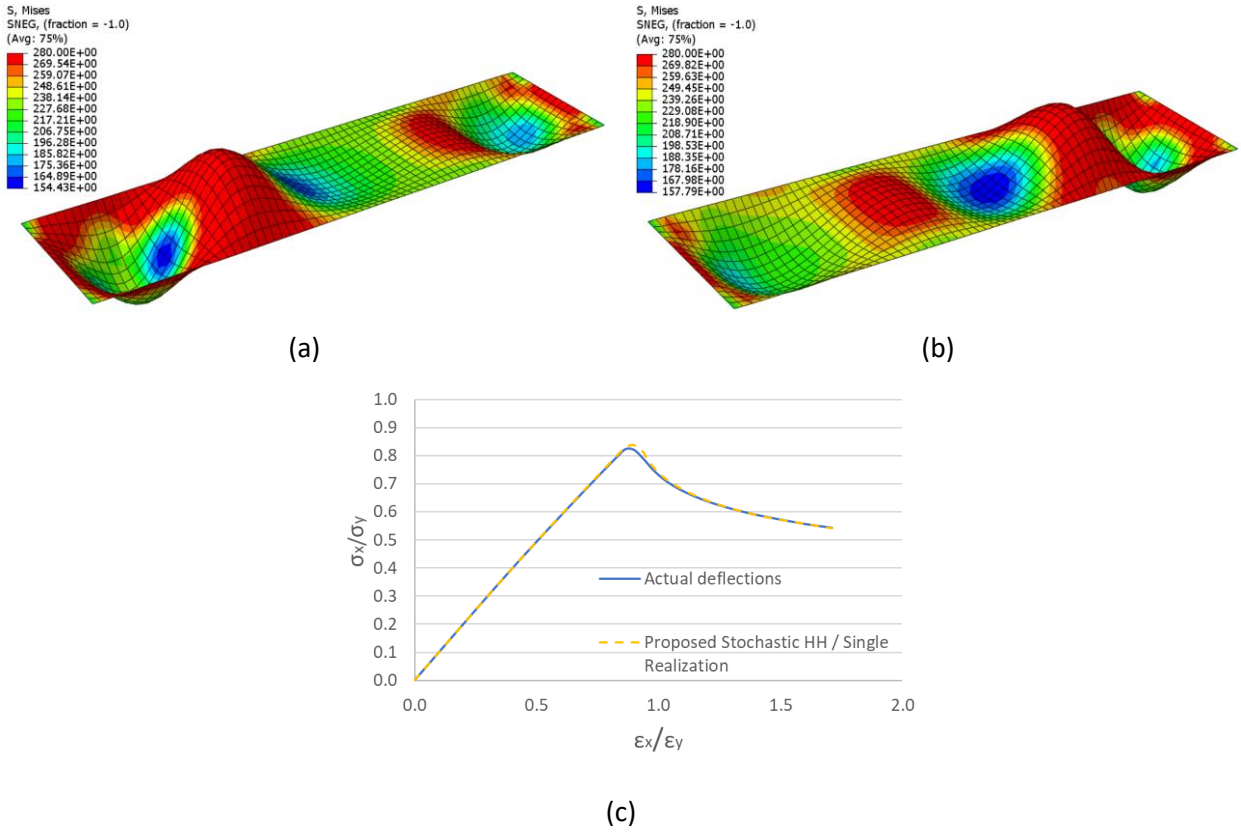

Figure 4.11. (a) Collapse mode for the actual initial deflection and (b) collapse mode for the selected individual sample function of the proposed SHH model. (c) Average stress-strain curve for panel no. 3 of the car carrier. A very good agreement between the selected individual sample function of the proposed stochastic model and the actual deflection behavior is observed.

Table 4.3. Sample functions average coefficients of deflection components in initial deflection for the car carrier plate panels.

A_{01}	A_{02}	A_{03}	A_{04}	A_{05}	A_{06}	A_{07}	A_{08}	A_{09}	A_{10}	A_{11}
-4.631	-0.036	-1.426	0.021	-0.639	-0.028	-0.305	0.003	-0.118	0.000	-0.027

4.2.4 Numerical investigation on a hull girder

The effect of the proposed stochastic imperfection model on the hull girder ultimate strength prediction of a VLCC tanker is examined under extreme sagging condition. Failure in sagging is investigated since it is identified as the most critical failure mode for double hull tankers. The buckling instability phenomenon occurring on the deck panels is influenced by the initial imperfections, highlighting the importance of their accurate modelling on the prediction of the overall hull girder strength. A comparison between the proposed stochastic imperfection model and the conventional/deterministic imperfections models as well as Smith's incremental-iterative solution is also performed in this section. Due to the numerous simulations required for a statistical description of capacity, neural networks (NNs) are efficiently trained and used to substitute the time-consuming FEM.

4.2.4.1 Vessel description

Thickness measurements reports have been acquired from a VLCC oil tanker with a deadweight of 300,000 t. The principal particulars of the vessel, along with the midship section properties calculated using the as-built scantlings are presented in Figure 4.12. The cross-section amidships is mainly constructed by high-tensile steel of type AH32, while the longitudinal stiffeners attached on the side shell plating of the neutral axis zone are made of mild steel. Longitudinal stiffeners are primarily of type "Tee". Angle-bar profiles are met only on few locations, e.g., deck stringer plates.

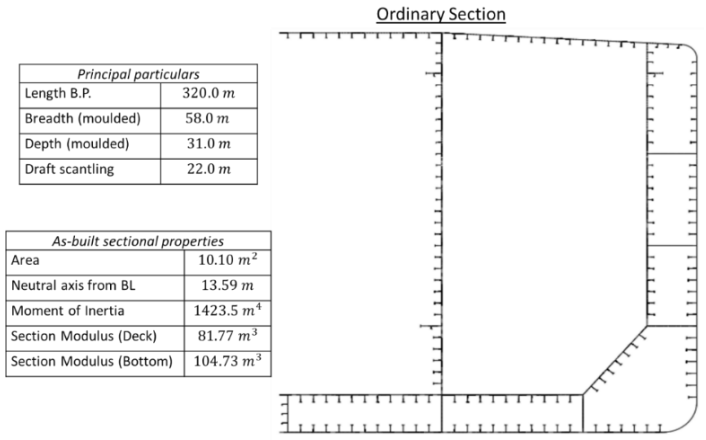

Figure 4.12. Principal particulars and midship section drawing of the examined VLCC tanker.

4.2.4.2 Finite Element (FE) modelling

The establishment of the FE model has been implemented on the ABAQUS software. It is of primary concern to develop a FE model that gives reliable predictions in conjunction with reasonable computational efforts. In the analysis that follows, the selection of the basic modelling parameters that influence the above aspects is described.

Length extent of the FE model

A one-bay FE model has been established for the determination of the hull-girder ultimate capacity (see Figure 4.13). This FE model extent has been considered acceptable for simulating pure bending, see e.g., Dow and Smith (1984), Hughes and Paik (2010), and ISSC (2018). A three-bay FE model has been also tested in Georgiadis and Samuelides (2021)a to examine the effect of boundary conditions on the resulted structural behavior. It was shown that the two FE model extents give identical results in terms of hull girder ultimate strength prediction and collapse mode. Thus, only the results from the one-bay FE model will be presented in the present thesis.

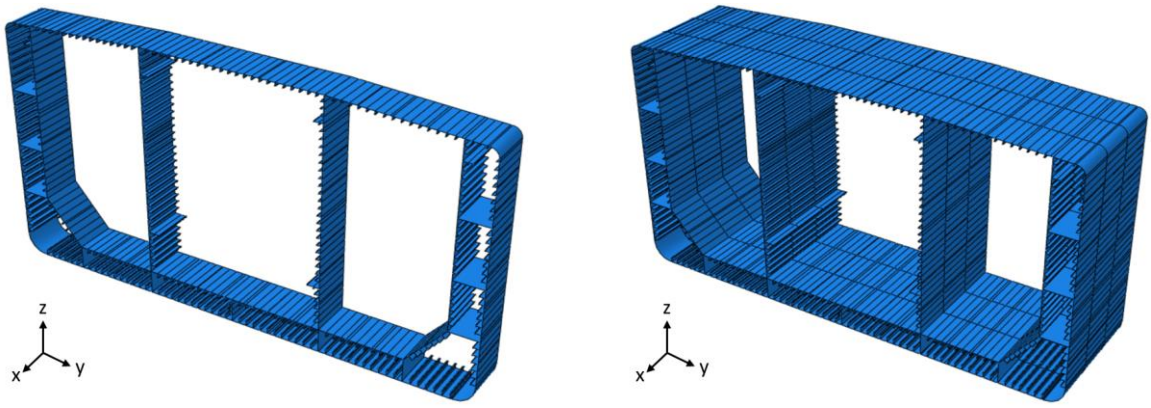

(a) (b)

Figure 4.13. The geometry of (a) the one-bay and the (b) three-bay FE model. The x, y, z axes correspond to the longitudinal, transverse and vertical direction of the FE model, respectively.

Material modelling

The stress-strain curve of the material used is represented by a bilinear model with a constant tangent modulus equal to 1000 MPa. The mechanical properties of the constructive mild and high-tensile steels used are based on their characteristic values as these recorded in Table 4.4.

Analyses solver

The problem of ultimate strength prediction is generally a static one. Hence, analogous techniques have been employed for its solution. The arc-length method has been primarily used, but convergence issues due to instability phenomena were encountered during the simulation. Therefore, a quasi-static analysis has been successfully implemented through the dynamic implicit solver of ABAQUS software to overcome these difficulties. In order to ensure that no inertia effects are present, it is verified that the kinetic energy of the deformable body through the whole simulation is only a small portion (less than 1%) of the internal energy of the whole model. In addition, in cases where the arc-length method was allowed to capture the entire path of the moment-curvature diagram, results between the two different solvers were in full agreement.

Boundary conditions and constraints

The boundary conditions of the FE model should be applied on such a way that simulate the real behavior of the structure. The fore and aft edges of the cross-section are coupled with an associated reference node. The prescribed degrees of freedom (DoF) assigned to the reference node coincide with the coupled nodes of the above end edges. The multi-point beam constraint (MPC-beam) used ensures that the cross-section remains plane throughout the whole simulation.

The boundary conditions applied on the two edges are in accordance with Table 4.5, where $u_{\mathrm{x}}, u_{\mathrm{y}}, u_{\mathrm{z}}$ indicate translations on the longitudinal, transverse and vertical axis, respectively and $r_{\mathrm{x}}, r_{\mathrm{y}}, r_{\mathrm{z}}$ denote the rotations around each corresponding axis. A prescribed rotation around y-axis equal to 0.0025 rad is imposed incrementally on each reference node leading to a sagging condition. In order to avoid the existence of axial forces on the longitudinal direction, translation on x-axis is set free at the fore end. All the remaining DoF are restraint. It is verified at the end of the analyses though, that reaction stresses on the restricted DoF are negligible, in an effort to simulate pure bending.

Table 4.4. Material properties' characteristic values, after IACS (2019).

Material properties	**Symbol**	**Value**	**Units**
Young's modulus	E	206	GPa
Poisson's ratio	ν	0.3	-
Yield stress (Mild/AH32)	σ_y	235 / 315	MPa
Inelastic tangent modulus	E_T	1000	MPa

Table 4.5. Applied boundary conditions on the cross-section end edges.

DoF	Ref. node fore	Ref. node aft
u_x	free	-
u_y	-	-
u_z	-	-
θ_x	-	-
θ_y	-0.0025 rad	0.0025 rad
θ_z	-	-

Mesh discretization

The discretization of the FE model is achieved using the four-nodes reduced integration shell elements (S4R) type, while five integration points are used through the thickness of the element. This type is selected mainly upon previous researches and recommendations on the study of the ultimate strength of stiffened plate structures, see e.g., Amlashi and Moan (2008), and Hughes and Paik (2010).

The mesh density is selected on the basis of a convergence analysis. Following Bathe (2006), mesh refinement is performed by subdividing a previously used element into two or more elements; thus, the old mesh is "embedded" in the new mesh. In addition, a fine mesh is selected for the deck zone (above 2/3 of vessel's depth) in order to capture accurately the relevant modes of failure occurring mainly due to buckling instability and a coarser mesh is used for the remaining region (neutral axis zone and bottom) in order to reduce the computational time and at the same time retain the accuracy on the results. This strategy has also been adopted by Amlashi and Moan (2008).

Deck's zone mesh density is tested using $400, 300, 200, 100, 75$ and 50 mm size of elements. The remaining zones were examined using $200, 300$ and 400 mm of element sizes. An aspect ratio of element size close to one is achieved for the deck region. The results of the convergence study are presented in Figure 4.14, where it is noticed that a stable plateau has been reached for a mesh smaller than 100 mm on the deck zone (notice that the difference between the 50 mm and the 100 mm mesh is less than 1%).

The following number of elements are recorded in the stiffened plates of deck:

- 6 elements along the web height of deck longitudinal stiffeners
- 1 element along the flange half-width of deck longitudinal stiffeners
- 9 elements between longitudinal stiffeners
- 51 elements between transverse web frames

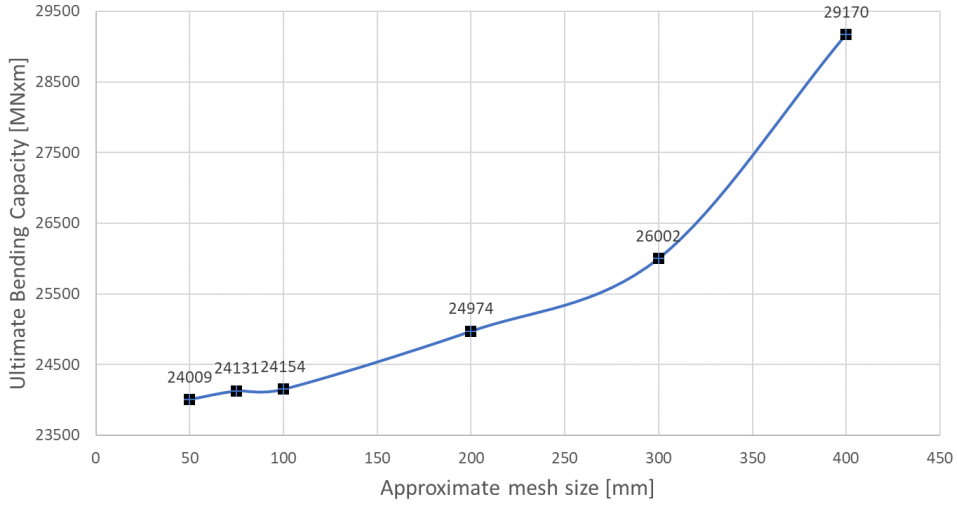

Figure 4.14. Mesh convergence analysis.

The above selection satisfies the recommendations of ISSC (2018). For the remaining zones, an element size equal to 300 mm is chosen. A close-up view on the adopted mesh is shown in Figure 4.15 for the deck and the bottom region. The final FE model resulted in a total of $814{,}668$ DoF. The final selected mesh is considered sufficient to proceed with the examination of the ultimate capacity of the vessel and the application of imperfections.

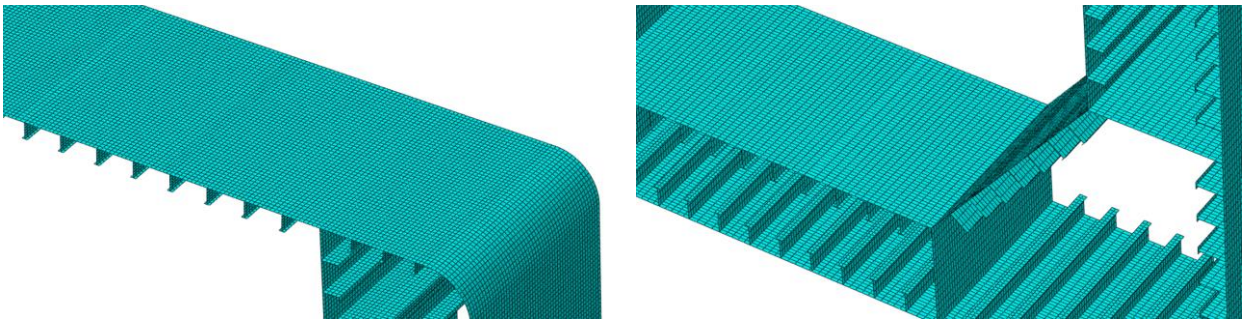

(a) (b)

Figure 4.15. A close-up view on the adopted mesh on (a) deck zone and (b) neutral/bottom zone.

Initial imperfections

Imperfections have been assigned to the FE nodes of the deck structure since overall strength in sagging is dominated by the buckling failure of this area. It was considered unnecessary though to model the imperfections on the side shell or longitudinal bulkheads since deformations on the deck will automatically trigger compatible buckling patterns in the

adjacent members. The final imperfect geometry has been obtained by linearly superimposing the three deflection modes described in Section 2.4.4.1, namely: (i) global column-type deflection, (ii) stiffener sideway deflection, and (iii) local plate deflection. In addition, the proposed stochastic HH model is tested as local plate deflection shape. Both directions of global deflection (towards plate and towards stiffener side) have been examined in the NLFEA and the one with the most conservative outcome is retained. In addition, and following the suggestions of Ueda and Yao (1985), the cases where $m = m + 1$ and $m = m + 2$ have been examined since the elastic buckling-mode is not necessarily the most conservative case when the collapse of panel is tested (see also Figure 4.10).

4.2.4.3 Application of stochastic imperfection model

The method of spectral representation is applied to generate Gaussian sample functions with a prescribed mean value $\overline{w}_0$, standard deviation σ_X and correlation length ℓ_c. Information from literature regarding the statistical description of $\overline{w}_0$ and σ_X is vague. This motivates the use of random variables for the description of their statistical uncertainty. A probabilistic model from available literature sources is thus established as follows.

Antoniou (1980) carried out a regression analysis using data from plates' deflections on newly built ships. He established a formula which suggests that the mean amplitude of initial distortions along the centerline of the plate $\overline{w}_0$ can be expressed as a function of the plate's slenderness β and the thickness of the adjacent longitudinal stiffeners t_w as:

$$\frac{\overline{w}_0}{t_p} = 0.091\beta^2\left(\frac{t_w}{t_p}\right) \tag{4.8}$$

when $t_w/t_p < 1$ and $\beta > 2.6$. In addition, in his study suggested that the mean plus two standard deviation amplitude for the examined case study when $b/t_p > 40$ and $t_p \geq 14\ \text{mm}$ can be obtained using Eq. (4.9) as:

$$\frac{\overline{w}_0 + 2\sigma_X}{t_p} = 0.014\frac{b}{t_p} - 0.32 \tag{4.9}$$

In the present study, the scantlings of the deck stiffened panel are equal to $b = 910\ \text{mm}$, $t_p = 19.5\ \text{mm}$, $t_w = 15\ \text{mm}$ and the slenderness ratio is $\beta_p = 1.825$. Thus, the solution of Eq. (4.8) and Eq. (4.9) leads to a pair of $\overline{w}_0$ ($\overline{w}_0/t_p$) and σ_w (σ_w/t_p) equal to 4.5 mm (0.231) and 1.0 mm (0.051), respectively. It is assumed that this pair corresponds to the mean values of the respective random variables.

Smith et al. (1988) recommended a magnitude of $w_{0p}^{max}/t_p = 0.1\beta^2$ for an average level of imperfections that correspond to the mean value of measured data. This equals to $w_{0p}^{max}/t_p = 0.333$ for the specified deck plate characteristics and provides an upper limit for the variability of $\overline{w}_0\ /t_p$.

The authors also conducted a statistical analysis to the data of Ueda and Yao (1985) where a series of 189 measurements from 21 deck panels has been considered. Ueda and Yao (1985) obtained a number of measurements from a total of 33 panels; however, 12 panels have been excluded in the present study because the plate characteristics differ significantly to the ones of the examined vessel. The ensemble average and standard deviation of the deflections have been computed resulting in the values of 2.52 mm and 1.64 mm, respectively.

From the three above literature surveys and assuming a uniform distribution to describe the variability related to the mean amplitude $\overline{w}_0/t_p$ a mean value equal to 0.231 and an upper (lower) limit of 0.333 (0.128) are derived. These values lead to a coefficient of variation equal to 0.013. Similarly, the variability of random field's standard deviation σ_X is determined by assuming a lognormal distribution. The mean value is set equal to 1.0 mm following Eq. (4.8). The 90% quantile of the distribution is set equal to 1.64 mm, which corresponds to the (ensemble) standard deviation derived from the data of Ueda and Yao (1985). This leads to a 5% probability of exceeding the 2.0 mm and a resulting coefficient of variation CoV equal to 0.50 (or 0.026 in terms of σ_X/t_p). Table 4.6 summarizes the PDFs of the statistical moments chosen for consideration on the present VLCC tanker along with their mean value and coefficient of variation.

The following comments and remarks are made:

- The generated sample functions have the same first and second order statistics when performing a single NLFEA simulation, considering that on a real case scenario similar behavior of initial distortions is encountered for all the deck panels.
- The spatial correlation of the initial deflection between adjacent panels is neglected, and thus, sample functions, i.e., initial deflection states, are generated independently on each panel.
- Although the HH model is preserved by obtaining a negative value of $\overline{w}_0$ (deflection of plate towards stiffener direction), there are points which exhibit a positive deflection. This is something that coincides with reality as it has been noticed from Ueda and Yao (1985). Hence, such sample functions are included in the analyses too.
- The ultimate strength produced with constant values of $\overline{w}_0$, σ_X and ℓ_c is more or less constant, i.e., one value of ultimate strength is considered. This means that different realizations (or sample functions) of initial imperfections do not affect the magnitude of response significantly.
- The only available data for the description of the correlation length parameter comes from the study of Ueda and Yao (1985). Therefore, ℓ_c/a is taken equal to 0.332 as derived from the post-processing of these data (see Eq. (4.7)).

An illustration of the imposed imperfection models applied on the deck panels of the FE model is shown in Figure 4.16, where a mean representative value of the field parameters is selected. Global stiffened plate panel imperfections and local initial sideways deflections on stiffeners are preserved for the proposed stochastic model, with Eq. (2.6) and Eq. (2.7) giving their analytical form.

Table 4.6. Probability distributions of the statistical moments associated with the generated random field.

Parameter	Symbol	Distribution	Mean value	CoV
Mean amplitude (dimensionless)	$\overline{w}_0/t_p$	Uniform	0.231	0.013
Standard deviation (dimensionless)	σ_X/t_p	Lognormal	0.051	0.026

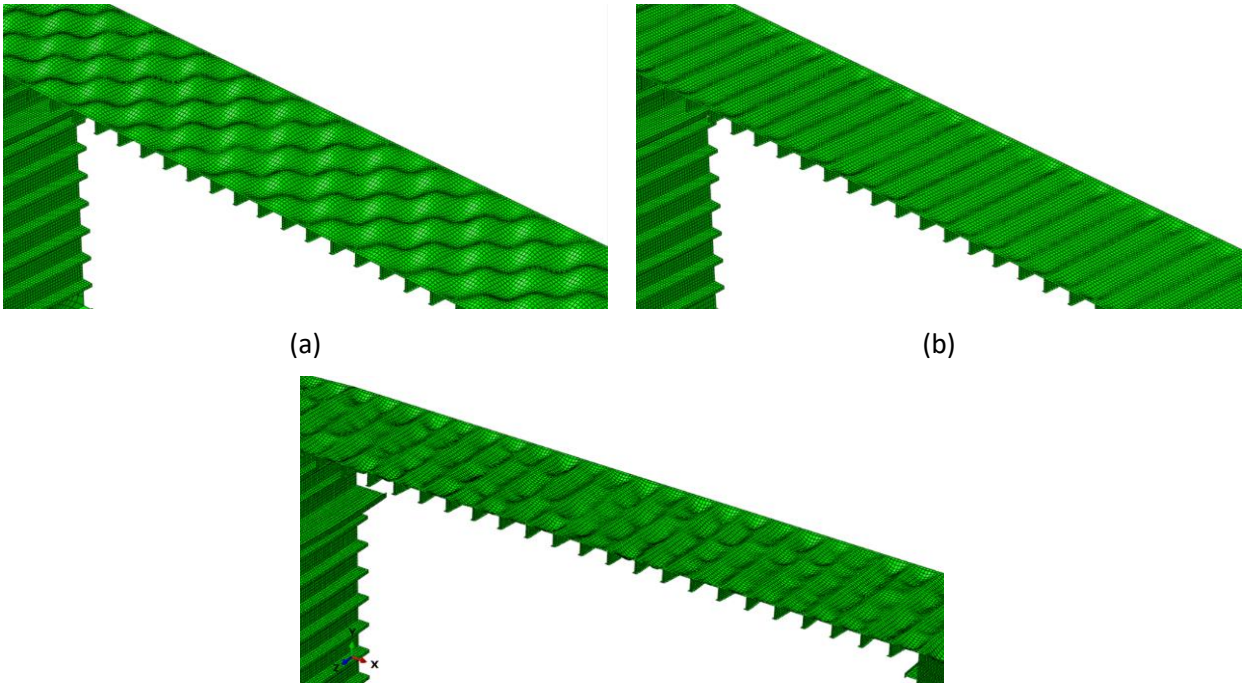

(a) (b)

(c)

Figure 4.16. Applied imperfect geometry on the deck stiffened panels; (a) buckling mode (BM) model and (b) hungry-horse (HH) model and (c) stochastic hungry-horse (SHH) model (amplified).

4.2.4.4 Assessment of hull girder ultimate strength

Deterministic approach

The results from the hull girder NLFEA simulations are presented here in order to investigate the effect of initial imperfections on the ultimate load carrying capacity of the target vessel. Results of bending moment versus curvature $M-\chi$ curves are presented in Figure 4.17 for all the described imperfection models, including the perfect geometry and the average stochastic imperfection model. In the latter case, representative average values of the field ($\overline{w}_0/t_p = 0.231$, $\sigma_X/t_p = 0.051$, $\ell_c/a = 0.332$) are selected under a common reference base between the imperfect models.

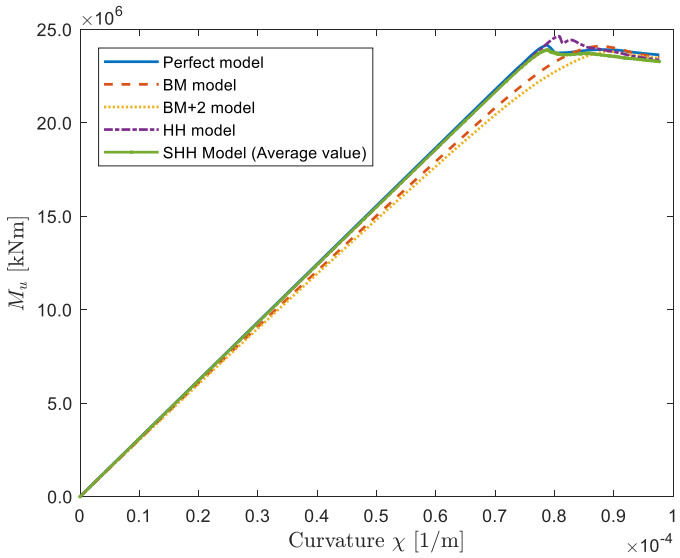

Figure 4.17. Bending moment M vs. curvature χ diagram derived from NLFEA adopting different imperfection models.

It can be seen that the response of all the models, except that of the BM model, displays a linear behavior up to about 90% of the maximum bending moment capacity when a sudden decrease of bending stiffness takes place. On the other hand, the BM model loses its stiffness gradually as a result of the a priori imposed mode of failure. Using two modes higher than the elastic-buckling half-waves on the plates ($m_x = m_x + 2$), a slightly decreased magnitude of strength is obtained ($\sim 1.5\%$). This is in accordance with Ueda and Yao (1985) who concluded that one or two modes higher than the elastic-buckling mode usually gives the most conservative result when collapse behavior of panels is examined. This is also confirmed from the results of Figure 4.10 for plates. The hull girder ultimate bending capacity for all applied imperfection models is presented in Table 4.7.

Table 4.7. Hull girder ultimate bending capacity for different imperfection models.

Imperfection Model	**Ultimate Bending Capacity** $(\mathrm{MN} \times \mathrm{m})$
Perfect	$24{,}154$
Buckling-mode (BM)	$24{,}101$
Buckling-mode (BM+2) $(m_{\mathrm{x}} = m_{\mathrm{x}} + 2)$	$23{,}815$
Hungry-horse (HH)	$24{,}638$
Stochastic HH (average)	$23{,}843$
IACS CSR Smith's model	$24{,}013$

Another interesting fact observed from the results of Table 4.7 is that the BM model gives slightly higher predictions than the stochastic average model. At a first sight, this contradicts with the results of Figure 4.10, where the BM model is the most conservative one. However, the progressive collapse analysis of a hull-girder is a much more complex phenomenon than the one of a plate. When hull-girder analysis takes place, three initial distortion components (global distortion, stiffener distortion and plate distortion) that are considered as critical, when examined individually, are linearly superimposed. In doing so, there is no evidence that this superimposition leads to the minimum possible buckling or collapse capacity when the "buckling-mode" imperfection model of plates is applied. It is clear from the above analyses, that the shape and amplitude of the initial deflections as obtained from the stochastic imperfection model can lead to a more conservative prediction of the overall ultimate strength.

A detailed picture on the deck structure at the time of collapse is presented in Figure 4.18 for the BM, the HH and the average stochastic model. The vertical displacement field on the deck plates, along with the Von Mises stresses distribution is illustrated. The conventional imperfection models exhibit a symmetry that is observed on the deflection patterns, both on the vertical deflections of plates, as on the transverse deflections of longitudinal stiffeners. This symmetry vanishes when the random field is applied. Apparently, the reality approaches the asymmetric condition of the stochastic field patterns.

Probabilistic approach

The probabilistic evaluation of hull girder strength applying the recommended SHH imperfection model follows. Neural networks have been successfully trained in order to provide a rapid mapping between the input uncertain parameters of the stochastic field, i.e., w_0 and σ_X and the hull girder ultimate strength M_u. Latin-Hypercube (LH) technique proposed by

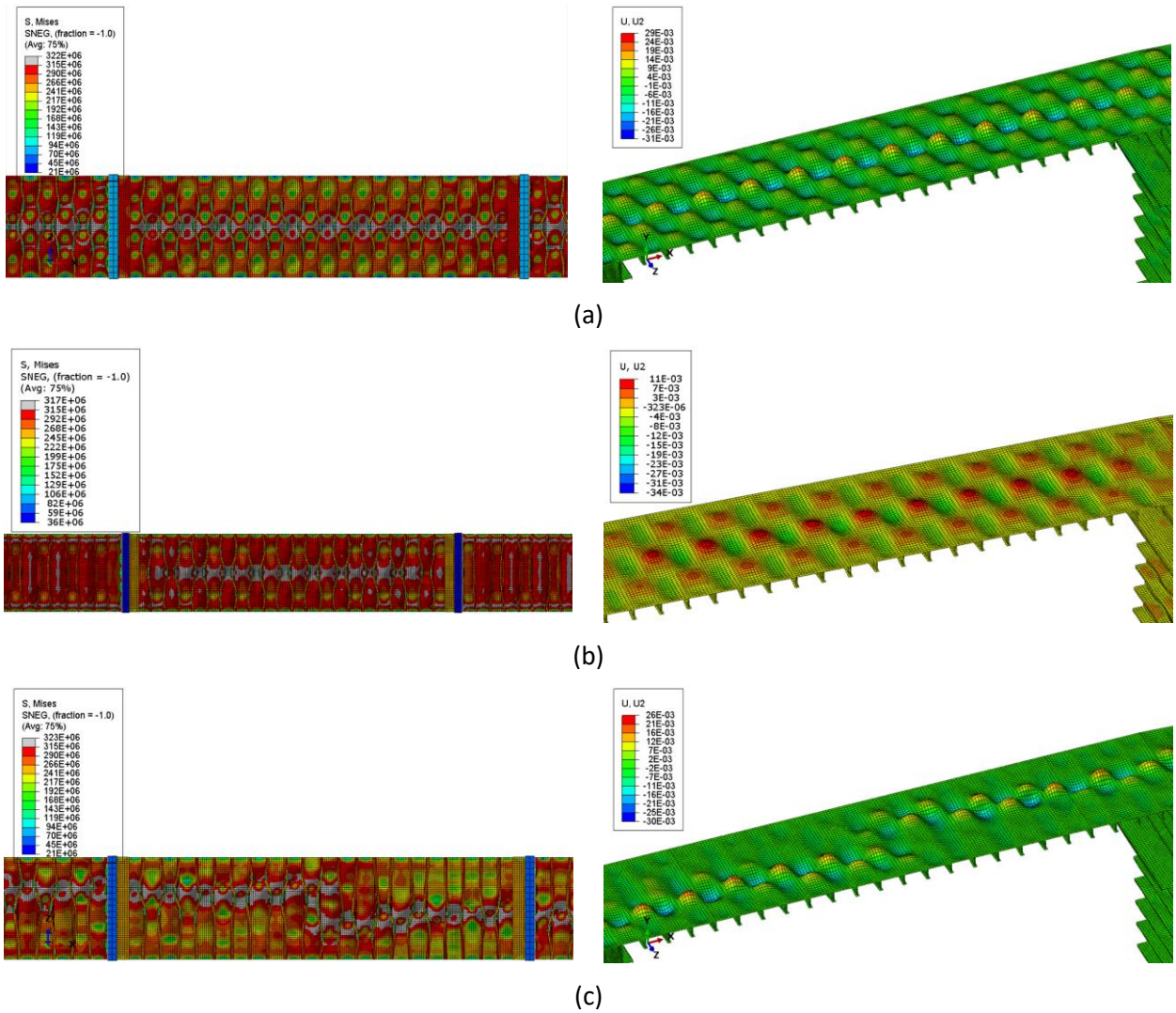

Figure 4.18. A close-up view on the center cargo tank deck panels indicating the Von Mises stresses (left column) and vertical displacements (right column) when ultimate strength is reached. From top to bottom: a) buckling-mode, b) hungry-horse and c) mean stochastic imperfection model (amplified).

Stein (1987) has been used to sample uniformly in the input space considering that the two parameters act independently on each other. A number of 40 training points (input pairs) have been generated and used to obtain an equivalent number of target output data by performing NLFEA simulations. Regarding the network's architecture, one hidden layer has been selected for all tested configurations, whereas the number of neurons is examined. The predominant network configuration has six neurons in the hidden layer, two fixed input variables and one output (abbreviation: $2-6-1$). The performance of the best network is presented in Table 4.8. The network's performance is translated in terms of standardized mean square error (MSE), maximum error and mean error percentage of the test subset data.

A number of 10,000 samples is generated using MCS and an equivalent number of output samples is obtained using the selected NN in trivial computational time. The mean value and coefficient of variation of hull girder ultimate strength are presented in Table 4.9. The low magnitude of coefficient of variation CoV indicates a low variability on the resulted ultimate strength that is due to the consideration of amplitude measures (mean value and standard deviation) as random variables. The histogram of the output response is illustrated in Figure 4.19. A kernel distribution is fitted to the data.

Table 4.8. Performance of the selected NN architecture.

NN configuration	**MSE**	**Max error** (%)	**Mean error** (%)
$2-6-1$	0.008	0.26	0.074

Table 4.9. Sample mean and coefficient of variation of ultimate bending capacity.

Number of samples	**Mean value** $(\mathrm{MN}\times\mathrm{m})$	**CoV**
10,000	23,790	0.007

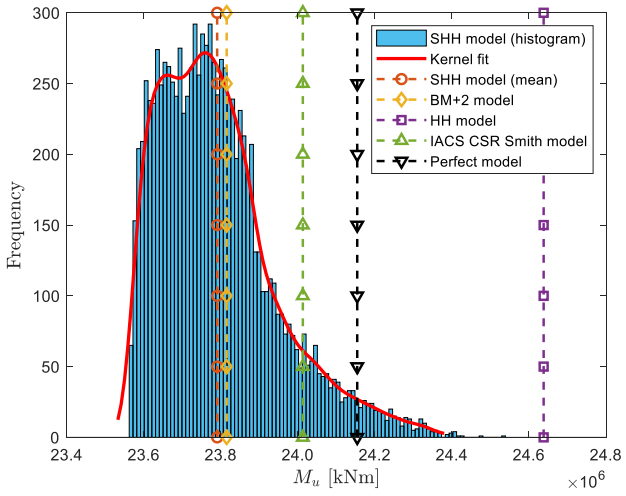

Figure 4.19. Histogram of the stochastic ultimate strength when 10,000 samples are generated using Monte Carlo simulation. Comparison with the conventional imperfection models and the IACS CSR Smith's incremental-iterative method.

The outcomes from the different models adopted in the present study are also presented in Figure 4.19. The resulted ultimate bending capacity of the proposed imperfection model (mean value) is lower than that of the idealized HH imperfection model by approximately 4%. A reasonable explanation of the above is the fact that the straight path that is present on the

idealized HH model prevents the development of localized wave-lengths along the panel which in turn, trigger the buckling to occur more rapidly. This difference is more profound (about 7%) in the case where the idealized HH model is applied without considering the 10% difference in the amplitudes of initial deflections between the adjacent plates (see also the results of Table 4.7). In the latter case, the imposition of the same amplitude and shape in the same direction restrains the plate buckling because of no presence of the asymmetric deflection component. On the other hand, the stochastic imperfection model produces the same levels of strength with the BM imperfection model, when in the latter model, two modes higher than the elastic-buckling mode are selected for local plate deflection. The resulted hull girder ultimate bending moment capacity by the IACS CSR Smith's model is also indicated for comparison and validation issues. The deviation between Smith's model and NLFEA when no imperfections are applied (perfect model) is less than 1%, revealing a very good agreement between the two models.

4.2.5 Concluding remarks

A new approach capable of simulating the spatial inherent randomness of initial geometric imperfections of ships' steel plates has been introduced in Section 4.2. Localized random initial deflections observed at the geometry of real steel plates motivate the use of random fields theory for their representation. The statistical description of the generated field, including the first/second order statistics and its autocorrelation form, is determined by exploiting actual data found from literature sources. The impact of the proposed stochastic imperfection model on the probabilistic-based ultimate strength assessment of plates (see Section 4.2.3) and hull girders (see Section 4.2.4) has been investigated.

The main findings out of this study are summarized as follows:

- The proposed stochastic HH imperfection model provides a very good agreement with the actual predictions of plates' ultimate strength (see Section 4.2.3). For the examined dataset, the conventional/idealized HH imperfection model generally overestimates the true ultimate strength, while it performs well only in cases where localized dents are not very profound in steel plates. On the other hand, the more theoretical BM imperfection model seems too conservative on its predictions.

- The ultimate strength assessment of plates is governed by the presence and magnitude of localized dents (see Section 4.2.3.3). This fact has been initially reported by Smith et al. (1988), and Dow and Smith (1984) and is confirmed here. It has been verified that the proposed stochastic imperfection model is able to generate such an imperfect geometry.

- With respect to hull-girder ultimate strength assessment, the proposed stochastic HH imperfection model gives closer estimates with the BM model than the idealized HH

model (see Section 4.2.4.4). Application of the conventional HH model result in about $1.0 - 4.5\%$ higher strength predictions than the stochastic one. This is something that should be considered from the scientific body, as conventional HH mode is generally associated with "realistic" operational conditions. In addition, variations on the statistics (mean value and standard deviation) of the stochastic imperfection model leads to very low levels of variability on the overall strength ($\mathrm{CoV} < 1\%$). This is due to the fact that hull girder collapse is dominated from the global/column-type mode, not the plate's collapse mode. Application of the stochastic imperfections on the global mode would possibly result in larger variations of overall capacity. This issue remains open for future research.

- Uncertainties considered on the parameters of the model (mean value, standard deviation and correlation length) can be represented by appropriate distribution models. As soon as more data become available, this can be used to refine/update the initial knowledge on the above parameters and improve predictions.

- The proposed stochastic imperfection model is able to account and quantify effectively different shapes of imperfections through the adjustment of the correlation length parameter ℓ_c. This is extremely useful in practice because the representation of actual hull geometry can be captured, e.g., after measurement inspections on construction stage or in-service, and further analyzed using FEM tools.

- A surrogate model (neural network) has been developed that is able to be learned with rather limited training samples of NLFEA and generalize effectively by retaining the accuracy of NLFEA and at the same time, reducing by orders of magnitudes the computational effort needed. The full spectrum of input uncertainties associated with the imperfect hull geometry is explored and a full probabilistic description of hull girder ultimate capacity is achieved. This is especially useful when a reliability assessment is subsequently carried out and the full PDF is required, without the need to employ the incremental-iterative Smith method.

Overall, it should be noted that for the establishment of the proposed stochastic imperfection model, and its use for design or assessment purposes in ship structures, further data should be acquired - both in as-built and in-service conditions - to tune the statistics and the autocorrelation form of the proposed model. Moreover, application of a similar stochastic model on the local sideways stiffener's deflection and global (column-type) deflection modes could be performed when up-to-date information from different types of ships and structural configurations becomes available.

4.3 The effect of non-uniform thickness variability on the ultimate strength of stiffened plate elements

4.3.1 Background

General (or uniform) corrosion is commonly idealized by uniformly reducing the thickness of a plate element. In reality, however, steel plates exhibit non-uniform thickness variation. Methods to simulate general corrosion have been primarily restricted on uniformly reducing the thickness of the plate element. Nevertheless, with the advancement of computer capabilities, more sophisticated modelling techniques that try to simulate the actual uneven patterns of thickness distribution over the surface of a steel plate have been emerged. In this direction, the framework of random fields can be used to model explicitly the spatial uncertain character of general corrosion.

During the last years, particular interest has been placed on the impact of thickness non-uniformity on the ultimate strength reduction under in-plane compressive loads of aged steel plates exposed in marine environments. A review study upon this subject can be found in Wang et al. (2014). Various discretizing techniques of random fields generation for representing thickness uneven patterns have been used, including the EOLE method, see e.g., Teixeira and Soares (2008), the spectral representation method, see e.g., Rahbar-Ranji (2012) and the KL expansion method, see e.g., Woloszyk and Garbatov (2020). Parametric studies for different correlation lengths and aspect ratios of plates have been carried out and results have been compared against random uniform reduction of thickness. Rahbar-Ranji (2012) used the spectral representation method based on an empirical construction of the power spectrum from actual data of scanned plates. Woloszyk and Garbatov (2020) tuned the parameters of the stochastic field based on experimental measurements and they additionally examined the effect of irregularities on the reduction of material mechanical properties.

The present study investigates the influence of non-uniform thickness distribution on the ultimate strength of a representative stiffened plate element subject to compression. The study aims at evaluating the validity of uniform thickness reduction in the formulation of analytical LSC. The stochastic variability of thickness is represented through a two-dimensional homogeneous non-Gaussian random field. The spectral representation method is employed to generate realizations of the stochastic field. The stochastic response of the system's output, i.e., stress-strain curves and maximum stress, is obtained by means of MCS method. A case study for a deck stiffened panel of a VLCC tanker is presented. The performance of the FE model is compared against the analytical LSC formulations prescribed by IACS CSR. Material properties' variation as well as residual stresses are neglected in this study for reasons of simplicity.

4.3.2 Description of spatial uncertain thickness variability

In the present study, the thickness loss over the surface of the plate element is described by a two-dimensional non-Gaussian homogeneous and isotropic random field as follows:

$$t(u_{\mathrm{x}}, u_{\mathrm{y}}) = \bar{t} + \hat{X}(u_{\mathrm{x}}, u_{\mathrm{y}}) \tag{4.10}$$

where, $\bar{t}$ denotes the mean thickness and $\hat{X}(u_{\mathrm{x}}, u_{\mathrm{y}})$ is a zero-mean 2D homogeneous stochastic field that describes the fluctuations of thickness around its mean value.

The random field is assumed to be *homogeneous* in the sense that its marginal distribution is invariant under arbitrary shift in space. In addition, the random field is assumed to be *isotropic*, i.e., its autocorrelation function is assumed to be independent of the direction. The above assumptions are rather rational since no evidence is provided proving the opposite side, i.e., that the corrosion process over the surface of a steel plate depends on the direction or its marginal distribution is dependent on specific locations.

Typically, a lognormal or a Weibull distribution model are used to quantify corrosion variability for given time instances of aged ship structures, see e.g., Guo et al. (2008), and Woloszyk and Garbatov (2020). Here, a Weibull distribution model is considered to describe the marginal distribution of thickness loss over the plate's surface. This selection is documented based on the data base provided by IACS (2016). The analyzed data, which are presented in Section 4.3.3.2, well fit to a Weibull distribution model[13].

The zero-mean 2D homogeneous random field is generated using the multidimensional spectral representation method proposed by Shinozuka and Deodatis (1996). As non-Gaussian sample functions are required, a translation process following Eq. (3.43) is adopted. The two-sided power spectral density function S_{XX} is assumed to correspond to an autocorrelation function of square exponential type whose functional form is given by:

$$S_{XX}(\kappa_1, \kappa_2) = \frac{\sigma_X^2}{4\pi} \ell_{c_1} \ell_{c_2} \exp\left[-\frac{1}{4}\left(\ell_{c_1}^2 {\kappa_1}^2 + \ell_{c_2}^2 {\kappa_2}^2\right)\right] \tag{4.11}$$

where, ℓ_{c_1}, ℓ_{c_2} denote the correlation length parameters that influence the shape of the field and they are proportional to the correlation distances of the stochastic field along the x, y axes, respectively. The correlation structure adopted herein has been assumed to be independent of

[13] It should be noted here that the consideration of Weibull distribution is based on data extracted from various sources. Here, we are interested in representing the thickness loss over the surface of specific plate elements. A more proper analysis would require a 3D scanning of the surface of the examined plate elements and a subsequent statistical processing. However, this information is not currently available.

the direction. This is equivalent to a *fully separable* correlation structure. In that case, the autocorrelation function, R_{XX}, takes the following form:

$$R_{XX}(v_1, v_2) = \sigma_X^2 \rho_{XX}(v_1)\rho_{XX}(v_2) = \sigma_X^2 \exp\left[-\frac{|v_1|^2}{\ell_{c_1}^2} - \frac{|v_2|^2}{\ell_{c_2}^2}\right] \tag{4.12}$$

where, v_1 and v_2 denote the relative distance between arbitrary locations in the x and y directions, respectively. It is noted that Eq. (4.11) and Eq. (4.12) are directly linked with an analytical relation based on the Fourier transform.

The selection of correlation length parameters ℓ_{c_1}, ℓ_{c_2} is selected based on available literature data. Previous studies performed by Rahbar-Ranji (2012), Neumann and Ehlers (2019), and Garbatov and Soares (2019) have indicated that, in general, a small correlation length (less than 100 mm) is appropriate to model the correlation structure of steel plate elements in aged ship structures. In the present study, the correlation length on the two directions has been chosen equal to $\ell_c = \ell_{c_1} = \ell_{c_2} = 50$ mm, which is in symphony with the above studies. More information for this selection is provided in Section 4.3.3.2.

4.3.3 Numerical investigation

The effect of model selection and quantification method is analyzed on a deck stiffened panel from a VLCC tanker that is subject to pure compression. In particular, the models used for the description of its structural performance in terms of a stress-strain relationship are: (i) the analytical LSC prescribed by IACS CSR, and (ii) the FE method, which is examined in terms of non-linear material behavior and non-linear geometry. The uncertainty quantification techniques applied for the description of thickness are: (i) the Random Variable (RV) approach and (ii) the Random Field (RF) approach. Overall, three different case studies are examined:

1. IACS CSR analytical LSC using uniform thickness (RV approach)
2. SFEM using uniform thickness (RV approach)
3. SFEM using non-unform thickness (RF approach)

In the framework of SFEM, Monte Carlo simulation (MCS) in conjunction with Latin-Hypercube technique is employed to propagate the input thickness uncertainties through the system and evaluate the ultimate strength of the stiffened plate panel model by means of statistical terms. A step-by-step process followed to embody a stochastic framework approach in a general-purpose finite element software such as Abaqus is provided in Georgiadis and Samuelides (2021)b.

The analytical LSC formulations of IACS CSR take into consideration three different failure modes: (i) beam-column buckling, (ii) torsional buckling and (iii) web local buckling. For brevity, the analytical relationships for these formulations are not given herein and the reader is referred to IACS (2019).

4.3.3.1 FE modelling

The FE model adopted in the present study is illustrated in Figure 4.20. The length of the model extends between a $1/2 + 1 + 1/2$ span and its breadth over a $1/2 + 1/2$ bay. The above FE range is selected based on the recommendations from Tanaka et al. (2014). The aspect ratio of length over breadth in the mid-span region is equal to 5.6. The material behavior is assumed to follow a bilinear elastic-plastic model and the steel used for the construction of the stiffened panel is a high-tensile steel of AH-32 type. The nominal values of material properties are listed in Table 4.10 along with the geometric characteristics of the stiffened panel.

The buckling and ultimate strength of plates and stiffened panels are closely related to the plate slenderness ratio β_p and the column slenderness ratio λ_c. The examined stiffened panel results in $\beta_p = 2.0$ and $\lambda_c = 0.42$ using the as-built scantlings. According to a survey carried out by Zhang and Khan (2009) on the structural design of 12 double hull oil tankers and 10 bulk carriers, the present values of the examined stiffened panel are typical for such types of ships and close to the average values.

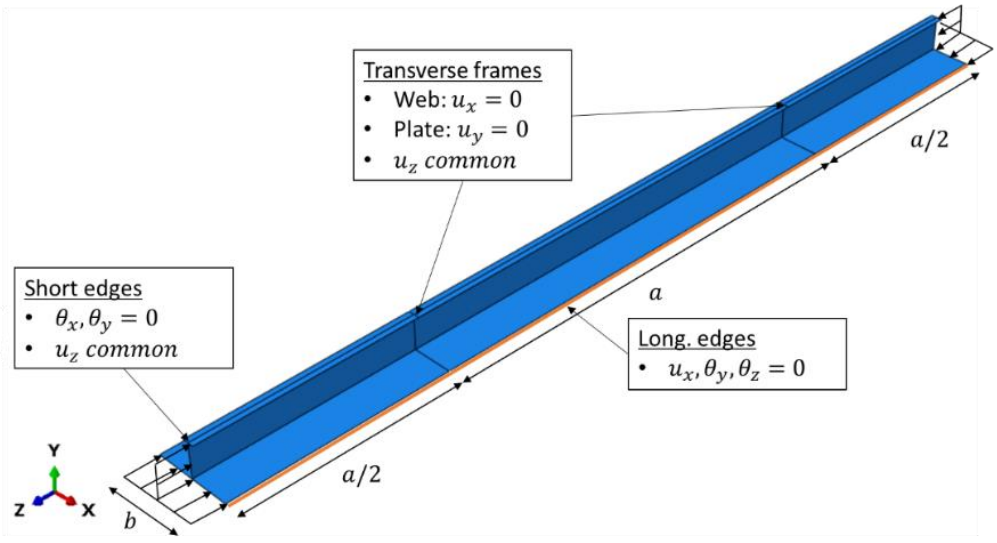

Figure 4.20. FE model of the examined deck stiffened panel subject to uniform compression.

Table 4.10. Stiffened panel's geometric and material characteristics.

Item	Symbol	Value	Units
Plate length	a	5120	mm
Plate width	b	910	mm
Plate thickness	t_p	19.5 (17.5) *	mm
Web height	h_w	400	mm
Web thickness	t_w	15.0 (13.0) *	mm
Flange breadth	b_f	130	mm
Flange thickness	t_f	20.0 (18.0) *	mm
Yield stress	σ_y	315	MPa
Young's modulus	E	206	GPa
Poisson's ratio	ν	0.3	-
Tangent modulus	E_t	1000	MPa

*As-built (CSR net-50 thickness).

The FE model is subject to uniform compression at its free end edges. The effect of transverse web frames has been modelled applying a restriction of plate's displacement in the vertical direction and a restriction on web's displacement in the transverse direction. Also, it is assumed that displacement in the longitudinal direction for all nodes is equal. A symmetry condition along the unloaded longitudinal edges has been imposed, i.e., $u_{\mathrm{x}} = r_{\mathrm{y}} = r_{\mathrm{z}} = 0$. In the loaded end edges fore and aft, a uniform compression has been applied and a restriction for the x-y plane to remain vertical.

A dynamic implicit solver (quasi-static analysis) has been used in order to overcome any instabilities present when static algorithms are employed. It is ensured that the kinetic energy arises for the whole model during the simulation is negligible.

The discretization of the FE model is executed using the quadratic four-node shell elements of reduced integration (S4R). First, a mesh convergence study has been carried out indicating that a 50 mm element size is sufficient to achieve an acceptable solution. However, a more refined discretization using a 25mm element size has been adopted for the region between the unsupported length of the panel in order to sufficiently capture the random field fluctuations (see also Section 4.3.3.2).

Values generated from spectral representation are assigned on the centroid of each element using the midpoint method. Therefore, the thickness of each element is represented by a single random variable. The nodes are located on the middle surface of the shell element and therefore, discontinuities localized at the element boundaries (bottom and top surface) exist. In

general, the midpoint method tends to over-represent the variability of the random field within each element. However, the error induced is almost negligible, especially in our case where a very fine mesh has been used on the area of interest.

The use of solid elements for the description of thickness random fluctuations has been rejected due to the high computational effort required. Moreover, it has been shown that differences between shell and solid elements on the collapse strength of steel plates are slight, see Teixeira and Soares (2008).

4.3.3.2 FEM stochastic thickness representation

Marginal distributions

The marginal distributions used for the description of corrosion wastage t_c for the plate, the web and the flange members of the examined deck stiffened panel are determined based on the CSR empirical database, see IACS (2016). Two candidate analytical distributions have been selected to fit the empirical distributions: the lognormal and the Weibull distribution. The analytical distributions are determined to match the target mean value and standard deviation of the collected data. Then, the 50%, 90%, 95% and 97.5% quantiles between the target and analytical distributions are compared. It is shown in Georgiadis and Samuelides (2021)b that the Weibull distribution is the best representative for all structural members since the statistical descriptors of the Weibull distribution model give a better approximation of the corresponding data, especially on the tails of the data. In summary, the marginal distributions used for the description of the corrosion wastage t_c variation are given in Table 4.11. The marginal PDFs of net-50 thickness $t_{\mathrm{n}-50}$ are finally obtained by application of Eq. (2.15).

Table 4.11. Marginal distributions for the description of corrosion wastage t_c at the 25-year design life. The empirical database by IACS (2016) with over 600,000 measurements from bulk carriers and oil tankers has been used to fit the empirical data with the analytical Weibull distribution model.

Structural member	Distribution	Mean value (mm)	Standard deviation (mm)
Plate	Weibull	1.73	0.995
Web	Weibull	1.25	0.590
Flange	Weibull	1.21	0.570

Correlation structure and FE discretization

The correlation structure of the generated random fields is described by the 2D power spectrum and the associated autocorrelation function of Eq. (4.11) and Eq. (4.12), respectively. The correlation length parameter has been chosen equal to $\ell_c = 50$ mm (see Section 4.3.2).

This value satisfies the condition of aliasing (see Eq. (3.56) - (3.57)), as well the following criterion, suggested by Sudret and Der Kiureghian (2000), that relates the appropriate random field mesh size with the correlation length parameter:

$$\text{RF mesh size} = \frac{\ell_c}{4} \sim \frac{\ell_c}{2} \tag{4.13}$$

Taking into consideration the above, an approximate RF mesh size of $25\ \text{mm}$ is adopted. The structural mesh on the area of interest (between the unsupported length) is forced to be equal with the RF mesh. The selected magnitude of the correlation length parameter implies practically that finite elements in a close area (approx. $100 \times 100\ \text{mm}$) act independently from the adjacent areas.

Cross-correlation structure

Statistical independence between the generated fields of each structural member, namely, plate, web and flange, is considered. In reality, it is very likely that a certain degree of cross-correlation might exist between the thickness waste for different structural members exposed in the same environmental conditions. However, the hypothesis of independence between the random fields is true due to the following reasoning. As the correlation length tends to infinity the random field tends to approximate the random variable approach since a full dependence between all locations exists. In such a case, cross-correlation is as important as in the RV approach case study. On the other hand, when correlation length approaches zero (white-noise random field[14]), as in the present examined case, all the elements act independently from each other and hence, the existence of cross-correlation becomes negligible. In addition, Graham and Deodatis (2001) have shown that cross-correlation effect does not influence considerably the response variability when static problems are treated (it is shown that this remark is not valid when a dynamic random eigenvalue problem is examined). Overall, it becomes apparent that the statistical independence assumption will not practically influence the accuracy of the results for the case of RF approach.

For the case of RV approach, a correlation matrix between the input random variables must be established, as this may have an influence on the response quantity of interest. It is reasonable to assume that a strong correlation exists between the web and the flange of the stiffener due to the fact that these members are exposed on the same corrosive environment. On the other hand, deck's plate surface is displayed on two different environments. Therefore, it is considered reasonable to select a moderate dependence between plate and stiffener's members. Finally, a correlation of $\rho = 0.8$ is selected among stiffener's members thickness reduction and a value of $\rho = 0.5$ among the plate and stiffener' members. Figure 4.21 provides

[14] A white-noise is a stochastic field that is characterized by complete randomness.

an overview of the dependence between the three input random variables, i.e., plate, web and flange thickness waste. In the same figure, a number of samples has been generated using the Latin-Hypercube technique. In the diagonals, the histogram of each corresponding random variable is displayed.

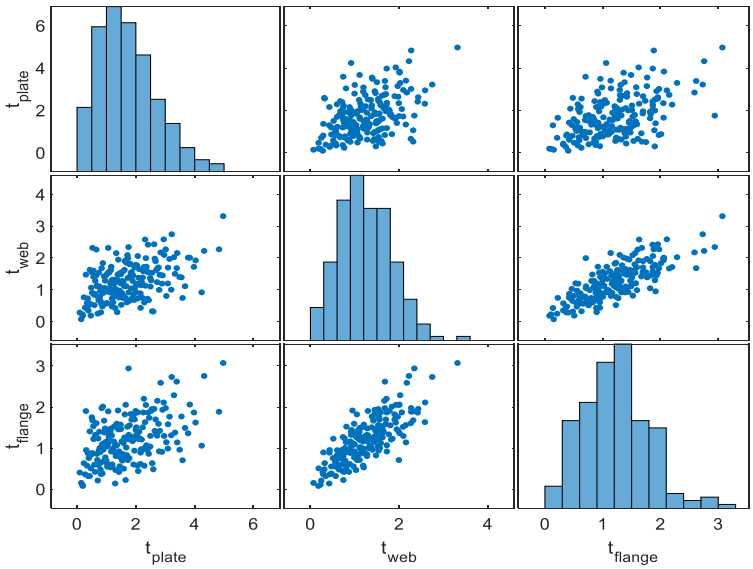

Figure 4.21. Multivariate scatter plot of the thickness waste reduction in mm for plate, web and flange adopted for uniform thickness reduction (RV approach).

A random realization of the adopted random field is presented in Figure 4.22 for the surface of plate, web and flange. It can be observed that an excellent match between the target statistics and the sample functions has been obtained in terms of marginal distributions. A random realization for the uniform (RV) and non-uniform (RF) thickness approach on the examined FE model is illustrated in Figure 4.23. Since the critical failure mode occurs at the mid-span region of the FE model, thickness variation has been applied solely on this area. Thickness magnitudes outside the mid-span region follow the as-built scantlings.

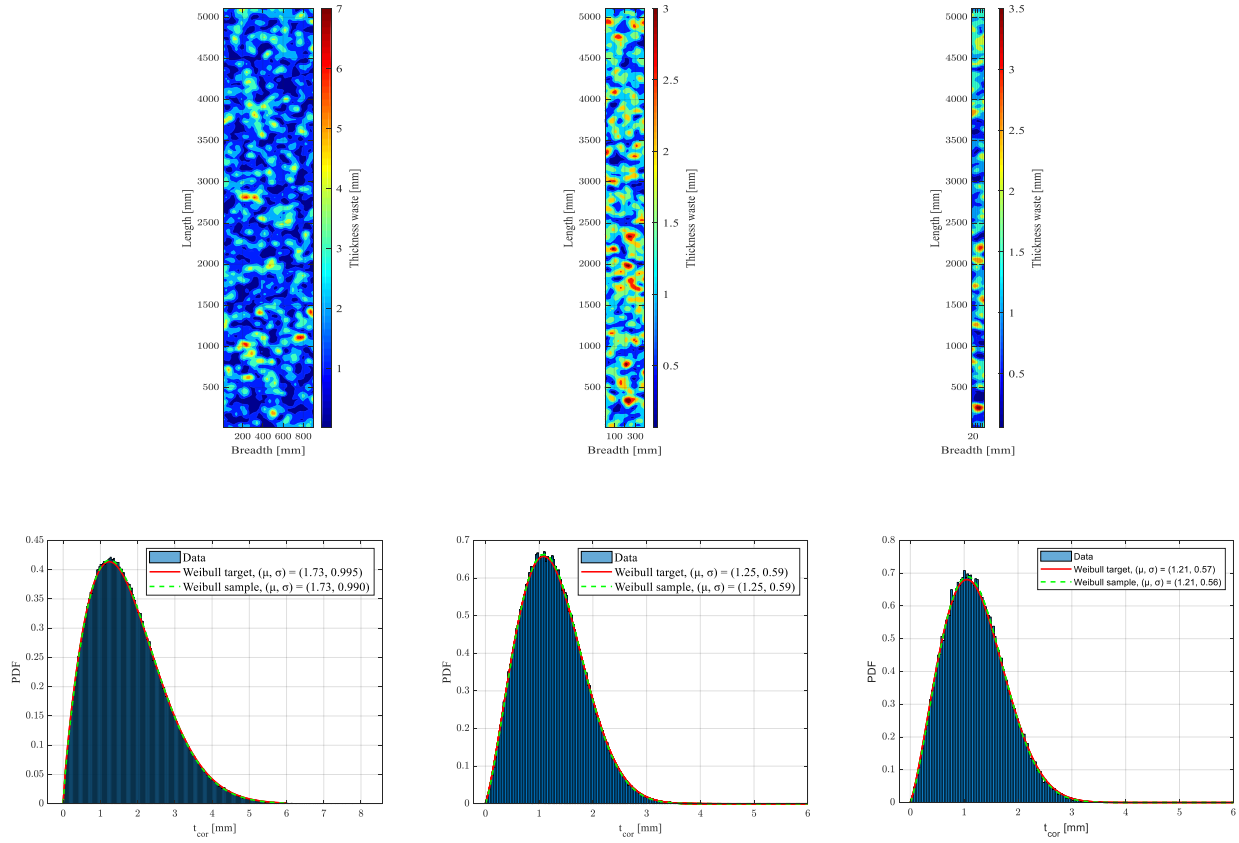

(a) (b) (c)

Figure 4.22. A realization of the 2D thickness RF for (a) plate, (b) web and (c) flange using the pre-assigned target distribution models and correlation structure.

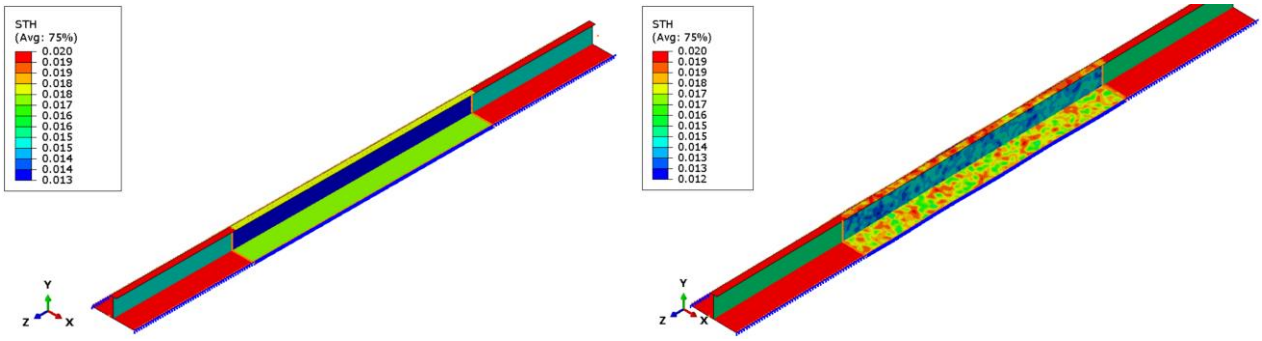

(a) (b)

Figure 4.23. A random realization of random thickness using (a) the RV approach and (b) the RF approach on the FE model under examination.

4.3.3.3 Results

A preliminary study is first implemented between the numerical FE model and the analytical LSC curves from CSR using the net-50 scantling approach. The results from the analysis are presented in Figure 4.24a in the form of normalized stress-strain curves. The normalization of stresses takes place using the yield strength of the material and that of strains using the yield strain. It is found that a very good agreement between the two different models exists when the critical failure mode of CSR is taken into consideration. The ultimate stress is equal to $\sigma_u = 262$ MPa for NLFEA and $\sigma_u = 258$ MPa for CSR model. Failure occurs under flexural-torsional buckling mode in both models. This can be seen from the contour plot of Von Mises stresses in Figure 4.24b.

It is noted that the hardening effect model which is taken into account in the NLFEA has a very slight effect on the maximum strength and the overall structural behavior, while the failure mode does not change. The incorporation of hardening effect on the FE model has been selected to give a more realistic perspective of the actual material behavior.

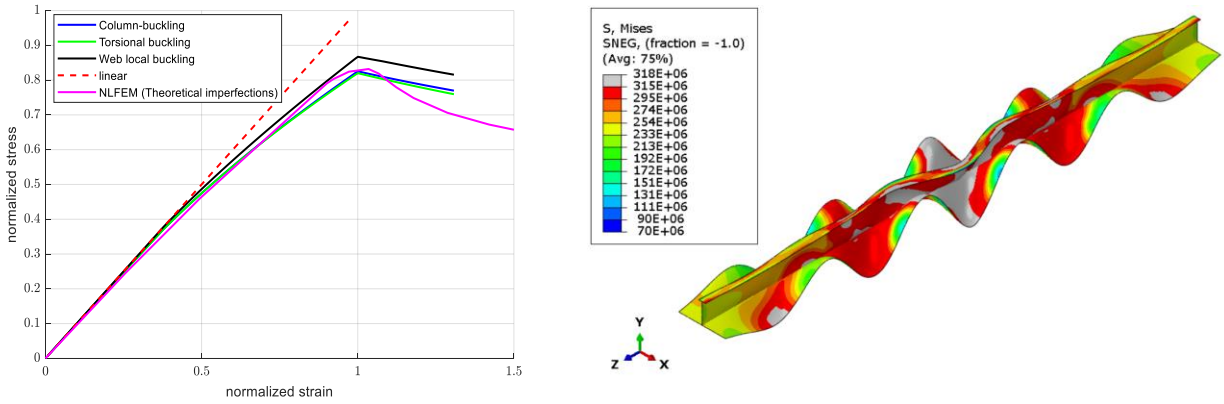

(a) (b)

Figure 4.24. (a) Normalized stress-strain curves under axial compression for the two different models; CSR and NLFEA. (b) Collapse mode of the examined stiffened panel using NLFEA (amplified). Grey color indicates the zones beyond the yield strength point.

The results from the stochastic modelling of thickness variation follow. The geometric location of ultimate stresses is presented in Figure 4.25 for the RF and the RV approach, along with the normalized stress-strain curves of CSR using the net-50 scantlings. MCS-LHS has been adopted using a sample size of $K = 200$, which is considered satisfactory for the particular problem to achieve convergence on the output sample statistics. A large variation is observed in the normalized stress when the RV approach is used. In contrast, when the RF approach is used, the variation on ultimate stress seems almost negligible. It is of interest that, in the case of the FE

analyses, a variation on the normalized strain occurs for both RV and RF approach with a degree of variability equal to 1.5% and 2.3%, respectively. This variation is more apparent in the RF approach (see Figure 4.25). This is due to the fact that curves do not exhibit a pronounced peak value (a stable plateau is observed), as opposed to the RV approach, where the generated curves display a smoother behavior when reaching the peak region (see Figure 4.26). In addition, interpolation between equilibrium points as those defined by the quasi-static solver of numerical analysis may lead to a shift of the peak to the left or the right.

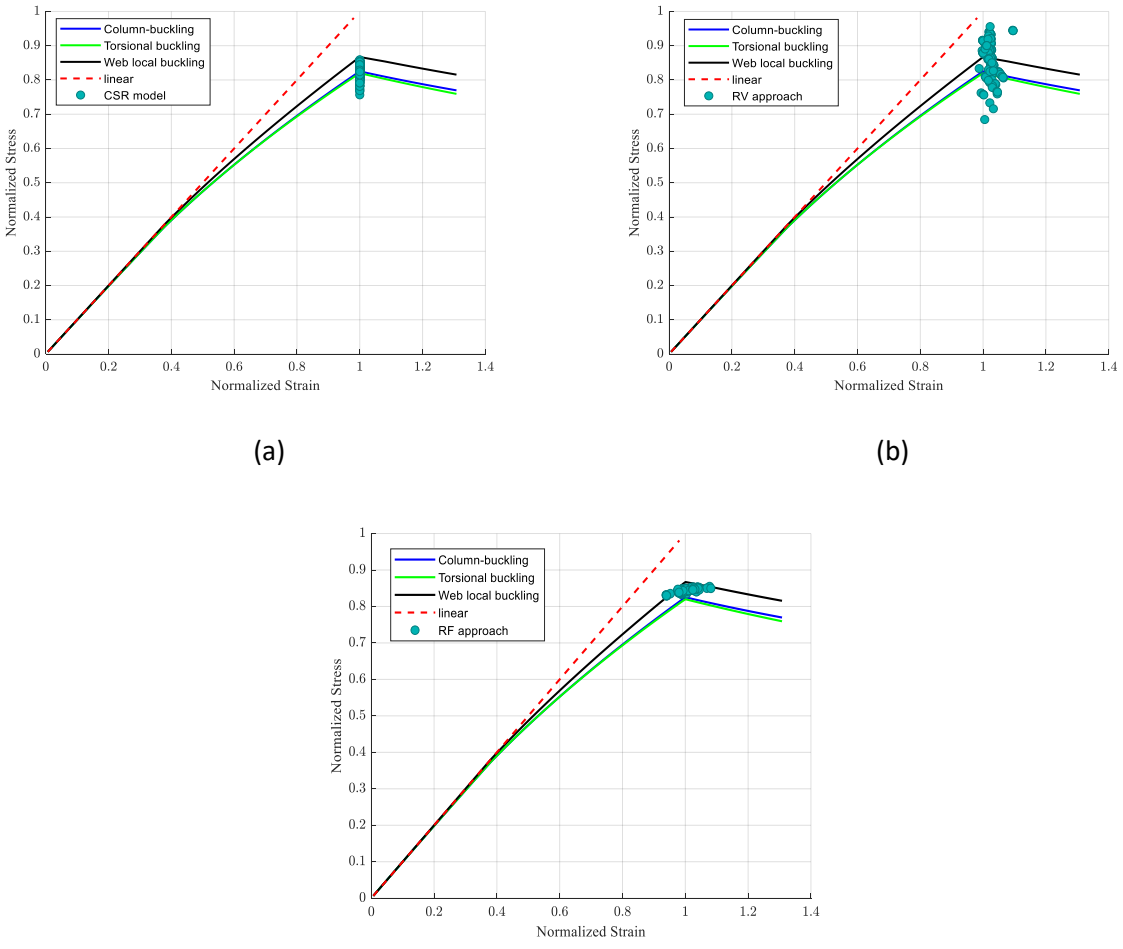

Figure 4.25. The geometrical location of maximum stresses using (a) IACS CSR LSC, (b) RV approach using SFEM, and (c) RF approach using SFEM. The three curves depict the results using IACS CSR net-50 scantlings.

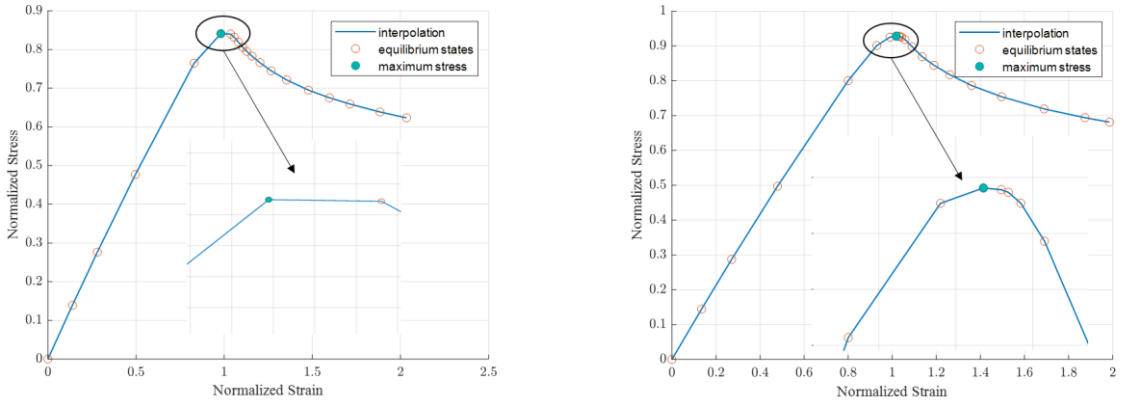

(a) (b)

Figure 4.26. A typical stress-strain curve generated from a single NLFEA with the (a) RF approach and (b) RV approach. A stable plateau is observed when RF approach is considered, whereas a more profound peak is displayed using RV approach.

Figure 4.27 depicts the corresponding histograms of ultimate stresses for the three different cases and the most appropriate distribution model fit. The quantification of output results with respect to the ultimate strength is summarized in Table 4.12. Using the SFEM, and the RF quantification method, the mean value of the maximum stresses is found to be 266 MPa, while the coefficient of variation is 0.7 %. For the same model and the case of the RV approach, a mean value equal to 271 MPa and a CoV of 5.6% is obtained. A comparison between the CSR and the SFEM when uniform thickness reduction is applied reveals a 4.2% difference in their mean values and a value of CoV more than two times for the SFEM. The above differences, although relatively small, can be attributed to model selection reasons and material hardening effects. The modeling of thickness non-uniformity has slight differences with respect to the magnitude of the mean value (about 2% for each model), but a more profound effect on the ultimate strength variability. The low degree of variability for the RF case is quite rational since a small correlation length has been selected for the modeling of spatial dependence.

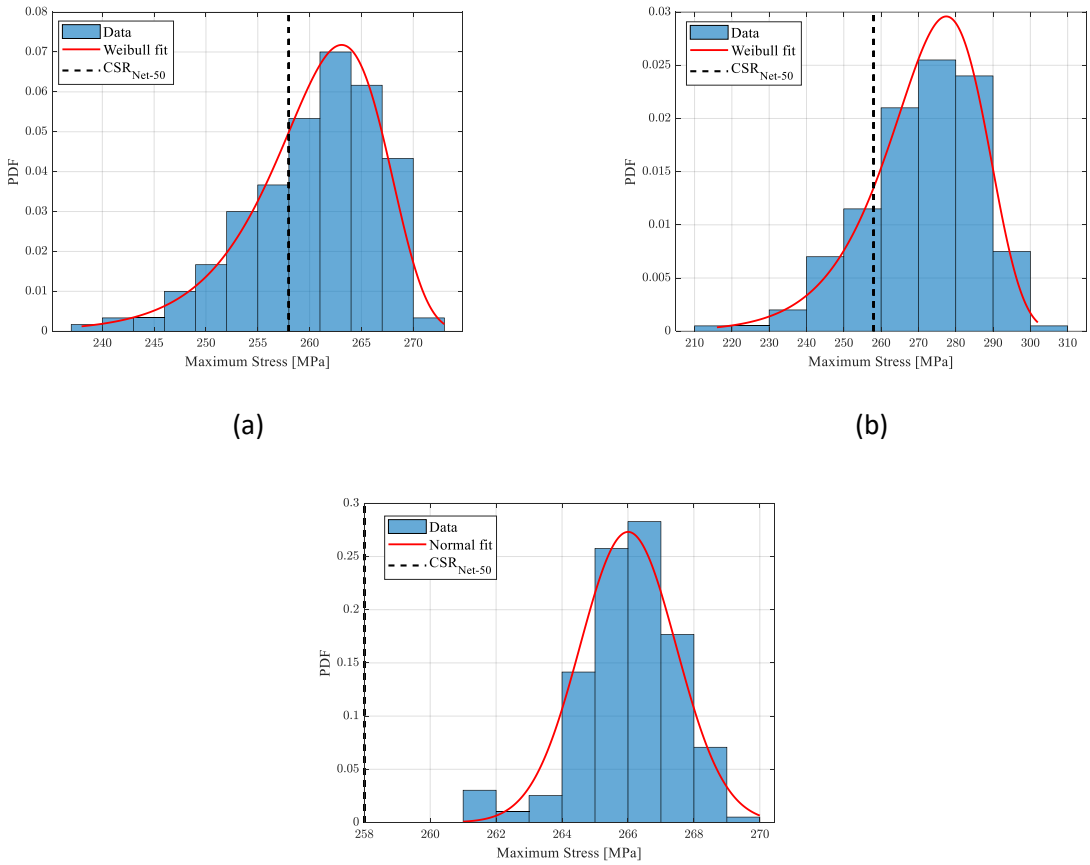

Figure 4.27. Histogram of maximum stresses for $K = 200$ along with fitted probability distributions. (a) IACS CSR approach (LSC), (b) RV approach, and (c) RF approach. IACS CSR net-50 result is given with a black dot line as a fixed quantity.

Table 4.12. Ultimate strength variability for different models and quantification approaches.

Model	**Quantification method**	**Mean value** (MPa)	**CoV** (%)	**Min value** (MPa)	**Max value** (MPa)
CSR	Deterministic	258	-	-	-
	RV approach	260	2.5	234	271
FEM	Deterministic	262	-	-	-
SFEM	RV approach	271	5.6	216	301
	RF approach	266	0.5	261	269

4.3.4 Concluding remarks

The computation of LSC prescribed by IACS CSR highly affects the hull girder ultimate bending moment capacity computed by Smith's method. The main scope of this study was to examine the assumption of uniform thickness reduction in the formulation of LSC. To this end, two different quantification approaches, i.e., a random variable (RV) and a random field (RF) approach, have been adopted for the simulation of uniform and non-uniform corrosion loss. Their influence is evaluated on the ultimate strength of a representative stiffened plate element, which is the main structural component for Smith's model implementation. In addition, the effect of model selection, i.e., FEM vs. analytical LSC, on the predicted ultimate strength has been investigated. The stochastic FEM framework has been employed to effectively combine the probabilistic modelling of input uncertain parameters and the well-founded finite element method technique for the solution of complex non-linear problems.

Summarizing, the following conclusions are drawn out of this study:

- The uniform thickness reduction adopted by LSC (IACS CSR model) provides a lower mean value (about 2%) and a much higher variability on the predicted ultimate strength against the non-uniform thickness reduction (SFEM RF approach). The latter approach displays this small variability due to the weak correlation structure adopted, that tends to simulate a white-noise stochastic field. In addition, the net-50 scantling approach leads to a below-average value for all probability density functions (see Figure 4.27 and Table 4.12). The above results indicate that the uniform thickness reduction in LSC is conservative and reasonable for the design of ship structures.

- The model itself has a considerable impact on the stochastic response of the structure. Particularly, the uniform thickness loss representation using the analytical curves of IACS CSR and the SFEM resulted in a 4.2% difference in their mean values and a value of coefficient of variation more than two times for the SFEM.

- The computational cost of RF modelling is much higher than the one of RV modelling approach.

It should be highlighted that the predicted probabilistic-based ultimate strength using the RF approach is highly dependent on the prescribed correlation structure. In the present study, literature sources have been used to establish a "realistic" correlation structure. However, in-situ information about the spatial distribution of thickness in aged structures is necessary to gain further confidence on the results. In addition, it would be more beneficial to develop a model on a vessel-specific basis or a fleet of sister vessels since spatial thickness distribution depends on many factors, including ship's age, operational profile, exact location, etc. Finally, as the results are based on a single case study, their generalization would require further research on various geometries of ship-type stiffened panels.

4.4 Main findings

An essential step in the course of this thesis is the construction of a high-fidelity FE model used for the hull girder ultimate strength assessment. In particular, an advanced FE model could explicitly accommodate various influencing factors, including spatially varying quantities such as imperfections, thickness and material characteristics[15], as well other phenomena, such as the double bottom effect observed in bulk carriers and container ships, the interdependence of failure modes between adjacent structural elements and so on. Such a model would be able to replace (missing) real-life results and update the model uncertainty associated with the simplified IACS CSR Smith's method[16]. The findings drawn from the present chapter contribute on the development of the aforementioned high-fidelity FE model with the following way.

From the perspective of imperfections, we concluded that the general impact of the applied stochastic model against the conventional deterministic imperfection models is considerable, but its variability on the resulted hull girder ultimate strength is quite small (see also Section 4.2.5). Therefore, a representative outcome of the hull girder collapse strength associated with the stochastic imperfection model application shall be used later in Section 6.2. In addition, the outcomes applying the BM and HH imperfection model shall be also employed.

From the perspective of thickness, the main finding was that RV and RF approaches give comparable results on the expected ultimate strength of the examined structure. As RV approach simulates in a satisfactory manner the corrosion diminution, and taking also into consideration the high computational cost associated with RF modelling, we do not consider it necessary to model the corrosion as a random field. Therefore, no modification is implemented in the formulation of LSC relationships of IACS CSR Smith's model. It is highlighted here that the modelling of thickness variability using random fields on such a large scale as that of a hull girder would be prohibitive since the modelling effort and the computational cost would be enormous. This is the reason why the non-uniform thickness representation has been tested on a representative stiffened plate element, which is the main structural component in the framework of Smith's incremental-iterative method.

[15] To the author's knowledge, data for the spatial variation of material properties, e.g., yield strength or Young's modulus, of structural elements used at the construction of a ship structure has not been found in the literature.

[16] The procedure for implementing the updating task is developed in Section 6.2.

5 Bayesian analysis

5.1 Introduction

Engineers are often faced with uncertainties related to the input parameters of a system and/or the model itself. At the same time, information related to the system's performance – often of limited amount – may become available in the form of observations, measurements or other sources, during the construction or operation. It is then desirable to quantify the effect of this information and combine it with existing knowledge (generally expressed in the form of initial distribution models) in order to reduce uncertainties and improve the performance of the system. *Bayesian analysis* framework provides a formal and systematic tool to implement this task, and is particularly appropriate when different sources and types of information need to be combined effectively.

In practice, different approaches can be applied to perform a Bayesian updating depending on the problem at hand. An outline of the different strategies applicable to the problem of Bayesian updating is illustrated in Figure 5.1. Let us consider a model $\mathcal{M}$ of the real physical system. Input uncertain parameters of the model are collected into a vector of random variables $\boldsymbol{X} = [X_1, \dots, X_n]^T$ with corresponding joint probability density function $f_{\boldsymbol{X}}(\boldsymbol{x})$. Often, the parameters that define the distribution model f_X of a single random variable X, such as the mean value and variance, can be uncertain. In that case, a random vector $\boldsymbol{\theta}$ can be formulated to characterize their randomness[17]. At any time, observations related to the system's performance or input parameters may become available. The scope of Bayesian updating is then to update the random vector $\boldsymbol{X}$ or $\boldsymbol{\theta}$ conditional on these measurements, either directly or indirectly. The procedure of using measurements associated with the system output $\mathcal{M}(\boldsymbol{x})$, e.g., deformations or displacements, to update the input uncertain model parameters $\boldsymbol{X}$ or $\boldsymbol{\theta}$ is commonly referred as *Bayesian inverse analysis*. On the other hand, if direct measurements of the QoI are acquired, e.g., measurements of yield stress from a steel plate, these can be used to learn its initial distribution model f_X either explicitly through X or implicitly through learning its associated parameters $\boldsymbol{\theta}$. The process of updating explicitly the distribution model f_X is a *classical Bayesian updating* problem, while the process of learning the parameters $\boldsymbol{\theta}$ of a distribution f_X is known as *Bayesian statistical inference* problem.

In this chapter, the fundamental theory of Bayesian analysis for application on common engineering problems is reviewed. Bayes' theorem is presented in Section 5.2 and reinterpreted in Section 5.3 for the updating of model input parameters $\boldsymbol{X}$, and in Section 5.4 for statistical inference on parameters $\boldsymbol{\theta}$. The selection of prior is discussed in Section 5.5 while the general

[17] Commonly, the uncertain parameters $\boldsymbol{\theta}$ that define a distribution model f_X are called *hyperparameters*.

formulation of the likelihood function is presented in Section 5.6. Finally, in Section 5.7, some basic methods to deal with the updating scheme are reviewed.

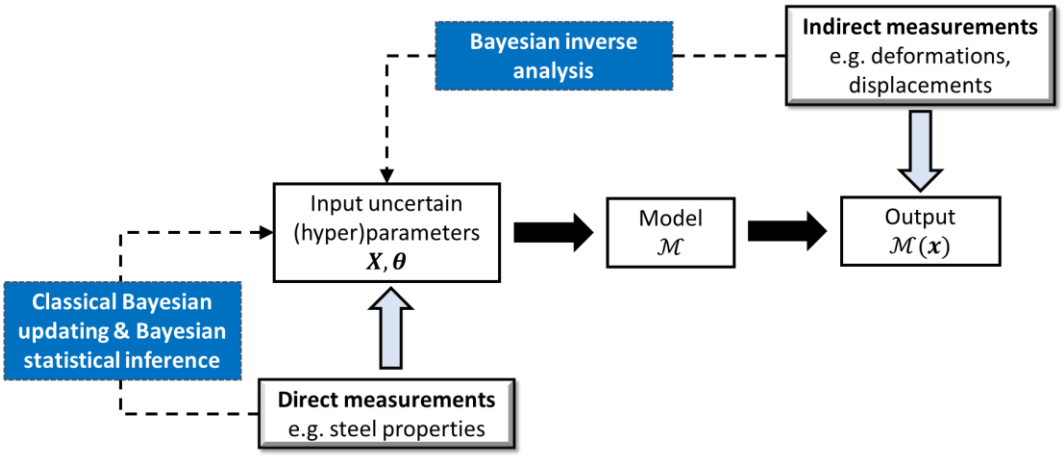

Figure 5.1. Outline of the Bayesian updating problem.

5.2 Bayes' theorem

Bayes' rule[18] describes how the conditional probability of an event A given the occurrence of another event E can be computed from the unconditional probability $\Pr(A)$ and from $\Pr(E|A)$. In a mathematical manner this is written as:

$$\Pr(A|E) = \frac{\Pr(E|A)\,\Pr(\mathrm{A})}{\Pr(\mathrm{E})} \propto \Pr(E|A)\,\Pr(\mathrm{A}) \tag{5.1}$$

In practice, Bayes' theorem provides a formal way to quantify the reduction in uncertainty on the event A through knowledge of the event E. Eq. (5.1) decomposes into three principal terms:

- $\Pr(A)$ is the *prior* probability, representing the knowledge before seeing the event E.
- $\Pr(E|A)$ is the *likelihood*, describing the probability of the event E given A to occur.
- $\Pr(A|E)$ is the *posterior* probability, representing the new knowledge on A after observing the event E.

[18] Named after Thomas Bayes (1701-1761), a British mathematician, philosopher and minister.

The proportionality constant in Eq. (5.1) signifies that $\Pr(E)$ can be ignored for the purpose of inference on A. The term $\Pr(E)$ is also a measure of the plausibility of the *evidence* and can be computed by application of total probability theorem.

Bayes' theorem can be extended to *discrete* and *continuum* random variables. The focus in this thesis is placed on the continuous case since all the numerical applications that are presented deal with continuous quantities.

5.3 Bayesian updating of model parameters

Consider a model $\mathcal{M}$ of a physical system and the associated uncertainties gathered into a vector of random variables $\boldsymbol{X} = [X_1, \dots, X_n]^T$ whose prior joint PDF is denoted by $f'_{\boldsymbol{X}}(\boldsymbol{x})$. The prior joint PDF describes the background knowledge about parameters $\boldsymbol{X}$. When information in observed data is acquired, this can be collected into a vector $\boldsymbol{d}$. The representation of this data set is performed through the formulation of the likelihood function $L(\boldsymbol{x})$. The posterior PDF $f''_{\boldsymbol{X}}(\boldsymbol{x})$ of $\boldsymbol{X}$ after observing the data $\boldsymbol{d}$ is then computed by application of Bayes' rule as:

$$f''_{\boldsymbol{X}}(\boldsymbol{x}) = {c_E}^{-1} L(\boldsymbol{x}) f'_{\boldsymbol{X}}(\boldsymbol{x}) \tag{5.2}$$

The posterior distribution can be also symbolized as $f_{\boldsymbol{X}|\boldsymbol{D}}(\boldsymbol{x}|\boldsymbol{d})$ to express how $\boldsymbol{X}$ vector changes conditional on the data $\boldsymbol{d}$. Similarly, the likelihood function can be also denoted as $L(\boldsymbol{x}|\boldsymbol{d})$ or $f_{\boldsymbol{D}|\boldsymbol{X}}(\boldsymbol{d}|\boldsymbol{x})$. It is stressed however, that the likelihood is a function of $\boldsymbol{x}$, even though it describes the probability of observing the measurement outcome[19]. Note that Eq. (5.2) is a generalization of Eq. (5.1) for continuous random variables. The constant c_E is a normalizing constant that ensures that the posterior PDF integrates to one.

$$c_E = \int_{-\infty}^{\infty} \dots \int_{-\infty}^{\infty} L(\boldsymbol{x}) f'_{\boldsymbol{X}}(\boldsymbol{x}) dx_1 \dots dx_n \tag{5.3}$$

In analogy with $\Pr(E)$ of Eq. (5.1), c_E is referred to as the model evidence and expresses the plausibility of the model $\mathcal{M}$. Usually, the difficulty in Bayesian updating lies in the evaluation of the constant c_E. Common methods for the solution of Bayesian updating problem will be reviewed in Section 5.7.

[19] Likelihood function states that: "Given a fixed parameter state of the system $\boldsymbol{X} = \boldsymbol{x}$, what is the probability of observing a particular set of data $\boldsymbol{d}$?"

5.4 Bayesian statistical inference

Bayesian statistical inference is closely related to classical statistical inference, see e.g., Ang and Tang (2007). In classical statistical inference, an unknown physical quantity is expressed by its distribution model f_X and its associated true – but unknown – hyperparameters $\boldsymbol{\theta}$. This distribution represents a "population" of the real physical system. When a data set (sample) of that population is observed, this can be used to estimate the true parameters of distribution model f_X. In other words, the exact values of the population parameters are generally unknown. The best that we can do is to estimate their values based on a finite set of samples (observations) of the population.

Common methods of classical statistical inference include the *method of moments* and the *maximum likelihood estimate* (MLE). The main difference between MLE and Bayesian statistical inference is the *prior*. In Bayesian statistics, a prior distribution is defined on the hyperparameters $\boldsymbol{\theta}$ of the distribution f_X to reflect our initial uncertain knowledge on them. Bayesian updating is well-suited in cases where the sample set observed is small and the existing information about the hyperparameters $\boldsymbol{\theta}$ is vague. In analogy with Eq. (5.2), the Bayesian updating problem now reads:

$$f''_{\boldsymbol{\theta}}(\boldsymbol{\theta}) = {c_E}^{-1} L(\boldsymbol{\theta}) f'_{\boldsymbol{\theta}}(\boldsymbol{\theta}) \tag{5.4}$$

The main difference from Eq. (5.2) is that all functions are now expressed with respect to the hyperparameters $\boldsymbol{\theta}$. The constant c_E is thus defined as:

$$c_E = \int_{-\infty}^{\infty} \dots \int_{-\infty}^{\infty} L(\boldsymbol{\theta}) f'_{\boldsymbol{\theta}}(\boldsymbol{\theta}) d\theta_1 \dots d\theta_n \tag{5.5}$$

As the interest in most applications usually lies on the evaluation of the basic random variable $\boldsymbol{X}$, one can apply the total probability theorem to derive the so-called posterior *predictive distribution* $\tilde{f}_X(x)$ of a single random variable X as:

$$\tilde{f}_X(x) = \int_{-\infty}^{\infty} \dots \int_{-\infty}^{\infty} f_{\boldsymbol{X}|\boldsymbol{\theta}}(x|\boldsymbol{\theta}) f''_{\boldsymbol{\theta}}(\boldsymbol{\theta}) d\theta_1 \dots d\theta_n \tag{5.6}$$

One can notice that the predictive distribution $\tilde{f}_X(x)$ is the expected value of $f(x|\boldsymbol{\theta})$ with respect to the posterior distribution of $\boldsymbol{\theta}$. The solution of the integral in Eq. (5.6) can be performed using the same approach followed for the computation of Bayesian updating problem. If, for example, samples from $f''_{\boldsymbol{\theta}}(\boldsymbol{\theta})$ are available, a Monte Carlo integration can be

adopted. On the other hand, if an analytical formulation for $f''_{\boldsymbol{\theta}}(\boldsymbol{\theta})$ is available, then an analytical expression is usually available for the predictive PDF as well.

In some cases, it is desirable to neglect the whole spectrum of (statistical) uncertainty associated with the hyperparameters $\boldsymbol{\theta}$ and obtain some *point estimators* for the posterior hyperparameters $\boldsymbol{\theta}$. The *posterior mean* is the most common Bayesian estimator derived as:

$$\widehat{\boldsymbol{\theta}}''_{\text{mean}} = \int_{-\infty}^{\infty} \dots \int_{-\infty}^{\infty} \boldsymbol{\theta} f''_{\boldsymbol{\theta}}(\boldsymbol{\theta}) d\theta_1 \dots d\theta_n \tag{5.7}$$

The *posterior maximum* or *maximum a-posteriori* (MAP) estimate is an alternative point estimate. It is the mode of the posterior distribution, i.e., the most likely value for $\boldsymbol{\theta}$:

$$\widehat{\boldsymbol{\theta}}''_{MAP} = \arg\max f''_{\boldsymbol{\theta}}(\boldsymbol{\theta}) \tag{5.8}$$

Note that for a non-informative prior distribution of $\boldsymbol{\theta}$, the posterior maximum estimate coincides with the classical *maximum likelihood estimate* (MLE). In general, the derivation of posterior maximum estimate should be preferred in cases where the uncertainty in the hyperparameters is small. When the uncertainty on the posterior is significant, the predictive distribution as defined in Eq. (5.7) should be utilized instead. However, the computation of MAP estimate is computationally advantageous over the mean estimate since it does not involve the solution of a multi-fold integral.

5.5 Prior distribution

Prior distributions play a vital role in Bayesian analysis and in most cases their selection is subjective. Priors represent our best knowledge on the uncertain model parameters $\boldsymbol{X}$ or $\boldsymbol{\theta}$ before seeing the data. The uncertainty on the parameters is expressed through the establishment of proper probability distribution models. Initial information may be acquired from different sources, such as experts' (subjective) knowledge, literature survey or previous observations on similar projects. In the framework of Bayesian analysis, it is feasible to effectively combine different sources of information. For instance, an expert's opinion can be used as prior information, and previous on-field observations as the remaining information to form the likelihood function.

Priors can have different levels of informativeness, see Van de Schoot et al. (2021). There are three main classification of priors that are used in literature to reflect the degree of uncertainty (or certainty) associated with parameters $\boldsymbol{X}$ or $\boldsymbol{\theta}$: (i) informative, (ii) weakly informative and (iii) diffuse (or non-informative). An *informative prior* is one that reflects a high degree of certainty about the model parameters. Mathematically, this level of informativeness can be

accomplished by assigning a small value of variance on the respective distribution model. In the contrary, a *non-informative prior* signifies the case where no specific knowledge of a parameter is available. A non-informative prior can be mathematically expressed by a relatively flat density function, such as for example a uniform distribution with bounds 0 to +∞ or generally, by assigning a very high degree of variability on the prior distribution. Finally, a *weakly informative prior* has a moderate amount of certainty, being neither too non-informative nor too restrictive. Such priors will have in general a very limited effect on the posterior distribution. A demonstration of the effect of the different types of priors on the posterior distribution for a given likelihood function is illustrated in Figure 5.2. It should be noted that the interpretation of a prior - as informative, weakly informative or diffuse - strongly depends on the formulation of the likelihood function in which it will be paired. For instance, if the likelihood is very informative, even a prior distribution with a moderate variance may have no effect on the posterior.

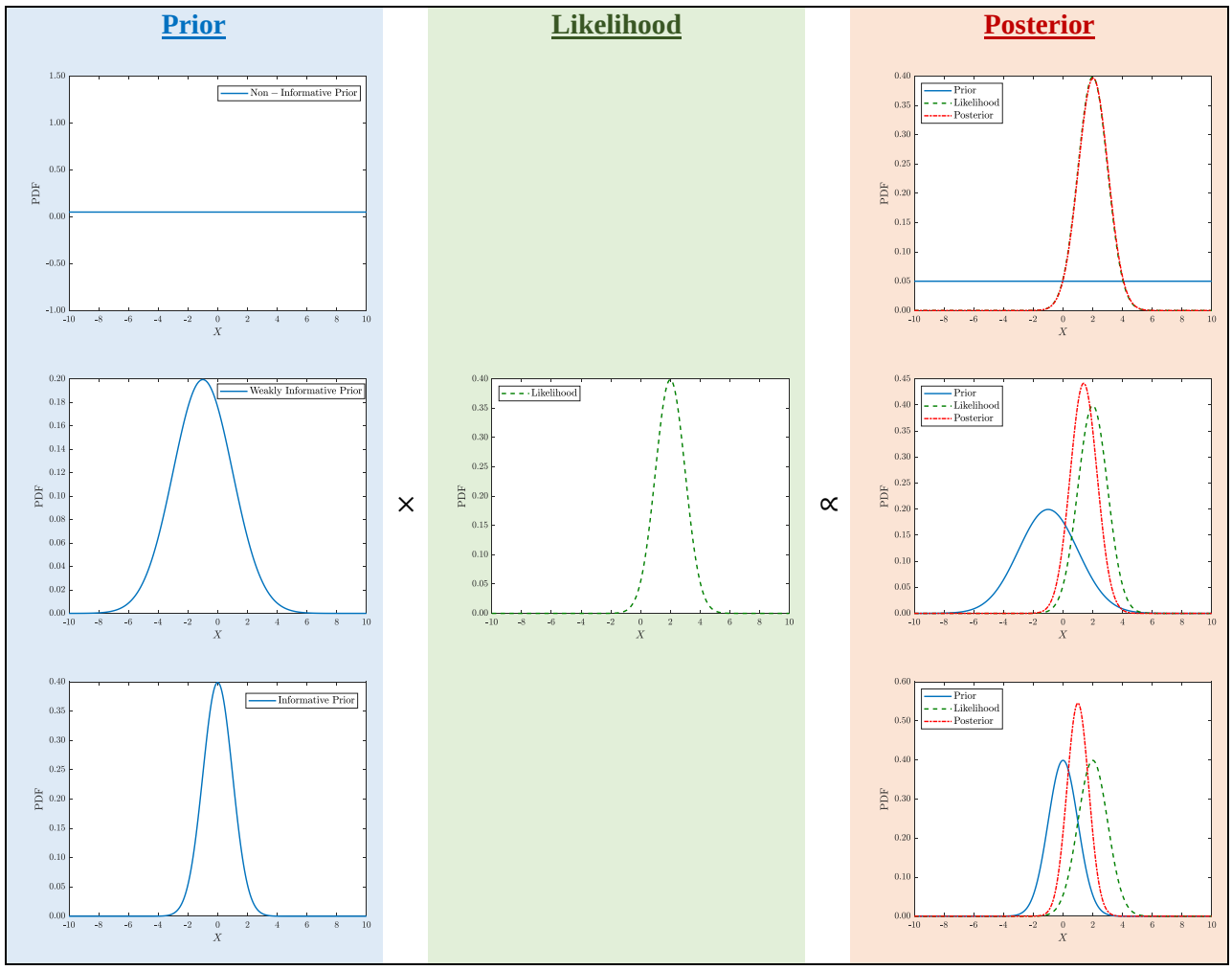

Figure 5.2. Illustration of the effect of prior on the posterior distribution for a given likelihood function.

5.6 Likelihood function

Information acquired in the form of measurements or observations is represented by the likelihood function. For continuous random variables $\boldsymbol{X}$, the likelihood function is defined as being proportional of the probability that one observes a measurement d_i conditional on a given parameter state (for fixed parameters), i.e., $\boldsymbol{X} = \boldsymbol{x}$, that is:

$$L(\boldsymbol{x}) \propto \Pr(d_i|\boldsymbol{X} = \boldsymbol{x}) \tag{5.9}$$

If multiple measurements $\boldsymbol{d} = \{d_1, \dots, d_m\}$ become available, likelihood functions L_i with $i = 1, \dots, m$ can be established for all of them individually. For *statistically independent* measurements, i.e., knowing the value of any measurement does not provide any information regarding the probability of observing other measurements, the joint likelihood takes the following form:

$$L(\boldsymbol{x}) = \prod_{i=1}^{m} L_i(\boldsymbol{x}) \tag{5.10}$$

In real applications, one is may interested in implementing the Bayesian updating process when measurements become available sequentially in time. Assuming independence between measurements collected at different time instances $\{\tau_1, \dots, \tau_{m_\tau}\}$, the likelihood function of Eq. (5.10) can be extended as:

$$L(\boldsymbol{x}) = \prod_{j=1}^{m_\tau} \prod_{i=1}^{m} L_i(\boldsymbol{x}; \tau_j) \tag{5.11}$$

where, m_τ is the total number of the time instances in which measurements are observed. For numerical stability enhancement, it is often convenient to work with the natural logarithm of the likelihood function instead of the joint likelihood function. Taking the natural logarithm on each side, Eq. (5.11) becomes:

$$\ln L(\boldsymbol{x}) = \sum_{j=1}^{m_\tau} \sum_{i=1}^{m} \ln L_i(\boldsymbol{x}; \tau_j) \tag{5.12}$$

Note also that the logarithm of a function has its maximum at the same location as the function itself. This is particular useful for the evaluation of Eq. (5.2) using sampling-based techniques as only the *shape* of the likelihood, and not its absolute magnitude, is needed to be known. In the

following, the derivation of the likelihood function for different classes of measurements is presented.

5.6.1 Direct measurements of a parameter X

Consider that a measurement x_i of the single random variable X is obtained[20]. We distinguish between a *perfect* and an *imperfect* measurement. For a perfect measurement, there would be no uncertainty on X, and thus the random variable would become a constant parameter with value $X = x_i$. There is no need for Bayesian updating in that case. The analytical form of the likelihood function would be the *Dirac delta* function with argument $x_i - x$:

$$L_i(x) = \delta(x_i - x) = \begin{cases} 1, & x_i = x \\ 0, & x_i \neq x \end{cases} \tag{5.13}$$

In practice, however, measurements are subject to one or numerous errors due to measurement inaccuracies. The measurement error ε is modelled probabilistically by its PDF f_ε which is commonly assumed to follow a Gaussian distribution. Error can be of *additive* or *multiplicative* type. In case of an additive error, the measurement is equal to the true value plus the error, $x_i = X + \varepsilon$, or equivalently, $\varepsilon = x_i - X$. The probability of observing a measurement x_i given that the true value is $X = x$, is equal to ε_i taking the value $x_i - x$. The likelihood function then reads:

$$L_i(x) = f_\varepsilon(x_i - x) \tag{5.14}$$

In case of a *multiplicative* error, it is $x_i = \varepsilon X$, so that $\varepsilon = x_i/X$. The likelihood function then becomes:

$$L_i(x) = f_\varepsilon\left(\frac{x_i}{x}\right) \tag{5.15}$$

5.6.2 Indirect measurements of model output

Consider a model denoted by $\mathcal{M}$ and its prediction $\mathcal{M}(\boldsymbol{x})$ for a given parameter state $\boldsymbol{X} = \boldsymbol{x}$. Let d_i denotes a single measurement corresponding to that model prediction. An error ε expressing the deviation of the model prediction from the measurement is modelled through

[20] In the context of this thesis, measurements are generally denoted by the symbol $\boldsymbol{d}$. Here, however, x_i has been used to emphasize that the measurement corresponds to the random variable X.

the PDF f_ε. This deviation is due to measurement and model errors[21]. Assuming an additive error, the following relation holds: $d_i = \mathcal{M}(\boldsymbol{x}) + \varepsilon$. The likelihood function describing this observation reads then:

$$L_i(\boldsymbol{x}) = f_\varepsilon\big(d_i - \mathcal{M}(\boldsymbol{x})\big) \tag{5.16}$$

More generally, the likelihood function for observations that provide information on continuous quantities can be expressed as:

$$L_i(\boldsymbol{x}) = f_{D_i|\boldsymbol{X}}(d_i|\boldsymbol{x}) \tag{5.17}$$

where $f_{D_i|\boldsymbol{X}}$ is the conditional PDF of the measured quantity d_i given $\boldsymbol{X} = \boldsymbol{x}$. Typically, $f_{D_i|\boldsymbol{X}}$ is assumed to follow a Gaussian distribution model. In case of multiplicative observation error ε the relationship that holds is $d_i = \varepsilon\mathcal{M}(\boldsymbol{x})$. The likelihood then becomes:

$$L_i(\boldsymbol{x}) = f_\varepsilon\left(\frac{d_i}{\mathcal{M}(\boldsymbol{x})}\right) \tag{5.18}$$

5.6.3 Sampling from a population

Occasionally, a model parameter X cannot be learned explicitly, but the parameters $\boldsymbol{\theta}$ that define the distribution model f_X can be learned. For instance, consider a spatially varying random parameter, e.g., thickness distribution, which is implicitly modelled through a single random variable X with corresponding PDF f_X. In that case, the *inherent* variability of thickness cannot be reduced with further measurements, but the parameters $\boldsymbol{\theta}$ (e.g., mean value and variance) of the distribution model f_X can be learned. In other words, the measurements are realizations of X, which are used to learn the parameters $\boldsymbol{\theta}$ of the distribution model f_X. The likelihood function describing a single sample x_i of a continuous random variable X with PDF f_X is expressed as follows:

$$L_i(\boldsymbol{\theta}) = f_X(x_i|\boldsymbol{\theta}) \tag{5.19}$$

where, $f_X(x_i|\boldsymbol{\theta})$ is the PDF of X with parameters value $\boldsymbol{\theta}$, evaluated at x_i.

In case where an additive error term ε is postulated on the observation x_i, e.g., due to a measurement inaccuracy, the likelihood function will depend both on f_X conditional on $\boldsymbol{\theta}$ as

[21] Model errors can be implicitly accommodated in the input vector $\boldsymbol{X}$ by adding an additional random variable. In that case, the induced error ε will be totally attributed to measurement inaccuracy.

well as the functional relationship between the error term and the measurement. Applying the multiplication and chain rules, the so-called *marginalized* or *integrated likelihood* is obtained as, see also Nagel and Sudret (2016):

$$L_i(\boldsymbol{\theta}) = \int_{-\infty}^{\infty} f_{X_i|X}(x_i|x) f_X(x|\boldsymbol{\theta}) dx = \int_{-\infty}^{\infty} f_{\varepsilon}(x_i - x) f_X(x|\boldsymbol{\theta}) dx \tag{5.20}$$

where the term $f_{X_i|X}(x_i|x)$ denotes the PDF of measuring the value x_i given the true value is $X = x$. For an additive error where $x_i = X + \varepsilon$, this term becomes equal to $f_{\varepsilon}(x_i - x)$, where a Gaussian distribution is considered to express the variability of the error. In analogy with Eq. (5.10), if $i = 1, \dots, m$ independent measurements are observed, then the joint likelihood function becomes:

$$L(\boldsymbol{\theta}) = \prod_{i=1}^{m} L_i(\boldsymbol{\theta}) \tag{5.21}$$

5.7 Posterior distribution

The quantification of the uncertainty related to the posterior distribution of model parameters $\boldsymbol{X}$ can be expressed using point estimates, such as the posterior mean and the MAP that we saw in Section 5.4. An alternative way to account for the uncertainty on the posterior model parameters is to estimate the so-called *credible intervals*. Credible intervals are used in the framework of Bayesian statistics and are opposed to *confidence intervals* which are adopted from a frequentist point of view. The use of credible intervals is more intuitive and their definition is simple: the $p\%$ credible interval represents a range in which the parameter value lies with $p\%$ probability. Credible intervals are defined through quantiles: e.g., the 2.5% and the 97.5% quantile of the posterior distribution are the limits of the 95% credible interval.

The calculation of the posterior distribution is implemented through Eq. (5.2) or Eq. (5.4), after determining the prior and the likelihood. In general, the selection of the appropriate computational strategy depends on the problem at hand and especially, on the number of random variables, their distribution model, the number of measurements and the computational cost of the respective model. Analytical solutions are rarely available in practice, while numerical integration methods (e.g., quadrature rule) are only applicable for a small number of input vector (in the order of 3). In most engineering applications, advanced sampling-based techniques, such as *Markov Chain Monte Carlo* (MCMC) and *Bayesian updating using structural reliability* (BUS) methods are needed for the solution of the Bayesian updating problem.

In the following, common methods for calculating the posterior distribution are reviewed. The emphasis is placed on the methods used in the context of the present thesis. A detailed presentation of the algorithms is beyond the scope of this thesis. A deeper insight is given for the reader in the relevant references.

5.7.1 Analytical solution (conjugate priors)

An analytical solution of the basic Bayesian updating problem is possible for given pairs of prior-likelihood distribution models. Knowledge of the so-called *conjugate priors* is extremely useful as they provide accuracy and low computational effort. Various forms of conjugate priors pairs can be found in Raiffa and Schlaifer (1961).

A common conjugate prior is the following case: Consider a normal random variable X with uncertain mean value $\mu_X = \theta$ and known standard deviation σ_X. If the likelihood of the parameter θ is the normal distribution with mean θ and fixed standard deviation σ_X, the conjugate prior is the normal distribution with mean μ'_θ and standard deviation σ'_θ. If m samples are taken with sample mean $\bar{x}$, the posterior distribution of θ is the normal distribution with parameters:

$$\mu''_\theta = \frac{\frac{\mu'_\theta}{\sigma'^2_\theta} + \frac{m\bar{x}}{\sigma_X^2}}{\frac{1}{\sigma'^2_\theta} + \frac{m}{\sigma_X^2}} \tag{5.22}$$

$$\sigma''_\theta = \left[\frac{1}{\sigma'^2_\theta} + \frac{m}{\sigma_X^2}\right]^{-1/2} \tag{5.23}$$

Note that in the above formulations the posterior mean μ''_θ depends on the average value and the number of observations, while the posterior standard deviation σ''_θ is affected only by the number of observations, and *not* on their actual outcome. In other words, the more samples are observed, the higher is the reduction of uncertainty that is achieved.

5.7.2 Sampling-based approaches

5.7.2.1 Markov Chain Monte Carlo methods

The most common sampling-based method used for the evaluation of the Bayesian updating problem is based on Markov Chain Monte Carlo (MCMC) technique. MCMC is a method that asymptotically generates dependent samples from the target (posterior) distribution. The sampling process is called Markovian in the sense that the next generated sample depends only on the current sample and not on the samples generated previously. For a comprehensive introduction to MCMC the reader is referred to the book of Gilks et al. (1996).

A well-known MCMC algorithm is the Metropolis-Hastings algorithm, after Metropolis et al. (1953), and Hastings (1970). The Metropolis-Hastings algorithms proceeds by generating each new state of the Markov chain from a proposal distribution $q\left(\cdot \left| \boldsymbol{x}^{(i)} \right.\right)$ conditional on the current state $\boldsymbol{x}^{(i)}$ and then accepts or rejects the sample with a certain degree of acceptance probability that depends on the current and the proposed state. Typical choices of the proposal distribution are symmetric distributions, such as the normal or uniform distribution, centered on the current state $\boldsymbol{x}^{(i)}$. The Metropolis-Hastings algorithm for generating K states of a Markov chain with stationary distribution equal to the posterior distribution $f_X''(\boldsymbol{x})$ can be summarized as follows:

Metropolis-Hastings algorithm:

1. Choose an initial guess $\boldsymbol{x}^{(0)}$
2. Set $i = 1$
3. Generate a candidate sample $\boldsymbol{\xi}$ from the proposal distribution $q\left(\boldsymbol{\xi} \left| \boldsymbol{x}^{(i-1)} \right.\right)$
4. Compute the acceptance probability p_a as:
$$p_a\left(\boldsymbol{x}^{(i-1)}, \boldsymbol{\xi}\right) = \min\left\{\frac{f_X''(\boldsymbol{\xi}) q\left(\boldsymbol{x}^{(i-1)} \left| \boldsymbol{\xi} \right.\right)}{f_X''(\boldsymbol{x}^{(i-1)}) q\left(\boldsymbol{\xi} \left| \boldsymbol{x}^{(i-1)} \right.\right)}, 1\right\}$$
5. Generate a sample p from the standard uniform distribution $p \sim U(0,1)$
6. Set:
$$\boldsymbol{x}^{(i)} = \begin{cases} \boldsymbol{\xi}, & \text{if } p < p_a\left(\boldsymbol{x}^{(i-1)}, \boldsymbol{\xi}\right) \\ \boldsymbol{x}^{(i-1)}, & \text{otherwise} \end{cases}$$
7. Set $i = i + 1$
8. Stop if $i = K$, else go to Step 2.

Note that the Metropolis-Hastings algorithm does not require the posterior distribution to be normalized. This is particular useful for Bayesian updating as the posterior distribution is known only up to a proportionality level. A problem with MCMC methods is the difficulty of ensuring

convergence to the target posterior distribution after an initial burn-in phase[22], see Plummer et al. (2006). Moreover, it is often difficult to choose a proposal density that can sample efficiently in high dimensional posterior densities. A method that partly alleviates the problem of burn-in in the original MCMC is the so-called transitional MCMC method, see Ching and Chen (2007). However, its performance deteriorates with increasing the dimension of the parameter space, see Betz et al. (2016).

5.7.2.2 Bayesian Updating with Structural reliability methods (BUS)

An alternative sampling-based approach of MCMC is the *Bayesian updating with structural reliability methods (BUS)*, originally proposed by Straub and Papaioannou (2015). BUS reinterprets the Bayesian updating problem by using structural reliability methods. The basic concept of BUS approach is presented below.

The principal idea behind BUS is to add a parameter P uniformly distributed in $[0,1]$ additionally to the space spanned by random variables $\boldsymbol{X}$. The updating problem is then expressed as a structural reliability problem in the augmented outcome space $[\boldsymbol{x}; p]$. In analogy with the failure domain $\Omega_{\mathcal{F}}$ defined in the reliability problem (see Section 7.2), the observation domain Ω_o is defined as:

$$\Omega_o = \{p \leq cL(\boldsymbol{x})\} \tag{5.24}$$

where c is a positive constant that ensures $cL(\boldsymbol{x}) \leq 1$ for all $\boldsymbol{x}$. It is proved by Straub and Papaioannou (2015) that samples generated from the prior and falling into the observation domain Ω_o are distributed according to the posterior distribution. In analogy with structural reliability analysis, the limit state function $h(\boldsymbol{x}, p)$ is introduced here to describe the observation ("failure") domain Ω_o:

$$h(\boldsymbol{x}, p) = p - cL(\boldsymbol{x}) \tag{5.25}$$

where, $h(\boldsymbol{x}, p) \leq 0$ if $[\boldsymbol{x}; p] \in \Omega_o$ and $h(\boldsymbol{x}, p) > 0$ if $[\boldsymbol{x}; p] \notin \Omega_o$.

Rejection sampling

In its simplest version, the BUS approach reduces to a classical *rejection sampling* method where the prior distribution is applied as an envelope distribution and the likelihood is applied as a filter, see Gelfand and Smith (1992). The basic steps of the algorithm are presented below:

[22] The number of steps until the Markov chain approximately reaches its stationary target distribution is called the *burn-in period*.

Rejection sampling algorithm:

1. $i = 1$
2. Generate a sample $\boldsymbol{x}^{(i)}$ from the prior joint distribution $f'_{\boldsymbol{X}}(\boldsymbol{x})$
3. Generate a sample $p^{(i)}$ from the standard uniform distribution $p \sim U(0,1)$
4. If $\left[\boldsymbol{x}^{(i)}, p^{(i)}\right] \in \Omega_o$
    a. Accept $\boldsymbol{x}^{(i)}$
    b. Set $i = i + 1$
5. If $i = K$ stop, otherwise go to Step 2.

The posterior samples resulting from the above algorithm are statistically independent. A measure for the efficiency of the rejection sampling algorithm is the probability of acceptance p_{acc} which is given by the following relation, see Straub and Papaioannou (2015):

$$p_{acc} = \int_{\boldsymbol{X}} cL(\boldsymbol{x}) f'_{\boldsymbol{X}}(\boldsymbol{x}) d\boldsymbol{x} \tag{5.26}$$

The probability of acceptance represents the probability that samples $[\boldsymbol{x}; p]$ from the prior distribution fall into Ω_o, that is:

$$p_{acc} = \Pr(\Omega_o) = \Pr[h(\boldsymbol{x}, p) \leq 0] \tag{5.27}$$

An estimate of the acceptance probability $\hat{p}_{acc}$ can be obtained simply by dividing the number of samples falling into the observation domain Ω_o by the total number of generated samples K. Following Eq. (5.26), an estimate of the evidence $\hat{c}_E$ associated with the updating problem can be obtained as:

$$\hat{c}_E = c^{-1} p_{acc} \tag{5.28}$$

An illustration of the rejection sampling algorithm is provided in Figure 5.3a for the case of a univariate standard normal prior PDF $f'_X(x)$ and a single observation $x_i = 2$ with an associated normally distributed additive error term $\varepsilon \sim N(0, \sigma_\varepsilon = 0.5)$. Here, the constant c is chosen as: $c = 1/\max[L(x)] = 1.253$. A total number of $K = 500$ samples has been generated from the prior. Samples falling into the shaded green area, i.e., the observation domain Ω_o, are accepted. These samples follow the posterior distribution $f''_X(x)$. A very good agreement between the empirical and the exact solution, which is available for the present problem, is achieved by examining the analytical/exact CDF with the empirical CDF (see Figure 5.3b). For that particular

problem, the exact acceptance probability, as computed by Eq. (5.26), is $p_{acc} = 0.09$. An estimate of the acceptance probability can be obtained by dividing the number of samples falling into the domain Ω_o by the total number of generated samples: $\hat{p}_{acc} = 50/500 = 0.1$.

The above rate of acceptance quickly reduces as the number of dimensions and measurements increases. Then, the rejection sampling algorithm becomes insufficient to accommodate the Bayesian updating problem. The BUS approach overcomes this difficulty by resorting to efficient structural reliability methods for representing the observation domain. Such an efficient structural reliability method is the Subset simulation (SuS). An outline of BUS-SuS method is given below, while for a detailed presentation of the method and the algorithms used for its implementation, the reader is referred to the papers of Straub and Papaioannou (2015), and Betz et al. (2018).

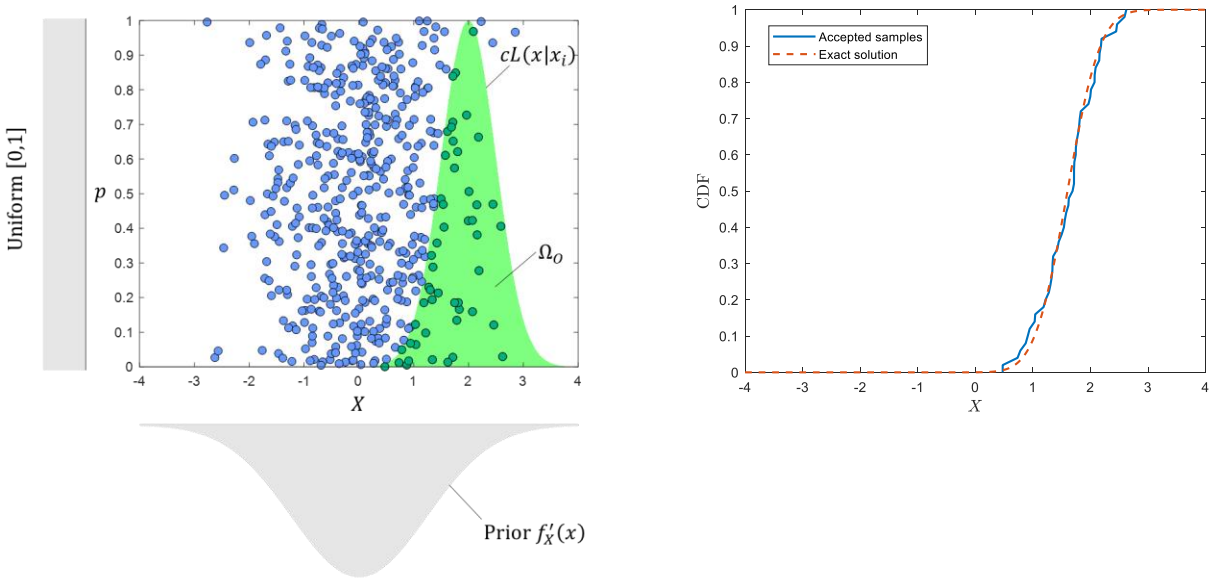

(a) (b)

Figure 5.3. (a) Illustration of the rejection sampling algorithm. Pairs of samples generated from the prior distribution $f'_X(x)$ and the standard uniform distribution that fall inside the observation domain Ω_o (green shaded area) are distributed according to the posterior. (b) CDFs of the exact/analytical solution and the empirical distribution constructed from the accepted samples are in very good agreement.

(a)BUS-SuS

Subset simulation (SuS) has been introduced by Au and Beck (2001) and is a particular efficient method to compute small failure probabilities in high-dimensional problems encountered in the reliability analysis of engineering systems. SuS expresses the observation domain Ω_o as the intersection of N intermediate nested intermediate domains (or events) $D_0 \supset D_1 \supset \cdots \supset D_N$, in which D_0 is the certain event and $D_N = \Omega_o$. The probability $\Pr(\Omega_o)$ is then expressed as:

$$\Pr(\Omega_o) = \Pr\left[\bigcap_{i=0}^{N} D_i\right] = \prod_{i=1}^{N} \Pr(D_i|D_{i-1}) \tag{5.29}$$

The above expression states that the possibly small probability $\Pr(\Omega_o)$ can be expressed as a product of conditional probabilities with higher probability level. The events D_i are defined as $D_i = \{h(\boldsymbol{x}, p) \leq b_i\}$, where b_i are positive threshold levels satisfying the following condition $b_0 = \infty > b_1 > \cdots > b_n = 0$. The thresholds b_i are selected adaptively such that each conditional probability equals a target probability p_0, with p_0 typically chosen as $p_0 = 0.1$. This is accomplished by generating $j = 1, \ldots, K$ samples from $\left\{\boldsymbol{x}_i^{(j)}, p_i^{(j)}\right\}$ conditional on the intermediate events D_i and then setting b_i as the p_0-quantile of the corresponding limit state function values. Samples conditional on the certain event D_0 are obtained by crude Monte Carlo simulation. Samples conditional on the events D_i for $i = 1, \ldots, N-1$ are obtained by MCMC using as seeds $K_s = p_0 K$ samples conditional on D_{i-1} for which $h(\boldsymbol{x}, p) \leq b_i$.

As discussed in Betz et al. (2018), the formulation of the limit state function has an impact on BUS-SuS. In general, a smooth transition between the intermediate events is needed for an efficient performance of the method. This can be achieved by introducing an alternative, yet equivalent, representation of the limit state function applying the natural logarithm for each term in Eq. (5.25):

$$h(\boldsymbol{x}, p) = \ln(p) - \ln(c) - \ln[L(\boldsymbol{x})] \tag{5.30}$$

Note that both limit state function formulations have the same failure domain while the use of the logarithms provides the additional advantage of numerical stable solutions.

Eventually, the probability $\Pr(\Omega_o)$ can be approximated by:

$$\Pr(\Omega_o) \approx p_0^{N-1} \hat{p}_n \tag{5.31}$$

where $\hat{p}_n$ is the estimate of the conditional probability $\Pr(D_i|D_{i-1})$ given by the ratio of the number of samples for which $h(\boldsymbol{x}, p) \leq 0$ over the total number of samples K generated conditional on the intermediate level D_{i-1}. The number of samples K generated in each intermediate domain should be selected large enough (usually larger than 1000) to guarantee an accurate estimate of p_0, see Betz et al. (2018).

An improved version of BUS-SuS approach termed *adaptive BUS-SuS (aBUS-SuS)* has been proposed by Betz et al. (2018). The main benefit of aBUS-SuS is that it does not require the knowledge of the constant c as input. In contrast, the constant c is adaptively learned. The method is recommended in cases where (log)-likelihood evaluations are associated with high computational cost.

6 Hull girder ultimate strength assessment: Uncertainty reduction methods

6.1 Introduction

In this chapter, novel methods for reducing the uncertainty associated with the assessment of hull girder ultimate strength of ship structures are developed. Bayesian techniques are employed for the accomplishment of this purpose. The scope of this chapter is to update the basic random variables that constitute the resistance model R in Eq. (2.1), namely, the model uncertainty factor X_r and the (time-varying) hull girder ultimate strength M_u. The impact of the novelties introduced in this chapter is analyzed in Chapter 7 through the implementation of a reliability analysis in an oil tanker and two container ships.

In Section 6.2, a methodology for a rigorous management of the uncertainties related to the model error parameter X_r is established. Particularly two stages are introduced. In the first one, a Bayesian updating scheme is employed to build a general-purpose ship-type dependent model uncertainty factor X_r. A recommendation is made for the determination of X_r within the context of reliability assessment on container ships and oil tankers. In the second stage, the derived model uncertainty factor X_r is further refined for application on a target vessel. A demonstration is presented where the model uncertainty factor X_r extracted for the global fleet of container ships is adapted for the unique case of "MOL Comfort" accident, sank in the Indian Ocean in 2013.

In Section 6.3, a Bayesian approach is adopted to learn and update the parameters of a time-dependent corrosion model using actual measurements from inspections. Updated thickness predictions are provided for the structural elements composing the cross section of midship section area by combining the information acquired from inspections with existing knowledge from global-fleet statistics. The focus is placed on a more accurate estimation of uniform thickness diminution based on a limited number of available measurements. The impact of using measurements from a single and sequential inspections is investigated. Results are validated against actual data from the last inspection of the examined vessel.

6.2 A Bayesian method for the determination and quantification of the strength model uncertainty factor

6.2.1 Background

The strength model uncertainty factor X_r is generally the most influential basic random variable of the reliability problem in ultimate limit state, see e.g., Campanile et al. (2016)c, Chen (2016), Parunov et al. (2014), Corak and Soares (2018). The determination of an appropriate ship-type dependent distribution model for X_r is thus of great practical importance. As real-scale observations from hulls' collapse are not available, the true value of hull girder ultimate strength is generally unknown. As a result, the quantification of X_r usually involves the combination of engineering judgment and results obtained from high-fidelity models, e.g., NLFEA. A need arises to develop a solid framework for efficiently combining the different sources of information. To this end, a systematic and formal method to manage the uncertainty related to model uncertainty X_r is presented in this section. The framework of Bayesian analysis whose basic theory was introduced in Chapter 5 is used for this purpose.

In the current study, advanced NLFEA results are used to formulate the likelihood function. Finite element simulations are seen as a trustworthy source of information used to replace real-life data[23]. In this regard, Xu et al. (2015) investigated the reliability of a Suezmax oil tanker by calibrating the results obtained from the simplified IACS CSR Smith's method with an advanced and "realistic" FE model. NLFEA can provide a refined version of the actual structure by explicitly covering aspects that are not considered in the simplified Smith's method (see also the discussion of Section 4.4). It should be noted, however, that the assessment of hull girder ultimate strength using non-linear finite element techniques is associated with an uncertainty, usually attributed to modelling aspects and user's skills (human error). This "measurement inaccuracy" type of uncertainty – although generally unknown up to an extent – can be explicitly quantified through the framework of Bayesian analysis.

Overall, the present study is structured as follows. In Section 6.2.2, the methodology and the mathematical formulation to update and learn the population statistics of the model uncertainty factor X_r are presented. For this purpose, different sources of subjective and objective type of information are combined effectively under the framework of Bayesian analysis to learn the parameters of the distribution model. The main objective is the establishment of an appropriate ship-type dependent model uncertainty factor X_r used for reliability assessment and potentially, for the development of design code formats. In Section 6.2.3, the goal is to learn the model uncertainty factor X_r explicitly for application on vessel-specific purposes. This is achieved using information from a target or a sister vessel whose

[23] As stated by Bathe (2006), a finite element simulation can be considered as a "laboratory experiment" performed on a digital environment.

specific characteristics, e.g., true imperfections, structural configuration, etc., are known and they can be embodied in an advanced FE model to evaluate the hull girder ultimate strength. In Section 6.2.4, we demonstrate the proposed methodology by applying it in oil tankers and container ships. Aiming at the specific characteristics of the individual type of vessels, a new recommendation for the quantification of strength model uncertainty factor X_r is presented. In addition, and following the methodology presented in Section 6.2.3, a suitable distribution model for X_r in the case of "MOL Comfort" container ship is proposed in order to evaluate the variability of its capacity at the time of accident.

6.2.2 Method for the determination of a global-based model uncertainty factor

The fundamental theory of learning the parameters of a distribution model f_X using Bayesian analysis has been presented in Section 5.4. In the present problem, the random variable of model uncertainty factor X_r with corresponding distribution model f_X is of interest. According to the definition given in Eq. (2.5), X_r reflects the *model* error, namely, in our case, the deviation of IACS CSR Smith's model prediction vs. real-life result. To reflect this uncertainty, X_r is modelled as a random variable with normal PDF, i.e., $X_r \sim N(\mu_X, \sigma_X)$.

The standard deviation σ_X expresses the uncertainty or deviation of model prediction vs. true value. In the ideal case where our model was a perfect replica of the physical system, σ_X would be equal to zero. However, since the true value for the problem at hand is not known, it is practically impossible to compute this deviation or learn it by data. Therefore, the uncertainty on σ_X parameter is treated as irreducible and is set equal to $\sigma_X = 0.10$, which is the most widely adopted value in the literature (see Section 2.4.2).

The mean μ_X expresses the bias of the reference model prediction. For instance, $\mu_X = 1.00$ denotes an unbiased estimate of model prediction. In our problem, the mean parameter μ_X is considered unknown and its quantification is inferred combining different sources of information, including experts' judgement from literature sources, as well observations from a limited number of high-fidelity NLFEA. The overall scope is then to provide the "best" estimate of the mean value μ_X using a Bayesian approach. Although this estimate would be different for each type of ship due to the unique structural characteristics, the methodology remains the same. A graphical overview of the proposed concept is illustrated in Figure 6.1.

6.2.2.1 Prior belief on mean parameter

To construct the prior probabilistic model of mean uncertain parameter μ_X, someone can rely on different potential sources. Among them, the most commonly used are: (i) available information from past observations/projects of similar type, (ii) literature sources, and (iii) experts' assessments. In the case where prior information is vague, a so-called non-informative or weakly informative prior can be chosen (see Section 5.5). In the present analysis, prior

knowledge is based on the available information associated with the specific type of ship that is investigated.

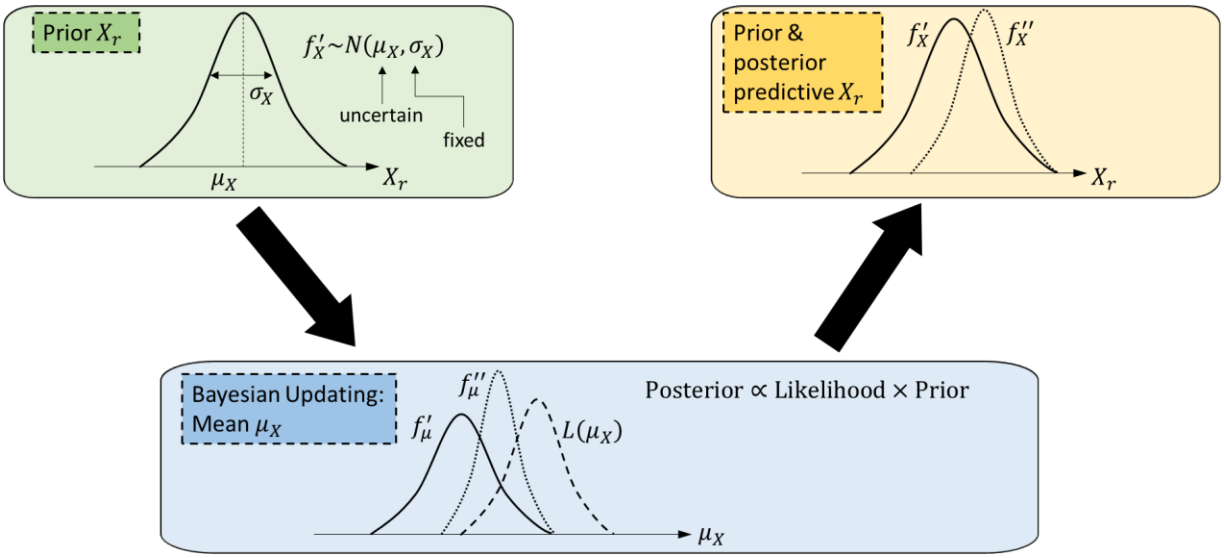

Figure 6.1. Outline of the procedure for the determination of mean value μ_X and associated strength model uncertainty factor X_r distribution model.

6.2.2.2 Likelihood formulation

In the absence of real-scale measurements, information about the hull girder collapse comes from high-fidelity NLFEA results. Recalling Eq. (2.5), the true – but unknown – value of the nominator is here approximated by the outcome of a NLFEA result. Therefore, a single observation $x_i \equiv x_r$ can be expressed by the following ratio:

$$x_r \equiv x_i = \frac{M_u^{FEM}}{M_u^{CSR}} \tag{6.1}$$

where, M_u^{FEM} denotes the "measurement" obtained from a single NLFEA simulation, and M_u^{CSR} is the corresponding result using the IACS CSR Smith's model. An error is associated with the ratio x_i due to the uncertainty on the NLFEA prediction and the transformation, i.e., M_u^{FEM}/M_u^{CSR}. NLFEA prediction error generally includes modelling and users' error. Transformation error is the result of deviations on Smith's model prediction observed between different participants[24]. The formulation of the likelihood function follows.

[24] Although one would expect this portion of error to be relatively small.

Let us assume that x_i is subject to an additive error term ε, so as: $x_i = X + \varepsilon$, and X denotes the true but unknown value. In that case, the analytical form of the likelihood is provided by Eq. (5.20), which for the present case reads:

$$L_i(\mu_X) = \int_{-\infty}^{\infty} f_{X_i|X}(x_i|x) f_X(x|\mu_X) dx = \int_{-\infty}^{\infty} f_\varepsilon(x_i - x) f_X(x|\mu_X) dx \tag{6.2}$$

where,

$$f_X(x|\mu_X) = \frac{1}{\sigma_X\sqrt{2\pi}} \exp\left[-\frac{1}{2}\left(\frac{x-\mu_X}{\sigma_X}\right)^2\right]$$

and $f_\varepsilon(x_i - x)$ is a univariate zero-mean Gaussian PDF $\varepsilon \sim N(0, \sigma_\varepsilon)$. The uncertainty for each sample x_i is reflected on σ_ε, which has been estimated equal to $\sigma_\varepsilon = 0.05$ (see Appendix G for further details). For multiple and independent on each other observations, the likelihood function becomes:

$$L(\mu_X) = \prod_{i=1}^{m} \int_{-\infty}^{\infty} f_\varepsilon(x_i - x) f_X(x|\mu_X) dx \tag{6.3}$$

6.2.2.3 Posterior distribution of mean parameter and predictive distribution

The posterior PDF of mean $f''_{\mu_X}(\mu_X)$ is computed using Bayes' theorem (see Eq. (5.4)) as:

$$f''_{\mu_X}(\mu_X) = c_E^{-1} L(\mu_X) f'_{\mu_X}(\mu_X) \tag{6.4}$$

A rejection sampling algorithm is employed to derive the posterior distribution. In the general case, the posterior predictive distribution of the basic random variable X_r, which is of interest, is obtained following Eq. (5.6):

$$\tilde{f}_X(x) = \int_{-\infty}^{\infty} f_X(x|\mu_X) f''_{\mu_X}(\mu_X) d\mu_X \tag{6.5}$$

In the present case study, the predictive distribution of X_r is computed employing a Monte Carlo integration using the posterior samples of $f''_{\mu_X}(\mu_X)$ generated from the employed rejection sampling algorithm.

6.2.3 Method for the adjustment of global-based model uncertainty factor for vessel-specific purposes

In the case where information from the hull condition of a target or sister ships is available, then updating can be performed on the model uncertainty factor X_{r} directly. The methodology to implement a Bayesian updating on such a case is presented here. In the present analysis, we are interested in updating only a single random variable. Therefore, the $\boldsymbol{X}$ vector on Eq. (5.2) reduces to a univariate random variable $X \equiv X_r$, and the basic problem of Bayesian updating reads:

$$f_X''(x) = c_E^{-1} L(x) f_X'(x) \tag{6.6}$$

The necessary information and mathematical tools to construct the prior PDF, the likelihood function and finally, the way to reach on the posterior distribution is analyzed in the remaining section.

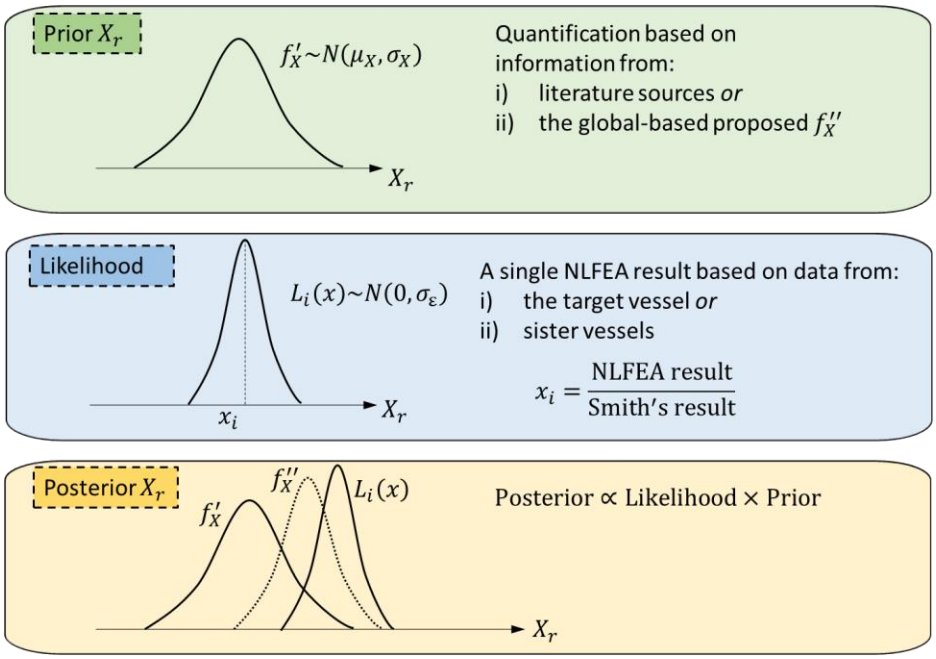

Figure 6.2. Outline of the updating process followed to derive the posterior X_r for a target vessel based on the actual data and structural configuration of that vessel or a sister vessel.

6.2.3.1 Prior probabilistic model

Initial knowledge on the strength model uncertainty factor can be based either on available literature sources, see e.g. Mansour & Hovem (1994), Paik and Frieze (2001), Hørte et al. (2007) or the updated/posterior PDF of the population statistics' learning (see Section 6.2.2).

6.2.3.2 Likelihood formulation

A single observation x_i is assumed to be taken from the target or a sister vessel after performing a detailed NLFEA and an associated Smith's model evaluation. An error term ε is added on the measurement to reflect the deviation from the true value X, so as: $x_i = X + \varepsilon$, where $\varepsilon \sim N(0, \sigma_\varepsilon)$. A zero-mean Gaussian PDF is postulated on ε_i so that the likelihood function takes the following form:

$$L_i(x) = f_\varepsilon(\varepsilon) = f_\varepsilon(x_i - x) = \frac{1}{\sigma_\varepsilon \sqrt{2\pi}} \exp\left[-\frac{1}{2}\left(\frac{x_i - x}{\sigma_\varepsilon}\right)^2\right] \tag{6.7}$$

The error term σ_ε for each measurement can be taken equal to $\sigma_\varepsilon = 0.05$, after Appendix G. This error is assumed to cover the uncertainties mentioned in Section 6.2.2.2.

6.2.3.3 Posterior distribution

The posterior distribution of the uncertain parameter X_r is evaluated using Eq. (6.6). An analytical solution to the present problem is available since the prior and the likelihood follow the normal distribution (conjugate priors). Following Section 5.7.1, the posterior PDF has the normal distribution with parameters:

$$\mu_X'' = \frac{\frac{\mu_X'}{\sigma_X'^2} + \frac{m\bar{x}}{\sigma_\varepsilon^2}}{\frac{1}{\sigma_X'^2} + \frac{m}{\sigma_\varepsilon^2}} \tag{6.8}$$

$$\sigma_X'' = \left[\frac{1}{\sigma_X'^2} + \frac{m}{\sigma_\varepsilon^2}\right]^{-1/2} \tag{6.9}$$

where, $m = 1$ for a single observation and $\bar{x}$ is the average (actual) value of the unique observation.

6.2.4 Determination of model uncertainty factor for oil tankers and container ships

The methodology developed in Section 6.2.2 is used as a basis to determine reasonably an appropriate model uncertainty factor X_r for the fleet of oil tankers (see Section 6.2.4.1) and container ships (see Section 6.2.4.2).

6.2.4.1 Numerical application on oil tankers

Failure in sagging is identified as the most critical failure mode for double hull tankers due to the way loads acting on the hull and due to the structural arrangement of these types of vessels, see e.g., Hørte et al. (2007). In sagging condition, the buckling of deck stiffened panels generally dominates the overall hull girder collapse for these types of ships. Since buckling phenomenon is highly affected by initial geometric imperfections, the proper consideration of the latter is a crucial parameter for the hull girder ultimate strength assessment. In contrast with the IACS CSR Smith's method, the FE model can explicitly accommodate the imperfect geometry of the hull structure and assess its impact on hull structure collapse. This information is exploited here through the inclusion of selected NLFEA which are used to calibrate the Smith's model prediction.

Prior belief on mean uncertain parameter μ_X

For oil tankers, our prior belief on mean uncertain parameter μ_X comes from literature sources, mainly as the result of experts' judgment. The most widely adopted values for mean value for the justification of X_r are $\mu_X = 1.00$ and $\mu_X = 1.05$ (see also Table 2.1). However, as the value of $\mu_X = 1.05$ – firstly introduced by Hørte et al. (2007) – was originally selected with some bias on a series of NLFEA results carried out by DNV (2004), we are going to omit its consideration from the prior and include it only in the formulation of the likelihood. Parunov et al. (2007) carried out parametric studies on the statistical parameters of X_r. They varied the values of μ_X in the range of 0.95 to 1.05. Here, we associate these values to the 15% and 85% quantiles, respectively, and we fit a normal distribution. The resulted prior PDF f'_{μ_X} has a mean value $\mu_0 = 1.00$ and standard deviation $\sigma_0 = 0.05$.

Likelihood

Information acquired from NLFEA results is used to formulate the likelihood function. The dataset has been selected taking into consideration:

1. Different imperfection models to describe the imperfect geometry of deck panels
2. Various types of ships

In summary, the dataset used to formulate the likelihood function given in Eq. (6.3) is presented in Table 6.1. The ship types that are examined are one VLCC, two Suezmax and one Product/Chemical tanker. The initial imperfect geometry for all case studies[25] consists of a linear superposition of: (i) a column-type global half-wave mode, (ii) a local half-wave stiffener

[25] An exception to this is the result of the Product/Chemical tanker whose imperfection model is not known.

sideways deflection, and (iii) a local plate deflection shape (see also Section 2.4.4). Both "theoretical" and "realistic" imperfection models have been adopted in the data set. For theoretical models, local plate's initial geometry is in symphony with the critical buckling mode shape (BM), whereas for the realistic models, the conventional hungry-horse (HH) model has been used. In addition, a single representative (average) result from the newly proposed stochastic HH model has been added in the dataset (see Section 4.2.4).

DNV (2004) conducted a series of NLFEA using different scantlings and imperfection models. From this series, Hørte et al. (2007) adopted a single NLFEA outcome, $x_i = 1.05$, corresponding to the net-50 scantling approach and the HH imperfection model. This value has been considered in the data set of the present study (see Table 6.1). However, we have additionally considered the result obtained from the theoretical imperfection model, $x_i = 1.01$, because as shown from the results of Section 4.2.4.4, the conventional HH model may overestimate the true strength. This the reason why more theoretical models have been considered in the dataset too.

Table 6.1. Hull girder ultimate strength results as a ratio of NLFEA result to IACS CSR Smith's model prediction.

Ship type	Imperfection model	Ratio x_i	Reference
Suezmax #1	Buckling-mode (BM)	1.01	DNV (2004)
	Hungry-horse (HH)	1.05	
Suezmax #2	Buckling-mode (BM)	1.08	Xu et al. (2017)
VLCC	Buckling-mode (BM)	0.99	From Table 4.7
	Hungry-horse (HH)	1.03	
	Stochastic HH (SHH)	0.99	
Product/Chemical	Buckling-mode (BM)	0.98	Andric et al. (2014)

Posterior distribution of mean value μ_X and predictive distribution of model error X_r

The results of the updating process are presented in Figure 6.3. As shown from Figure 6.3a, the likelihood (data) distribution has approximately equal effect with the prior on the resulted posterior distribution. This is due to the relative strong prior belief for the problem at hand and the considerable degree of uncertainty associated with observations. As a result, the inclusion of added information does not alter significantly our prior belief on the mean uncertain parameter μ_X. In turn, as shown from Figure 6.3b, the effect on the predictive posterior distribution $\tilde{f}_X$ is almost negligible.

Note that the predictive distribution $\tilde{f}_X$ depicted in Figure 6.3b includes the statistical uncertainty on the mean value. This is the reason why $\tilde{f}_X$ is wider, i.e., it has a larger standard

deviation, than the "true" distribution f_X. Standard practices upon the quantification of X_r do not take into account the uncertainty on the statistical parameters. Consequently, the following distribution model is recommended:

$$X_r \sim N(\mu_X = 1.01, \sigma_X = 0.10) \tag{6.10}$$

Overall, Figure 6.6a summarizes the common literature approaches for the quantification of X_r in the context of reliability analysis of oil tankers and the proposed X_r.

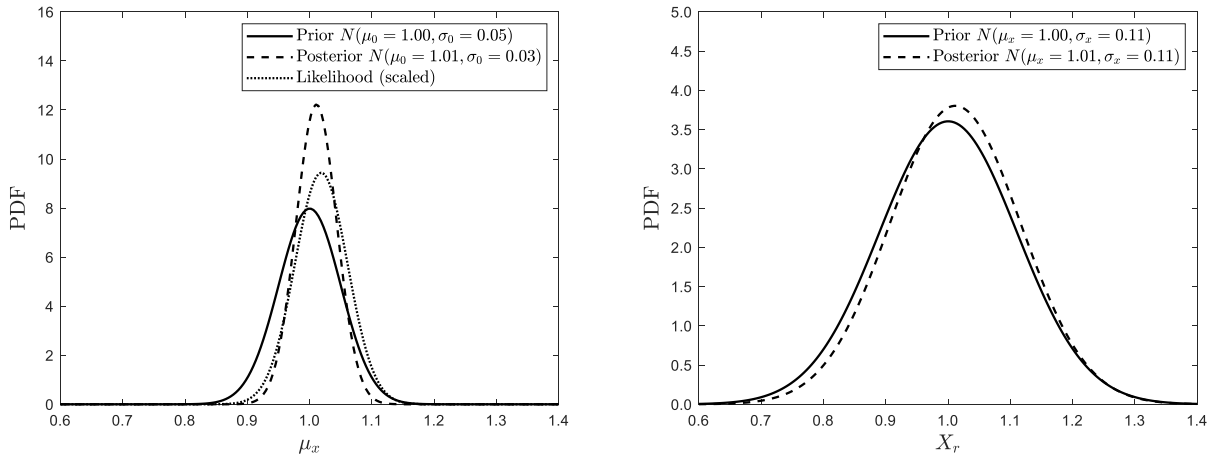

(a) (b)

Figure 6.3. Determination of strength model uncertainty factor X_r for oil tankers. (a) Bayesian updating of the mean value μ_X, and (b) prior and posterior predictive distributions of X_r. Note that predictive distributions include the statistical uncertainty of its mean value.

6.2.4.2 Numerical application on container ships

In contrast with tankers, the most unfavorable condition for container ships is the hogging. Hogging is also the most commonly experienced condition for these types of ships because of the result of the two following load effects: (i) buoyancy forces acting on the midship part are larger than those acting on the fore and aft parts, and (ii) cargo distribution is extended over the full length of the vessel. Recent studies have revealed the fact that lateral loads acting on the double bottom structure of container ships have a negative impact on the overall ultimate strength assessment when the ship is in hogging condition. This phenomenon is referred as the *double bottom effect* (see Appendix F for a detailed description). The consideration of the double bottom effect can be adequately captured through high-fidelity NLFEA. On the contrary, the conventional IACS CSR Smith's method cannot account for it.

Prior belief on mean uncertain parameter μ_X

In the case of container ships, prior belief on μ_X is based on two different sources of available information: (i) literature sources, and (ii) past NLFEA results conducted on a wide range of ship sizes. For the first source, structural reliability studies conducted on container ships show that the most commonly used value for μ_X is 1.00, see e.g. Parunov et al. (2014), Corak and Soares (2018) and Shi and Gao (2021). However, sufficient evidence for this selection is missing. For the second source of information, the results of NLFEA presented by Matsumoto et al. (2016) are used. In their analysis, the ratio between hull girder ultimate strength calculation using NLFEA to the conventional IACS CSR Smith's method prediction was extracted for 18 container ships of various sizes (4,000 – 10,000 TEU). The effect of double bottom has been explicitly considered by the authors in NLFEA while no initial imperfections were used. The results indicated a reduction of hull girder ultimate capacity because of the double bottom effect. Particularly, it was found that the mean value of the ratio X_r was equal to 0.86, whereas lower and upper bounds varied approximately from 0.7 to 1.0.

In the present analysis, we assume that 0.86 corresponds to the most probable value before observing any new data and that the value of 1.00 observed in literature - which also coincides with the maximum value obtained from Matsumoto et al. (2016) - corresponds to about 5% probability of exceedance. Then, we fit a normal distribution. The resulted prior PDF f'_{μ_X} has a mean value $\mu_0 = 0.86$ and standard deviation $\sigma_0 = 0.09$.

Likelihood

A series of NLFEA results performed on 6 post-Panamax vessels aims to increase our initial knowledge on the mean uncertain parameter μ_X and consequently, on the resulted model error X_r. The data used to formulate the likelihood have been retrieved by ClassNK (2014). In the investigation report, the ratio x_r of the ultimate strength calculated by 3-hold model elasto-plastic analysis to the ultimate strength calculated by IACS CSR Smith's method has been presented for the 6 vessels. The results are reproduced in Figure 6.4. The FE simulations accounted for the double bottom effect, while no initial imperfections were considered in the FE modelling in order to examine the impact of double bottom effect on the resulted strength.

Posterior distribution of mean value μ_X and predictive distribution of X_r

The results from the updating process of μ_X along with the posterior predictive distribution of X_r are illustrated in Figure 6.5. The error postulated in NLFEA results leads to a quite large variation of the likelihood function, similar to the previous case study for tankers. However, in contrast with tankers, the prior belief here is less informative. It turns out that the posterior distribution f''_{μ_X} is mainly affected from the likelihood. After removing the statistical uncertainty from the posterior predictive distribution, we come up with the recommended distribution model for model uncertainty factor X_r:

$$X_r \sim N(\mu_X = 0.83, \sigma_X = 0.10) \tag{6.11}$$

Figure 6.6b illustrates the proposed model uncertainty factor X_r along with the one commonly adopted for reliability assessment of container vessels in literature. It is noticed that this result is considerable different with the one adopted in previous research studies. This is because, in the past studies, the quantification of model uncertainty factor X_r exclusively relied on Smith's – most probable value – prediction. However, this is misleading since the conventional IACS CSR Smith's method does not take into account the double bottom effect. In the contrary, NLFEA take into account this effect. Double bottom effect is a phenomenon which is actually related to a reduction of the ultimate strength, and it can lead to serious damages or even ship losses, see ClassNK (2014). For this reason, it is beneficial to use the suggested distribution model when performing a reliability analysis on container ships at the design phase. Alternatively, intrusive methods should be used to appropriately modify the Smith's method in order to consider the effect. A recent study published by Tatsumi et al. (2020) accounted exactly for this fact.

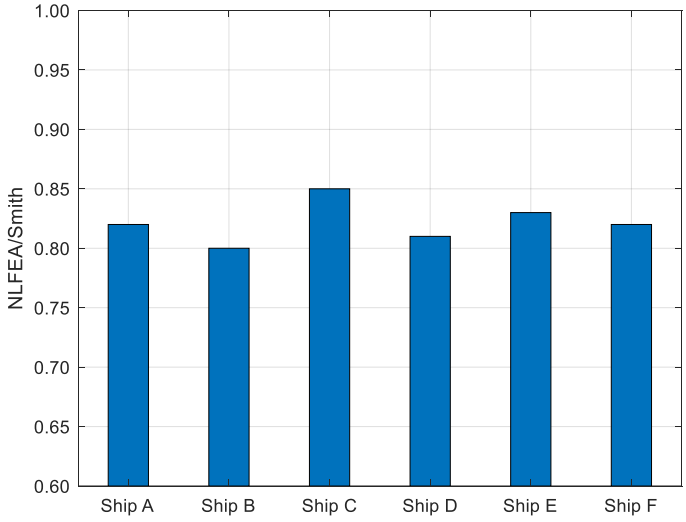

Figure 6.4. Ratio x_r of hull girder ultimate strength calculated by 3-hold model elasto-plastic analysis and IACS CSR Smith's model prediction, after ClassNK (2014).

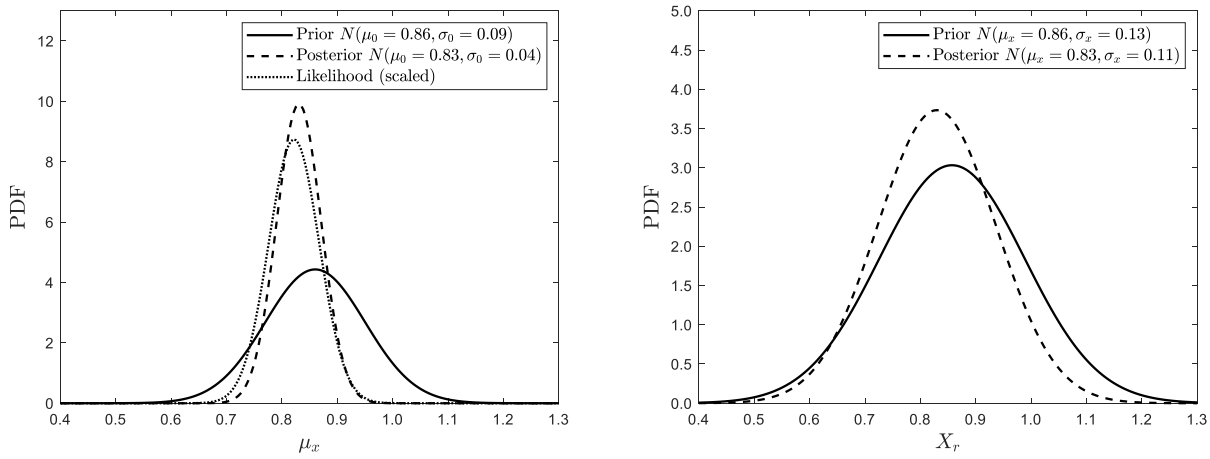

(a) (b)

Figure 6.5. Determination of strength model uncertainty factor X_r for container ships. (a) Bayesian updating of the mean value μ_X, and (b) prior and posterior predictive distributions of X_r. Note that predictive distributions include the statistical uncertainty of its mean value.

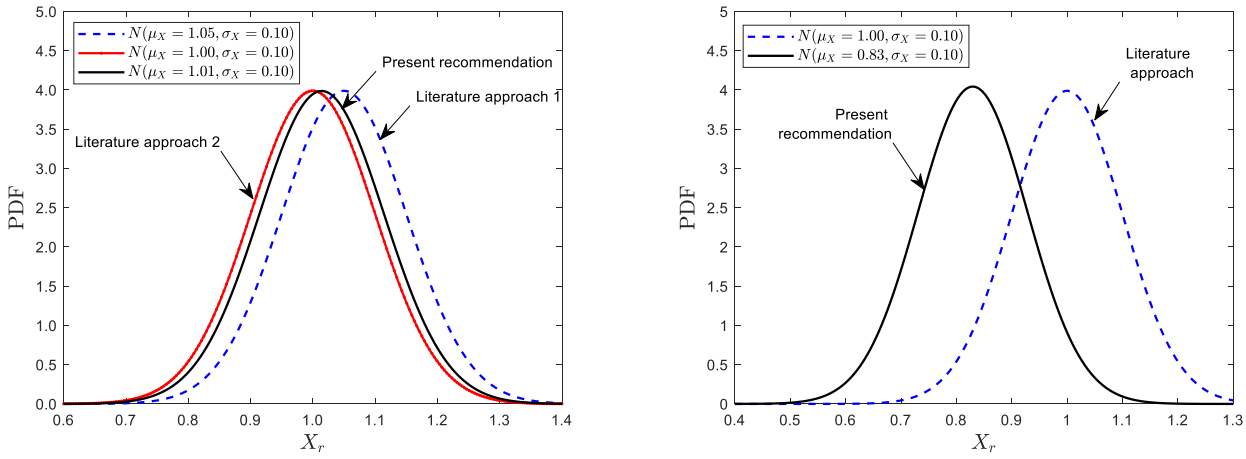

(a) (b)

Figure 6.6. Recommended distribution model for the quantification of strength model uncertainty factor X_r for (a) oil tankers and (b) container ships, along with existing practices from literature. Note that the statistical variability associated with the mean value μ_X has been substituted by its mean estimate.

6.2.4.3 Vessel-specific case study: Determination of model uncertainty factor for "MOL Comfort"

We now examine how the model uncertainty factor X_r can be further refined when available information from a target vessel becomes available (see Section 6.2.3). Bayesian updating is performed to evaluate the model error X_r for the case of "MOL Comfort" at the time of its accident. Particularly, the formulation of the prior distribution model f_X' coincides with the recommended global-based X_r for container ships (see Section 6.2.4.2). A single observation is used to formulate the likelihood. This value corresponds to the ratio[26] $x_i = 0.72$, see ClassNK (2014). An additive error is associated with this value – due to the difference of NLFEA prediction and real-life result – equal to $\sigma_\varepsilon = 0.05$ (as computed in Appendix G). The results of the Bayesian updating process are shown in Figure 6.7.

It is found that the updated PDF is very close to the likelihood since the variability of the likelihood is significantly lower than that of prior. Prior here becomes weakly informative. The posterior PDF $X_r \sim N(\mu_X = 0.74, \sigma_X = 0.04)$ can be used in the formulation of limit state function (LSF) when assessing the reliability of "MOL Comfort" at the time of accident.

It should be noted here that the reliability of the "MOL Comfort" *before* its construction would be evaluated using the derived model uncertainty factor X_r of the previous section. However, *after* the construction, the actual characteristics of the ship at the time of accident have been here considered. For example, deformations of bottom plates on sister ships were measured and used to simulate the true imperfect geometry. Information on the sea state condition prevailing at the time of accident has been also exploited to apply the actual loads acting at the structure. Such types of data have been embodied in a high-fidelity FE model which was then used to predict the ultimate hull girder strength. The results revealed a significant reduction on the model uncertainty factor.

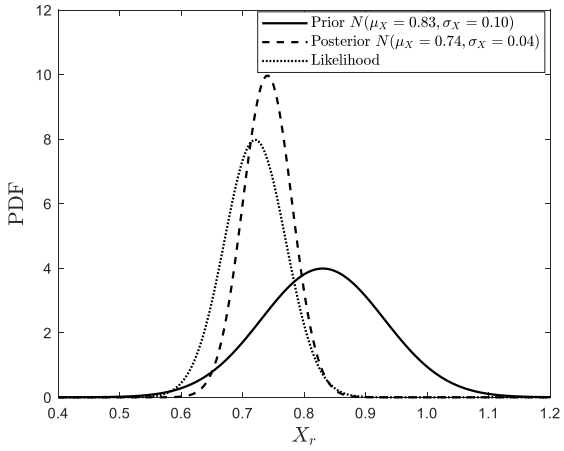

Figure 6.7. Updating the model uncertainty factor X_r for the case of "MOL Comfort" accident.

[26] This value has been derived applying the nominal yield strength values both on NLFEA and Smith's method.

6.2.5 Concluding remarks

A robust methodology for the probabilistic modelling of the strength model uncertainty factor in ultimate strength assessment has been presented in this section. The mathematical framework of Bayesian analysis is proved to be a powerful tool for that purpose, able to provide a formal way of dealing with small amount of available data while combining efficiently different sources of information.

The recommended Bayesian updating scheme can be performed dually; firstly, combining available information from different sources, such as, literature, experts' accumulated knowledge and past NLFEA studies, to learn the "population" statistics and build a general-purpose model, and secondly, using information of the particular characteristics of hull structure of a target - or sister ships - to adjust the model uncertainty factor explicitly. Undoubtfully, the best practice would be to consider both of the updating approaches in a sequential manner, that is, to use the results from the population learning as the prior information and then perform the direct updating of the model error parameter X_r (see Section 6.2.4.3).

A summary of the information and the results obtained after the implementation of Bayesian updating for model uncertainty factor X_r is illustrated in Figure 6.8. Two types of ships were analyzed throughout this section, i.e., container ships and tankers. In each case, the updating was performed by appropriately quantifying the available sources of information. For oil tankers, the results showed that the probabilistic modelling of capacity can be entirely rely on the IACS CSR Smith' model prediction. In contrast, for container ships, Smith's method must be corrected by NLFEA in order to consider the double bottom effect in extreme hogging conditions. The exclusion of this phenomenon can severly overestimate the true strength. The correction of Smith's method is reflected on the proposed model uncertainty factor X_r. Alternatively, a correction in the method of Smith itself can be implemented intrusively, see Tatsumi et al. (2020).

During the construction of a specific vessel, information from the hull structure condition can be acquired and used to update a "digital twin" of the vessel, that is, a purpose-built FE model. Of course, this information can be also added during operation or inspection surveys. It is possible then to explicitly update the model uncertain parameter X_r. A demonstration of this methodology has been analytically presented in Section 6.2.4.3 for the case of "MOL Comfort" at the time of accident. The results showed that a considerable decrease on the uncertainty of model error can be achieved in this way. This, in turn, would determine a more reliable safety index for the specific vessel.

Overall, a well-documented and robust methodology has been presented in Section 6.2 for a rational determination of model uncertainty factor. Subjective and objective types of information have been effectively addressed through the framework of Bayesian analysis. The proposed methodology allows for the explicit quantification of NLFEA uncertainty and has the capability of incorporating new data with a systematic approach.

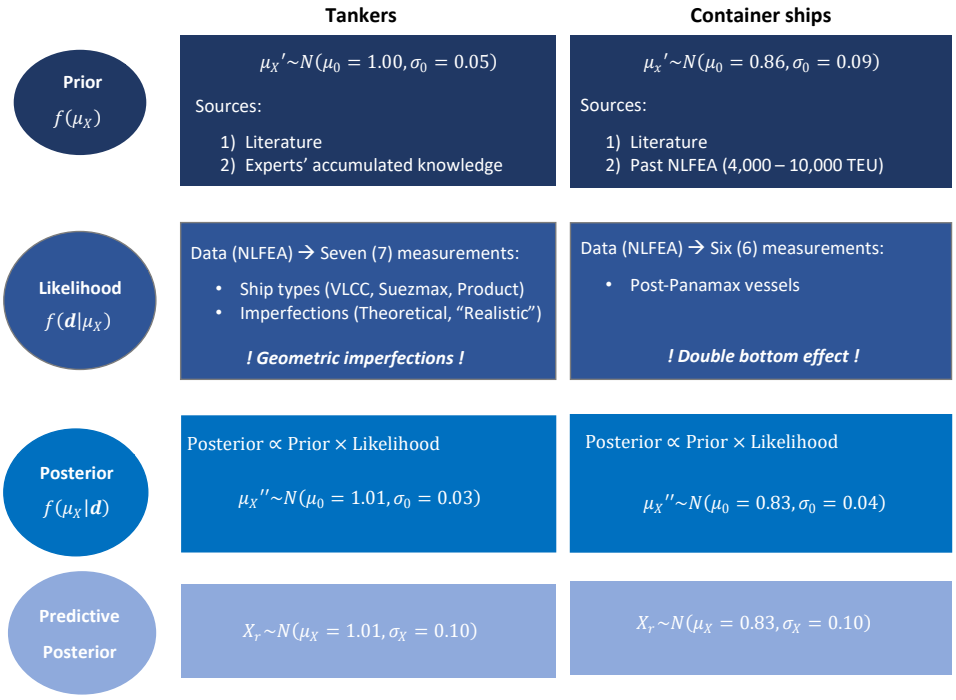

Figure 6.8. Summary of information and results obtained by implementing the Bayesian updating scheme for container ships and oil tankers. The recommended predictive posterior of model uncertainty factor X_r shall be used for application in reliability assessment.

6.3 A Bayesian approach for learning and updating the corrosion model parameters

6.3.1 Background

Several probabilistic corrosion models have been established so far, aiming at quantifying the thickness loss due to uniform/general corrosion. Most of the models have been developed empirically based on thickness measurements collected over a wide range of ships of similar type. Although these models provide a relatively good approximation of thickness prediction over time and a useful guide for design purposes, they are prone to a large degree of uncertainty (see Section 2.4.5).

Marching into the digital-twin era, condition assessment of structures tends to be more unique. In this direction, information related to the hull structure condition that may come into light at the construction stage and/or during operation become more and more relevant. Often, thickness measurement reports acquired from inspections surveys remain unexploited. The inclusion of such information into existing generic (global-based) empirical corrosion models

could mitigate the uncertainties of model parameters and provide improved corrosion predictions for the remaining life of the target vessel.

Methods for updating corrosion predictions of steel plates conditional on inspection data have been recently developed in the field of ship structures. Lampe and Hamann (2018) presented an updating scheme for predicting general corrosion on structural elements of an ageing ship by considering inspection data. In particular, it was shown how the parameter values of the employed corrosion model can be adjusted based on available inspection measurements and improve the accuracy of the corrosion model. Mohammadrahimi and Sayebani (2019) used a Bayesian approach to model the time-dependent corrosion wastage for the deck panel of bulk carriers. A set of about $4{,}000$ measurements were used for the updating. Kim and Straub (2017) investigated the effect of spatial variability of corrosion on the reliability of ships considering hypothetical measurements from inspections. A hierarchical spatial model was adopted to represent the spatial variability of corrosion. A Bayesian updating scheme was developed to investigate the effect of different spatial corrosion models and the number of inspected elements on the resulting reliability.

The main objective of the present study is to develop a practical and useful methodology able to predict thickness diminution of steel plates due to general/uniform corrosion. To this end, we employ a Bayesian approach to incorporate new data acquired on field into a global-based time-dependent corrosion model, and provide updated predictions for vessel-specific purposes. As Bayesian techniques are particularly useful in cases where a limited number of measurements is available, we attempt to offer reliable results using only a small portion of the available data. Such a solution could be beneficial for reducing the inspection effort and mitigating the associated costs. In addition, decisions associated with lifetime extension and maintenance policy can be arranged with that way. In addition, the effect of the updating process on the reliability of the target ship is investigated later in Chapter 7. The present study differs from the existing ones presented in the literature so far as it combines the following:

- A different procedure for implementing the Bayesian updating scheme in ship structures is proposed.
- Sequential Bayesian updating using a minimum amount of data from each inspection is performed.
- The updating is performed on the entire set of structural elements of midship section and thus, it provides a holistic view of its structural resistance.
- A validation of the method based on observations from the last inspection is obtained for all elements.

The present study is an extension of the work published by Georgiadis and Samuelides (2019).

6.3.2 Methodology

An outline of the methodology followed for the derivation of updated thickness predictions is illustrated in Figure 6.9. Broadly speaking, the whole procedure can be classified into three main steps: (i) data processing, (ii) Bayesian updating of corrosion model parameters, and (iii) validation and interpretation of the results.

In the first stage, the various environmental classes that characterize the corrosion growth for different groups of elements are identified. UT measurement reports carried out at the 15th, 18th and 20th year of the service life of target vessel are processed (see Section 6.3.3). Readings are then classified into 22 groups (or classes) based on the environmental conditions that prevail on each area and their impact on the time-dependent corrosion progress, see Paik et al. (2003)a.

In the second stage, the Bayesian updating of corrosion model parameters takes place. The mathematical formulation of the problem is thoroughly presented in Section 6.3.4. Bayesian updating is implemented using data (i) from the first inspection and (ii) the first and second inspection. A limited number of data is used for the updating process for the reasons explained in Section 6.3.1.

In the third step, the updated model predictions for all elements are presented and validated against the actual measurements from the last inspection. Mean predictions and associated credible intervals of the parameter of interest, i.e., corrosion wastage, are depicted as a function of time. A close investigation on the deck plates of the vessel is analyzed in Section 6.3.5.

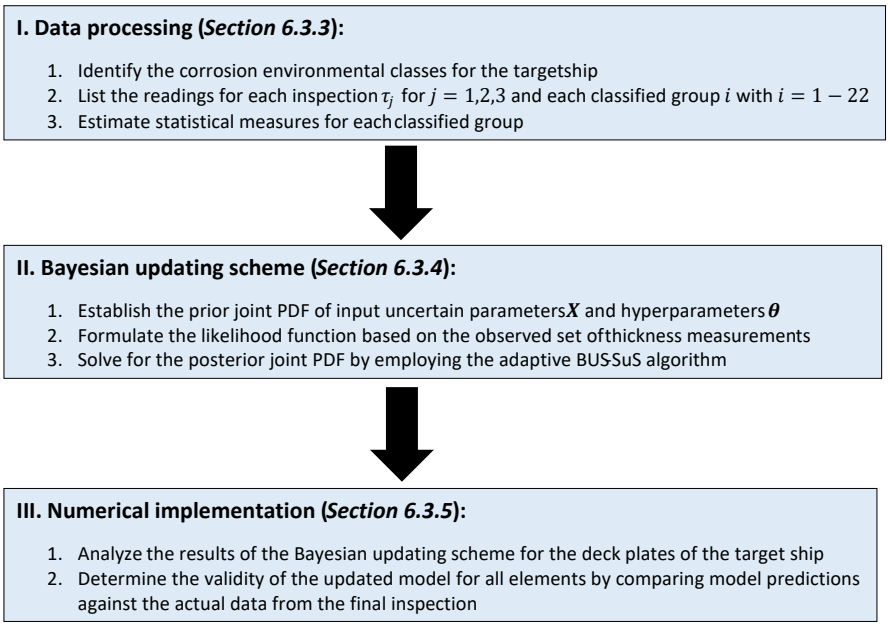

Figure 6.9. Overview of the proposed methodology.

6.3.3 Data processing

6.3.3.1 Corrosion environmental classes

Different corrosion environmental classes have been identified based on the recommendation of Paik et al. (2003)a. Application on the examined VLCC results in a total of 21 environmental classes (or groups) as shown in Figure 6.10. The characteristics of the target vessel have been presented in Section 4.2.4.1.

Each class is characterized by a time-invariant and uncertain annual corrosion rate that follows the Weibull distribution with scale parameter λ and shape parameter k (see Table 6.2). The corresponding mean values and CoVs have been computed for each group by assuming a linear corrosion propagation law and that corrosion initiates after 7.5 years of service (see Section 2.4.5.1). These assumptions arise additional uncertainties[27] on the values listed in Table 6.2. This fact will be explicitly considered in the framework of Bayesian analysis as will be shown later in Section 6.3.4.1.

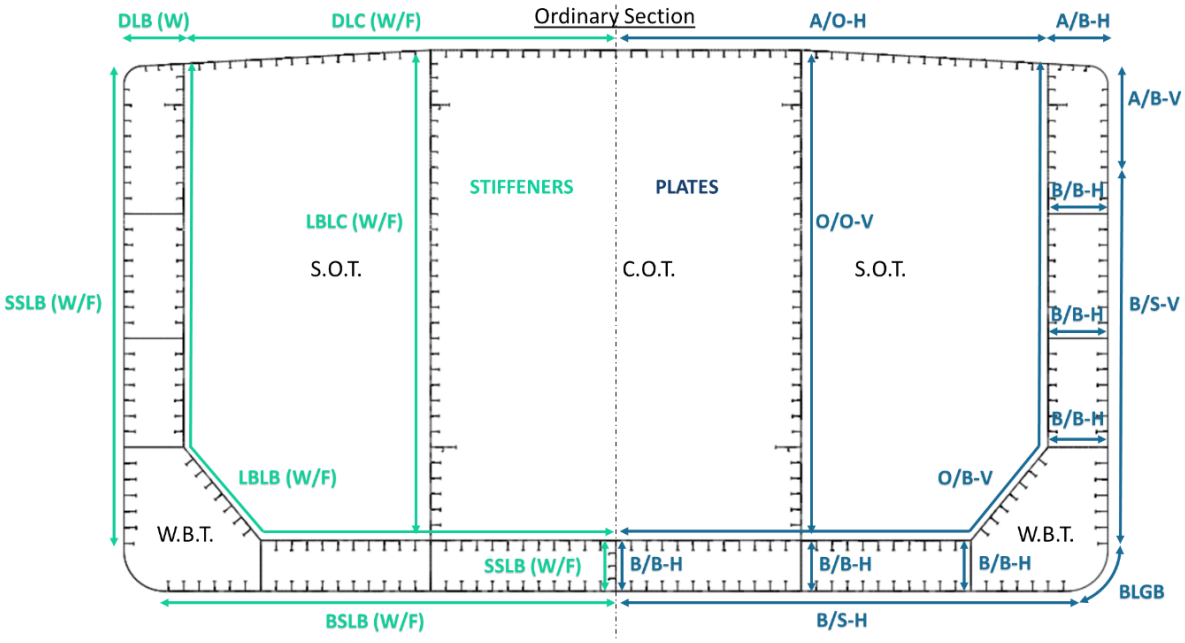

Figure 6.10. Classified corrosion environmental groups for the target VLCC according to Paik et al. (2003)a.

[27] It is reminded here that primary sources of uncertainties related to model parameters arise due to the fact that measurements have been collected from the global fleet of oil tankers covering a wide range of operational profiles, maintenance policies, etc. (see also the discussion in Section 2.4.5).

Table 6.2. Mean value and CoV with associated Weibull distribution parameters λ (scale parameter), k (shape parameter) for the annualized corrosion rate C_1 of each group, after Paik et al. (2003)a.

ID	Group	Mean (mm/year)	CoV	Scale parameter λ	Shape parameter k
1	A/O-H	0.0581	0.8262	0.0620	1.2163
2	A/B-H	0.1084	0.8183	0.1159	1.2286
3	A/B-V	0.0661	1.1341	0.0622	0.8839
4	B/S-V	0.0622	1.0030	0.0621	0.9970
5	BLGB	0.0619	0.8821	0.0648	1.1361
6	B/S-H	0.0597	0.9901	0.0599	1.0100
7	B/B-H	0.1408	0.2704	0.1550	4.1661
8	O/B-V	0.1012	0.7994	0.1088	1.2592
9	O/O-V	0.0577	0.8162	0.0617	1.2319
10	DLC (W)	0.0716	0.8902	0.0747	1.1254
11	DLC (F)	0.0588	1.0032	0.0587	0.9968
12	DLB (W)	0.2403	0.9165	0.2485	1.0923
13	DLB (F)	0.2403	0.9165	0.2485	1.0923
14	SSLB (W)	0.1413	1.0097	0.1407	0.9904
15	SSLB (F)	0.0882	0.8966	0.0919	1.1172
16	BSLB (W)	0.1367	0.7802	0.1478	1.2921
17	BSLB (F)	0.1127	1.0121	0.1121	0.9881
18	LBLB (W)	0.1960	0.9993	0.1961	1.0007
19	LBLB (F)	0.1782	0.9941	0.1786	1.0059
20	LBLC (W)	0.0550	0.8129	0.0589	1.2372
21	LBLC (F)	0.0508	1.0012	0.0508	0.9988

6.3.3.2 Thickness measurements data

The UT measurement report of the examined ship is available for the first, second and third inspection survey. Since we are interested in estimating the corrosion wastage at midship section area, recordings corresponding to cargo tank no. 3 are of relevance here. Outliers have not been removed from the data set on the basis that all measurements collected from the inspector are considered trustworthy. Therefore, large deviations on corrosion wastage observed within an environmental class may attributed to non-uniformity of corrosion and the fact of measuring different locations on each inspection.

The sample statistics of corrosion wastage for each group are summarized in Table 6.3. Inner bottom plates and side longitudinal bulkhead plates have been divided into two separate groups because it was noticed that the degree of corrosion penetration has a substantial difference among them. The higher level of corrosion growth is present at the deck plates and longitudinal stiffeners of cargo tanks, as well, at the inner bottom plates. In general, the area inside oil tanks is more corrosive than the area inside ballast tanks. For the majority of groups, the thickness diminution is relatively small (less than $1\ \mathrm{mm}$ on average). Moreover, it is seen that corrosion does not grow linearly with time, but rather stabilizes between second and third inspection.

Table 6.3. Sample statistics of corrosion wastage for all plates and stiffeners located at the midship section region of the examined VLCC. Thickness measurements are grouped in 22 environmental classes.

Group	Inspection 1			Inspection 2			Inspection 3		
	Samples	Mean (mm)	St. dev. (mm)	Samples	Mean (mm)	St. dev. (mm)	Samples	Mean (mm)	St. dev. (mm)
A/O-H	183	1.50	0.52	167	1.55	0.46	168	1.66	0.51
A/B-H	56	0.14	0.06	54	0.59	0.41	54	0.47	0.26
A/B-V	40	0.17	0.11	42	0.27	0.08	40	0.28	0.07
B/S-V	82	0.15	0.09	134	0.26	0.09	122	0.27	0.07
BLGB	40	0.16	0.10	30	0.20	0.11	30	0.23	0.10
B/S-H	214	0.18	0.09	216	0.19	0.11	216	0.21	0.10
B/B-H	164	0.14	0.06	118	0.16	0.07	100	0.17	0.06
O/B-V [(1)]	190	0.96	0.22	188	1.88	0.80	196	1.25	0.72
O/B-V [(2)]	178	0.28	0.10	200	0.27	0.12	260	0.39	0.14
O/O-V	178	0.28	0.12	208	0.29	0.14	208	0.33	0.31
DLC (W)	156	0.49	0.17	360	1.18	0.43	208	1.49	0.31
DLC (F)	156	0.49	0.21	360	0.84	0.47	208	0.83	0.10
DLB (W)	40	0.28	0.13	72	0.21	0.08	54	0.25	0.08
DLB (F)	40	0.27	0.14	72	0.26	0.13	54	0.26	0.08
SSLB (W)	210	0.21	0.09	210	0.22	0.11	208	0.19	0.08
SSLB (F)	210	0.19	0.07	210	0.26	0.14	208	0.23	0.09
BSLB (W)	312	0.19	0.09	378	0.19	0.07	380	0.24	0.07
BSLB (F)	312	0.20	0.09	378	0.24	0.08	380	0.27	0.07
LBLB (W)	560	0.21	0.09	526	0.25	0.10	526	0.33	0.09
LBLB (F)	560	0.20	0.08	526	0.27	0.10	526	0.31	0.09
LBLC (W)	178	0.41	0.21	300	0.30	0.10	300	0.40	0.15
LBLC (F)	178	0.34	0.17	300	0.33	0.13	300	0.38	0.17

Notes:

[(1)] Inner bottom plates.

[(2)] Side longitudinal bulkhead plates.

6.3.4 Bayesian Updating scheme

6.3.4.1 Problem description

Let us consider the model $\mathcal{M}$ of Eq. (2.12) which predicts the corrosion diminution of a steel plate in mm as a function of time τ and the input random vector $\boldsymbol{X} = [X_1, X_2, X_3]^T$:

$$\mathcal{M}(\boldsymbol{X};\tau) = \begin{cases} X_1(\tau - X_2)^{X_3}, & \tau \geq X_2 \\ 0, & \tau < X_2 \end{cases} \tag{6.12}$$

This model assumes uniform/general thickness reduction of steel, and thus, it does not consider the actual spatial variability - non-uniformity - of corrosion within the plate's surface. The consideration of spatial variability would require the explicit modelling of thickness using random fields. However, the random field approach has not been adopted in the present thesis for the following reasons. First, the computational cost and modelling effort for performing the updating for the entire hull girder and for different time instances would be enormous. Second, information on the exact measurements' location is not available for the problem at hand. Third, results from this study are used later for implementing IACS CSR Smith's algorithm. Nevertheless, Smith's model requires the assignment of a single value of thickness, namely, a uniform thickness diminution is considered for a given structural member.

In the present study, we keep the analysis simple, and without loss of generality, we model the spatial variability of corrosion through a random variable (RV) approach. This random variable represents the *inherent* variability of thickness within an area of interest. Therefore, its distribution model cannot be learned explicitly, since this type of variability can be diminished only up to a certain level with an increasing number of measurements. However, the statistical parameters of the distribution model can be learned (this is the case discussed in Section 5.6.3). For the problem at hand, a prior joint distribution $f_{\boldsymbol{\Theta}}(\boldsymbol{\theta})$ is established on the hyperparameters $\boldsymbol{\theta}$ of the basic random variables $\boldsymbol{X}$. Measurements $\boldsymbol{d}$ corresponding to the model outcome $\mathcal{M}(\boldsymbol{x})$ are then used to reduce the uncertainties considered in the model through updating $f_{\boldsymbol{\Theta}}(\boldsymbol{\theta})$ by means of a Bayesian inverse analysis. A schematic description of the learning process is illustrated in Figure 6.11.

The formulation of the Bayesian updating problem takes the following functional form:

$$f_{\boldsymbol{\Theta}|\boldsymbol{D}}(\boldsymbol{\theta}|\boldsymbol{d}) \propto f_{\boldsymbol{D}|\boldsymbol{\Theta}}(\boldsymbol{d}|\boldsymbol{\theta}) f_{\boldsymbol{\Theta}}(\boldsymbol{\theta}) \tag{6.13}$$

where the proportionality constant is equal to:

$$c_E = \left[\int_{\boldsymbol{\theta}} f_{\boldsymbol{D}|\boldsymbol{\theta}}(\boldsymbol{d}|\boldsymbol{\theta}) f_{\boldsymbol{\theta}}(\boldsymbol{\theta}) d\boldsymbol{\theta}\right]^{-1} \tag{6.14}$$

Briefly, the solution of the updating problem requires:

1. The description of a joint PDF $f_{\boldsymbol{X}|\boldsymbol{\theta}}(\boldsymbol{x}|\boldsymbol{\theta})$ for $\boldsymbol{X}$ parameters conditional on the uncertain hyperparameters $\boldsymbol{\theta}$
2. The establishment of a prior joint PDF $f_{\boldsymbol{\theta}}(\boldsymbol{\theta})$
3. The formulation of the likelihood function $f_{\boldsymbol{D}|\boldsymbol{\theta}}(\boldsymbol{d}|\boldsymbol{\theta})$ as a function of $\boldsymbol{\theta}$ given an observation set $\boldsymbol{d}$
4. The calculation of the posterior joint PDF $f_{\boldsymbol{\theta}|\boldsymbol{D}}(\boldsymbol{\theta}|\boldsymbol{d})$ for $\boldsymbol{\theta}$ conditional on the observation set $\boldsymbol{d}$
5. The final evaluation of the unconditional posterior predictive distributions $\tilde{f}_{\boldsymbol{X}}(\boldsymbol{x})$

The above steps are thoroughly described in the remaining section.

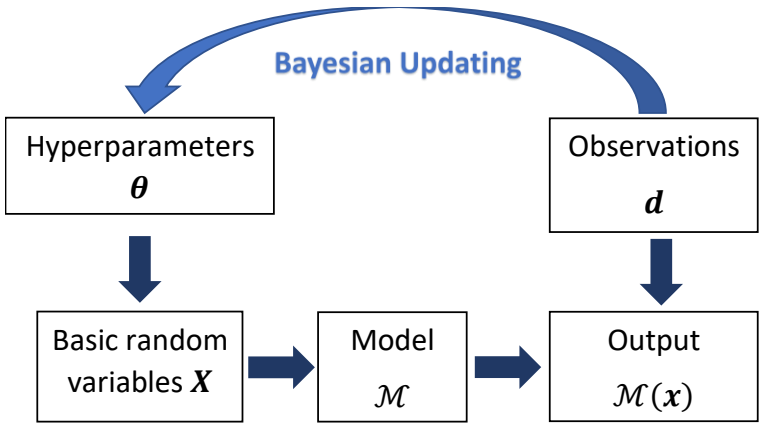

Figure 6.11. Learning the hyperparameters $\boldsymbol{\theta}$ of model parameters $\boldsymbol{X}$ through indirect measurements $\boldsymbol{d}$ that correspond to the model outcome $\mathcal{M}(\boldsymbol{x})$.

Probabilistic modelling of input parameters $\boldsymbol{X}$ and prior hyperparameters $\boldsymbol{\theta}$

Model input parameters $\boldsymbol{X}$ are expressed by their joint PDF. To make the dependence of the model parameters to their corresponding parameters explicit, we express $\boldsymbol{X}$ conditional on $\boldsymbol{\theta}$, i.e., $f_{\boldsymbol{X}|\boldsymbol{\theta}}(\boldsymbol{x}|\boldsymbol{\theta})$. The uncertainty associated with the hyperparameters $\boldsymbol{\theta}$ is represented by their joint PDF $f_{\boldsymbol{\theta}}(\boldsymbol{\theta})$. In the following, we establish the individual PDF of each variable X_i separately, after assuming independence among them. In addition, the distribution models for the hyperparameters $\boldsymbol{\theta}$ are defined.

The annual corrosion rate parameter X_1 follows a Weibull distribution model with uncertain shape parameter λ_{X_1} and scale parameter k_{X_1} (see Section 2.4.5.1). Since both parameters are positive definite a bivariate lognormal distribution is a rational selection for their joint representation. The prior correlation coefficient ρ between the two random variables λ_{X_1} and k_{X_1} is calculated for each environmental class[28]. The values listed in Table 6.1 are set as their expected values. Following the short discussion in Section 6.3.3.1, a high degree of variability is assumed for both parameters to reflect their high statistical uncertainty. Their coefficient of variation CoV is thus set equal to 30%.

The coating life (or corrosion initiation) parameter X_2 is represented by a lognormal distribution with parameters η_{X_2} and ζ_{X_2}. These parameters express the mean and standard deviation of the underlying normal distribution of $\ln X_2$, and can be related to the mean μ_{X_2} and coefficient of variation CoV_{X_2} of X_2 using the relationships of Eq. (C.7) and (C.8)**.**

Coating life is expected to vary in the range of 5 to a maximum of 15 years (see Section 2.4.5.1). Assigning a 10% probability of non-exceeding the value of 5 years, the resulted coefficient of variation of the parameter is equal to $\mathrm{CoV}_{X_2} = 0.30$. This value is assumed known and is modelled as a fixed quantity. We use inspections data to learn the mean value μ_{X_2} of coating life parameter which is assumed unknown. Mean value typically ranges between 5 to 10 years. Typically, a mean value equal to 7.5 years is considered in literature (see Section 2.4.5.1). From this information, we set the mean equal to 7.5 and the coefficient of variation equal to 10%. We then fit a lognormal distribution to represent the variability on μ_{X_2}.

The corrosion progress (trend) parameter X_3 is assumed to follow a Beta distribution with lower limit a_{X_3} and upper limit b_{X_3}, and shape parameters $\alpha_{X_3}, \beta_{X_3} > 0$. We will here parametrize the Beta distribution with the mean value of parameter μ_{X_3} and its standard deviation σ_{X_3}, so that $X_3 \sim Beta\left(\mu_{X_3}, \sigma_{X_3}, \left[\mathrm{a}_{X_3}, \mathrm{b}_{X_3}\right]\right)$. This selection is made because the first and second order statistics are more intuitive than the shape parameters. The relations that link the parameters of Beta distribution with its mean and standard deviation are given in Eq. (C.15) and (C.16).

---

[28] An estimate of the prior correlation coefficient ρ between the two uncertain parameters λ and k can be obtained by implementing the following procedure:

1. Create a $K \times K$ (with $K \sim 10^5$) matrix of random numbers from the original Weibull distribution with fixed shape k and scale parameters λ. The random numbers of each array $1 \times K$ follow the prescribed Weibull distribution.
2. For the i-th array ($i = 1,2, \dots, K$), the associated parameters $\lambda^{(i)}$ and $k^{(i)}$ can be found after computing the mean value and standard deviation of the i-th array.
3. The correlation coefficient ρ_0 between the parameters λ and k is calculated for the obtained $\boldsymbol{\lambda}$ and $\boldsymbol{k}$ vectors with corresponding size $K \times 1$. Finally, the correlation coefficient ρ between $\log(k)$ and $\log(\lambda)$ is then estimated from the $\log(\boldsymbol{k})$ and $\log(\boldsymbol{\lambda})$ vectors.

Corrosion progress is generally assumed to vary in the range 0.30 (lower bound) and 1.50 (upper bound). However, the majority of the scientific body advices that values of corrosion trend mostly lie between 0.30 (optimistically) to 1.00 (pessimistically) (see Section 2.4.5). Here, we set 1.00 as the 95% quantile of the Beta distribution with lower and upper bounds 0.30 and 1.50. The resulted mean value and coefficient of variation are equal to $\mu_{X_3} = 0.75$ and $\mathrm{CoV}_{X_3} = 0.20$. We assume that the variability of the parameter X_3 is known and we model the mean value μ_{X_3} as a random variable. Based on literature sources, the mean value μ_{X_3}typically lies between 0.50 and 1.00, see e.g., Melchers (1999)b. Setting its mean equal to 0.75 and assuming that 0.50 and 1.00 correspond to the bounds of plausible values, we fit a lognormal distribution to represent the variability in μ_{X_3}. The resulting coefficient of variation is equal to 0.15.

Overall, the vector of hyperparameters $\boldsymbol{\theta}$ consists of the following four uncertain parameters $\boldsymbol{\theta} = \left[\lambda_{X_1}, k_{X_1}, \mu_{X_2}, \mu_{X_3}\right]^T$ whose prior distribution models are listed in Table 6.5. It is assumed that μ_{X_2} and μ_{X_3} act independently among each other and among the other two hyperparameters. The probabilistic description of $\boldsymbol{X}$ vector is summarized in Table 6.4.

Table 6.4. Distribution models of corrosion model parameters $\boldsymbol{X}$.

Parameter	Symbol	Distribution	Mean value	CoV
Annual corrosion rate [mm/year]	$C_1 \equiv X_1$	Weibull	*uncertain*	*uncertain*
Coating life [years]	$\tau_c \equiv X_2$	Lognormal	*uncertain*	0.30 (*fixed*)
Corrosion progress	$C_2 \equiv X_3$	Beta	*uncertain*	0.20 (*fixed*)

Table 6.5. Prior distribution models of hyperparameters $\boldsymbol{\theta}$.

Hyperparameter	Symbol	Distribution	Mean value	CoV
Scale parameter	$\lambda_{X_1} \equiv \theta_1$	Bivariate lognormal	*As in Table 6.2*	0.30
Shape parameter	$k_{X_1} \equiv \theta_2$		*As in Table 6.2*	0.30
Mean value	$\mu_{X_2} \equiv \theta_3$	Lognormal	7.50	0.10
Mean value	$\mu_{X_3} \equiv \theta_4$	Lognormal	0.75	0.15

Likelihood formulation

Measurements are mathematically represented by the likelihood function. Let us consider that a single measurement d_i is recorded at a given time instance τ. This measurement corresponds to a given model outcome $\mathcal{M}(\boldsymbol{x})$ and is prone to an error due to measurement and model uncertainties[29]. Assuming an additive error term ε, this single measurement can be written as follows:

$$d_i = \mathcal{M}(\boldsymbol{x};\tau) + \varepsilon \tag{6.15}$$

We further postulate a zero-mean normal distribution model with standard deviation σ_ε to describe this error, that is, $\varepsilon \sim N(0,\sigma_\varepsilon)$. The analytical form of the marginalized likelihood function for a single measurement reads (see Eq. (5.20)):

$$L_i(\boldsymbol{\theta};\tau) = \int_{-\infty}^{\infty} \dots \int_{-\infty}^{\infty} f(d_i|\boldsymbol{x}) f(\boldsymbol{x}|\boldsymbol{\theta}) dx_1 \dots dx_n \tag{6.16}$$

It is stressed that the integration is performed with respect to $\boldsymbol{x}$ vector and thus, likelihood is expressed as a function of $\boldsymbol{\theta}$. For the problem at hand, the precise expression of the likelihood function becomes:

$$L_i(\boldsymbol{\theta};\tau) = \int_{0.3}^{1} \int_{0}^{\tau} \int_{0}^{\infty} f_\varepsilon(d_i - x_1(\tau - x_2)^{x_3}) f_{X_1}(x_1|\theta_1,\theta_2) f_{X_2}(x_2|\theta_3) f_{X_3}(x_3|\theta_4) dx_1 dx_2 dx_3 \tag{6.17}$$

For a set of multiple measurements m independent on each other, obtained at a given time instance τ, the likelihood is evaluated as the product of individual marginalized likelihoods:

$$L(\boldsymbol{\theta};\tau) = \prod_{i=1}^{m} L_i(\boldsymbol{\theta};\tau) \tag{6.18}$$

If we further assume independence of measurements between different time instances $\{\tau_1, \dots, \tau_{m_\tau}\}$, we can express the likelihood function as (see Eq. (5.11)):

[29] *Measurement error* may be attributed to inaccuracy of measurement tool and location error. Location error may become significant if the corrosion of plates is not entirely uniform (as in practice) and the precise location of readings at different time instances is uncertain. On the other hand, *model error* involves the assumption of an "ideal" uniform thickness diminution within an area. Although this may be accepted for practical use, it does not represent real life. It can be said that location error is included in model error component.

$$L(\boldsymbol{\theta};\tau_1,\dots,\tau_{m_\tau}) = \prod_{j=1}^{m_\tau}\prod_{i=1}^{m} L_i(\boldsymbol{\theta};\tau_j) \tag{6.19}$$

Posterior distribution of $\boldsymbol{\theta}$ and predictive distribution of basic random variables $\boldsymbol{X}$

The solution of Eq. (6.13) is implemented using the adaptive version of BUS-SuS approach presented in Section 0. Samples of the posterior PDFs of $\boldsymbol{\theta}$ are thus generated. The posterior predictive distribution $\tilde{f}_X$ for each X_i is thus evaluated by marginalizing out the hyperparameters $\boldsymbol{\theta}$ according to the following relations:

Posterior predictive distribution for X_1:

$$\tilde{f}_{X_1}(x) = \int_0^\infty \int_0^\infty f_{X_1}(x|\theta_1,\theta_2) f''(\theta_1,\theta_2) d\theta_1 d\theta_2 \tag{6.20}$$

Posterior predictive distribution for X_2:

$$\tilde{f}_{X_2}(x) = \int_0^\infty f_{X_2}(x|\theta_3) f''(\theta_3) d\theta_3 \tag{6.21}$$

Posterior predictive distribution for X_3:

$$\tilde{f}_{X_3}(x) = \int_0^\infty f_{X_3}(x|\theta_4) f''(\theta_4) d\theta_4 \tag{6.22}$$

In each case, the evaluation of the unconditional distribution of X_i is implemented employing a Monte Carlo simulation where samples from the posterior PDFs $f''(\boldsymbol{\theta})$ are used.

6.3.5 Numerical implementation on a VLCC tanker

The proposed Bayesian updating scheme is used here to demonstrate its benefit on real problems. A relatively limited number of measurements from the full set of available readings, as displayed in Table 6.3, is randomly selected to update the corrosion wastage prediction for each group. Measurements from the last inspection are kept off record and used only for validation purposes. A close investigation is implemented here for the deck plates located at

the cargo area of the target vessel[30]. For this group, the impact of different number of observations on the updating scheme is examined (see Table 6.6). Then, we generalize our results for the remaining 21 groups using a standard number of measurements, i.e., using 10 measurements from each inspection. The effect of the random selection of m measurements is discussed in Section 6.3.5.1.

The error associated with each measurement is assumed equal to $\sigma_{\varepsilon} = 0.10\ \mathrm{mm}$. This covers the uncertainty which arises from the *measurement tool* and the *effect of location*. In the former case, error due to inaccuracies in the measuring device may occur. The latter case is referred to the fact that if the inspector repeats the survey, observations on different locations from the original will be recorded. This, in turn, would possibly result in a somewhat different set of measurements.

The adaptive version of BUS-SuS algorithm that was briefly reviewed in Section 5.7.2 is employed here to sample from the posterior distributions of hyperparameters $\boldsymbol{\theta}$. The posterior predictive distributions of the basic random variables $\boldsymbol{X}$ are then obtained using a Monte Carlo simulation and following Eq. (6.20)-(6.22). The number of samples per subset level D_i has been selected equal to $K = 3000$ and the probability of accepted samples for each subset level is set equal to $p_0 = 0.1$. The above selections have been mainly based on the recommendations presented by Betz et al. (2018).

Due to the high computational cost needed for evaluating the logarithm of the joint likelihood function (see Eq. (5.12)) for a given set of input parameters $\boldsymbol{\theta}$, neural networks have been efficiently trained and used adaptively at each conditional subset to accelerate the aBUS-SuS algorithm. This concept has been originally presented by Giovanis et al. (2017). An outline of the procedure is presented below.

Table 6.6. Number of measurements considered for each specified scenario for the implementation of Bayesian updating scheme. Application on A/O-H group.

Scenario	Data	
	Inspection 1	Inspection 2
1	5	-
2	10	-
3	20	-
4	5	5
5	10	10
6	20	20

[30] Deck plates have been selected because they display the highest level of corrosion diminution among all groups and deviate the most from prior model prediction. In other words, the “worst-case” scenario is examined here.

At each subset level we construct a NN surrogate of the logarithm of the likelihood function $\ln L(\boldsymbol{\theta}|\boldsymbol{d})$. This surrogate will be used to accelerate the generation of $i = 1,2,\dots,K$ samples conditional on the intermediate domain D_i required to proceed to the next level of SuS. The NN is trained with a limited number of training samples. A training point is defined as a duad $\{\boldsymbol{\theta}^{(i)}, y^{(i)}\}$, where $y^{(i)} = \ln L(\boldsymbol{\theta}^{(i)}|\boldsymbol{d})$. The input vector $\boldsymbol{\theta}$ consists of 5 parameters and the output y is a scalar parameter.

In the present study, a feed-forward back propagation network with one hidden layer and 5 neurons in that layer has been selected. The NN has been trained with 100 training points, which have been considered sufficient for most of the cases. For increasing dimensionality of the problem, i.e., for measurements equal to and above 20, the number of training points has been set equal to 200. The error of NN is controlled applying the criteria presented in Giovanis et al. (2017). In general, a reduction on the computational cost more than 80-90% has been achieved as compared with the standard aBUS-SuS algorithm, while maintaining the accuracy of the standard algorithm.

6.3.5.1 Results

The results from the updating process are presented in this section for all classified groups. A deeper insight is provided for the deck plates of cargo tanks (A/O-H group). The results from the sensitivity study regarding the random selection of m measurements are also presented in the end of this section.

Deck plates of cargo area (A/O-H group)

The results from the single and the sequential updating process are given in Table 6.8 - Table 6.16 for the deck plates exposed to the cargo tanks. The quantitative description of various quantities of interest, including the hyperparameters $\boldsymbol{\theta}$, the basic random variables $\boldsymbol{X}$ and the model prediction $\mathcal{M}(\boldsymbol{x})$, is depicted before and after observing the measurements.

The model predictions of thickness loss are presented in Table 6.12. In general, it is observed that with increasing number of observations, the updated model prediction approaches the actual values. Although the initial model prediction underestimates the true data, a small number of observed samples (only 5 measurements) is sufficient to approximate the actual dataset corresponding to the 20th year of service. Already after 10 measurements, the expected model prediction is very close to the mean value of the observed set, while the validation set of measurements is enveloped within the 95% credible interval of model prediction. Moreover, it is observed that the inherent variability of predicted thickness loss reduces (with a decreasing rate) as the number of measurements increases. This substantiates the fact that the dispersion of the parameter cannot be reduced beyond a certain level which depends on its inherent variability.

The following insights are drawn regarding the input uncertain parameters $\boldsymbol{\theta}$ and $\boldsymbol{X}$ after the implementation of the updating scheme:

- The posterior PDFs of the scale parameter λ_{X_1} and shape parameter k_{X_1} of the prescribed Weibull distribution clearly deviate from our initial belief. The density function of the posterior shape parameter deviates the most. Particularly, the expected value of both hyperparameters' PDF has been increased, while their variability (CoV) has been decreased. As a result, the expected value of annual corrosion rate X_1 has been considerably increased, whereas its inherent variability has been decreased by more than 50%, in the cases where more than 20 measurements have been considered.

- The mean value of corrosion initiation μ_{X_2} shifts to lower values. This indicates that the corrosion starts earlier than expected. The statistical uncertainty of μ_{X_2} has been slightly diminished after seeing the data. As a result, the corrosion initiation X_2 has been shifted to lower values, but its inherent variability is constant since it has been assumed known.

- The expected value of the corrosion trend μ_{X_3} is more or less the same with our initial belief ($\mu_{X_3} \approx 0.75$). However, the variability of the parameter has been significantly decreased with measurements. The result out of this process is that the posterior distribution of the corrosion progress X_3 is more or less the same as the initial consideration. As in the previous case of coating life parameter, the inherent variability of X_3 remains the same because it has been assumed known from the beginning.

All groups

The results for all group members are summarized in Table 6.17 and Table 6.18. A priori, we assume the same PDF for coating life X_2 and corrosion trend X_3. However, after the updating, we may result in different PDF for each classified area. The results from this table are used to assess the hull girder ultimate strength of the ship and its subsequent reliability later in Chapter 7. In Table 6.17, the *inherent* variability of the basic random variables $\boldsymbol{X}$ has been only considered. To this end, the statistical uncertainty of the associated hyperparameters $\boldsymbol{\theta}$ has been described by the mean posterior point estimate, following Eq. (5.7). A schematic representation of the prior and posterior model predictions along with the 95% credible interval is depicted for each group in Appendix H. The following conclusions are drawn from these results.

Posterior model predictions show a very good agreement with actual inspection data almost in all cases. In particular, the posterior means are very close to the corresponding mean observed values while, in majority, the 95% credible interval envelops the true data. With the increase of measurements, the credible intervals are becoming narrower. This fact indicates a reduction in the uncertainty associated with our predictions. In some cases, however, credible intervals are

seen to be broader than the initial prediction (e.g., A/O-H, O/B-V[1], DLC (W)). This is due to the high degree of inherent variability of thickness loss (high scatter of measurements) associated with these groups (see Table 6.3). It is also observed that for two groups, i.e., O/O-V, DLC (W), posterior predictions are not as close to the true values. This seems rational since the observations for the specific groups show anomalies and inconsistencies between consecutive inspections (see Table 6.3).

At this point, it should be emphasized that the integration of data does not necessarily reduce the variability of a parameter. In fact, if the initial prediction is associated with a low level of variability regarding this parameter, while true dispersion is large, then the inherent uncertainty of the parameter will increase after updating since the incorporation of data would lead the prediction closer to its true value. However, the uncertainty related to our imprecise state of knowledge will reduce because our knowledge about the hyperparameters of the parameters after seeing the data will improve.

Sensitivity study

A sensitivity study was carried out to examine the effect of randomly selecting m measurements. The study was conducted for the deck plates of cargo area (A/O-H) since the measurements of this group present one of the highest degrees of scatter and deviation from the original corrosion model prediction. Two cases have been considered, i.e., $m = 10$ and $m = 20$. The algorithm runs 10 times using randomly selected measurements each time. The results are presented in Table 6.7 in terms of mean thickness loss prediction $\overline{t_c}$ and coefficient of variation of thickness loss prediction CoV_{t_c} at the 20th year of service life. It was found that for all runs and measurements cases, the 95% credible interval of updated model prediction enclose the true values. Already after 10 measurements reliable results can be obtained, whereas very accurate predictions and an increase level of confidence is acquired for 20 measurements.

Table 6.7. Sensitivity study for randomly selecting m measurements in terms of mean value and CoV of thickness loss t_c at the validation year. The statistics for the two parameters are presented after running the algorithm 10 times.

Statistics descriptors	$m = 10$		$m = 20$	
	$\overline{t_c}$	CoV_{t_c}	$\overline{t_c}$	CoV_{t_c}
μ	1.23	1.04	1.69	0.71
CoV	13%	13%	5%	1%
Min	0.94	0.87	1.62	0.70
Max	1.47	1.24	1.90	0.73

Table 6.8. Histograms of hyperparameters $\boldsymbol{\theta}$ before and after the observations. Single updating. Deck plates (A/O-H group).

Data	Weibull scale parameter λ_{X_1}	Weibull shape parameter k_{X_1}	Lognormal mean parameter μ_{X_2}	Beta mean parameter μ_{X_3}
5	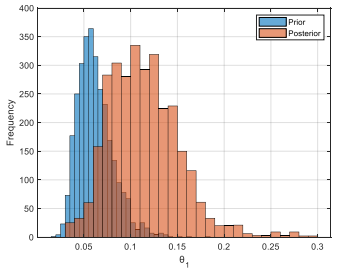	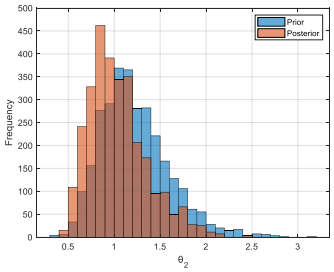	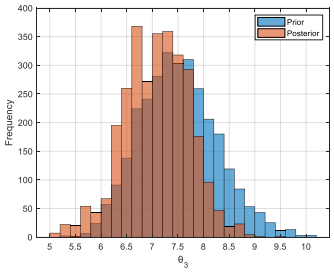	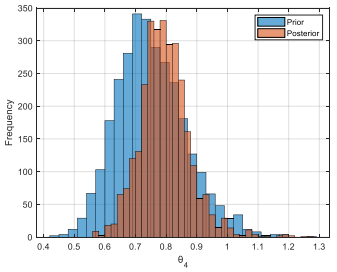
10	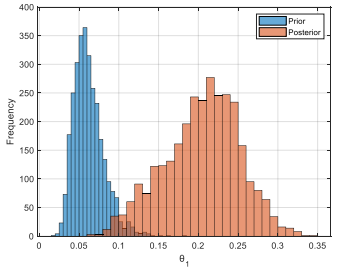	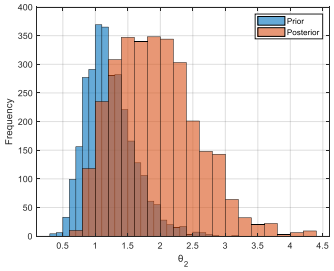	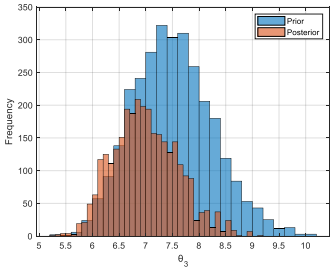	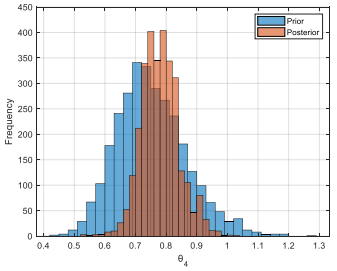
20	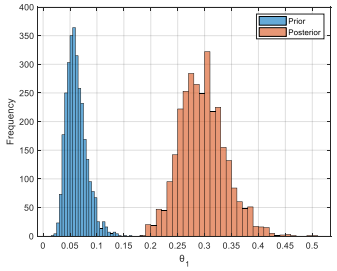	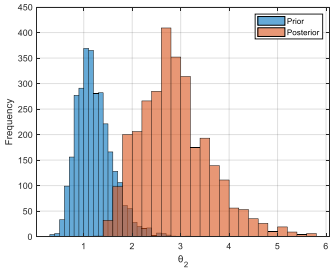	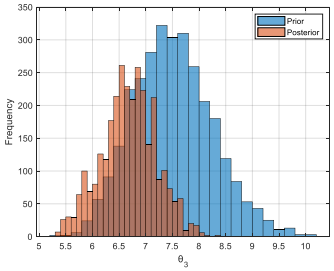	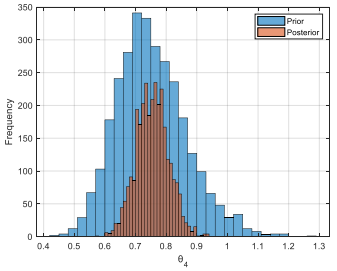

Table 6.9. Histograms of hyperparameters $\boldsymbol{\theta}$ before and after the observations. Sequential updating. Deck plates (A/O-H group).

Data	Weibull scale parameter λ_{X_1}	Weibull shape parameter k_{X_1}	Lognormal mean parameter μ_{X_2}	Beta mean parameter μ_{X_3}
[5,5]	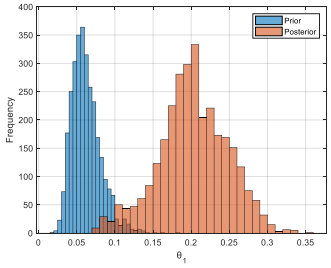	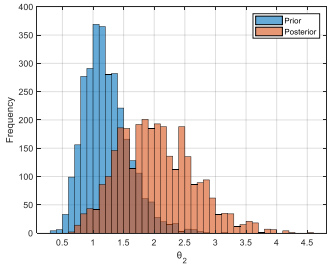	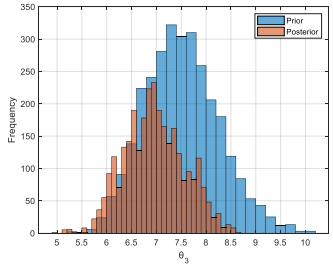	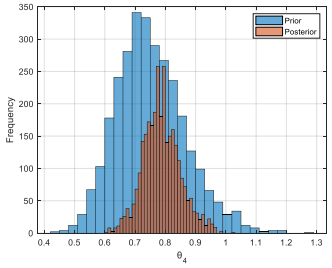
[10,10]	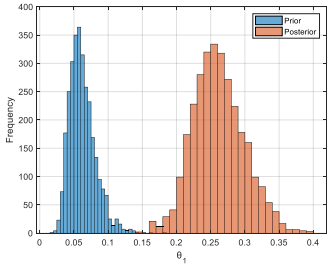	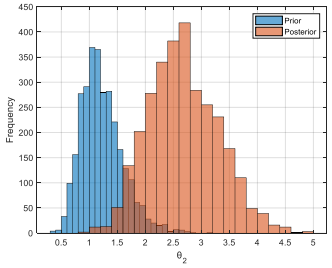	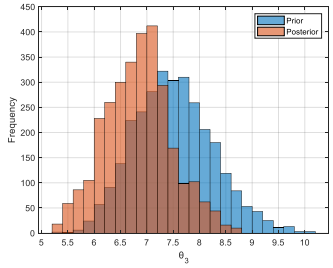	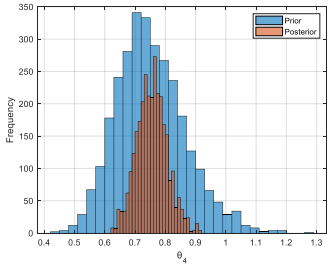
[20,20]	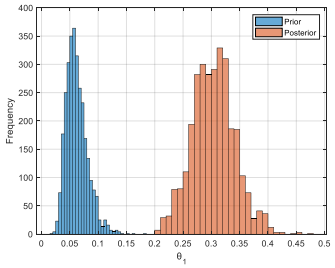	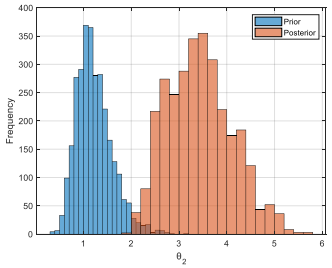	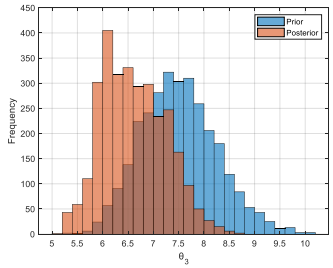	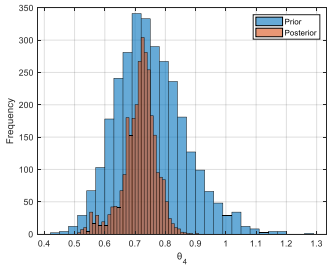

Table 6.10. PDFs for basic random variables $\boldsymbol{X}$ before and after the observations. Single updating. Deck plates (A/O-H group).

Data	Annual corrosion rate $X_1 \equiv C_1$	Corrosion time initiation $X_2 \equiv \tau_c$	Corrosion trend $X_3 \equiv C_2$
5	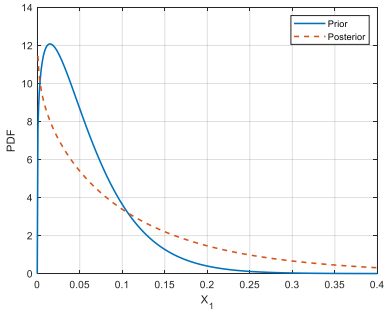	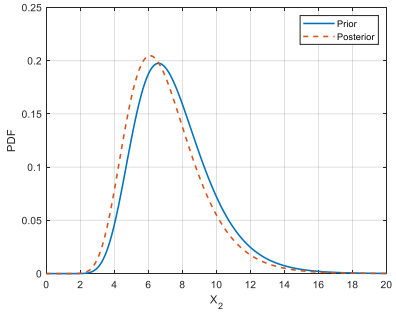	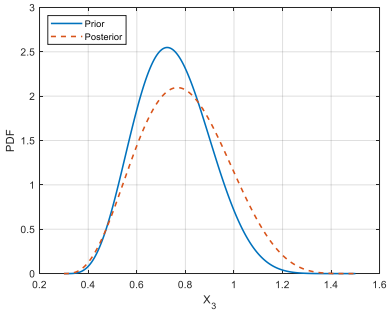
10	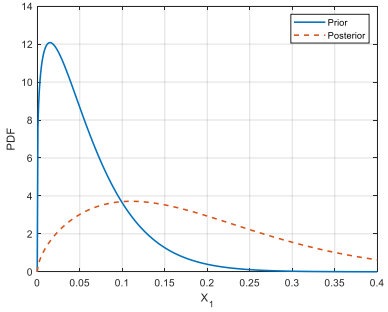	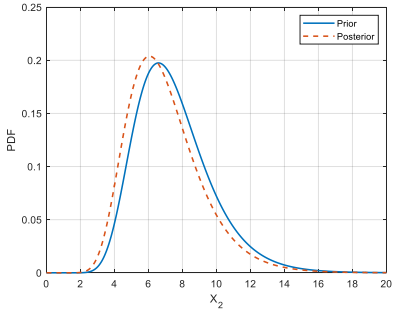	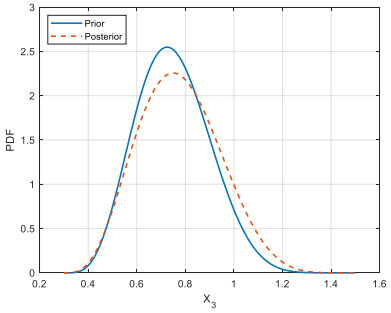
20	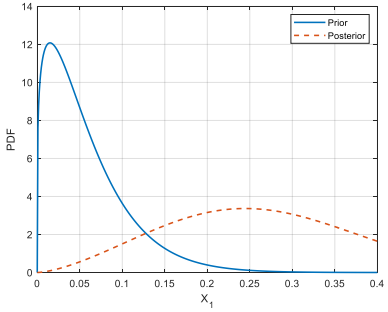	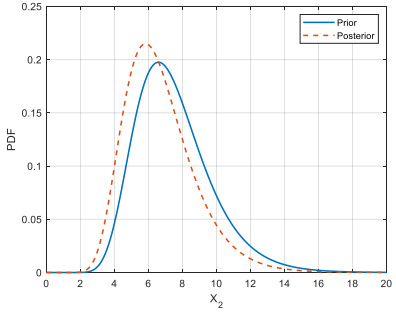	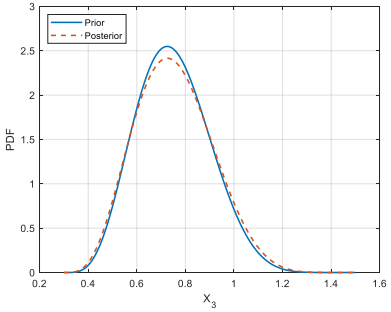

Table 6.11. PDFs for basic random variables $\boldsymbol{X}$ before and after the observations. Sequential updating. Deck plates (A/O-H group).

Data	Annual corrosion rate $X_1 \equiv C_1$	Corrosion time initiation $X_2 \equiv \tau_c$	Corrosion trend $X_3 \equiv C_2$
[5,5]	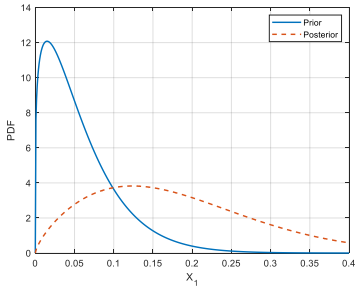	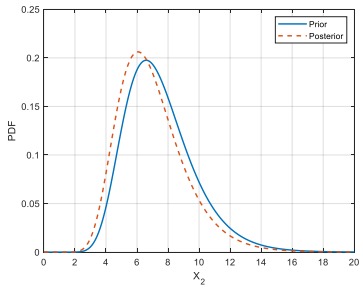	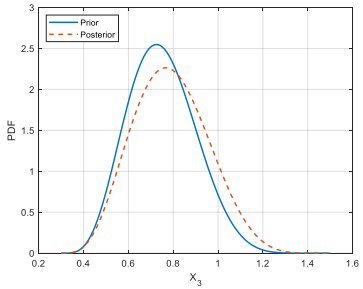
[10,10]	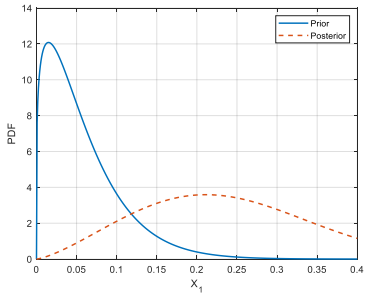	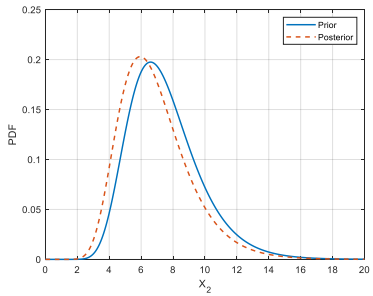	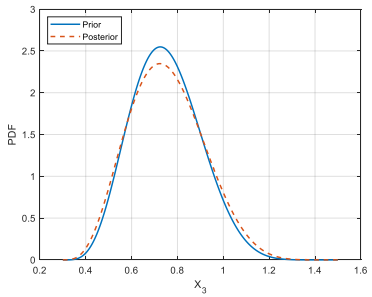
[20,20]	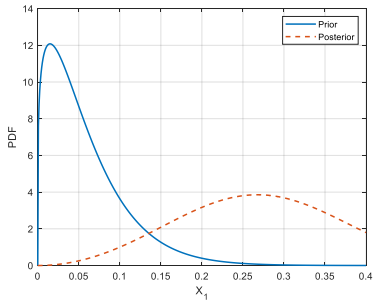	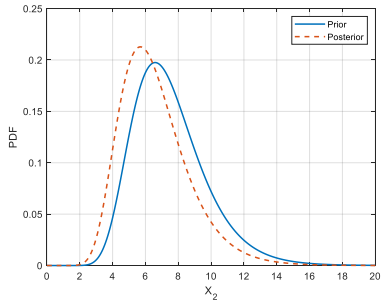	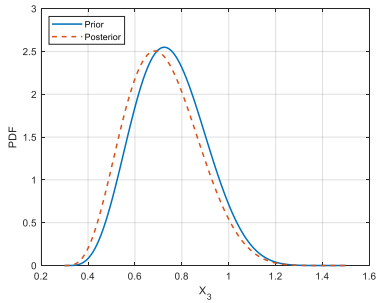

Table 6.12. Prior and posterior time-varying model predictions of corrosion wastage for the deck plates of cargo tanks (A/O-H). Results are tested against actual data from the last inspection (the 2.5% and 97.5% quantiles of the data are depicted with red color).

	Prior	**Posterior**		
		$m = 5$	$m = 10$	$m = 20$
Single updating	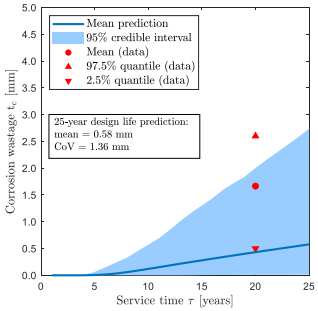	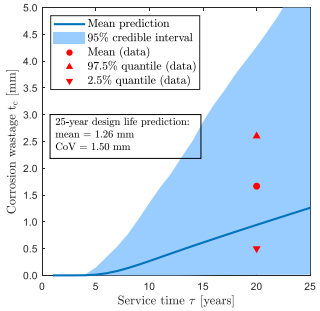	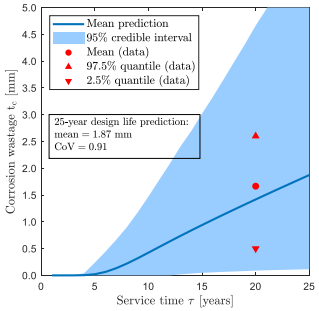	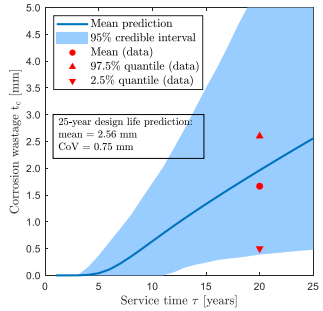
		$m = [5, 5]$	$m = [10, 10]$	$m = [20, 20]$
Sequential updating		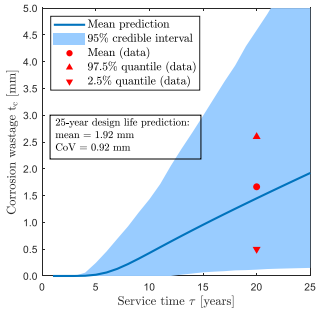	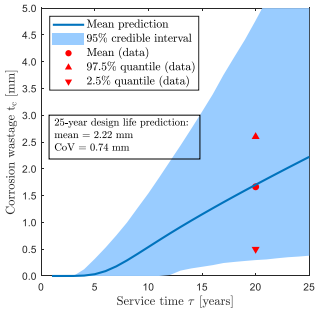	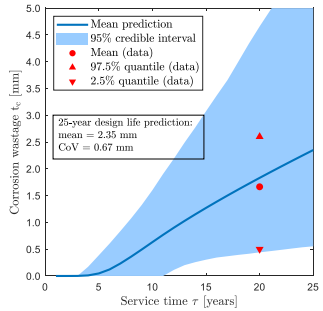

Table 6.13. Prior and posterior of the mean and CoV of the corrosion model hyperparameters $\boldsymbol{\theta}$. Single updating. Application on deck plates of cargo tank.

Hyperparameter	Prior		Posterior $m = 5$		Posterior $m = 10$		Posterior $m = 20$	
	Mean	CoV	Mean	CoV	Mean	CoV	Mean	CoV
Scale parameter a_{X_1}	0.062	0.30	0.114	0.33	0.205	0.23	0.296	0.14
Shape parameter k_{X_1}	1.216	0.30	1.039	0.30	1.932	0.33	2.885	0.25
Mean coating life μ_{X_2}	7.50	0.10	7.10	0.09	7.00	0.09	6.70	0.08
Mean corrosion progress μ_{X_3}	0.75	0.15	0.80	0.10	0.78	0.08	0.76	0.07

Table 6.14. Prior and posterior of the mean and CoV of the corrosion model hyperparameters $\boldsymbol{\theta}$. Sequential updating. Application on deck plates of cargo tank.

Hyperparameter	Prior		Posterior $m = [5, 5]$		Posterior $m = [10, 10]$		Posterior $m = [20, 20]$	
	Mean	CoV	Mean	CoV	Mean	CoV	Mean	CoV
Scale parameter a_{X_1}	0.062	0.30	0.202	0.22	0.261	0.14	0.304	0.13
Shape parameter k_{X_1}	1.216	0.30	2.030	0.30	2.679	0.23	3.438	0.20
Mean coating life μ_{X_2}	7.50	0.10	7.00	0.09	6.80	0.09	6.60	0.09
Mean corrosion progress μ_{X_3}	0.75	0.15	0.79	0.08	0.76	0.07	0.72	0.08

Table 6.15. Prior and posterior of the mean and CoV of the thickness model parameters $\boldsymbol{X}$. Single updating. Application on deck plates of cargo tank. Inherent variability of the parameters is depicted only, without considering for statistical uncertainty of hyperparameters.

Parameter	**Prior**		**Posterior** $m = 5$		**Posterior** $m = 10$		**Posterior** $m = 20$	
	Mean	**CoV**	**Mean**	**CoV**	**Mean**	**CoV**	**Mean**	**CoV**
Annual corrosion rate X_1	0.058	0.83	0.115	0.95	0.181	0.53	0.258	0.38
Coating life X_2	7.50	0.30	7.00	0.30	7.00	0.30	6.60	0.30
Corrosion progress X_3	0.75	0.20	0.79	0.20	0.78	0.20	0.75	0.20

Table 6.16. Prior and posterior of the mean and CoV of the thickness model parameters $\boldsymbol{X}$. Sequential updating. Application on deck plates of cargo tank. Inherent variability of the parameters is depicted only, without considering for statistical uncertainty of hyperparameters.

Parameter	**Prior**		**Posterior** $m = [5, 5]$		**Posterior** $m = [10, 10]$		**Posterior** $m = [20, 20]$	
	Mean	**CoV**	**Mean**	**CoV**	**Mean**	**CoV**	**Mean**	**CoV**
Annual corrosion rate X_1	0.058	0.83	0.181	0.51	0.236	0.39	0.274	0.32
Coating life X_2	7.50	0.30	7.00	0.30	6.90	0.30	6.60	0.30
Corrosion progress X_3	0.75	0.20	0.79	0.20	0.75	0.20	0.72	0.20

Table 6.17. Prior and posterior statistical values for corrosion model parameters for all groups using $m = 10$ from the first inspection.

Group	Prior						Posterior					
	X_1		X_2		X_3		X_1		X_2		X_3	
	Mean	**CoV**	**Mean**	**CoV**	**Mean**	**CoV**	**Mean**	**CoV**	**Mean**	**CoV**	**Mean**	**CoV**
A/O-H	0.058	0.83	7.50	0.30	0.75	0.20	0.181	0.53	7.00	0.30	0.78	0.20
A/B-H	0.108	0.82	7.50	0.30	0.75	0.20	0.072	0.82	7.70	0.30	0.63	0.20
A/B-V	0.066	1.13	7.50	0.30	0.75	0.20	0.060	1.00	7.40	0.30	0.67	0.20
B/S-V	0.062	1.00	7.50	0.30	0.75	0.20	0.051	0.86	7.50	0.30	0.65	0.20
BLGB	0.061	0.88	7.50	0.30	0.75	0.20	0.052	0.79	7.50	0.30	0.66	0.20
B/S-H	0.060	0.99	7.50	0.30	0.75	0.20	0.053	0.79	7.50	0.30	0.65	0.20
B/B-H	0.141	0.27	7.50	0.30	0.75	0.20	0.070	0.33	7.70	0.30	0.60	0.20
O/B-V[1]	0.101	0.80	7.50	0.30	0.75	0.20	0.176	0.49	7.10	0.30	0.74	0.20
O/B-V[2]	0.101	0.80	7.50	0.30	0.75	0.20	0.087	0.61	7.50	0.30	0.64	0.20
O/O-V	0.058	0.82	7.50	0.30	0.75	0.20	0.061	0.58	7.40	0.30	0.68	0.20
DLC (W)	0.072	0.89	7.50	0.30	0.75	0.20	0.098	0.59	7.20	0.30	0.70	0.20
DLC (F)	0.059	1.00	7.50	0.30	0.75	0.20	0.084	0.64	7.10	0.30	0.72	0.20
DLB (W)	0.240	0.92	7.50	0.30	0.75	0.20	0.169	0.88	7.60	0.30	0.64	0.20
DLB (F)	0.240	0.92	7.50	0.30	0.75	0.20	0.168	0.94	7.70	0.30	0.65	0.20
SSLB (W)	0.141	1.01	7.50	0.30	0.75	0.20	0.098	0.92	7.60	0.30	0.65	0.20
SSLB (F)	0.088	0.90	7.50	0.30	0.75	0.20	0.068	0.75	7.50	0.30	0.64	0.20
BSLB (W)	0.137	0.78	7.50	0.30	0.75	0.20	0.094	0.74	7.60	0.30	0.63	0.20
BSLB (F)	0.113	1.01	7.50	0.30	0.75	0.20	0.088	0.86	7.50	0.30	0.65	0.20
LBLB (W)	0.196	1.00	7.50	0.30	0.75	0.20	0.142	0.97	7.70	0.30	0.66	0.20
LBLB (F)	0.178	1.00	7.50	0.30	0.75	0.20	0.126	1.00	7.60	0.30	0.63	0.20
LBLC (W)	*0.056*	*0.81*	*7.50*	*0.30*	*0.75*	*0.20*	*0.077*	*0.60*	*7.10*	*0.30*	*0.72*	*0.20*

(Table continued)

LBLC (F)	0.051	1.00	7.50	0.30	0.75	0.20	0.063	0.66	7.20	0.30	0.71	0.20

Table 6.18. Prior and posterior statistical values for corrosion model parameters for all groups using $m = [10,10]$ measurements from each inspection.

Group	Prior						Posterior					
	X_1		X_2		X_3		X_1		X_2		X_3	
	Mean	**CoV**	**Mean**	**CoV**	**Mean**	**CoV**	**Mean**	**CoV**	**Mean**	**CoV**	**Mean**	**CoV**
A/O-H	0.058	0.83	7.50	0.30	0.75	0.20	0.236	0.39	6.90	0.30	0.75	0.20
A/B-H	0.108	0.82	7.50	0.30	0.75	0.20	0.087	0.76	7.50	0.30	0.66	0.20
A/B-V	0.066	1.13	7.50	0.30	0.75	0.20	0.060	0.73	7.50	0.30	0.65	0.20
B/S-V	0.062	1.00	7.50	0.30	0.75	0.20	0.051	0.70	7.50	0.30	0.63	0.20
BLGB	0.061	0.88	7.50	0.30	0.75	0.20	0.050	0.66	7.50	0.30	0.62	0.20
B/S-H	0.060	0.99	7.50	0.30	0.75	0.20	0.045	0.74	7.50	0.30	0.62	0.20
B/B-H	0.141	0.27	7.50	0.30	0.75	0.20	0.058	0.31	7.80	0.30	0.54	0.20
O/B-V[1]	0.101	0.80	7.50	0.30	0.75	0.20	0.223	0.44	7.10	0.30	0.74	0.20
O/B-V[2]	0.101	0.80	7.50	0.30	0.75	0.20	0.078	0.61	7.50	0.30	0.63	0.20
O/O-V	0.058	0.82	7.50	0.30	0.75	0.20	0.061	0.56	7.30	0.30	0.65	0.20
DLC (W)	0.072	0.89	7.50	0.30	0.75	0.20	0.142	0.50	7.30	0.30	0.72	0.20
DLC (F)	0.059	1.00	7.50	0.30	0.75	0.20	0.108	0.60	7.20	0.30	0.72	0.20
DLB (W)	0.240	0.92	7.50	0.30	0.75	0.20	0.130	0.80	7.60	0.30	0.56	0.20
DLB (F)	0.240	0.92	7.50	0.30	0.75	0.20	0.126	0.76	7.60	0.30	0.58	0.20
SSLB (W)	0.141	1.01	7.50	0.30	0.75	0.20	0.087	0.87	7.60	0.30	0.59	0.20
SSLB (F)	0.088	0.90	7.50	0.30	0.75	0.20	0.065	0.67	7.60	0.30	0.61	0.20
BSLB (W)	0.137	0.78	7.50	0.30	0.75	0.20	0.083	0.68	7.50	0.30	0.59	0.20
BSLB (F)	0.113	1.01	7.50	0.30	0.75	0.20	0.078	0.73	7.40	0.30	0.60	0.20
LBLB (W)	0.196	1.00	7.50	0.30	0.75	0.20	0.103	0.87	7.80	0.30	0.57	0.20
LBLB (F)	0.178	1.00	7.50	0.30	0.75	0.20	0.101	0.78	7.70	0.30	0.58	0.20

(Table continued)

LBLC (W)	0.056	0.81	7.50	0.30	0.75	0.20	0.071	0.58	7.20	0.30	0.68	0.20
LBLC (F)	0.051	1.00	7.50	0.30	0.75	0.20	0.067	0.58	7.20	0.30	0.67	0.20

6.3.6 Discussion and concluding remarks

In Section 6.3, we presented a Bayesian approach to update corrosion wastage predictions of steel plates for an oil tanker based on UT measurements from inspection surveys. The method is capable of incorporating new data sequentially, that is, to combine existing knowledge with measurements that become available at different time instances during service life. The spatial distribution of corrosion has been implicitly considered using a random variable approach. Using a Bayesian inverse analysis, we used measurements that correspond to the model outcome in order to learn the statistics of the basic random variables of the employed time-dependent corrosion model. In summary, the following insights are gained:

- The updated model is able to give accurate predictions of future corrosion trends using a limited number of observed samples. Particularly, a set of 10 measurements collected from the first and the second inspection provide a very good agreement with the validation set for all groups. The method is capable of giving reliable predictions even if the initial model predictions deviate by far from the true values, as this demonstrated for the case of deck plates.

- The high level of uncertainty and scatter of data related to annual corrosion rate remains a matter of conflict and skepticism in scientific body. This uncertainty is the result of developing empirical corrosion models that have been based on data from vessels with various operational profiles and maintenance strategies. In this study, the high statistical uncertainty associated, mainly, with the annual corrosion rate parameter is significantly reduced with the inclusion of only a small set of measurements. A reduction of the associated statistical variability by more than 50% can be achieved in some cases.

- The more measurements are considered, the higher is the reduction of uncertainty. From the results of the sensitivity study, it was found that 10 measurements are considered sufficient to have a reliable estimate in terms of 95% credible interval, while 20 measurements are adequate to obtain confident predictions on the mean value too.

It is also noted that in real cases, added knowledge on the corrosion initiation may become available. This information can be explicitly considered in the model. For example, if we know that corrosion initiated between the 8^{th} and 10^{th} year of service, we can quantify this information by selecting a lognormal probabilistic model with reduced variability or a Beta distribution model with lower and upper bounds the 8 and 10 years, respectively.

Overall, the developed methodology can considerably reduce the uncertainties related to corrosion model parameters and its associated prediction. The high degree of uncertainty related to the conventional empirical corrosion models motivates the need for the establishment of vessel-specific corrosion models. In particular, the updating procedure proposed in this section can be implemented in a more refined scale by establishing a corrosion degradation model for each plate of a ship.

7 Reliability Analysis

7.1 Introduction

The main objective of this chapter is to examine the effect of the proposed strength model uncertainty factor (see Section 6.2) and the updated corrosion model predictions (see Section 6.3) on the performance of ship structures in ultimate limit state. After introducing the general reliability problem in Section 7.2, the framework of time-dependent reliability of deteriorating ship structures is addressed in Section 7.3. Then, two numerical applications are analyzed in Section 7.5. In the first one, the updating of time-dependent reliability of a VLCC tanker conditional on thickness measurements acquired from subsequent inspections is performed. In the second application, the safety level of two container ships at a given time instance is computed using the existing and the recommended approach for the quantification of strength model uncertainty factor X_r (see Section 6.2). The differences on the failure probabilities using the two approaches are compared and discussed for each case.

Note that it is possible to directly update the reliability without the need to first update the model parameters $\boldsymbol{X}$, see e.g., Straub (2011). However, such an approach has not been implemented in the present thesis as the interest lies mainly on the updating of model parameters.

7.2 The general reliability problem

In reliability analysis, the interest is on the evaluation of the failure probability of a system. Consider a vector $\boldsymbol{X} = [X_1, \dots, X_n]^T$ consisting of a set of basic random variables that characterize a system. In general, the vector $\boldsymbol{X}$ describes uncertainties regarding material properties, geometric characteristics, loads (or load effects) and calculation models. A failure domain $\Omega_{\mathcal{F}}$ can be defined as the collection of the outcomes of $\boldsymbol{X}$ for which the so-called *limit state function* (LSF) or *performance function* $g(\boldsymbol{x})$ takes non-positive values, that is, $\Omega_{\mathcal{F}} = \{g(\boldsymbol{x}) \leq 0\}$. The probability of failure of the system can be evaluated as:

$$P_f = \Pr[\mathcal{F}] = \Pr[g(\boldsymbol{x}) \leq 0] = \int_{\Omega_{\mathcal{F}}} f_{\boldsymbol{X}}(\boldsymbol{x}) d\boldsymbol{x} \tag{7.1}$$

where, $f_{\boldsymbol{X}}(\boldsymbol{x})$ denotes the joint PDF of $\boldsymbol{X}$ vector. The computation of Eq. (7.1) is the solution of the reliability problem.

For the elementary case where a resistance term R and a load term S define the problem, i.e., $\boldsymbol{X} = [R, S]^T$, the LSF becomes $g(\boldsymbol{x}) = r - s$. Then, the probability of failure can be written as follows:

$$P_f = \Pr[r - s \leq 0] = \Pr[r \leq s] = \iint_{\Omega_{\mathcal{F}}} f_{RS}(r, s) dr ds \tag{7.2}$$

In case where R, S are independent, it holds that $f_{RS}(r, s) = f_R(r) f_S(s)$. Eq. (7.2) can be written then in a single integral form known as the *convolution integral*:

$$P_f = \Pr[r - s \leq 0] = \int_S F_R(s) f_S(s) ds \tag{7.3}$$

where the integration takes place over the S domain (typically from 0 to ∞). A schematic description of the elementary reliability problem is illustrated in Figure 7.1. Note that the probability of failure corresponds to the volume of joint density function $f_{RS}(r, s)$ that lies within the failure domain $\{g(\boldsymbol{x}) \leq 0\}$.

Often, a more convenient way to describe the reliability of a structural system is the reliability index. The *generalized reliability index* β is defined as:

$$\beta = -\Phi^{-1}(P_f) \tag{7.4}$$

where, Φ^{-1} is the inverse cumulative distribution function (CDF) of the standard Normal distribution. A one-to-one mapping exists between the failure probability and the reliability index. As shown in Figure 7.2, for increasing values of reliability index, the failure probability of a system decreases monotonically.

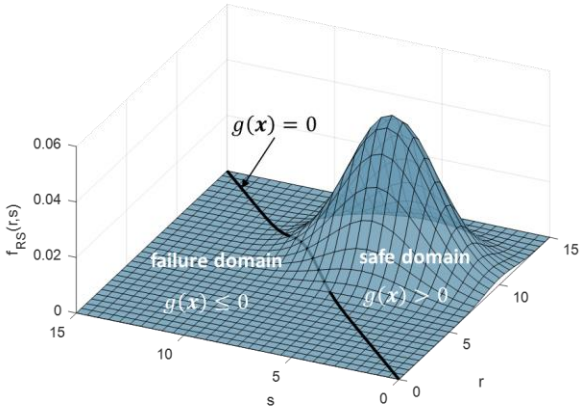

Figure 7.1. A 3D illustration of the reliability problem for the elementary case of two random variables R, S.

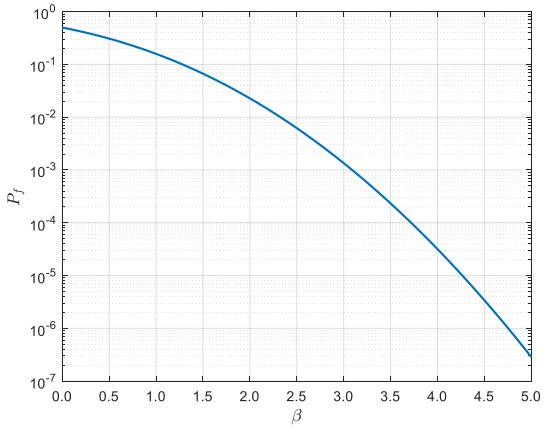

Figure 7.2. Relationship between failure probability P_f and reliability index β.

7.3 Time-variant reliability analysis of deteriorating ship structures

An overview of the basic theory of time-dependent reliability with some focus on deteriorating ship structures is presented in this section. For a more detailed analysis, the reader is referred to the books of Ditlevsen and Madsen (1996) and Melchers (1999)a. A comprehensive review on the subject of time-dependent deterioration of structural systems in general is provided by Straub et al. (2020).

The loads (or load effects) acting on the hull structure of a ship during its lifetime should be ideally modelled as stochastic process. Moreover, if deterioration effects (e.g., corrosion, fatigue) are considered, the resistance should be also represented by a stochastic process. In fact, if no repair and renewal actions are performed, resistance will monotonically decrease with time. In the simplest case, where a ship structure is characterized by a time-varying resistance term $R(\tau)$ and a load (effect) $S(\tau)$, the *point-in-time* or *instantaneous failure probability* can be defined as:

$$P_f(\tau) = \Pr[g(\boldsymbol{X}, \tau) \leq 0] = \Pr[R(\tau) - S(\tau) \leq 0] = \Pr[R(\tau) \leq S(\tau)] \tag{7.5}$$

The difference $Q(\tau) = R(\tau) - S(\tau)$ is called the *safety margin* and is also a stochastic process. Note that Eq. (7.5) is an extension of the basic reliability problem of Eq. (7.2) and evaluates the failure probability of the ship for an arbitrary time instance over the service life. However, Eq. (7.5) has no actual meaning if the structure has already failed in previous years. In practice, one should consider the stochastic processes $R(\tau)$ and $S(\tau)$ for $\tau \in [0, T]$ considering that failure may occur at any time up to time T. The *cumulative failure probability* $P_{f,c}$ that describes this event is then defined as:

$$P_{f,c}(T) = \Pr\left\{\left[\min_{\tau\in[0,T]} g(\boldsymbol{X},\tau)\right] \le 0\right\} \tag{7.6}$$

The cumulative failure probability that is referred to the entire 25-year design life of ship, is called the *lifetime failure probability*. In the general case, computation of Eq. (7.6) requires the solution of a *first-passage* problem, i.e., the probability that the safety margin $Q(\tau)$ exceeds a threshold level (zero), see Melchers (1999)a. However, difficulties arise on the computation of this problem, while the establishment of a stochastic process that defines the load (or load effect) for the entire history of a ship structure is practically impossible. To this end, an approximation method is usually adopted for the solution of Eq. (7.6) by transforming the time-variant reliability problem into a series of time-invariant reliability problems with the following way.

Consider that time is discretized into a sequence of intervals $j = 1,2,\dots$ such that the j-th interval corresponds to $\tau \in \left(\tau_{j-1}, \tau_j\right]$. The interval failure probability P_f^j is then defined as the event of failure in $\tau \in \left(\tau_{j-1}, \tau_j\right]$:

$$P_f^j(\tau) = \Pr\left\{\left[\min_{\tau\in\left(\tau_{j-1},\tau_j\right]} g(\boldsymbol{X},\tau)\right] \le 0\right\} \approx \Pr\left[R\left(\tau_j\right) \le S_{\max,j}\right] \tag{7.7}$$

where, $S_{\max,j} = \max_{\tau\in\left(\tau_{j-1},\tau_j\right]} S(\tau)$ is the maximum load for the given reference period (e.g., annual). $S_{\max}$ corresponds to an extreme value distribution and its formulation requires the implementation of an extreme value analysis on $S(\tau)$. Note that the formulation of Eq. (7.7) is in analogy with Eq. (7.5), namely, it neglects the occurrence of previous failure events. The $\Pr\left[R\left(\tau_j\right) \le S_{\max,j}\right]$ can be thus evaluated by a time-invariant reliability analysis. The cumulative failure probability up to time T is the union of the interval failure probabilities leading up to time T, which corresponds to the solution of a system reliability problem, see Straub et al. (2020). A robust and simple approach to compute the system reliability by means of Monte Carlo simulation is introduced in the next section (see Eq. (7.12)).

The formulation of Eq. (7.7) is valid when a single load process is acting on the structure. In practice, however, more than one stochastic load effects $\{S_1(\tau), S_2(\tau), \dots\}$ are present. In that case, it would be very pessimistic to combine the maximum (extreme values) for all loads. As an improvement, *load combination techniques* should be used to obtain an equivalent extreme value distribution of the combined load effect of all random variables.

In the formulation of hull girder reliability problem, a commonly used method to combine effectively multiple loads is given by Turkstra (1970). Turkstra's rule states that if one of the time-varying loads is dominant, the load combination problem can be formulated by applying the *extreme value distribution* on that load and an *arbitrary-point-in-time* distribution on the

other load(s). For instance, if two time-varying load processes act on a structure, the distribution of the total load S_t can be obtained using the following relation:

$$S_t = \max\{(S_1 + S_{2,ex}), (S_{1,ex} + S_2)\} \tag{7.8}$$

where, S_1 and S_2 are the arbitrary-point-in-time load distributions and $S_{1,ex}$ and $S_{2,ex}$ are the corresponding extreme value distributions for the given reference period. The difference between an arbitrary-point-in-time distribution and an extreme value distribution can be seen in Figure 7.3.

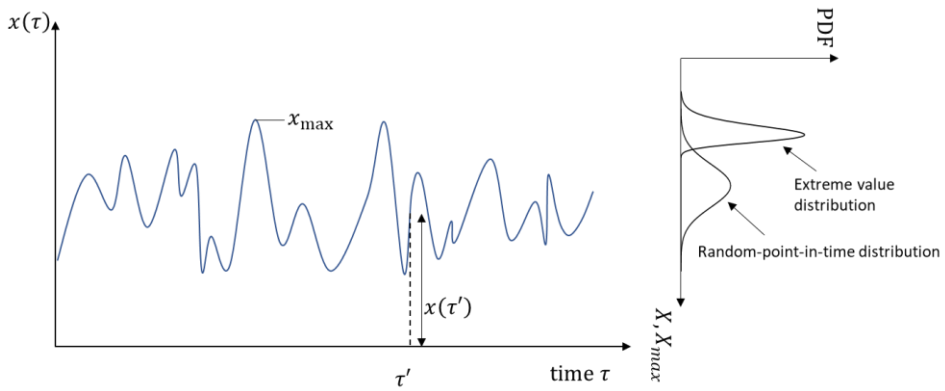

Figure 7.3. Illustration of a time-varying realization $x(\tau)$ of a stochastic process $X(\tau)$. The random-point-in-time distribution and the extreme value distribution of maxima are depicted for $X(\tau)$.

7.4 Common methods for the evaluation of failure probability

The solution of the general reliability problem of Eq. (7.1) is generally not a trivial task. An analytical solution of the problem exists only when the LSF is linear and the random variables $\boldsymbol{X}$ are normally distributed. However, in most practical applications, the LSF is non-linear and the random vector $\boldsymbol{X}$ consists of one or more non-Gaussian variables. Then, the selection of the solution method depends mainly on the order of magnitude of failure probability for the ad-hoc problem. For ship structures examined in ULS, this order of magnitude is usually between 10^{-2} and 10^{-5}, see e.g., Hørte et al. (2007). For such cases, the First Order Reliability method (FORM) and the crude Monte Carlo simulation (MCS) method are particularly efficient. An outline of these two methodologies is given below[31].

[31] It is noted that for smaller probabilities of failure (in the order of $10^{-6} - 10^{-8}$), the above methods become insufficient. In that cases, more advanced sampling techniques based on MCMC and BUS methods are needed.

7.4.1 Monte Carlo simulation for application to structural reliability analysis

An outline of the MCS method is given in Appendix C. In terms of reliability, where the interest lies on evaluating the probability of a failure event, MCS proceeds by first generating a number of samples $\boldsymbol{x}^{(i)}$, $i = 1, \dots, K$ from the input vector $\boldsymbol{X}$ and then calculating the failure probability by applying the following relation:

$$P_f \approx p_f^{MCS} = \frac{1}{K}\sum_{i=1}^{K} \mathrm{I}\left[g\left(\boldsymbol{x}^{(i)}\right) \leq 0\right] \tag{7.9}$$

where, p_f^{MCS} is an unbiased estimator of the true probability of failure P_f and $\mathrm{I}[\cdot]$ is the indicator function which takes value one if the argument is true and zero otherwise, that is:

$$\mathrm{I}\left[g\left(\boldsymbol{x}^{(i)}\right) \leq 0\right] = \begin{cases} 1, & g\left(\boldsymbol{x}^{(i)}\right) \leq 0 \\ 0, & \text{otherwise} \end{cases} \tag{7.10}$$

The estimator p_f^{MCS} is thus obtained by dividing the number of failures $n_f = \sum_{i=1}^{K} \mathrm{I}\left[g\left(\boldsymbol{x}^{(i)}\right) \leq 0\right]$ to the total number of generated samples K. Using MCS, the computation of (instantaneous) failure probability for the j-th time interval can be obtained as:

$$\Pr\left[\mathcal{F}(\tau_j)\right] \approx \frac{1}{K}\sum_{i=1}^{K} \mathrm{I}\left[g\left(\boldsymbol{x}^{(i)}, \tau_j\right) \leq 0\right] \tag{7.11}$$

Similarly, the calculation of cumulative failure probability up to time τ_n with $n = 1,2, \dots$ can be computed as:

$$\Pr[\mathcal{F}(\tau_n)] \approx \frac{1}{K}\sum_{i=1}^{K} \mathrm{I}\left\{\left[\min_{j=1:n} g\left(\boldsymbol{x}^{(i)}, \tau_j\right)\right] \leq 0\right\} \tag{7.12}$$

The strong benefit of using MCS is its independence on the LSF formulation and the number of random variables of the problem. In addition, MCS provides a set of measure indexes (confidence and credible intervals) to assess the uncertainty on the estimated probability of failure p_f^{MCS}. Credible intervals are preferred in this thesis over confidence intervals as they provide a more intuitive description of the uncertainty.

7.4.1.1 Estimation of confidence intervals for p_f^{MCS}

The estimator p_f^{MCS} is itself a random variable whose coefficient of variation depends on the (unknown) failure probability P_f and the total number of samples K. Moreover, $\mathrm{I}\left[g\left(\boldsymbol{x}^{(i)}\right)\right]$ for $i = 1, \dots, K$ can be considered as a Bernoulli process that has a mean value equal to P_f. Consequently, for a certain P_f, the number of failures n_f in K (independent) trials follows a binomial distribution. Therefore, the mean value of the estimator p_f^{MCS} is:

$$\mathrm{E}\left[p_f^{MCS}\right] = \frac{n_f}{K} \tag{7.13}$$

The variance of the estimator p_f^{MCS} is:

$$\mathrm{Var}\left[p_f^{MCS}\right] = \frac{P_f\left(1 - P_f\right)}{K} \tag{7.14}$$

The coefficient of variation of the estimator p_f^{MCS} is:

$$\mathrm{CoV}\left[p_f^{MCS}\right] = \frac{\sqrt{P_f - P_f^2}}{P_f\sqrt{K}} \approx \frac{1}{\sqrt{P_f K}} \tag{7.15}$$

The importance of Eq. (7.15) lies on the fact that knowing the order of magnitude of failure probability p_F provides the required number of samples (LSF evaluations) to achieve a desired level of CoV. For instance, for a CoV equal to 10%, the required number of samples to achieve a failure probability in the order of 10^{-3} is approximately equal to $K = 10^5$. It is also shown that p_f^{MCS} converges to the true failure probability P_f as $K \to \infty$.

7.4.1.2 Estimation of credible intervals for p_f^{MCS}

In a Bayesian context, the (posterior) uncertainty about the probability of failure p_f follows a standard Beta distribution with parameters $n_f + 1$ and $K - n_f + 1$, that is, $p_f \sim Beta\left(n_f + 1, K - n_f + 1\right)$. Its probability distribution function then reads:

$$f_{P_f|n_f,K}\left(p_f\right) = \frac{p_f^{n_f}\left(1 - p_f\right)^{K - n_f}}{B\left(n_f + 1, K - n_f + 1\right)} \tag{7.16}$$

where, $\mathrm{B}(\cdot)$ is the Beta function with arguments $n_f + 1$ and $K - n_f + 1$.

The posterior *expectation* value of p_f is:

$$\mathrm{E}\left(p_f \middle| n_f, K\right) = \frac{n_f + 1}{K + 2} \tag{7.17}$$

The posterior *variance* of p_f is:

$$\mathrm{Var}\left(p_f \middle| n_f, K\right) = \frac{\left(n_f + 1\right)\left(K - n_f + 1\right)}{(K + 2)^2 (K + 3)} \tag{7.18}$$

The posterior *coefficient of variation* of p_f is:

$$\mathrm{CoV}\left(p_f \middle| n_f, K\right) = \sqrt{\frac{K - n_f + 1}{\left(n_f + 3\right)\left(n_f + 1\right)}} \tag{7.19}$$

7.4.2 First Order Reliability Method (FORM)

FORM was first introduced by Hasofer and Lind (1974) and is still an attractive method for computing the probability of failure of a system. Broadly speaking, FORM transforms all random variables $\boldsymbol{X}$ into an equivalent set of standard normal random variables $\boldsymbol{Z}$, and then approximates the LSF by a linear first-order polynomial function. The basic methodology consisting FORM is summarized below. An illustration of the approach is presented in Figure 7.4.

The first step of FORM is to transform the LSF $g(\boldsymbol{x})$ from the original space into standard normal space $G(\boldsymbol{z})$ and perform the integration on the standardized domain, namely:

$$P_f = \int_{g(\boldsymbol{x}) \le 0} f_{\boldsymbol{X}}(\boldsymbol{x})\, d\boldsymbol{x} = \int_{G(\boldsymbol{z}) \le 0} f_{\boldsymbol{Z}}(\boldsymbol{z})\, d\boldsymbol{z} \tag{7.20}$$

FORM evaluates the above integral by linearizing the LSF at the so-called *design point* or *most probable failure point (MPFP)* $\boldsymbol{z}^*$. This point is the location on the limit state surface which is closest to the origin. The evaluation of the design point $\boldsymbol{z}^*$ can be obtained by solving the following constrained optimization problem:

$$\boldsymbol{z}^* = \arg\min \|\boldsymbol{z}\| \text{ subject to the constraint: } G(\boldsymbol{z}) = 0 \tag{7.21}$$

where, $\|\boldsymbol{z}\| = \sqrt{\boldsymbol{z}^T\boldsymbol{z}}$ is the norm of the vector $\boldsymbol{z}$, which corresponds to the distance of $\boldsymbol{z}$ from the origin. The problem can be solved with a variety of optimization problems, see e.g., Rackwitz and Flessler (1978), and Liu and Der Kiureghian (1991). Assuming that the LSF is continuous and differentiable near $\boldsymbol{z}^*$, we can approximate $G(\boldsymbol{z})$ through its linearization at $\boldsymbol{z}^*$, that is:

$$G(\boldsymbol{z}) \cong G'(\boldsymbol{z}) = \nabla G(\boldsymbol{z}^*)(\boldsymbol{z} - \boldsymbol{z}^*) \tag{7.22}$$

where, $\nabla G(\boldsymbol{z}^*) = [\partial G/\partial z_1|_{\boldsymbol{z}=\boldsymbol{z}^*}, \dots, \partial G/\partial z_n|_{\boldsymbol{z}=\boldsymbol{z}^*}]$ is the gradient row vector evaluated at the design point in standard normal space. The FORM approximation to the failure probability is then:

$$P_f \approx \Pr[G'(\boldsymbol{Z}) \leq 0] = \Phi[-\beta_{\text{FORM}}] \tag{7.23}$$

where, Φ is the CDF of standard normal distribution. The distance between the design point and the origin corresponds to the first order reliability index, defined as:

$$\beta_{\text{FORM}} = \|\boldsymbol{z}^*\| \tag{7.24}$$

The main advantage of using FORM is the information that provides regarding the sensitivity of basic random variables $\boldsymbol{X}$ on the probability of failure through the so-called α-factors. The sensitivity measures are obtained through knowledge of the design point $\boldsymbol{z}^*$ as follows:

$$\boldsymbol{\alpha} = -\frac{\nabla G(\boldsymbol{z}^*)}{\|\nabla G(\boldsymbol{z}^*)\|} \tag{7.25}$$

The relation between the reliability index β_{FORM}, the design point $\boldsymbol{z}^*$ and the i-component of $\boldsymbol{\alpha}$ row-vector is given by the following relation:

$$a_i = \frac{z_i^*}{\beta_{\text{FORM}}} \tag{7.26}$$

where, z_i^* is the value of the i-th coordinate at the design point. Basic random variables X_i whose absolute value of a_i is high have a strong impact on the reliability index β_{FORM}, and vice versa.

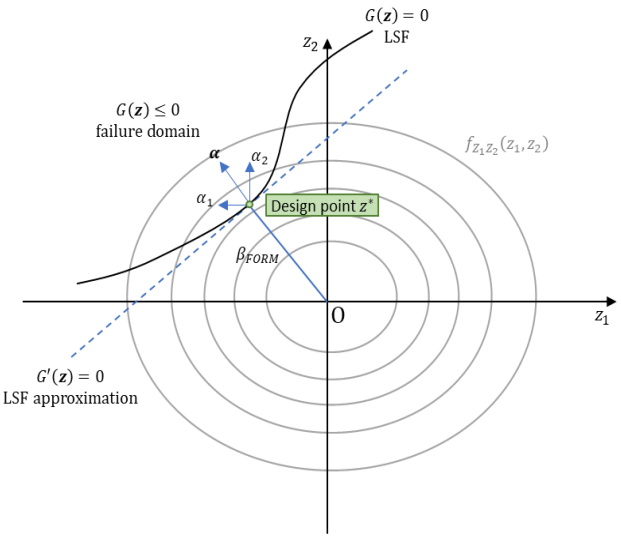

Figure 7.4. Illustration of the FORM approach.

7.5 Numerical investigations

7.5.1 Application 1: Reliability updating of a VLCC tanker based on inspections data

The reliability assessment and updating of a double hull VLCC tanker using inspections results from the 15th and 18th year of its service life is presented. In each inspection survey, we consider the collection of 10 measurements for each classified group (for the classification of groups see Figure 6.10). The updating of reliability takes place by considering the posterior corrosion model parameters that have been already presented in Table 6.17 and Table 6.18. For comparison, the effect of Paik's linear corrosion model and IACS CSR net-50 scantling approach on the reliability of the vessel is also evaluated. The calculations are performed using the recommended and the existing strength model uncertainty factor X_r as well (see Section 6.2.4.1).

7.5.1.1 Limit State Function (LSF) formulation

Failure in sagging is considered as the most unfavorable scenario for double hull oil tankers. The time-dependent LSF of hull girder collapse under extreme sagging conditions can be determined using the following relation, see e.g., Hørte et al. (2007), Hussein and Soares (2009):

$$g(\boldsymbol{X}, \tau) = X_r M_u(\tau) - \left(X_{sw} M_{sw} + X_{st} X_{nl} M_{wv,ex}\right) \tag{7.27}$$

where, M_{sw} and X_{sw} denote the uncertainty on still water bending moment load and the corresponding model uncertainty factor, $M_{wv,ex}$ is the annual extreme wave-induced bending moment load subject to two model uncertainty factors; X_{st} and X_{nl}, corresponding to linear and non-linear response calculations, respectively. The ultimate bending moment capacity M_u is computed by IACS CSR Smith's method as a function of time τ due to corrosion deterioration. The term M_u also includes the randomness of material properties, i.e., yield strength and Young's modulus.

7.5.1.2 Probabilistic representation of time-variant hull girder ultimate bending capacity

The incremental-iterative IACS CSR Smith's method is employed to calculate the hull girder ultimate bending capacity of the ship under longitudinal bending. It is considered that the hull girder ultimate strength decreases over time due to uniform corrosion degradation.

Two versions of Paik's corrosion wastage model (see Section 2.4.5.1) are applied to estimate the time-varying thickness reduction $t_c(\tau)$ of steel plates and stiffeners: (i) the *linear*, and (ii) the *generalized* corrosion model. The linear corrosion model is the one that is commonly adopted in literature. It assumes that C_1 parameter follows a Weibull distribution, while $C_2 = 1.0$ and $\tau_C = 7.5$ years. On the other hand, the generalized version is considered to be more representative of real-life as it takes into account the uncertainty on the corrosion time initiation and the non-linearity of corrosion progress. This is accomplished here by setting τ_C and C_2 as random variables. The generalized corrosion model has been adopted in Section 6.3 for the implementation of the updating scheme. In addition, a partial correlation model is applied here to characterize the large-scale spatial dependence of corrosion growth between the elements around the midship section (see also Section 2.4.5.2). Finally, we take into account that a structural element that reaches its *renewal thickness* is replaced by its original (as-built) thickness[32].

Regarding material properties variation, the recommendations of Section 2.4.3 have been followed. In particular, a lognormal distribution has been used to describe the variability on the yield strength with mean value equal to 269 MPa (348 MPa) and coefficient of variation 0.08 (0.06) for mild (high-tensile steel), and a normal distribution to quantify the variability on Young's modulus with mean value equal to 210 GPa and coefficient of variation 10%. Temporal and spatial variation of material characteristics around midship section is neglected, namely, full correlation is considered both in time and space. It is also assumed that mechanical properties do not decay over time, that is, the same PDFs are valid at any point in time.

[32] The renewal thickness is specified by IACS (2019) equal to the 100% of net thickness t_n and depends on the location of an element around the midship section.

Table 7.1. Summarized random variables introduced for IACS CSR Smith' model evaluation M_u.

Parameter	Symbol	Distribution	Mean value	CoV	Units
Annual corrosion rate	C_1	Weibull	(*)	(*)	mm/year
Coating life	τ_c	Lognormal	(*)	(*)	years
Corrosion progress	C_2	Beta	(*)	(*)	-
Yield stress (**)	σ_y	Lognormal	269 (348)	0.08 (0.06)	MPa
Young's modulus	E	Normal	210	0.10	GPa

Notes:

(*) For the generalized corrosion model, three sets of mean values and COVs are adopted from Table 6.17 and Table 6.18, namely: (i) prior, (ii) posterior after $m = 10$ measurements and (iii) posterior after $m = [10,10]$ measurements.

For the linear corrosion model, C_1 is assumed to follow the Weibull distribution with associated prior values as listed in Table 6.17 and Table 6.18, whereas coating life and corrosion progress are assumed fixed with $\tau_c = 7.5$ and $C_2 = 1.0$.

(**) Mean values and CoVs are referred to mild steel and high tensile AH32 type steel (mild/AH32).

7.5.1.3 Combination of loads

The formulation of Eq. (7.27) needs the combination of still water bending moment M_{sw} and wave-induced bending moment M_{wv}. It would be unrealistic and quite unfavorable scenario, however, to consider a linear superposition of their extreme values since it is unlikely that maximum values act at the same time during the service life of a ship, see also Huang and Moan (2008). Therefore, to effectively combine these two loads Turkstra's rule is applied (see Eq. (7.8)).

Previous applications of the Turkstra's rule have shown that annual extreme value distribution of vertical wave-induced bending moment dominates the ship hull girder annual failure probability over still water bending moment, see e.g., Hørte et al. (2007), and Teixeira and Guedes Soares (2009). Therefore, the following linear superposition that combines the annual extreme wave bending moment $M_{wv,ex}$ and the arbitrary point-in-time distribution of still water bending moment M_{sw} is used for the present study to describe the total load effect:

$$M_t = M_{wv,ex} + M_{sw} \tag{7.28}$$

The probabilistic formulations of annual random-point-in-time still water bending moment M_{sw} and extreme value distribution of wave bending moment $M_{wv,ex}$ are established below.

7.5.1.4 Probabilistic representation of still water bending moment (SWBM)

The uneven longitudinal distribution of loads (weights and buoyancy) acting on the hull structure of a ship results in the development of vertical SWBM. In reality, as the cargo load varies between different voyages – and between departure and arrival of one voyage as well – the SWBM alters too. Traditionally, the annual stochastic representation of SWBM is assumed to follow a normal distribution with mean value and standard deviation equal to $0.7M_{sw}^{max}$ and $0.2M_{sw}^{max}$, respectively, where M_{sw}^{max} denotes to the maximum value of SWBM as reported in the loading manual of the vessel. The following two simplifications are usually made for the stochastic description of SWBM: (i) the SWBM is considered fixed during one voyage, and (ii) the value of SWBM within one year is interpreted as a realization of the random-point-in-time (normal) distribution, and (iii) SWBM realizations are assumed independent between consecutive years. The above description is shown schematically in Figure 7.5.

Uncertainties on the prediction of SWBM are taken into account through a relevant model uncertainty factor X_{sw}. This factor reflects the uncertainty between the actual SWBM and the corresponding calculated value from the loading manual. X_{sw} is assumed to follow a normal distribution with mean value and standard deviation equal to 1.00 and 0.10, respectively, see e.g., Hørte et al. (2007).

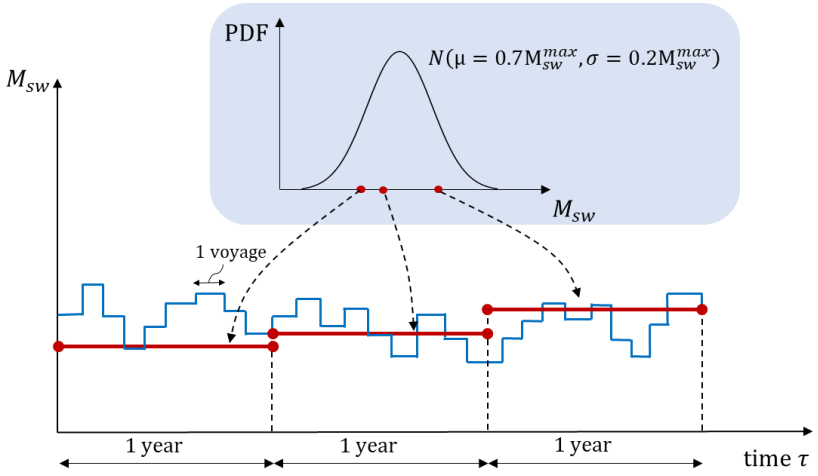

Figure 7.5. Distribution for still water bending moment (SWBM). A single realization corresponds to an annual random point-in-time value. A one-voyage SWBM value is approximated with an annual value.

7.5.1.5 Probabilistic representation of annual extreme wave-induced bending moment

The wave-induced bending moment (WVBM) results from the dynamic response of the hull girder due to the excitation of wave loads. The long-term prediction of WVBM M_{wv} at any point in time is assumed to follow the Weibull distribution with shape parameter k and scale parameter λ, see e.g., Hughes and Paik (2010). According to Gaspar et al. (2016), a representative value for the shape parameter is $k = 1.0$. On the other hand, the scale

parameter λ can be defined under the condition that the specified by the Rules characteristic wave-induced bending moment M_{wv}^{ch} will be exceeded at *any one* of the N cycles encountered during the design life of vessel with a probability 10^{-8}, i.e., $\Pr[M_{wv} > M_{wv,d}] = 10^{-8}$. This leads to the following relationship for the scale parameter λ:

$$\lambda = \frac{M_{wv}^{ch}}{(\ln N)^{1/k}} \tag{7.29}$$

The characteristic value of sagging wave-induced bending moment is defined by IACS (2019) as:

$$M_{wv}^{ch} = 0.110 C_w L_{BP}^2 \mathrm{B}(C_b + 0.7) \tag{7.30}$$

where, B equals the breadth of the vessel, C_b is the block coefficient and C_w equals to 10.75 for $300 < L_{BP} \leq 350$ m.

Since the interest here is in the evaluation of the (annual) extreme WVBM $M_{wv,ex}$, we require the extreme value distribution of long-term WVBM for a given return period *over N cycles*. This converges to the Gumbel distribution with CDF:

$$F_{M_{wv,ex}}(m_{wv,ex}) = \exp\left[-\exp\left(\frac{m_{wv,ex} - b_n}{a_n}\right)\right] \tag{7.31}$$

The scale parameter a_n and location parameter b_n of the Gumbel distribution are related to the Weibull parameters of the long-term WVBM, as follows:

$$b_n = \lambda(\ln N)^{1/k} \tag{7.32}$$

$$a_n = \frac{b_n}{k \ln N} \tag{7.33}$$

The number of wave cycles encountered over the reference period of one year is determined based on the North Atlantic wave environment, see e.g., Hørte et al. (2007). The mean representative wave period for this environment is about 8.0 sec. Taking into consideration that the vessel will travel on the full load departure (sagging) condition and at sea 42.5% annually, the annual number of wave cycles N_a encountered can be estimated. Finally, it is assumed that extreme WVBM is independent among different years.

The uncertainty on the linear response calculations is reflected on X_{st} which is represented by a normal random variable whose mean value and standard deviation equals to 1.00 and 0.10, respectively. The X_{nl} model uncertainty factor, which accounts for uncertainties on non-linear

effects, is also modelled with a normal distribution model with the same statistical parameters, see e.g., Hørte et al. (2007).

7.5.1.6 Results

A summary of the random variables used for the formulation of Eq. (7.27) is listed in Table 7.2. The calculation of hull girder ultimate strength M_u is performed applying MCS in conjunction with appropriately trained NNs. The vector of input parameters of the NN includes the Young's modulus E, the yield strength σ_y (both mild and high-tensile steel grade) and the values of thickness wastage t_c for each classified group (22 groups). In total, 25 parameters are assigned in the input vector for each time instance. The output of interest is the ultimate bending moment in sagging. However, ultimate strength in hogging was also computed by the employed NN. NNs have been trained using a rather limited number of Smith's model evaluation. In particular, 100 training points are sampled from the input parameter space each year using the Latin-Hypercube variance reduction technique. A NN is trained for each annual time interval separately.

Table 7.2. Summary of random variables used for the reliability problem of the VLCC tanker.

Item	Symbol	Distribution	Mean	St. dev.	Units
Ultimate bending capacity (*)	M_u	Lognormal	22,611	984	MN × m
Still water bending moment	M_{sw}	Normal	3,059	874	MN × m
Extreme wave bending moment	$M_{wv,ex}$	Gumbel	11,138	1,120	MN × m
Strength model uncertainty (**)	X_r	Normal	1.01 (1.05)	0.10	-
Still water model uncertainty	X_{sw}	Normal	1.00	0.10	-
Linear wave model uncertainty	X_{st}	Normal	1.00	0.10	-
Non-linear wave model uncertainty	X_{nl}	Normal	1.00	0.10	-

Notes:

(*) M_u calculation here corresponds to t_{n-50} scantlings prescribed by IACS (2019). See Table 7.3 for time-variant ultimate strength calculation.

(**) X_r is adopted equal to the proposed one from Section 6.2 and the one recommended by Hørte et al. (2007).

Time-varying Smith's model evaluation is illustrated in Figure 7.6 when the linear corrosion model is adopted. In the same figure, the 90% credible interval is identified to quantify the uncertainty bounds of the prediction. The hull girder ultimate strength starts to decay from the 8th year of service life since coating life duration is equal to 7.5 years for the linear corrosion

model. In total, $K = 5 \times 10^3 \times 25(\text{years}) = 125 \times 10^3$ model evaluations have been performed using NN-MCS. The overall reduction of the computational cost that has been achieved is more than 90%.

The sample statistics (mean value and coefficient of variation CoV) for hull girder ultimate strength prediction adopting the linear and generalized corrosion model are shown in Table 7.3. It has been found that the derived sample of annual sagging bending moment capacity well fits the lognormal distribution model. In addition, the following are noticed:

- The variability for both corrosion models ranges between 4.5% to 5% in all cases.
- At the design life of vessel, the expected value of hull girder ultimate strength adopting the posterior generalized corrosion model (after the incorporation of inspections data) is about 2% higher than the value corresponding to the linear corrosion model.
- With respect to the generalized corrosion model, a reduction of less than 1% is observed in the mean ultimate strength after seeing the data at the 15^{th} and 18^{th} year of service lifetime. This reduction seems logical since the amount of thickness loss on the deck plates – which, as it will be seen later, affects the overall strength in sagging – is higher in the posterior model, but not as much high in order to change the expected value of ultimate strength significantly. At the same time, the degree of variability remains the same after the incorporation of data in both inspections.

From the above conclusions it seems that the influence of thickness wastage uncertain parameters upon the variability of hull girder ultimate strength is minor. This fact motivated the author to carry out a sensitivity analysis in order to assess the relative influence of input variables on the variance of model output. A global sensitivity analysis was conducted by means of (i) depicting the scatterplots between input random variables and model output, and (ii) computing the variance-based sensitivity measures. Details are presented in Appendix I.

The main finding of the sensitivity analysis is that the variability related to material properties – and especially yield strength of high-tensile grade – dominate the variance of ultimate bending capacity in sagging condition. The contribution of thickness loss in the deck plates of cargo tank area seems to have a minor effect to the output variability, whereas the importance of thickness wastage uncertainty for all other groups is almost negligible. The above conclusion justifies this minor change in the variability of ultimate strength after the incorporation of inspections data.

The time-dependent resistance $R(\tau)$ and load $S(\tau)$ prediction is shown in Figure 7.7 for the case of linear corrosion model. The 90% credible interval is depicted for both cases too. In the same figure, a single realization of R and S is illustrated. For the specified scenario, it is observed that an event of failure occurs during the 24^{th} year of service life.

Table 7.3. Time-variant hull girder ultimate bending capacity in sagging.

Service time (years)	**Linear corrosion model**		**(Updated) Generalized corrosion model**	
	$\mathrm{E}[M_u]$ (GN × m)	$\mathrm{CoV}[M_u]$ (%)	$\mathrm{E}[M_u]$ (GN × m)	$\mathrm{CoV}[M_u]$ (%)
5	26.064	4.4	26.059	4.4
10	25.647	4.4	25.726	4.4
15 (1st inspection)	24.880	4.5	25.308 (25.099)	4.5(4.6)
18 (2nd inspection)	24.508	4.6	24.866 (24.693)	4.7 (4.7)
20	24.288	4.7	24.575	4.7
25	23.939	4.8	24.378	4.8

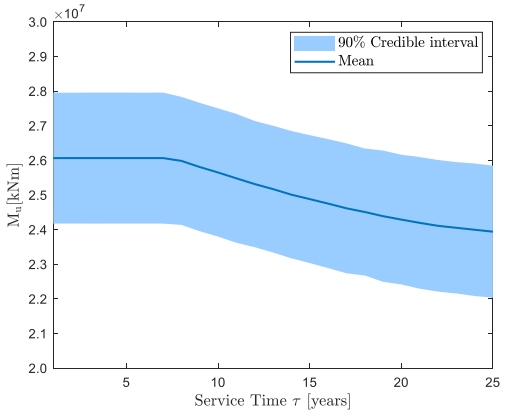

Figure 7.6. Time-variant hull girder ultimate strength reduction due to uniform corrosion degradation.

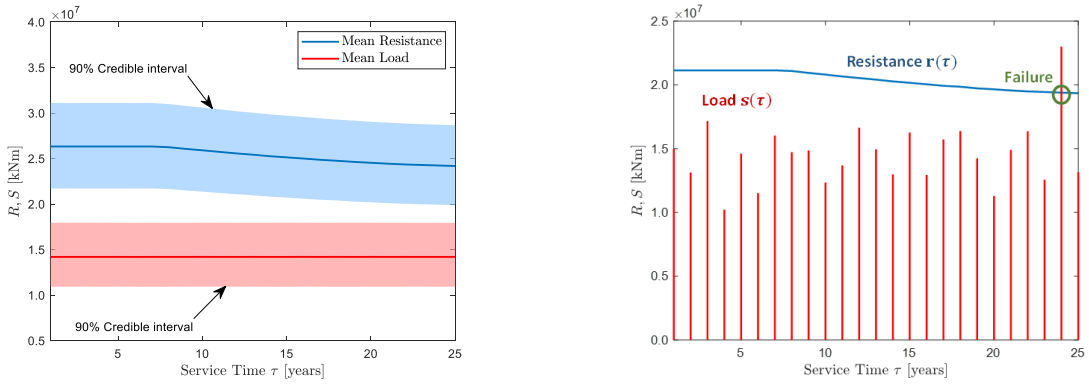

(a) (b)

Figure 7.7. (a) Time-dependent mean resistance $R(\tau)$ and annual extreme load event $S(\tau)$ along with the 90% credible interval, and (b) a single realization $r(\tau)$ of time-dependent resistance and extreme annual load $s(\tau)$. A failure event is recorded at the 24th year for the specific realization.

The calculations for the derivation of failure probability P_f and associated reliability index β are shown in Figure 7.8 and Figure 7.9 for the recommended and existing strength model uncertainty factor X_r, respectively. The results are presented for: (i) the linear corrosion model, (ii) the (updated) generalized corrosion model before and after the collection of data from inspections, and (iii) the IACS CSR t_{n-50} scantling approach corresponding to the design life of vessel. MCS has been used to estimate the instantaneous failure probability in annual time intervals $j = 1, \dots, 25$. The number of LSF evaluations in each year has been set equal to $K = 10^7$. For this number of samples and a magnitude of failure probability in the order of 10^{-3} to 10^{-2}, the error – translated by means of coefficient of variation – produced by MCS prediction is about 1%, following Eq. (7.15). The cumulative failure probability up to time τ_n is also computed through Eq. (7.12). From the results shown in Figure 7.8 and Figure 7.9, the following comments are made:

- The magnitude of annual failure probability at the design life of the vessel is in the order of 10^{-4} to 10^{-2} which is in good agreement with IACS CSR recommended values.

- The impact of the inspections data on the resulted reliability is low. This should come with no surprise as the decrease on the mean ultimate strength is small (see also Table 7.3). However, it should be stressed that this is not a generic conclusion.

- The linear and the updated generalized corrosion model give comparable results of failure probability. Although this finding cannot be generalized, since the outcome depends on the structural configuration of the examined ship and the effect of measurements as well, it can be noticed that the linear corrosion model provides a reasonable conservatism over the generalized, and more representative, corrosion model.

- The (instantaneous) annual failure probability using IACS CSR net-50 scantling approach provides a reasonable conservatism. However, in terms of cumulative failure probability, IACS CSR is not on the safe side. Particularly, the value of lifetime failure probability is approximately equal to 2×10^{-2} which is one order of magnitude smaller than the annual failure probability at the 25th year of service life (2×10^{-3} to 4×10^{-3}).

As a final note it is stated that the cumulative failure probability should be generally preferred for assessing the performance and the structural safety of a vessel, since it provides information from the entire history of ship, accounting for the fact that the ship may already have failed previously. In that case, the computation of instantaneous failure probability has no actual meaning.

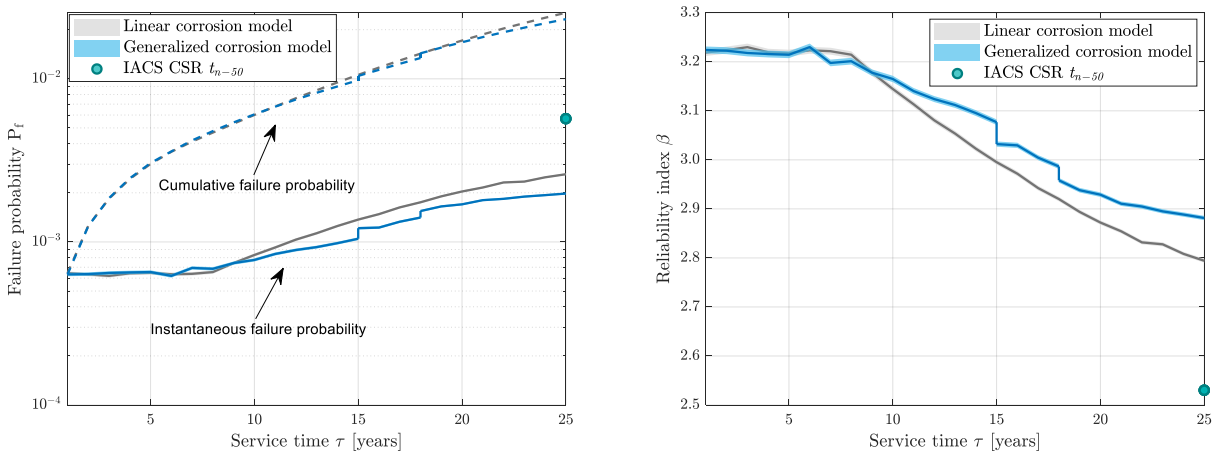

Figure 7.8. (a) Failure probability and (b) reliability index for linear corrosion model, updated corrosion model and net-50 scantling approach. The strength model uncertainty X_r has been set equal to $X_r \sim N(\mu_X = 1.01, \sigma_X = 0.10)$ which is the one proposed from Section 6.2.4.

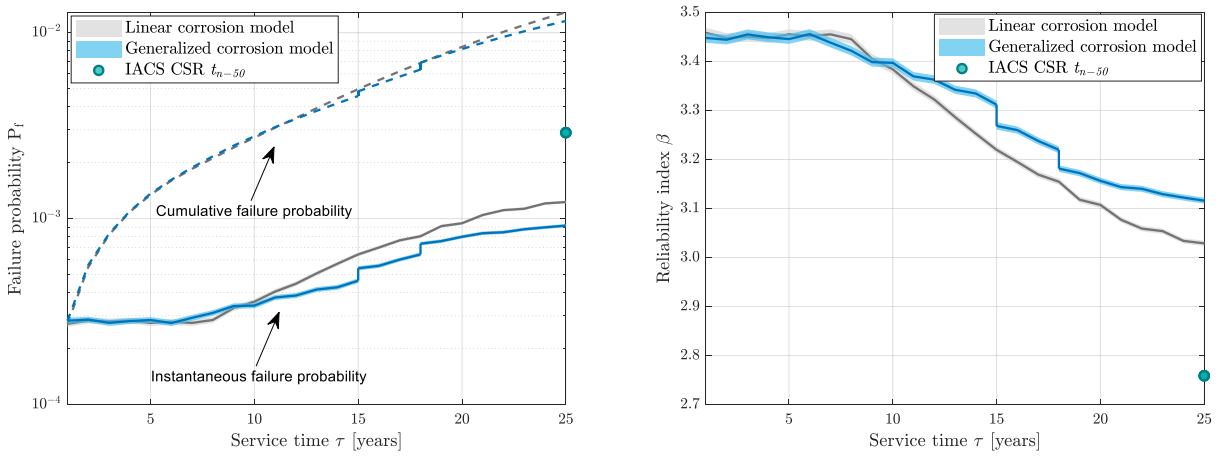

Figure 7.9. (a) Failure probability and (b) reliability index for linear corrosion model, updated corrosion model and net-50 scantling approach. The strength model uncertainty X_r has been set equal to $X_r \sim N(\mu_X = 1.05, \sigma_X = 0.10)$ which is the recommended from Hørte et al. (2007).

7.5.2 Application 2. Reliability assessment of two container ships

In this section, the reliability assessment under extreme hogging condition for a $4{,}400$ TEU and a $9{,}400$ TEU container ship is investigated. The scope of the present study is to evaluate the impact of the proposed model uncertainty factor X_r of Section 6.2 on the resulted probability of failure. For this reason, FORM has been employed to solve the reliability problem and identify the level of sensitivity of the basic random variables on the failure probability. The data for computing the basic random variables $\boldsymbol{X}$ that constitute the LSF for the above ships have been directly obtained from the paper of Corak and Soares (2018).

7.5.2.1 LSF formulation

The LSF formulation for the performance assessment of container ships in extreme hogging conditions reads:

$$g(\boldsymbol{X}) = X_r X_m M_u^{ch} - \left[X_{sw} M_{sw,ex} + k_w\left(X_{st} X_{nl} M_{wv,ex} + k_d X_d M_d\right)\right] \tag{7.34}$$

where, M_u^{ch} is the characteristic ultimate hull girder bending moment predicted by IACS CSR Smith method, M_{sw} is a random variable representing the annual extreme vertical SWBM, $M_{wv,ex}$ is a random variable expressing the annual extreme WVBM, M_d is a random variable that gives the annual extreme whipping bending moment due to bow flare slamming, k_w is a load combination factor between still water loads and wave-induced loads, k_d is another load combination factor that considers the interaction between wave and whipping bending moment. parameter X_d is also a random variable that denotes the uncertainty on whipping load prediction, whereas the random variables X_{sw}, X_{st}, X_{nl} have been defined in Eq. (7.27). Note that Eq. (2.2) has been used here to express the uncertainty on the computational model X_r and material yield strength X_m of the associated hull girder ultimate strength. The

The LSF of Eq. (7.34) can be seen as an extension of the LSF for oil tankers that takes into account the whipping bending moments. Whipping phenomenon is generally caused by the violent impact of wave loads on bow (bow flare slamming). Whipping bending moment is associated with high-frequency vibrations – as opposed with low-frequency rigid body vertical wave bending moments. Whipping should be taken into account for the ultimate limit state check as it can significantly increase the vertical wave bending moment.

A summary of the basic random variables forming the LSF is listed in Table 7.4. The evaluation of the hull girder ultimate capacity has been implemented using the as-built scantlings.

Table 7.4. A summary of the basic variables formulating the LSF for the 4,400 TEU and the 9,400 container ships.

		4,400 TEU vessel		9,400 TEU vessel	
Variable	**Distribution**	**Mean**	**CoV**	**Mean**	**CoV**
M_u^{ch}	fixed	9,893	-	20,199	-
$M_{sw,ex}$	Gumbel	3,317	0.1112	6,668	0.0396
$M_{wv,ex}$	Gumbel	3,846	0.0766	7,232	0.0781
$M_{d,ex}$	Gumbel	1,864	0.1470	6,113	0.1516
X_r	Normal	1.00 (0.83) *	0.10	1.00 (0.83) *	0.10
X_m	Lognormal	1.10	0.06	1.10	0.06
X_{sw}	Normal	1.00	0.05	1.00	0.05
X_{st}	Normal	1.00	0.10	1.00	0.10
X_{nl}	Normal	0.81	0.15	0.87	0.15
X_d	Normal	1.00	0.30	1.00	0.30
k_d	Normal	0.389	0.15	0.544	0.15
k_w	Normal	0.837	0.05	0.899	0.05

Note: (*) Existing vs. (recommended) approach.

7.5.2.2 Results

The results of the reliability analysis are shown in Table 7.5 for the two case studies. Probability of failures and associated reliability indexes are presented with respect to the existing and the proposed strength model uncertainty factor. Table 7.6 presents the importance of the respective random variable on the derived failure probability. An absolute value close to unity denotes a high effect whereas a value close to zero expresses a minor effect on the reliability problem.

Regarding the effect of strength model uncertainty factor X_r on the calculated reliability, the following two important insights are drawn from this study:

- The strength model uncertainty factor is the most influential parameter for the determination of safety level for both vessels.

- A significant reduction of the reliability index is observed using the recommended X_r. For the 4,400 TEU ship, the failure probability has increased by a factor of 36, whereas for the 9,400 TEU ship, the increase of failure probability is by a factor of 13.

The above results signify the importance of a proper quantification of X_r for the problem of reliability.

Table 7.5. Reliability index β_{FORM} and failure probability P_f calculated with FORM for the 4,400 TEU and 9,400 TEU container ships for different strength model uncertainty factor X_r.

Case study	X_r		$\Pr[F]$	β_{FORM}
	μ_X	σ_X		
Ship A. 4,400 TEU	1.00	0.10	8.3×10^{-4}	3.15
	0.83	0.10	3.0×10^{-2}	1.89
Ship B. 9,400 TEU	1.00	0.10	1.0×10^{-2}	2.32
	0.83	0.10	1.3×10^{-1}	1.11

Table 7.6. Derived sensitivity indexes (α-factors) for the two examined ships.

Random variables	**Ship A. 4,400 TEU**		**Ship B. 9,400 TEU**	
	$\mu_X = 1.00$	$\mu_X = 0.83$	$\mu_X = 1.00$	$\mu_X = 0.83$
M_u^{ch}	-	-	-	-
$M_{sw,ex}$	0.359	0.300	0.084	0.083
$M_{wv,ex}$	0.197	0.167	0.177	0.154
$M_{d,ex}$	0.073	0.068	0.212	0.169
X_r	-0.714	-0.764	-0.687	-0.734
X_m	-0.332	-0.314	-0.346	-0.329
X_{sw}	0.130	0.126	0.108	0.112
X_{st}	0.221	0.211	0.211	0.202
X_{nl}	0.310	0.303	0.301	0.296
X_d	0.136	0.136	0.333	0.315
k_d	0.074	0.072	0.192	0.169
k_w	0.141	0.133	0.175	0.160

8 Conclusions, originality and future directions

8.1 Conclusions

The hull girder ultimate strength assessment is one of the most critical measures of safety and a fundamental issue for the structural design of commercial vessels. The uncertainties associated with hull girder ultimate strength prediction dictate the use of probabilistic methods for its quantification. An overview of the uncertainties associated with hull girder ultimate strength prediction has been presented in Chapter 2. The main objective of this thesis is the assessment of hull girder ultimate strength and the updating of reliability through the management of the uncertainties related to geometric aspects (initial imperfections), deterioration processes (corrosion) and model aspects. For this reason, two basic mathematical tools have been introduced for uncertainty quantification and reduction, i.e., random fields and Bayesian analysis. In addition, machine learning techniques (neural networks) have been used when needed in conjunction with sampling-based approaches, such as MCS, to replace time-consuming models and accelerate the propagation of uncertainty through the model.

Random fields have been used within the framework of stochastic FE method as a tool to describe the spatial randomness of *initial geometric imperfections* and *uneven thickness distribution* on structural elements (see Chapter 4). The impact of stochastic initial imperfections on the ultimate strength of steel plates and hull girders has been examined in Section 4.2. It has been found that the developed stochastic imperfection model is able to accommodate the inherent randomness of initial deflections and predict the true ultimate strength of plates with better accuracy than the existing deterministic models (see Figure 4.10). It has been also showcased that the application of the proposed stochastic imperfection model on the hull girder resembles more the structural behavior of the critical buckling-mode (BM) imperfection model than the conventional hungry-horse (HH) model. The results from both analyses indicated that the conventional/idealized HH imperfection model does not necessarily represents a “realistic” condition as it is commonly assumed from literature body.

The effect of non-uniform thickness distribution on the ultimate strength of a representative stiffened panel has been investigated in Section 4.3. The main conclusion drawn from this study was that the uniform thickness approach adopted by IACS CSR seems reasonable and provides a satisfactory manner to simulate the actual uneven thickness distribution pattern, without loss of generality. The two modelling approaches (RF and RV approach) give comparable results in terms of mean ultimate strength prediction, although the variability is larger using the uniform thickness reduction. More case studies should be conducted to generalize the outcomes of the present work.

Bayesian methods have been applied in Chapter 6 of this thesis on two numerical investigations: (i) the quantification of *model uncertainty* associated with hull girder ultimate

strength description (see Section 6.2) and (ii) the updating of *corrosion model predictions* (see Section 6.3). In the first investigation, a robust framework for the determination of the model uncertainty factor distribution on a ship-type dependent basis has been established. The proposed methodology combines systematically and efficiently the analytical IACS CSR Smith's model prediction along with high-fidelity NLFEA results and other sources of information, e.g., literature sources or subjective knowledge from experts. The updating scheme that has been performed on oil tankers resulted in a model uncertainty factor that is close to the existing ones, verifying with that way the current practices of scientific body. On the contrary, the derived distribution model for container ships indicated that the model uncertainty factor should be shifted to lower values than the one commonly adopted in literature in order to account for the double bottom effect. The consideration of the double bottom effect can be performed either by adjusting the model uncertainty factor using the proposed methodology or by intrusively modifying the Smith's method, see Tatsumi et al. (2020). It has been also shown how the model uncertainty factor can be further adjusted and be applied on a particular vessel, as demonstrated for the case of "MOL Comfort" at the time of accident.

In the second investigation of Chapter 6, the corrosion predictions of an existing double hull VLCC tanker are updated using thickness measurements data from consecutive inspections. An updating scheme is performed to learn the initial uncertain parameters of an empirical time-dependent corrosion model using inspections data. The results of the posterior model indicated a very good agreement with the actual data recorded from the final inspection of the examined ship. The statistical uncertainty of the model parameters and the uncertainty bounds of corrosion predictions have been reduced using only a limited number of measurements. The updated model can be used for reliability analysis purposes where a higher level of sophistication is needed.

Neural networks have been successfully employed in this thesis to replace time-consuming model evaluations. MCS is the simplest method for propagating the uncertainty from input uncertain parameters through the model and calculating the stochastic response of the system. However, MCS becomes inefficient when the computational cost of model evaluations becomes unmanageable. NNs can alleviate this problem as they can be trained with a rather limited number of model evaluations and substitute the respective model with a black-box. In this thesis, NNs have been efficiently trained and used in three particular cases: (i) for the prediction of hull girder ultimate strength by replacing NLFEA (see Section 4.2.4.4), (ii) for the acceleration of aBUS-SuS algorithm by replacing log-likelihood function evaluations (see Section 6.3.5), and (iii) for the computation of time-varying hull girder ultimate strength by replacing IACS CSR Smith's model (see Section 7.5.1). The use of NNs for all the above applications reduce the computational cost by orders of magnitude while retaining the accuracy of model predictions.

The ultimate goal of this thesis is to get an improved description of the resistance model used for the reliability assessment of ship structures in ultimate limit state. In doing so, the

implication of the developments presented in Chapter 6 has been examined on the reliability of an oil tanker and two container ships (see Chapter 7). Particularly, the reliability updating of an oil tanker conditional on inspection data has been investigated. The results from this study demonstrated that the effect of measurements on the time-dependent reliability of the examined vessel is small. However, this finding cannot be seen as a general rule as the effect of inspections data is ship-type dependent. In the second investigation of Chapter 7, the failure probability for two container ships has been calculated using the proposed strength model uncertainty factor from Section 6.2. The failure probability has been also computed with commonly adopted values of strength model uncertainty factor from literature. The results indicated that the adoption of the recommended distribution model for strength model uncertainty factor leads to significant larger failure probabilities. This is due to the following two reasons: (i) the recommended distribution model for strength model uncertainty factor has been shifted to significantly lower values as compared with the existing distribution model (see Section 6.2.4.2, Figure 6.6), and (ii) the sensitivity of the strength model uncertainty factor parameter in the reliability calculation is the highest among all the basic random variables. It has been concluded that the neglection of the double bottom phenomenon in extreme hogging conditions can lead to unrealistic and risky results regarding the reliability of container ships (see Section 7.5.2).

8.2 Originality of the work

The work undertaken has led to the following innovations:

- A new stochastic imperfection model has been introduced for the description of imperfect geometry of steel plates on ship structures. The model has been constructed by taking into consideration the general HH mode shape of weld-induced plates and the spatial randomness of imperfect geometry. The latter is addressed through random fields theory. Statistics from actual data have been used for the formulation of the stochastic model. In contrast with the existing deterministic imperfection models that use a standard shape and an average level of distortion, the recommended stochastic model is able to quantify the whole spectrum of input uncertain parameters and approximate better the reality, which is a result of manufacturing processes and random localized dents created during service. The proposed model has been validated against actual data in terms of ultimate strength prediction. In general, a better resemblance of actual collapse mode and ultimate strength assessment has been achieved using the proposed model in comparison with the existing imperfection models.

- A robust framework for determining the model uncertainty factor related to hull girder ultimate strength prediction on a ship-type dependent basis has been developed. Current practices suggest a model uncertainty factor that either has been based on

subjective judgment only, or combines information from NLFEA, but not with a systematic and rigorous manner. In addition, no room to effectively incorporate new data exists, while often the same model uncertainty factor is adopted irrespectively of the ship type under examination. The recommended Bayesian methodology alleviates all of the aforementioned weaknesses by: (i) systematically combining information from different sources, e.g., subjective knowledge can be used to formulate the prior and advanced NLFEA results can be used to construct the likelihood, and (ii) quantify the effect of a future observation, e.g., an advanced NLFEA result, through the likelihood and update the prior knowledge. In addition, the recommended methodology is generic in the sense that it can be applied for any type of ship or floating unit (e.g., FPSO/FLNG) where any type of data is available. In the present thesis, the methodology has been applied on oil tankers and container ships. It has been found that the recommended model uncertainty factor for oil tankers is in good symphony with commonly adopted literature practices. On the other hand, for container ships, it has been found that the model uncertainty factor currently used in literature leads to significantly higher levels of reliability. The proposed methodology, which takes into account the double bottom effect due to the presence of local loads, results in a more representative model uncertainty factor that should be used in the framework of reliability.

- A Bayesian methodology has been developed on a vessel-specific basis for a more reliable and accurate prediction of uniform corrosion trends considering data from inspections. It has been shown that a minimum number of measurements acquired from consecutive inspections, when combined with available statistics from the global fleet of tankers, can lead to a significant reduction of uncertainties associated with the parameters of the employed time-dependent empirical corrosion model. A validation of the proposed methodology with actual data has taken place on a double hull VLCC tanker.

- A surrogate model (neural network) has been developed that is able to be learned with rather limited training samples of NLFEA. The generalized NN generalize retains the accuracy of NLFEA while it reduces by orders of magnitudes the computational effort needed. The full spectrum of input uncertainties associated with the imperfect hull geometry is explored and a full probabilistic description of hull girder ultimate capacity is achieved. This is especially useful when a reliability assessment is subsequently carried out and the full PDF is required, without the need to employ the incremental-iterative Smith's method.

8.3 Future directions

Methods for the quantification and reduction of uncertainties related to hull girder ultimate strength and reliability assessment have been developed in this thesis. It has been showed that Bayesian analysis framework can provide a solution on the problem of model error quantification and determination. As a systematic method for the determination of model error was missing from literature, a new framework has been established that is able to consistently and efficiently combine different sources of information and quantify their effect. The ultimate goal from this study could be a more reliable estimate of the performance of existing ship structures, as well the establishment of a unified partial safety factor (PSF) format design criterion for container ships. The adoption of the proposed methodology to other types of ships, such as bulk carriers, FPSOs, would be also an option for the future.

The application of the proposed Bayesian methodology for the corrosion model updating is beneficial as it may serve as a decision-making tool on existing ship structures, e.g., reinforcements, replacements, life-time extension. A strong benefit of the proposed model is that it can give reliable results with only as few as 20 measurements. This can reduce unnecessary costs and time from inspection surveys. In addition, the extension of the corrosion model to a smaller scale, i.e., a plate (or strake) element level, can be implemented for a more detailed view of corrosion predictions. Such a model could operate as a digital-twin where prior knowledge will be updated with new information from inspections.

In addition, the following research directions are proposed:

- The extension of the proposed stochastic imperfection model on stiffener sideways and global beam-column mode deflection mode shapes as soon as related information become available.

- The performance of the reliability assessment of “MOL Comfort” at the time of accident as soon as the midship section plan of the ship becomes available to the public.

This page intentionally left blank

References

Abrahamsen P. (1997). *A review of Gaussian random fields and correlation functions*.

Akpan U., Koko T., Ayyub B., Dunbar T. (2002). Risk assessment of aging ship hull structures in the presence of corrosion and fatigue. *Marine Structures*, *15*, 211–231.

Amlashi H. K. K., Moan T. (2008). Ultimate strength analysis of a bulk carrier hull girder under alternate hold loading condition – A case study Part 1 : Nonlinear finite element modelling and ultimate hull girder capacity. *Marine Structures*, *21*(4), 327–352.

Andric J., Kitarovic S., Bical M. (2014). IACS incremental - iterative method in progressive collapse analysis of various hull girder structures. *Brodogradnja : Časopis Brodogradnje i Brodograđevne Industrije*, *65*(1), 65–78.

Ang A. H.-S., Tang W. H. (2007). *Probability Concepts in Engineering: Emphasis on Applications to Civil and Environmental Engineering* (2nd ed.). Wiley.

Antoniou A. C. (1980). On the maximum deflection of plating in newly built ships. *Journal of Ship Research*, *24*(1), 31–39.

Au S. K., Beck J. L. (2001). Estimation of small failure probabilities in high dimensions by subset simulation. *Probabilistic Engineering Mechanics*, *16*(4), 263–277.

Babazadeh A., Khedmati M. R. (2021). Progressive collapse analysis of a bulk carrier hull girder under longitudinal vertical bending moment considering cracking damage. *Ocean Engineering*, *242*.

Bathe K. J. (2006). Finite Element Procedures. In *Prentice Hall*.

Betz W., Papaioannou I., Beck J. L., Straub D. (2018). Bayesian inference with Subset Simulation: Strategies and improvements. *Computer Methods in Applied Mechanics and Engineering*, *331*, 72–93.

Betz W., Papaioannou I., Straub D. (2016). Transitional Markov Chain Monte Carlo: Observations and Improvements. *Journal of Engineering Mechanics*, *142*(5).

Bracewell R. (1965). *The Fourier transform and its applications*. McGraw–Hill.

Caldwell J. (1965). Ultimate longitudinal strength. *Trans RINA*, *107*, 411–430.

Campanile A., Piscopo V., Scamardella A. (2014). Statistical properties of bulk carrier longitudinal strength. *Marine Structures*, *39*, 438–462.

Campanile A., Piscopo V., Scamardella A. (2015). Statistical properties of bulk carrier residual strength. *Ocean Engineering*, *106*, 47–67.

Campanile A., Piscopo V., Scamardella A. (2016a). Incidence of residual stresses and steel properties variability on corroded bulk carrier reliability. *Ocean Engineering*, *128*, 58–80.

Campanile A., Piscopo V., Scamardella A. (2016b). Time-variant bulk carrier reliability analysis in

pure bending intact and damage conditions. *Marine Structures*, *46*, 193–228.

Campanile A., Piscopo V., Scamardella A. (2016c). Time-variant bulk carrier reliability analysis in pure bending intact and damage conditions. *Marine Structures*, *46*, 193–228.

Campanile A., Piscopo V., Scamardella A. (2017a). Incidence of load combination methods on time-variant oil tanker reliability in intact conditions. *Ocean Engineering*, *130*, 371–384.

Campanile A., Piscopo V., Scamardella A. (2017b). Incidence of load combination methods on time-variant oil tanker reliability in intact conditions. *Ocean Engineering*, *130*, 371–384.

Chen N. Z. (2016). Hull girder reliability assessment for FPSOs. *Engineering Structures*, *114*, 135–147.

Ching J., Chen Y. (2007). Transitional Markov Chain Monte Carlo Method for Bayesian Model Updating, Model Class Selection, and Model Averaging. *Journal of Engineering Mechanics*, *133*(7), 816–832.

Chojaczyk A. A., Teixeira A. P., Neves L. C., Cardoso J. B., Guedes Soares C. (2015). Review and application of Artificial Neural Networks models in reliability analysis of steel structures. *Structural Safety*, *52*(PA), 78–89.

ClassNK. (2014). *Investigation Report on Structural Safety of Large Container Ships. The Investigative Panel on Large Container Ship Safety*.

Corak M., Soares C. G. (2018). Structural Reliability Analysis of Container Ships under Combined Wave and Whipping Loads. *Journal of Ship Research*, *62*(3), 115–133.

Der Kiureghian A., Liu P. (1986). Structural reliability under incomplete probability information. *Journal of Engineering Mechanics*, *112*(1), 85–104.

Ditlevsen O., Madsen H. (1996). *Structural Reliability methods*. John Wiley & Sons.

DNV. (1992). *Structural reliability analysis of marine structures. Classification Notes No. 30.6*.

DNV. (2004). *Non-linear finite element analysis of hull girder collapse of a tanker*.

DNV. (2013). Determination of structural capacity by non-linear FE analysis methods. *DNV-RP-C2008*.

DNV. (2020). Allowable thickness diminution for hull structure. In *DNVGL-CG-0182*.

Dow R. S., Smith C. S. (1984). Effects of localized imperfections on compressive strength of long rectangular plates. *Journal of Constructional Steel Research*, *4*(1), 51–76.

Emi H., Kumano A., Yamamoto N., Nakamura Y., Baba N., Shihara H. (1991). A recent study on life assessment of ships and offshore structures. *NKK Technical Bulettin*, *9*, 24–49.

Enright M. P., Frangopol D. M. (1999). Condition prediction of deteriorating concrete bridges. *Structural Engineering*, 1118–1125.

Frieze P., Lin Y. (1991). Ship Longitudinal Analysis Strength Modeling for Reliability Analysis. *SNAME Transactions*.

Fujikubo M., Yao T., Khedmati M. R., Harada M., Yanagihara D. (2005). Estimation of ultimate

strength of continuous stiffened panel under combined transverse thrust and lateral pressure Part 1: Continuous plate. *Marine Structures*, *18*(5–6), 383–410.

Gannon L., Liu Y., Pegg N., Smith M. J. (2012). Effect of welding-induced residual stress and distortion on ship hull girder ultimate strength. *Marine Structures*, *28*(1), 25–49.

Gao D. W., Shi G. J., Wang D. Y. (2012). Residual ultimate strength of hull structures with crack and corrosion damage. *Engineering Failure Analysis*, *25*, 316–328.

Garbatov Y., Soares C. G. (2002). Bayesian Updating in the Reliability Assessment of Maintained Floating Structures. *Journal of Offshore Mechanics and Arctic Engineering*, *124*(3), 139.

Garbatov Y., Soares C. G. (2019). Spatial corrosion wastage modeling of steel plates exposed to marine environments. *Journal of Offshore Mechanics and Arctic Engineering*, *141*(3), 1–6.

Gaspar B., Soares C. G. (2013). Hull girder reliability using a Monte Carlo based simulation method. *Probabilistic Engineering Mechanics*, *31*, 65–75.

Gaspar B., Teixeira A. P., Guedes Soares C. (2016). Effect of the nonlinear vertical wave-induced bending moments on the ship hull girder reliability. *Ocean Engineering*, *119*, 193–207.

Gelfand A. E., Smith A. F. M. (1992). Bayesian Statistics without Tears: A Sampling–Resampling Perspective. *The American Statistician*, *46*(2), 84–88.

Georgiadis D. G., Samuelides M. S. (2019). A methodology for the reassessment of hull-girder ultimate strength of a VLCC tanker based on corrosion model updating. *Ships and Offshore Structures*, *14*(sup1), 270–280.

Georgiadis D. G., Samuelides M. S. (2021a). Stochastic geometric imperfections of plate elements and their impact on the probabilistic ultimate strength assessment of plates and hull-girders. *Marine Structures*, *76*.

Georgiadis D. G., Samuelides M. S. (2021b). The effect of corrosion spatial randomness and model selection on the ultimate strength of stiffened panels. *Ships and Offshore Structures*, *16*(S1), 140–152.

Gilks W. R., Richardson S., Spiegelhalter D. J. (1996). *Markov Chain Monte Carlo in Practice*. Chapman & Hall.

Giovanis D. G., Papaioannou I., Straub D., Papadopoulos V. (2017). Bayesian updating with subset simulation using artificial neural networks. *Computer Methods in Applied Mechanics and Engineering*, *319*, 124–145.

Gong C., Frangopol D. M. (2020). Time-variant hull girder reliability considering spatial dependence of corrosion growth , geometric and material properties. *Reliability Engineering and System Safety*, *193*, 106612.

Goodfellow I., Bengio Y., Courville A. (2016). *Deep Learning*. MIT Press.

Graham L., Deodatis G. (2001). Response and eigenvalue analysis of stochastic finite element systems with multiple correlated material and geometric properties. *Probabilistic Engineering Mechanics*, *16*(1), 11–29.

Grigoriu M. (1993). On the spectral representation method in simulation. *Probabilistic Engineering Mechanics*, *8*(2), 75–90.

Grigoriu M. (1998). Simulation of Stationary Non-Gaussian Translation Processes. *Journal of Engineering Mechanics*, *124*(2), 121–126.

Grigoriu M. (2002). *Stochastic Calculus. Applications in Science and Engineering*. Springer Science and Business Media.

Guia J., Teixeira A. P., Guedes Soares C. (2018). Probabilistic modelling of the hull girder target safety level of tankers. *Marine Structures*, *61*(January), 119–141.

Guo J., Wang G., Ivanov L., Perakis A. (2008). Time-varying ultimate strength of aging tanker deck plate considering corrosion effect. *Marine Structures*, *21*(4), 402–419.

Hagan M. T., Demuth H. B., Beale M. H., De Jesus O. (2014). *Neural Network Design*. PWS.

Hasofer A., Lind N. (1974). Exact and Invariant Second-Moment Code Format. *Jounral of the Engineering Mechanics Division*, *100*(1), 111–121.

Hastings W. K. (1970). Monte Carlo sampling methods using Markov chains and their applications. *Biometrika*, *57*(1), 97–109.

Hørte T., Wang G., White N. (2007). Calibration of the hull girder ultimate capacity criterion for double hull tankers. *PRADS*.

Huang W., Moan T. (2008). Analytical method of combining global longitudinal loads for ocean-going ships. *Probabilistic Engineering Mechanics*, *23*(1), 64–75.

Hughes O. F. ., Paik J. K. (2010). *Ship Structural Analysis and Design*. SNAME.

Hussein A. W., Soares C. G. (2009). Reliability and residual strength of double hull tankers designed according to the new IACS common structural rules. *Ocean Engineering*, *36*(17–18), 1446–1459.

IACS. (2016). *Technical background report list for CSR BC & OT*.

IACS. (2019). *Common Structural Rules for Bulk Carriers and Oil Tankers*. International Association of Classifiction Societies.

IMO. (2006). *Goal-based new ship construction standards. Linkage between FSA and GBS* (Issue MSC 81/INF.6).

ISSC. (2000). Ultimate Hull Girder Strength (Special task committe VI.2). *Proceedings of the 14th International Ship and Offshore Structure Congress*, *2*, 1–67.

ISSC. (2012). Ultimate Strength (Committe III.1). *Proceedings of the 18th International Ship and Offshore Structures Congress*, *1*, 338–424.

ISSC. (2018). Ultimate Strength (Comittee III.1). *Proceedings of the 20th International Ship and Offshore Structures Congress*, *July*.

Kim D. K., Park D. K., Kim H. B., Seo J. K., Kim B. J., Paik J. K., Kim M. S. (2012). The necessity of applying the common corrosion addition rule to container ships in terms of ultimate

longitudinal strength. *Ocean Engineering*, *49*, 43–55.

Kim H., Straub D. (2017). Reliability Analysis and Updating of Inspected Ship Structures subject to Spatially Variable Corrosion. *12th International Conference on Structural Safety & Reliability (ICOSSAR)*, 1656–1665.

Lampe J., Hamann R. (2018). Probabilistic model for corrosion degradation of tanker and bulk carrier. *Marine Structures*, *61*, 309–325.

Li S., Georgiadis D. G., Kyun D., Samuelides M. S. (2022). A comparison of geometric imperfection models for collapse analysis of ship-type stiffened plated grillages. *Engineering Structures*, *250*.

Li S., Kim D. K., Benson S. (2021). The influence of residual stress on the ultimate strength of longitudinally compressed stiffened panels. *Ocean Engineering*, *231*.

Lindley D. (1975). The Future of Statistics: A Bayesian 21st Century. *Advances in Applied Probability*, *7*, 106–115.

Liu P. L., Der Kiureghian A. (1991). Optimization algorithms for structural reliability. *Structural Safety*, *9*(3), 161–177.

Luque J., Hamann R., Straub D. (2014). Spatial model for corrosion in ships and FPSOs. *OMAE*, 1–11.

Ma Y., Zhang J., Wang L., Liu Y. (2013). Probabilistic prediction with Bayesian updating for strength degradation of RC bridge beams. *Structural Safety*, *44*, 102–109.

Mansour A. E., Hovem L. (1994). Probability-based ship structural safety analysis. *Journal of Ship Research*, *38*(4), 329–339.

Matsumoto T., Shigemi T., Ishibashi K., Sugimoto K., Kidogawa M. (2016). Examination of effect of lateral loads on the hull girder ultimate strength of large container ships. *OMAE*, 1–8.

Melchers R. (1999a). *Structural Reliability Analysis and Prediction*. John Wiley & Sons.

Melchers R. E. (1999b). Corrosion uncertainty modelling for steel structures. *Constructional Steel Research*, *52*, 3–19.

Melchers R. E. (2003). Probabilistic Models for Corrosion in Structural Reliability Assessment — Part 1 : Empirical Models. *Transactions of the ASME*, *125*, 264–271.

Melchers R. E. (2019). Predicting long-term corrosion of metal alloys in physical infrastructure. *Npj Materials Degradation*, *3*(1), 1–7.

Metropolis N., Rosenbluth A. W., Rosenbluth M. N., Teller A. H., Teller E. (1953). Equation of state calculations by fast computing machines. *Journal of Chemicl Physics*, *21*(1087).

Moan T., Ayala-Uraga E., Wang X. (2005). Reliability-based service life assessment of FPSO structures. *Transactions - Society of Naval Architects and Marine Engineers (SNAME)*, *112*, 314–342.

Mohammadrahimi A., Sayebani M. (2019). Using the Bayesian updating approach to develop time-dependent corrosion wastage model for deck panel of bulk carriers. *Marine*

Structures, *64*, 92–109.

Nagel J. B., Sudret B. (2016). A unified framework for multilevel uncertainty quantification in Bayesian inverse problems. *Probabilistic Engineering Mechanics*, *43*, 68–84.

Neumann K., Ehlers S. (2019). Power spectrum for surface description of corroded ship structure from laser scan. *Proceedings of the ASME 2019 38th International Conference on Ocean, Offshore and Arctic Engineering (OMAE)*, 1–7.

Okasha N. M., Frangopol D. M., Decò A. (2010). Integration of structural health monitoring in life-cycle performance assessment of ship structures under uncertainty. *Marine Structures*, *23*(3), 303–321.

Paik J. (2002). *Ultimate Limit State Analysis and Design of Plated Structures*. John Wiley & Sons.

Paik J., Frieze P. (2001). Ship structural safety and reliability. *Prog. Struct. Engng. Mater*, *3*, 198–210.

Paik J. K., Kim S. K., Lee S. K. (1998). Probabilistic corrosion rate estimation model for longitudinal strength members of bulk carriers. *Ocean Engineering*, *25*(10), 837–860.

Paik J., Lee J., Hwang J., Park J. (2003a). A Time-Dependent Corrosion Wastage Model for the Structures of Single- and Double-Hull Tankers and FSOs and FPSOs. *Marine Technology*, *40*(3), 201–217.

Paik J., Myung J., Ii Y., Sung J., Wook C. (2003b). Time-variant ultimate longitudinal strength of corroded bulk carriers. *Marine Structures*, *16*, 567–600.

Papaioannou I., Straub D. (2017). Georisk : Assessment and Management of Risk for Engineered Systems and Geohazards Learning soil parameters and updating geotechnical reliability estimates under spatial variability – theory and application to shallow foundations. *Georisk*, *11*(1), 116–128.

Papoulis A., Pillai S. (2002). *Probability, random variables, and stochastic processes*. McGraw-Hill.

Parunov J., Andric J., Corak M., Kitarovic S. (2014). Structural reliability assessment of container ship at the time of accident. *Engineering for the Maritime Environment*, 1–13.

Parunov J., Senjanović I., Guedes Soares C. (2007). Hull-girder reliability of new generation oil tankers. *Marine Structures*, *20*(1–2), 49–70.

Plummer M., Best N., Cowles K., Vines K. (2006). CODA: convergence diagnosis and output analysis for MCMC. *R News*, *6*(1), 7–11.

Qin S., Cui W. (2003). Effect of corrosion models on the time-dependent reliability of steel plated elements. *Marine Structures*, *16*(1), 15–34.

Rackwitz R., Flessler B. (1978). Structural reliability under combined random load sequences. *Computers and Structures*, *9*(5), 489–494.

Rahbar-Ranji A. (2012). Ultimate strength of corroded steel plates with irregular surfaces under in-plane compression. *Ocean Engineering*, *54*, 261–269.

Raiffa H., Schlaifer R. (1961). *Applied statistical decision theory.* Harvard University Graduate School of Business Administration (Division of Research); Bailey & Swinfen.

Ringsberg J. W., Darie I., Nahshon K., Shilling G., Augusto M., Benson S., Brubak L., Feng G., Fujikubo M., Gaiotti M., Hu Z., Jang B., Paik J., Slagstad M., Tabri K., Wang Y., Wiegard B., Yanagihara D. (2021). The ISSC 2022 committee III. 1-Ultimate strength benchmark study on the ultimate limit state analysis of a stiffened plate structure subjected to uniaxial compressive loads. *Marine Structures*, *79*.

Saltelli A., Ratto M., Andres T., Campolongo, Francesca Cariboni J., Gatelli D., Saisana M., Tarantola S. (2008). *Global Sensitivity Analysis: The Primer*. John Wiley.

Shi G., Gao D. (2021). Reliability analysis of hull girder ultimate strength for large container ships under whipping loads. *Structure and Infrastructure Engineering*, *17*(3), 319–330.

Shinozuka M., Deodatis G. (1991). Simulation of stochastic processes by spectral representation. *Applied Mechanics Reviews*, *44*(4), 191–204.

Shinozuka M., Deodatis G. (1996). Simulation of multi-dimensional Gaussian stochastic fields by spectral representation. *Applied Mechanics Reviews*, *49*(1), 29–53.

Shu Z., Moan T. (2011a). Reliability analysis of a bulk carrier in ultimate limit state under combined global and local loads in the hogging and alternate hold loading condition. *Marine Structures*, *24*(1), 1–22.

Shu Z., Moan T. (2011b). Reliability analysis of a bulk carrier in ultimate limit state under combined global and local loads in the hogging and alternate hold loading condition q. *Marine Structures*, *24*(1), 1–22.

Smith C. (1977). Influence of local compressive failure on ultimate longitudinal strength of a ship's hull. *International Symposium on Practical Design of Ships and Others Floating Structures (PRADS)*.

Smith C. S., Davidson P. C., Chapman J. C. (1988). Strength and stifness of ships' plating under in-plane compression and tension. *Trans. RINA*, *130*, 277–296.

Soares C. G., Dogliani M., Ostergaard C., Parmentier G., Pedersen P. T. (1996). Reliability based ship structural design. *Transactions - Society of Naval Architects and Marine Engineers*, *104*, 357–389.

Soares C., Garbatov Y. (1999). Reliability of corrosion protected and maintained ship hulls subjected to corrosion and fatigue. *Journal of Ship Research*, *43*(2), 65–78.

Sobol I. M. (1993). Sensitivity Estimates for Nonlinear Mathematical Models. *Mathematical Modelling and Computational Experiments*, *4*, 407–414.

Stefanou G. (2009). The stochastic finite element method: Past, present and future. *Comput. Methods Appl. Mech. Engrg.*, *198*, 1031–1051.

Stein M. (1987). Large sample properties of simulations using Latin Hypercube sampling. *Technometrics*, *29*(2), 143–151.

Straub D. (2011). Reliability updating with equality information. *Probabilistic Engineering*

Mechanics, *26*(2), 254–258.

Straub D., Papaioannou I. (2015). Bayesian Updating with Structural Reliability Methods. *J. Eng. Mech.*, *141*(3), 04014134.

Straub D., Schneider R., Bismut E., Kim H. J. (2020). Reliability analysis of deteriorating structural systems. *Structural Safety*, *82*.

Strauss A., Frangopol D. M., Kim S. (2008). Use of monitoring extreme data for the performance prediction of structures : Bayesian updating. *Engineering Structures*, *30*(12), 3654–3666.

Sudret B., Der Kiureghian A. (2000). *Stochastic Finite Element Methods and Reliability. A State-of-the-Art Report*.

Sun H., Bai Y. (2003). Time-variant reliability assessment of FPSO hull girders. *Marine Structures*, *16*, 219–253.

Tanaka S., Yanagihara D., Yasuoka A., Harada M., Okazawa S., Fujikubo M., Yao T. (2014). Evaluation of ultimate strength of stiffened panels under longitudinal thrust. *Marine Structures*, *36*, 21–50.

Tatsumi A., Fujikubo M. (2020). Ultimate strength of container ships subjected to combined hogging moment and bottom local loads, Part 1 : Nonlinear finite element analysis. *Marine Structures*, *69*, 102683.

Tatsumi A., Htoo H., Ko H., Fujikubo M. (2020). Ultimate strength of container ships subjected to combined hogging moment and bottom local loads, Part 2: An extension of Smith' s method. *Marine Structures*, *71*, 102738.

Teixeira A. P., Guedes Soares C. (2009). Reliability analysis of a tanker subjected to combined sea states. *Probabilistic Engineering Mechanics*, *24*(4), 493–503.

Teixeira A., Soares C. (2008). Ultimate strength of plates with random fields of corrosion. *Structure and Infrastructure Engineering*, *4*(5), 363–370.

Turkstra C. (1970). Theory of Structural Design Decisions. Study No.2. In *Solid Mechanics division*.

Ueda Y., Yao T. (1985). The influence of complex initial deflection modes on the behaviour and ultimate strength of rectangular plates in compression. *Journal of Constructional Steel Research*, *5*, 265–302.

Van de Schoot R., Depaoli S., King R., Kramer B., Märtens K., Tadesse M. G., Vannucci M., Gelman A., Veen D., Willemsen J., Yau C. (2021). Bayesian statistics and modelling. *Nature Reviews Methods Primers*, *1*(1).

Vanmarcke E. (2010). *Random Fields:Analysis and Synthesis*. World scientific.

Vasconcelos de Farias B., Netto T. A. (2012). FPSO hull structural integrity evaluation via Bayesian updating of inspection data. *Ocean Engineering*, *56*, 10–19.

Wang Y., Wharton J., Shenoi R. (2014). Ultimate strength analysis of aged steel-plated structures exposed to marine corrosion damage: A review. *Corrosion Science*, *86*, 42–60.

Woloszyk K., Garbatov Y. (2020). Random field modelling of mechanical behaviour of corroded thin steel plate specimens. *Engineering Structures*, *212*.

Xu M. C., Song Z. J., Pan J. (2017). Study on influence of nonlinear finite element method models on ultimate bending moment for hull girder. *Thin-Walled Structures*, *119*(June), 282–295.

Xu M. C., Teixeira A. P., Guedes Soares C. (2015). Reliability assessment of a tanker using the model correction factor method based on the IACS-CSR requirement for hull girder ultimate strength. *Probabilistic Engineering Mechanics*, *42*, 42–53.

Yamamoto N., Ikegami K. (1998). A Study on the Degradation of Coating and Corrosion of Ship' s Hull Based on the Probabilistic Approach. *Offshore Mechanics and Arctic Engineeering*, *120*, 1–8.

Yao T. (2003). Hull girder strength. *Marine Structures*, *16*, 1–13.

Yao T., Fujikubo M. (2016). Buckling and Ultimate Strength of Ship and Ship-like Floating Structures. In *Buckling and Ultimate Strength of Ship and Ship-like Floating Structures*. Elsevier.

Zayed A., Garbatov Y., Soares C. G. (2018). Corrosion degradation of ship hull steel plates accounting for local environmental conditions. *Ocean Engineering*, *163*(June), 299–306.

Zhang S., Khan I. (2009). Buckling and ultimate capability of plates and stiffened panels in axial compression. *Marine Structures*, *22*(4), 791–808.

Zhu B., Frangopol D. M. (2013). Reliability assessment of ship structures using Bayesian updating. *Engineering Structures*, *56*, 1836–1847.

This page intentionally left blank

Appendix A. Probability theory

The basic notions of probability theory are briefly introduced in this appendix. A thorough review of probability theory is out of the scope of this thesis. The reader who is interested is referred to the book of Ang and Tang (2007) for a deep insight of probability theory with focus on engineering applications.

A.1 Basics of probability theory

The theory of probability is concerned with *experiments* and their outcomes, where the term experiment is used in a more generic sense to express for example a random phenomenon or process. The collection of all possible outcomes of an experiment is called its *sample space* Ω. This space consists of a set of points (or elements) ω_i representing an individual outcome of an experiment called *sample points* or *realizations.* An event A represents a collection of sample points in the sample space Ω.

We use the notation $\Pr(A)$ to denote the probability of an event A. The basic axioms of probability theory are:

1. For any event A, the probability of A must lie between zero and one:

$$0 \leq \Pr(A) \leq 1 \tag{A.1}$$

2. The probability that is associated with the entire sample space Ω expresses a certain event and is equal to unity:

$$\Pr(\Omega) = 1 \tag{A.2}$$

3. If the events $A_1, A_2, \dots, A_n$ are *mutually exclusive*, i.e., they do not contain no sample points in common, the probability of their *union* is a sum of probabilities:

$$\Pr(A_1 \cup A_2 \cup \dots \cup A_n) = \sum_{i=1}^{n} \Pr(A_i) \tag{A.3}$$

The event that A *or* B occurs is the union of events $\{A \cup B\}$, whose probability can be expressed as:

$$\Pr(A \cup B) = \Pr(A) + \Pr(B) - \Pr(A \cap B) \tag{A.4}$$

where $\{A \cap B\}$ denotes the joint event that both A and B occur. If the events A and B are mutually exclusive, then $\Pr(A \cup B) = \Pr(A) + \Pr(B)$.

If all possible outcomes of an experiment are represented by a set of mutually exclusive events $A_1, A_2, \dots, A_n$, then it follows from axioms 2 and 3 that the associated probabilities sum to unity:

$$\Pr(A_1) + \Pr(A_2) + \cdots + \Pr(A_n) = 1 \tag{A.5}$$

The probability of the complement event $\bar{A}$ is defined as:

$$\Pr(\bar{A}) = 1 - \Pr(A) \tag{A.6}$$

The probability of an event A given that another event E has occurred expresses the *conditional probability* of A given B:

$$\Pr(A|B) = \frac{\Pr(A \cap B)}{\Pr(B)} \tag{A.7}$$

Rearranging Eq. (A.7), it yields that:

$$\Pr(A \cap B) = \Pr(A|B)\Pr(B) = \Pr(B|A)\Pr(A) \tag{A.8}$$

Two events A and B are called *independent*, i.e., the occurrence of one does not affect the probability of occurrence of the other, when:

$$\Pr(A|B) = \Pr(A) \tag{A.9}$$

or:

$$\Pr(A \cap B) = \Pr(A)\,\Pr(B) \tag{A.10}$$

The above can be generalized from more than two events. This theorem is known as the *multiplication rule*. If $B_1, B_2, \dots, B_n$ are a set of mutually exclusive events, then the probability of an event A can be determined from the *total probability theorem* as:

$$\Pr(A) = \sum_{i=1}^{n} \Pr(A \cap B_i) \overset{\text{Eq.(A.8)}}{=} \sum_{i=1}^{n} \Pr(A|B_i) \Pr(B_i) \tag{A.11}$$

The conditional probability of an event A given the occurrence of another event B can be computed by the combination of Eq. (A.7) and Eq. (A.8) yielding the so-called *Bayes' rule*:

$$\Pr(A|B) = \frac{\Pr(B|A)\Pr(A)}{\Pr(B)} \tag{A.12}$$

A detailed presentation of Bayes' rule is presented in Section 5.2 of the thesis.

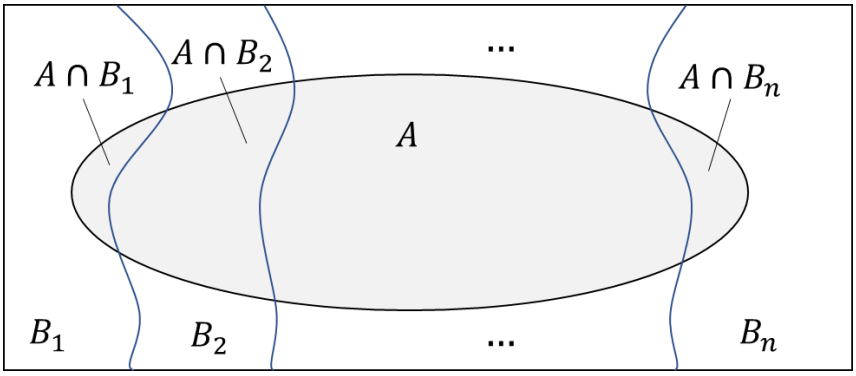

Figure.A.1. Illustration of total probability theorem.

This page intentionally left blank

Appendix B. Random variables

Throughout this thesis, a single random variable is represented by a capital letter X. A single realization (or outcome) of the random variable X is denoted by a small letter x. In the following, we will first define the description of a single random variable, and then we will extend to two or more random variables jointly.

B.1 Basic definitions

A random variable X is a function which maps a set of sample points ω_i from the sample space Ω to real numbers, that is: $X: \Omega \to \mathbb{R}$. A random variable can be discrete or continuous, depending on the type of the corresponding sample space. In the following, we will restrict our definitions to continuous random variables which is the main subject of this thesis.

A common way to describe the probability distribution of a random variable is through the use of a *cumulative distribution function* or CDF. The value of this function $F_X(x)$ is simply the probability of the random variable X being smaller or equal to a specific value x, that is:

$$F_X(x) = \Pr(X \leq x) \tag{B.1}$$

The following properties hold for the CDF of X:

$$0 \leq F_X(x) \leq 1 \tag{B.2}$$

$$F_X(-\infty) = 0 \tag{B.3}$$

$$F_X(\infty) = 1 \tag{B.4}$$

$$F_X(x_2) - F_X(x_1) = \Pr(x_1 \leq X \leq x_2) \tag{B.5}$$

Another classical measure to express the probability distribution of a random variable is through the *probability density function* or PDF. We define the PDF $f_X(x)$ of a variable X such that the probability that X takes values in an interval x to $x + dx$ is:

$$f_X(x)dx = \Pr(x \leq X \leq x + dx) \tag{B.6}$$

The following properties hold for the PDF of X:

$$\Pr(x \leq X \leq x + dx) = \int_{x}^{x+dx} f_X(x)dx \tag{B.7}$$

$$f_X(x) \geq 0 \tag{B.8}$$

$$\int_{-\infty}^{\infty} f_X(x)dx = 1 \tag{B.9}$$

The PDF can be determined if the CDF is known, since $f_X(x)$ is simply the derivative or slope of $F_X(x)$:

$$f_X(x) = \frac{dF_X(x)}{dx} \tag{B.10}$$

It also holds that:

$$F_X(x = a) = \Pr(-\infty \leq X \leq a) = \int_{-\infty}^{a} f_X(x)dx \tag{B.11}$$

B.2 Jointly distributed random variables

Most engineering problems deal with multiple random variables $\boldsymbol{X} = [X_1, \dots, X_n]^T$. It is then needed to establish a joint distribution model. For the elementary case of two continuous random variables X and Y, the probability that X lies in the interval $\{x, x + dx\}$ and Y lies in the interval $\{y, y + dy\}$ is $f_{XY}(x, y)dxdy$. The function $f_{XY}(x, y)$ is called the *joint probability density function* of joint PDF.

The probability of the joint occurrence of X and Y in some region in the sample space is determined by integration of the joint PDF over that region, that is:

$$\Pr(x_1 \leq X \leq x_2) \text{ and } \Pr(y_1 \leq Y \leq y_2) = \int_{x_1}^{x_2} \int_{y_1}^{y_2} f_{XY}(x, y)dxdy \tag{B.12}$$

Clearly, the joint PDF must satisfy the following conditions:

$$f_{XY}(x, y) \geq 0 \tag{B.13}$$

$$\iint_{-\infty}^{\infty} f_{XY}(x,y)dxdy = 1 \tag{B.14}$$

The joint CDF can be defined as:

$$F_{XY}(x,y) = \Pr[(X \leq x) \cap (Y \leq y)] \tag{B.15}$$

The joint density function is now the partial derivative of joint CDF:

$$f_{XY}(x,y) = \frac{\partial^2}{\partial x \partial y} F_{XY}(x,y) \tag{B.16}$$

The *marginal PDF* of is X_1obtained by integrating the joint PDF over all possible values of x_2:

$$f_X(x) = \int_{-\infty}^{\infty} f_{XY}(x,y)dy \tag{B.17}$$

Consider the case of two dependent random variables X and Y. If the value of one random variable is known $Y = y$, the distribution of the other becomes the *conditional distribution* of X given $Y = y$, and it follows from Eq. (A.7) that:

$$f_{X|Y}(x|y) = \frac{f_{XY}(x,y)}{f_Y(y)} \tag{B.18}$$

Note that $f_{X|Y}(x|y)$ is a univariate PDF. From the above definition of conditional distribution, the *chain rule* is defined as:

$$f_{XY}(x,y) = f_{X|Y}(x|y) f_Y(y) \tag{B.19}$$

Chain rule can be extended to a vector of random variables $\boldsymbol{X} = [X_1, \dots, X_n]^T$ as follows:

$$f_{\boldsymbol{X}}(\boldsymbol{x}) = f(x_n|x_{n-1}, \dots, x_1) f(x_{n-1}|x_{n-2}, \dots, x_1) \dots f(x_1) \tag{B.20}$$

Through the chain rule, conditional distributions are often an effective way to establish joint distributions.

B.3 Statistical descriptors of random variables

The *expectation* or the *first moment* μ_X of a random variable X with associated PDF $f_X(x)$ is:

$$\mu_X = \mathrm{E}[X] = \int_{-\infty}^{\infty} x f_X(x) dx \tag{B.21}$$

A common measure of the dispersion of the variable X is its *variance* σ_X^2 defined as the weighted average of the squared deviations from the mean:

$$\sigma_X^2 = \mathrm{Var}[X] = \mathrm{E}[(X - \mu_X)^2] = \int_{-\infty}^{\infty} (x - \mu_X)^2 f_X(x) dx \tag{B.22}$$

Alternatively, the variance can be written as:

$$\mathrm{Var}[X] = \mathrm{E}[X^2] - \mu_X^2 \tag{B.23}$$

The square root of the variance is the *standard deviation* σ_X of X:

$$\sigma_X = \sqrt{\mathrm{Var}[X]} \tag{B.24}$$

A dimensionless measure to quantify the degree of uncertainty of X is the *coefficient of variation* CoV_X:

$$\mathrm{CoV}_X = \frac{\sigma_X}{|\mu_X|} \tag{B.25}$$

The *covariance* of two random variables X_1 and X_2 is defined as the expectation of the product of the deviations from their respective means:

$$C[X_1, X_2] = \mathrm{E}\big[(X_1 - \mu_{X_1})(X_2 - \mu_{X_2})\big] = \iint_{-\infty}^{\infty} (x_1 - \mu_{X_1})(x_2 - \mu_{X_2}) f_{X_1 X_2}(x_1, x_2) dx_1 dx_2 \tag{B.26}$$

It holds also that:

$$C[X_1, X_2] = \mathrm{E}[X_1 X_2] - \mu_{X_1} \mu_{X_2} \tag{B.27}$$

If the random variables X_1 and X_2 are independent, the expectation of the product is the product of the expectations, that is:

$$\mathrm{E}[X_1 X_2] = \mathrm{E}[X_1] E[X_2] \tag{B.28}$$

From Eq. (B.27) and Eq. (B.28) it yields that for two independent random variables their covariance is zero $C[X_1, X_2] = 0$.

The dimensionless *coefficient of correlation* $\rho_{X_1 X_2}$ between X_1 and X_2 is defined by dividing Eq. (B.26) by the associated standard deviations:

$$\rho_{X_1 X_2} = \frac{C[X_1, X_2]}{\sigma_{X_1} \sigma_{X_2}} \tag{B.29}$$

It can be shown that the bounds of the correlation coefficient are:

$$-1 \leq \rho_{X_1 X_2} \leq 1 \tag{B.30}$$

This page intentionally left blank

Appendix C. Probability distribution models

C.1 Normal distribution

A random variable X follows the normal or (Gaussian) distribution with parameters μ and σ, denoted by $X \sim N(\mu, \sigma)$, if its PDF $f_X(x)$ is defined as:

$$f_X(x) = \frac{1}{\sigma\sqrt{2\pi}} \exp\left[-\frac{1}{2}\left(\frac{x-\mu}{\sigma}\right)^2\right] \tag{C.1}$$

The parameters μ and σ of the Normal distribution are identical to the mean and standard deviation of X, i.e., $\mu = \mu_X$ and $\sigma = \sigma_X$.

The standard normal distribution $\varphi(z)$ it comes from the generalized normal distribution with $\mu = 0$ and $\sigma = 1$. The PDF of the standard normal distribution reads:

$$\varphi(z) = \frac{1}{\sqrt{2\pi}} \exp\left[-\frac{1}{2}z^2\right] \tag{C.2}$$

and the CDF:

$$\Phi(z) = \int_{-\infty}^{z} \varphi(z)dz \tag{C.3}$$

Any normal distributed random variable X can be transformed to its standardized form Z by the transformation:

$$Z = \frac{X - \mu_X}{\sigma_X} \tag{C.4}$$

As no closed-form solution for the normal distribution exists, the above transformation can be used to evaluate the CDF of a normal random variable through the standard normal CDF as follows:

$$F_X(x) = \Phi\left(\frac{x-\mu_X}{\sigma_X}\right) \tag{C.5}$$

C.2 Lognormal distribution

If $X = \ln(Y)$ has a normal distribution with mean value μ_X and standard deviation σ_X, then the random variable Y will follow the lognormal distribution with parameters η and ζ, denoted by $X \sim LN(\eta, \zeta)$, with PDF:

$$f_Y(y) = \frac{1}{\zeta\sqrt{2\pi}} \exp\left[-\frac{1}{2}\left(\frac{\ln(y) - \eta}{\zeta}\right)^2\right], \quad y \geq 0 \tag{C.6}$$

The parameters η and ζ are associated with the mean μ_Y and coefficient of variation CoV_Y of Y as follows:

$$\zeta = \sqrt{\ln(1 + \mathrm{CoV}_Y^2)} \tag{C.7}$$

$$\eta = \ln(\mu_Y) - 0.5\zeta^2 \tag{C.8}$$

The CDF of Y can be evaluated in terms of the standard normal CDF $\Phi(\cdot)$ as:

$$F_Y(y) = \Pr(Y \leq y) = \Pr(X \leq \ln(y)) = \Phi\left(\frac{\ln(y) - \mu_X}{\sigma_X}\right) \tag{C.9}$$

C.3 Uniform distribution

A random variable X follows the uniform distribution with lower limit a and upper limit b, denoted by $X \sim U(\mathrm{a}, \mathrm{b})$, if its PDF $f_X(x)$ is defined as:

$$f_X(x) = \frac{1}{\mathrm{b} - \mathrm{a}}, \quad \mathrm{a} \leq x \leq \mathrm{b} \tag{C.10}$$

The PDF $f_X(x)$ of the uniform distribution is thus constant over the interval $[\mathrm{a}, \mathrm{b}]$. The CDF $F_X(x)$ of the uniform distribution is defined as:

$$F_X(x) = \frac{x - \mathrm{a}}{\mathrm{b} - \mathrm{a}} \tag{C.11}$$

The parameters a and b are related to the mean value μ_X and standard deviation σ_X of X variable as follows:

$$\mathrm{a} = \mu_X - \sigma_X\sqrt{3} \tag{C.12}$$

$$\mathrm{b} = \mu_X + \sigma_X\sqrt{3} \tag{C.13}$$

C.4 Beta distribution

A random variable X follows the beta distribution with shape parameters α and β, and lower and upper limits a and b, respectively, denoted by $X \sim Beta(\alpha, \beta, [\mathrm{a}, \mathrm{b}])$, if its PDF $f_X(x)$ is defined as:

$$f_X(x) = \frac{w^{\alpha-1}(1-w)^{\beta-1}}{\mathrm{B}(\alpha,\beta)(\mathrm{b}-\mathrm{a})}, \quad \mathrm{a} \le x \le \mathrm{b} \tag{C.14}$$

where, $\mathrm{w} = \frac{x-\mathrm{a}}{\mathrm{b}-\mathrm{a}}$ and $\mathrm{B}(\alpha, \beta)$ is the beta function with arguments α and β. The parameters α and β are related to the mean μ_X and standard deviation σ_X with the following relations:

$$\alpha = \frac{(\mathrm{a}-\mu_X)(\mathrm{ab}-\mathrm{a}\mu_X-\mathrm{b}\mu_X+\mu_X^2+\sigma_X^2)}{\sigma_X^2(\mathrm{b}-\mathrm{a})} \tag{C.15}$$

$$\beta = \frac{(\mu_X-\mathrm{b})(\mathrm{ab}-\mathrm{a}\mu_X-\mathrm{b}\mu_X+\mu_X^2+\sigma_X^2)}{\sigma_X^2(\mathrm{b}-\mathrm{a})} \tag{C.16}$$

The great value of the Beta distribution lies in the wide variety of shapes it can take simply by varying the parameters α and β. Beta distribution is particularly appropriate in cases where a variable must lie within a specified range $[\mathrm{a}, \mathrm{b}]$. Finally, for $\alpha = 1$ and $\beta = 1$, the Beta distribution is equivalent to the uniform distribution.

C.5 Weibull distribution

Let X be a random variable that follows the Weibull distribution with scale parameter λ and shape parameter k. The PDF $f_X(x)$ of the Weibull distribution is:

$$f_X(x) = \frac{k}{\lambda}\left(\frac{x}{\lambda}\right)^{k-1} \exp\left[-\left(\frac{x}{\lambda}\right)^k\right] \tag{C.17}$$

The CDF $F_X(x)$ of the Weibull distribution is:

$$F_X(x) = 1 - \exp\left[-\left(\frac{x}{\lambda}\right)^k\right] \tag{C.18}$$

The parameters λ and k of the Weibull distribution are associated with its mean μ_X and standard deviation σ_X as follows:

$$\mu_X = \lambda\Gamma\left(1 + \frac{1}{k}\right) \tag{C.19}$$

$$\sigma_X = \lambda\left[\Gamma\left(1 + \frac{2}{k}\right) - \Gamma^2\left(1 + \frac{1}{k}\right)\right] \tag{C.20}$$

where $\Gamma(\cdot)$ is the Gamma function.

C.6 Gumbel distribution

Let X be a random variable that follows the Gumbel distribution with scale parameter a_n and location parameter b_n. The PDF $f_X(x)$ of the Gumbel distribution is:

$$f_X(x) = \frac{1}{a_n}\exp\left[-\frac{x - b_n}{a_n} - \exp\left(-\frac{x - b_n}{a_n}\right)\right] \tag{C.21}$$

The CDF $F_X(x)$ of the Gumbel distribution is:

$$F_X(x) = \exp\left[-\exp\left(-\frac{x - b_n}{a_n}\right)\right] \tag{C.22}$$

The parameters a_n and b_n of the Gumbel distribution are associated with its mean μ_X and standard deviation σ_X as follows:

$$\mu_X = b_n + 0.5772a_n \tag{C.23}$$

$$\sigma_X = \frac{\pi}{\sqrt{6}}a_n \tag{C.24}$$

Appendix D. Monte Carlo simulation

D.1 Outline of Monte Carlo simulation (MCS) method

Monte Carlo simulation is a simple and powerful method for propagating the uncertainty from input model parameters $\boldsymbol{X} = [X_1, \dots, X_n]^T$ through the model $\mathcal{M}$ and calculate the variability of the response $\boldsymbol{Y}$ using simple relationships from statistics (see Figure D.1).

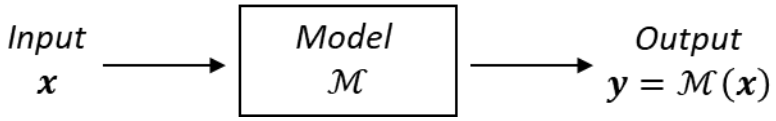

Figure D.1. Input-output relation.

The implementation of MCS consists of the following three simple steps which are briefly outlined below.

1. Generate (pseudo-)random samples $\boldsymbol{x}^{(i)}$, for $i = 1, \dots, K$ of the input random vector $\boldsymbol{X}$.

For the simple case of a single random variable X with associated CDF $F_X(x)$, a sample $x^{(i)}$ can be obtained by first generating a random sample $u^{(i)}$ from the standard uniform distribution $U(0,1)$ and then computing the inverse CDF F_X^{-1} on that single point:

$$x^{(i)} = F_X^{-1}\left(u^{(i)}\right) \tag{D.1}$$

The generation of a pseudo-random sample point uniformly distributed in the interval $[0,1]$ can be implemented by a computer code, e.g., in Matlab by calling the function *rand*. For the case where the input vector $\boldsymbol{X}$ consists of n random variables independent on each other, the above transformation can be applied on each variable separately to generate its associated samples.

To generate samples from a vector $\boldsymbol{X}$ of correlated random variables, the Nataf transformation can be used, see Der Kiureghian and Liu (1986). According to the Nataf transformation model, samples of uncorrelated normal random variables are generated, which are then transformed into correlated random variables by applying an appropriate orthogonal transformation. These correlated random variables are then marginally transformed into the desired random variables.

2. Run the model K times and evaluate its response as $\boldsymbol{y}^{(i)} = \mathcal{M}\left(\boldsymbol{x}^{(i)}\right)$.

Once the samples have been generated, the function $\mathcal{M}(\boldsymbol{x})$ must be evaluated K times. The model $\mathcal{M}$ can represent an analytical expression but can also represent an advanced FE numerical model. Often, model evaluations require a significant computational time. This is the basic disadvantage of MCS. For instance, for a time-consuming large-scale non-linear FE model, the use of MCS is almost prohibitive.

An alternative solution is the replacement of the basic model with a *surrogate model* or *meta model*. Surrogate models are trained (learned) by selected values of input parameters and corresponding basic model evaluations. Common surrogate models include simple polynomial models, Gaussian process models, neural networks, etc.

3. Analyze the generated samples $\boldsymbol{y}^{(i)}$ by means of statistics.

The generated samples $\boldsymbol{y}^{(i)}$, for $i = 1, \dots, K$ are processed by common statistical methods in order to derive sample means, sample standard deviations and other sample statistics. The expected value of a function $\mathcal{M}(\boldsymbol{X})$ is estimated by means of MCS as:

$$\mathrm{E}[\mathcal{M}(\boldsymbol{X})] \approx \frac{1}{K}\sum_{i=1}^{K} \mathcal{M}\left(\boldsymbol{x}^{(i)}\right) \tag{D.2}$$

However, since MCS generates a finite number of samples, it is subject to a *statistical uncertainty*. It is thus important for real problems to have an estimate of the accuracy of MCS.

D.2 Accuracy of MCS

We are interested in evaluating an estimate of the expected value of a scalar function Y, $\mathrm{E}[Y]$. Following Eq. (D.2), the MCS estimate is equal to the sample mean $\bar{Y} = \overline{\mathcal{M}(\boldsymbol{X})}$, where $\bar{Y}$ is itself a random variable with associated mean value and variance:

$$\mathrm{E}[\bar{Y}] = \mu_Y \tag{D.3}$$

$$\mathrm{Var}[\bar{Y}] = \frac{\sigma_Y^2}{K} \tag{D.4}$$

Eq. (D.3) shows that the MCS estimate is unbiased, i.e., on average MCS results in the true value μ_Y. On the other hand, Eq. (D.4) shows that for increasing number of samples K, the variance of the sample mean $\bar{Y}$ decreases. This relationship provides an indication of the uncertainty on the estimate.

If the quantity Y has a coefficient of variation CoV_Y, the standard deviation and the coefficient of variation of the MCS estimate read:

$$\sigma_{\mu_Y}^{MCS} = \sqrt{\frac{\sigma_Y^2}{K}} = \frac{\mathrm{CoV}_Y}{\sqrt{K}}\,\mu_Y \tag{D.5}$$

$$\mathrm{CoV}_{\mu_Y}^{MCS} = \frac{\sigma_{\mu_Y}^{MCS}}{\mu_Y} = \frac{\mathrm{CoV}_Y}{\sqrt{K}} \tag{D.6}$$

For example, for a value of $\mathrm{CoV}_Y = 0.2$ and $K = 1000$ samples, the coefficient of variation of the MCS estimate is only $\mathrm{CoV}_{\mu_Y}^{MCS} = 0.6\%$. As shown from the above, an important feature of MCS is that its accuracy does not depend on the number of random variables $\boldsymbol{X}$.

This page intentionally left blank

Appendix E. Neural Networks

The fundamentals of *neural networks* (NN) – with particular focus on feed-forward neural networks – are presented here in a synoptic manner. The reader who is interested for a more comprehensive understanding of NNs is referred to the books of Hagan et al. (2014) and Goodfellow et al. (2016). A review on the use of NNs in reliability analysis of steel structures can be found in Chojaczyk et al. (2015).

E.1 Structure and architecture of a neural network

A typical structure of a neural network is illustrated in Figure E.1. The structure of a NN consists of basic units which are called *neurons*. The neurons incorporate the basic elements of a network such as the weight matrix, the net input function and the activation function. The inputs are gathered into a vector $\boldsymbol{x} = [x_1, x_2, \dots, x_n]^T$. Each element of the input vector is connected with a neuron j through the weight matrix w_{ij}. Then, two actions take place. First the input data is combined with the weights to formulate the net input function u_j which is expressed by the following relation:

$$u_j = \sum_{i=1}^{n} x_i w_{ij} + e \tag{E.1}$$

where the constant e is the bias value which has the effect of increasing or lowering the net input of the activation function $f(\cdot)$. The latter, then, receives the result of the net input function u_j and gives the output y_j of the neuron j as:

$$y_j = f(u_j) \tag{E.2}$$

The weights and the bias are both adjustable parameters which are randomly initialized. The activation functions are chosen from the designer and play an essential role on the effectiveness of the network. Commonly used activation functions are the sigmoid and the linear transfer function. A learning rule is applied on the network in order the input-output relationship meets some specific goal.

The number of neurons that work on parallel is called a *layer*. Commonly, a neural network may consist of multiple layers and number of neurons within each layer. Apparently, the number of inputs and outputs of the network is selected from external specifications and coincides with the corresponding number of input-output variables of the problem. For example, a typical network architecture with two input variables, three neurons in the layer and one neuron in the

output layer is illustrated in Figure E.2. The layer whose output is not the network output is called *hidden layer*.

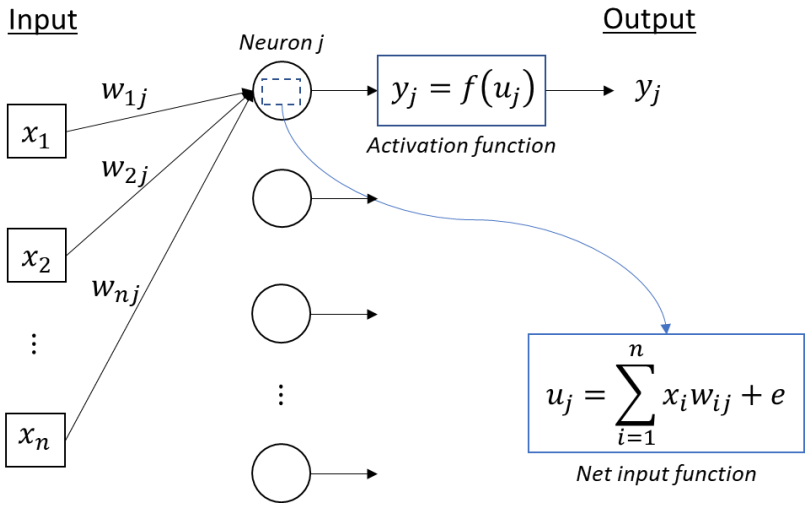

Figure E.1. A typical structure of an artificial neuron.

There are generally two broad categories or types of network architectures: the *single-layer* and the *multilayer* networks. The first type consists of the input vector and one output layer, whereas the second one has additional hidden layers between the input vector and the output layer. The network of Figure E.2 is characterized as a multilayer network. Multilayer networks are more powerful than single-layer networks. For instance, a two-layer network having a sigmoid first-layer activation function and a linear second layer can be trained to approximate most functions arbitrarily well. This is something a single-layer network cannot do, see also Hagan et al. (2014).

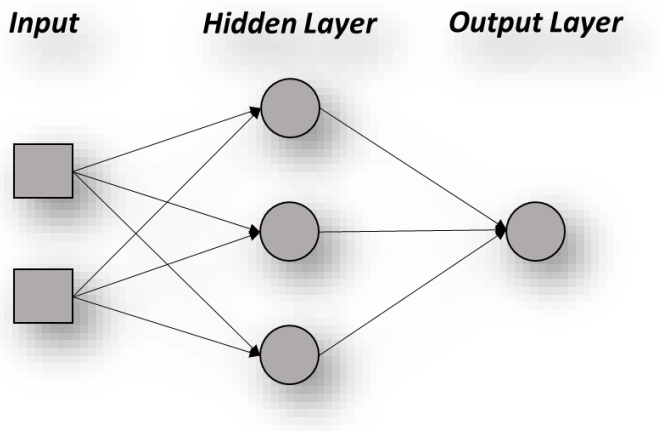

Figure E.2. A typical network architecture with one hidden layer.

E.2 Training of a feed-forward neural network

In order a network to generalize well it must be trained appropriately. Training depends on the quantity and the quality of the input-output training set, as well as the selected architecture. It is difficult to determine the exact number of input-output data a priori since this depends mainly on the size and the non-linearity of the problem under consideration. However, it is essential that the training data should be appropriately sampled from the input parameter space and span the whole range for which the network will be used.

A *feed-forward back-propagation* algorithm is commonly used for applications of function approximations as the ones examined in the present thesis. The term "feed-forward" describes the forward pass of the signal propagating from the input vector to the output layer throughout the network. The term "back-propagation" describes the signal that travels back adjusting the weights aiming to minimize the error and make the output response of the network move closer to the target values. During the forward pass, the weights of the neurons are all fixed. The actual response of the network (output signal) is subtracted from the desired (target) response values and an error is produced. The process is repeated until the *mean squared error* (MSE) of training data is minimized:

$$\mathrm{MSE} = \frac{1}{K}\sum_{i=1}^{K}(t_i - y_i)^2 \tag{E.3}$$

The symbol K denotes the number of input-output data in the training set, t is the target output and y the output produced by the network. The training algorithm that has been applied in the context of this thesis is the Bayesian regularization algorithm. This algorithm is an application of Bayes' rule and modifies the weights accordingly in order to maximize the conditional probability of them given the data.

This page intentionally left blank

Appendix F. The double bottom effect

Container ships travel most of their time in hogging condition. It can be said that the following three loads act almost always on the double bottom structure of a container ship:

1) Longitudinal compressive load due to vertical bending
2) Upward load due to bottom sea pressure
3) Transverse compressive load due to side sea pressure

The compressive stresses induced by the aforementioned combination of loads lead to the development of the *double bottom effect*. In particular, hull girder bending leads to the development of longitudinal compressive stresses σ_{CL_1} at the bottom structure. In addition, the transverse sea loads acting at the side plates and the upward sea loads acting at the bottom result in the generation of transverse compressive stresses σ_{CT_1} and σ_{CT_2} on the bottom plate. At the same time, local longitudinal compressive stresses σ_{CL_2} as a result of the upward loads induced by the sea pressure are developed on the outer bottom. The total induced longitudinal and transverse stresses are the linear superposition of the corresponding stresses that cause the double bottom effect. A schematic description of the phenomenon is depicted in Figure F.1.

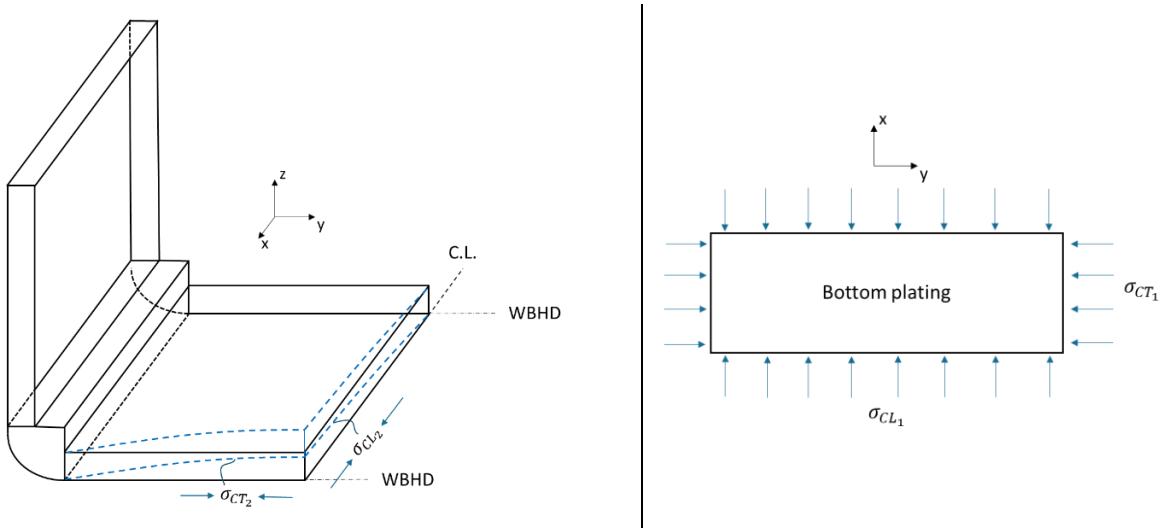

Figure F.1. Induced compressive stresses acting on the bottom plating of a container ship; longitudinal vertical bending moment σ_{CL_1}, transverse compressive load due to side sea loads σ_{CT_1} and upward loads due to bottom sea pressure $\sigma_{CL_2}, \sigma_{CT_2}$. The double bottom effect takes place within the length defined by two watertight bulkheads (WBHD).

This page intentionally left blank

Appendix G. Estimation of FEM error

Ideally, the quantification of FEM error could be estimated by comparing the result from a number of FEA participants with a reference full-scale result from the hull-girder collapse of a ship. Since this is not feasible, the data from the benchmark study of Ringsberg et al. (2021) will be used, where a full-scale experiment predicting the ultimate strength of a steel stiffened panel under uniaxial compressive loads was conducted. The results from the NLFEA are depicted in Figure G.1. The results from Phase 3-1 are considered as these correspond to the actual values and thus, the error induced is (mostly) attributed to the difference between FE modelling itself versus real-life.

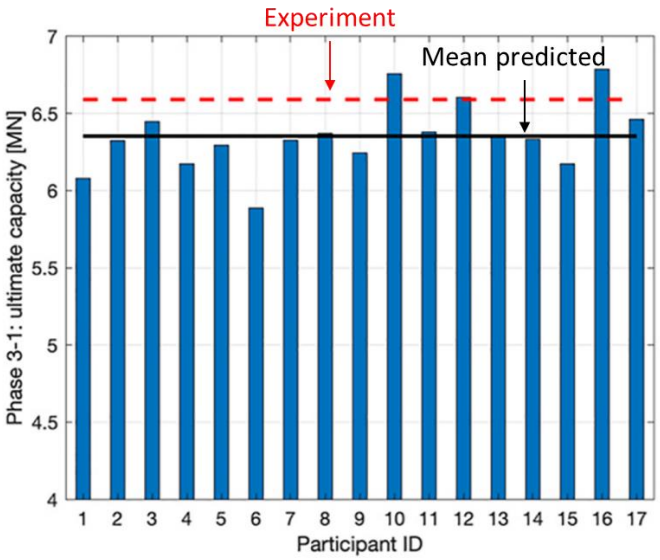

Figure G.1. FEA users' prediction along with experimental value, after Ringsberg et al. (2021). The solid line is the mean value from the FEA results, and the dashed line is the ultimate capacity from the reference experiment (true value).

In our analysis, we accept that the value received from the experimental result coincides with the true value. Then, we try to quantify the error between FEA participants and reality by postulating that a Gaussian distribution describes this error. In doing so, we employ a *maximum likelihood estimate (MLE)* approach.

Let us consider that the FEA prediction x_i is equal to the true value (experimental result) x_t plus an additive error ε. This can be written as:

$$x_i = x_t + \varepsilon \tag{G.1}$$

A zero-mean Gaussian distribution with *unknown* standard deviation σ_ε is used to describe this error, so as: $\varepsilon \sim N(0, \sigma_\varepsilon)$. The likelihood as a function of the unknown parameter σ_ε, and for a single FE prediction, is formulated as follows:

$$L_i(\sigma_\varepsilon) = f_\varepsilon(\varepsilon) = f_\varepsilon(x_i - x_t) = \frac{1}{\sigma_\varepsilon \sqrt{2\pi}} \exp\left[-\frac{1}{2}\left(\frac{x_i - x_t}{\sigma_\varepsilon}\right)^2\right] \tag{G.2}$$

In case of $i = 1, \dots, m$ FEA users, and assuming independence between each other, the likelihood becomes:

$$L(\sigma_\varepsilon) = \prod_{i=1}^{m} L_i(\sigma_\varepsilon) \propto \frac{1}{{\sigma_\varepsilon}^n} \exp\left[-\frac{1}{2}\sum_{i=1}^{m}\left(\frac{x_i - t}{\sigma_\varepsilon}\right)^2\right] \tag{G.3}$$

The MLE $\hat{\sigma}_\varepsilon$, i.e., the value of σ_ε that best describes the current data set, is obtained by maximizing the above equation (or the logarithm of the above equation), namely:

$$\hat{\sigma}_\varepsilon = \max \ln\big(L(\sigma_\varepsilon)\big) \tag{G.4}$$

After transforming the results of the benchmark study to the dimensionless values, i.e., the result from the experiment is taken equal to unity, and following a numerical replacement to the above relations, we get $\hat{\sigma}_\varepsilon = 0.05$.

Appendix H. Results: Corrosion model updating

Table H.1. Prior and posterior corrosion model prediction for all groups of the target VLCC vessel. 10 measurements from the first and the second inspection corresponding to the 15th year and the 18th year of service have been randomly selected from the full set. Results are compared with the validation set corresponding to the 20th year of service life (third inspection).

Group	Prior	Posterior $m = 10$	Posterior $m = [10,10]$
A/O-H	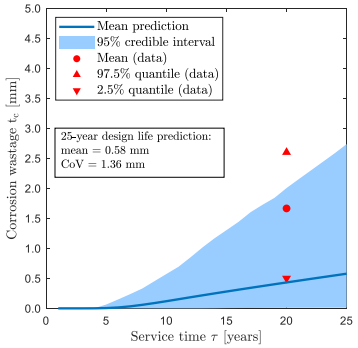	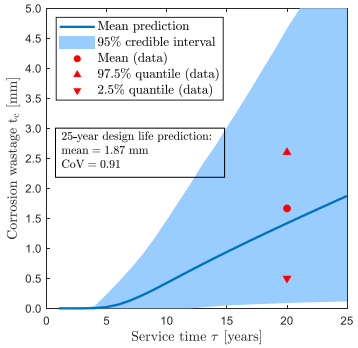	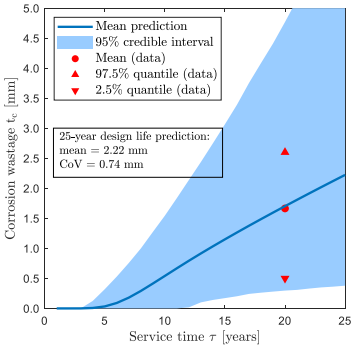
A/B-H	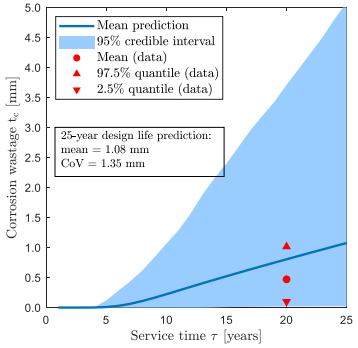	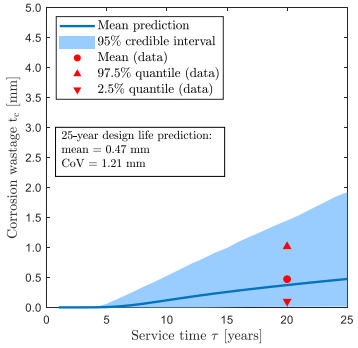	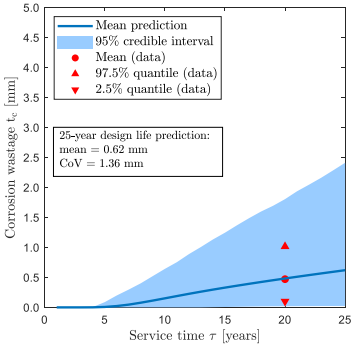

A/B-V

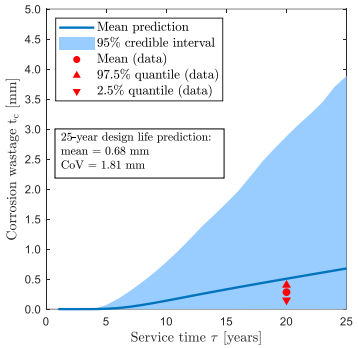
Mean prediction
95% credible interval
Mean (data)
97.5% quantile (data)
2.5% quantile (data)
25-year design life prediction:
mean = 0.68 mm
CoV = 1.81 mm
Corrosion wastage t_c [mm]
Service time τ [years]

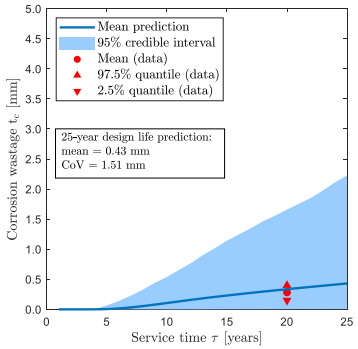
Mean prediction
95% credible interval
Mean (data)
97.5% quantile (data)
2.5% quantile (data)
25-year design life prediction:
mean = 0.43 mm
CoV = 1.51 mm
Corrosion wastage t_c [mm]
Service time τ [years]

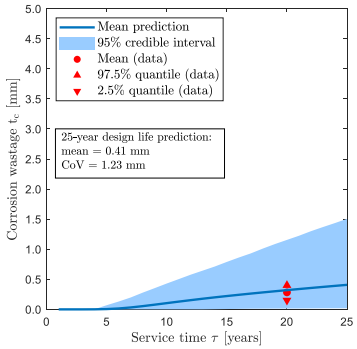
Mean prediction
95% credible interval
Mean (data)
97.5% quantile (data)
2.5% quantile (data)
25-year design life prediction:
mean = 0.41 mm
CoV = 1.23 mm
Corrosion wastage t_c [mm]
Service time τ [years]

B/S-V

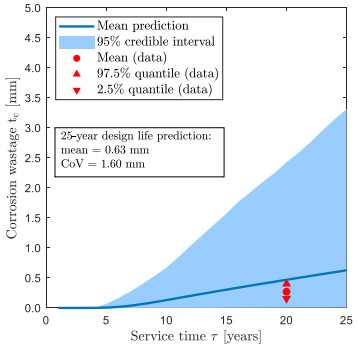
Mean prediction
95% credible interval
Mean (data)
97.5% quantile (data)
2.5% quantile (data)
25-year design life prediction:
mean = 0.63 mm
CoV = 1.60 mm
Corrosion wastage t_c [mm]
Service time τ [years]

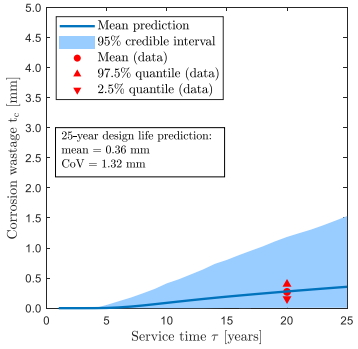
Mean prediction
95% credible interval
Mean (data)
97.5% quantile (data)
2.5% quantile (data)
25-year design life prediction:
mean = 0.36 mm
CoV = 1.32 mm
Corrosion wastage t_c [mm]
Service time τ [years]

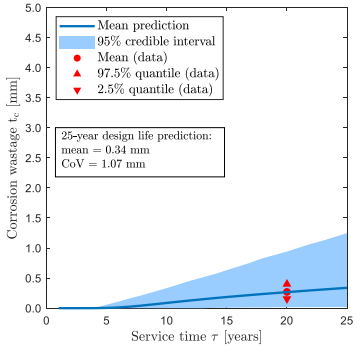
Mean prediction
95% credible interval
Mean (data)
97.5% quantile (data)
2.5% quantile (data)
25-year design life prediction:
mean = 0.34 mm
CoV = 1.07 mm
Corrosion wastage t_c [mm]
Service time τ [years]

BLGB

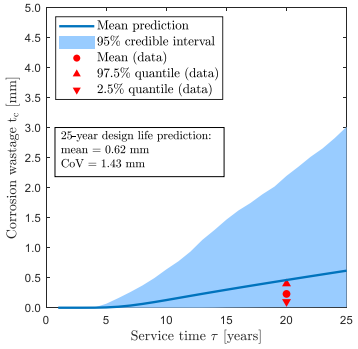
Mean prediction
95% credible interval
Mean (data)
97.5% quantile (data)
2.5% quantile (data)
25-year design life prediction:
mean = 0.62 mm
CoV = 1.43 mm
Corrosion wastage t_c [mm]
Service time τ [years]

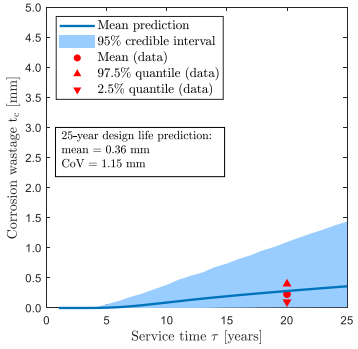
Mean prediction
95% credible interval
Mean (data)
97.5% quantile (data)
2.5% quantile (data)
25-year design life prediction:
mean = 0.36 mm
CoV = 1.15 mm
Corrosion wastage t_c [mm]
Service time τ [years]

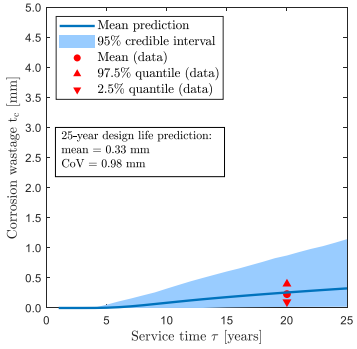
Mean prediction
95% credible interval
Mean (data)
97.5% quantile (data)
2.5% quantile (data)
25-year design life prediction:
mean = 0.33 mm
CoV = 0.98 mm
Corrosion wastage t_c [mm]
Service time τ [years]

B/S-H

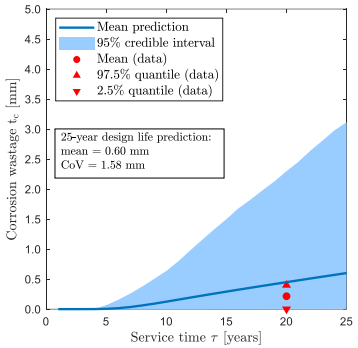
Mean prediction
95% credible interval
Mean (data)
97.5% quantile (data)
2.5% quantile (data)
25-year design life prediction:
mean = 0.60 mm
CoV = 1.58 mm
Corrosion wastage t_c [mm]
Service time τ [years]

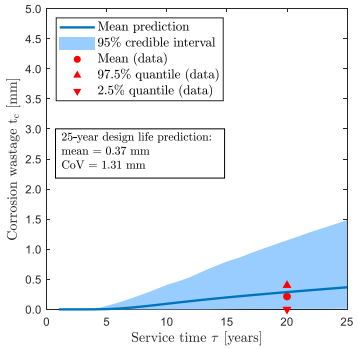
Mean prediction
95% credible interval
Mean (data)
97.5% quantile (data)
2.5% quantile (data)
25-year design life prediction:
mean = 0.37 mm
CoV = 1.31 mm
Corrosion wastage t_c [mm]
Service time τ [years]

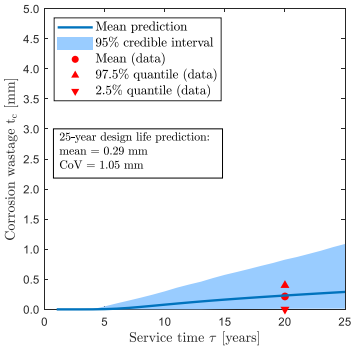
Mean prediction
95% credible interval
Mean (data)
97.5% quantile (data)
2.5% quantile (data)
25-year design life prediction:
mean = 0.29 mm
CoV = 1.05 mm
Corrosion wastage t_c [mm]
Service time τ [years]

B/B-H

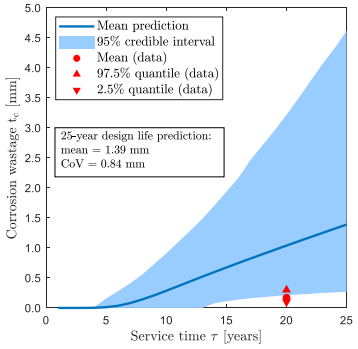
Mean prediction
95% credible interval
Mean (data)
97.5% quantile (data)
2.5% quantile (data)
25-year design life prediction:
mean = 1.39 mm
CoV = 0.84 mm
Corrosion wastage t_c [mm]
Service time τ [years]

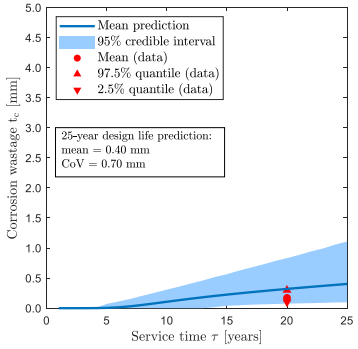
Mean prediction
95% credible interval
Mean (data)
97.5% quantile (data)
2.5% quantile (data)
25-year design life prediction:
mean = 0.40 mm
CoV = 0.70 mm
Corrosion wastage t_c [mm]
Service time τ [years]

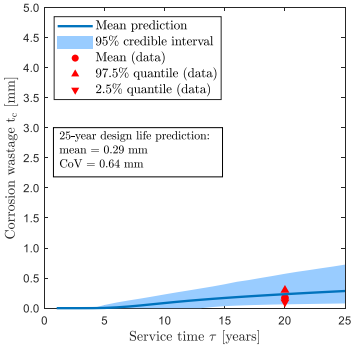
Mean prediction
95% credible interval
Mean (data)
97.5% quantile (data)
2.5% quantile (data)
25-year design life prediction:
mean = 0.29 mm
CoV = 0.64 mm
Corrosion wastage t_c [mm]
Service time τ [years]

O/B-V[1]

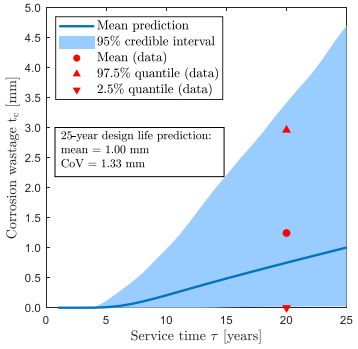
Mean prediction
95% credible interval
Mean (data)
97.5% quantile (data)
2.5% quantile (data)
25-year design life prediction:
mean = 1.00 mm
CoV = 1.33 mm
Corrosion wastage t_c [mm]
Service time τ [years]

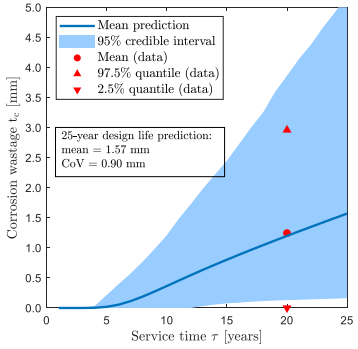
Mean prediction
95% credible interval
Mean (data)
97.5% quantile (data)
2.5% quantile (data)
25-year design life prediction:
mean = 1.57 mm
CoV = 0.90 mm
Corrosion wastage t_c [mm]
Service time τ [years]

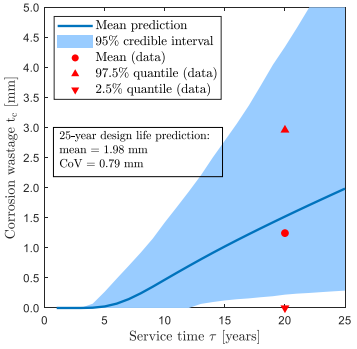
Mean prediction
95% credible interval
Mean (data)
97.5% quantile (data)
2.5% quantile (data)
25-year design life prediction:
mean = 1.98 mm
CoV = 0.79 mm
Corrosion wastage t_c [mm]
Service time τ [years]

O/B-V²

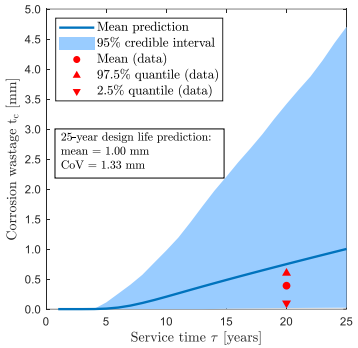

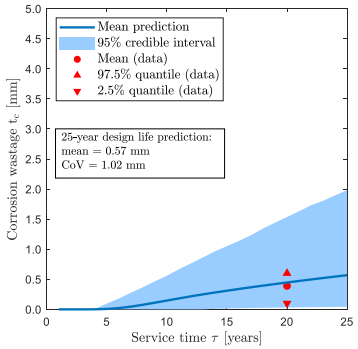

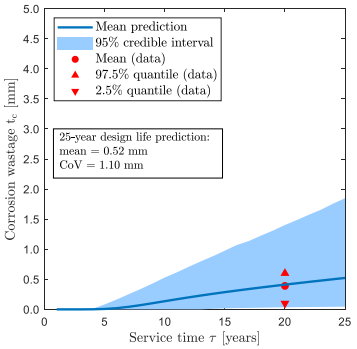

O/O-V

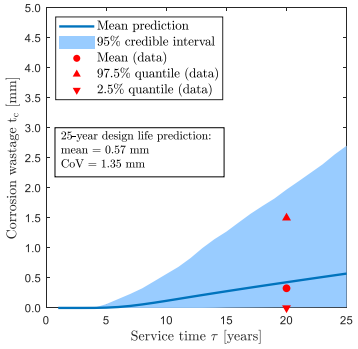

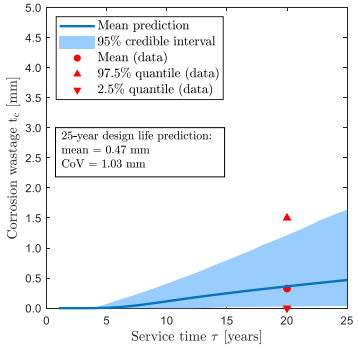

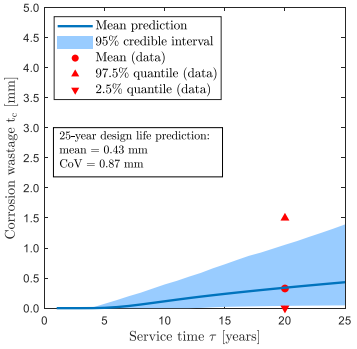

DLC (W)

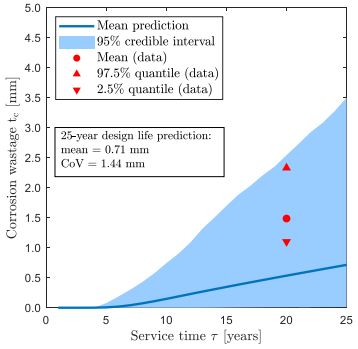

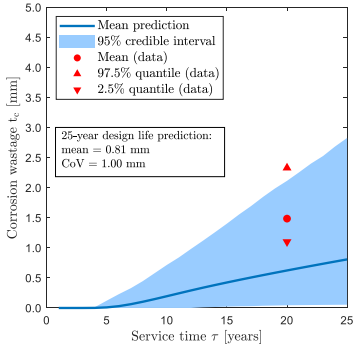

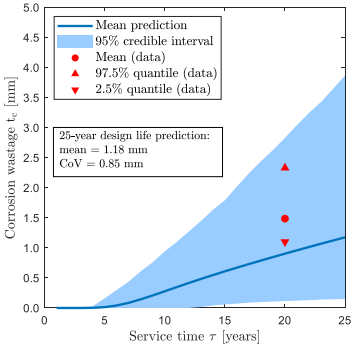

DLC (F)

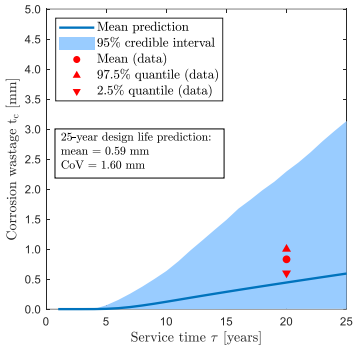

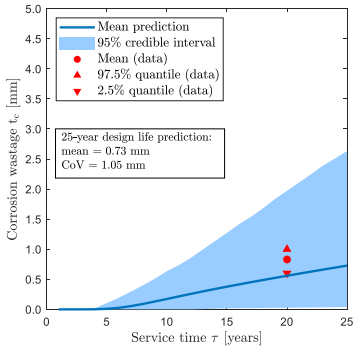

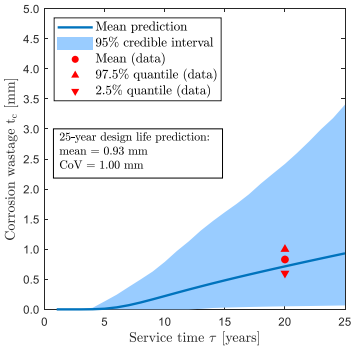

DLB (W)

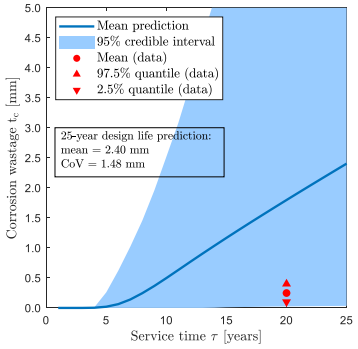

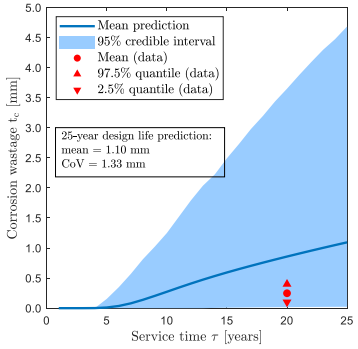

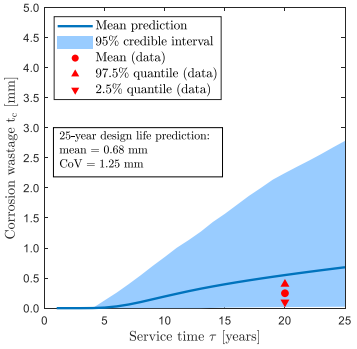

DLB (F)

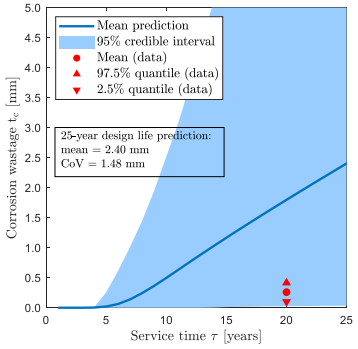

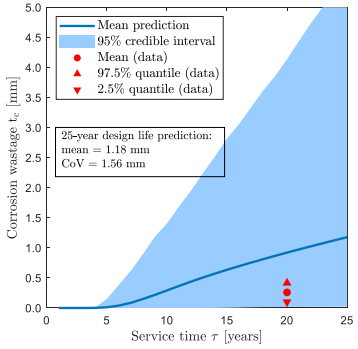

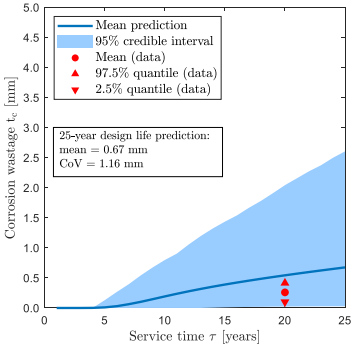

SSLB (W)

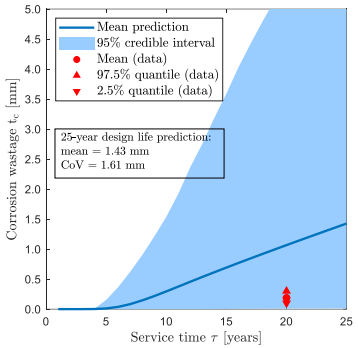

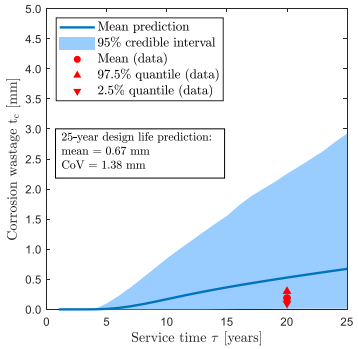

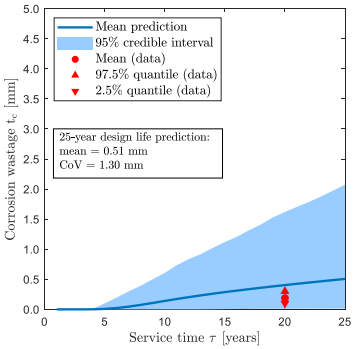

SSLB (F)

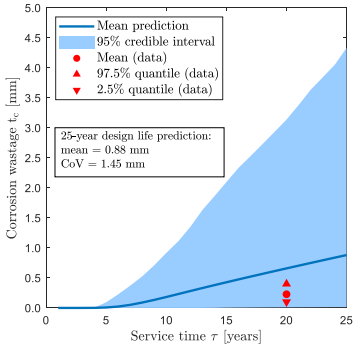

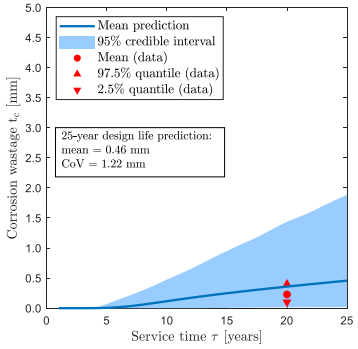

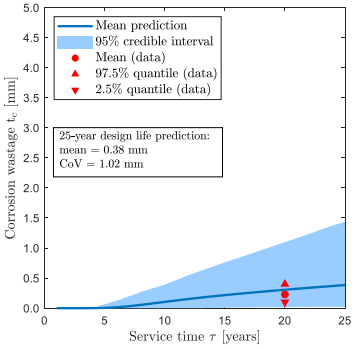

BSLB (W)

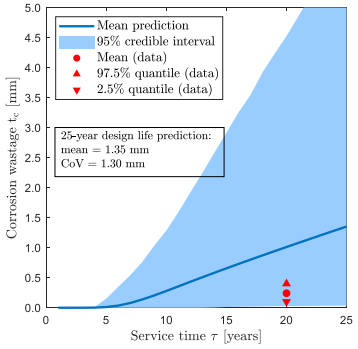

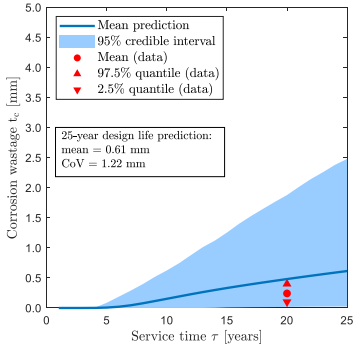

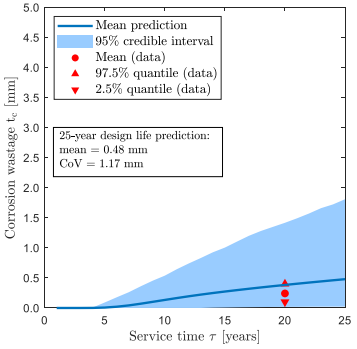

BSLB (F)

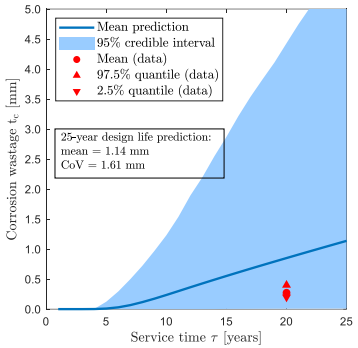

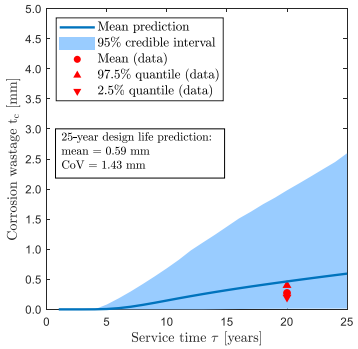

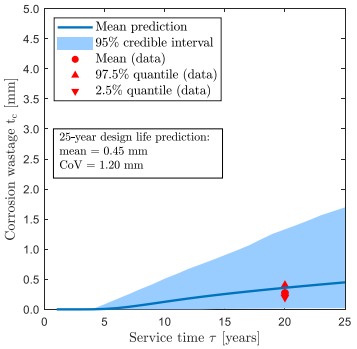

LBLB (W)

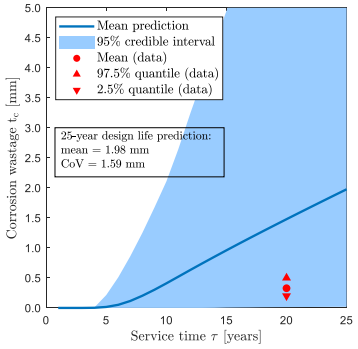

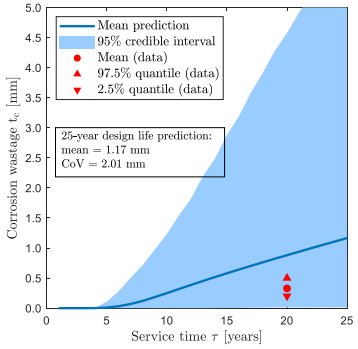

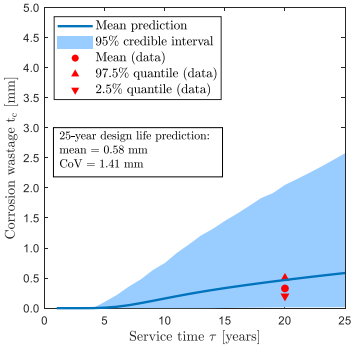

LBLB (F)

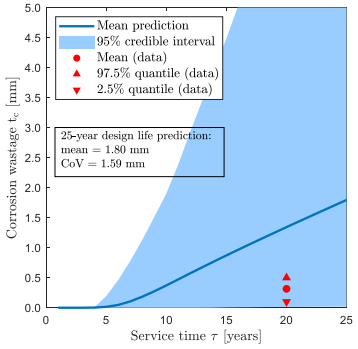

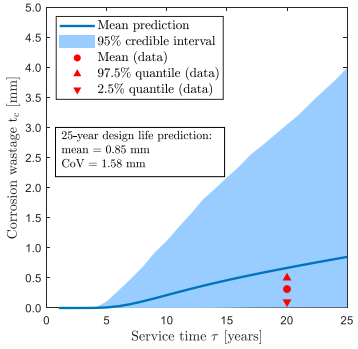

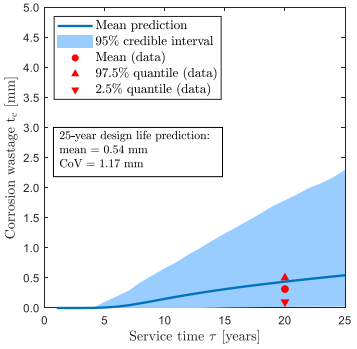

LBLC (W)

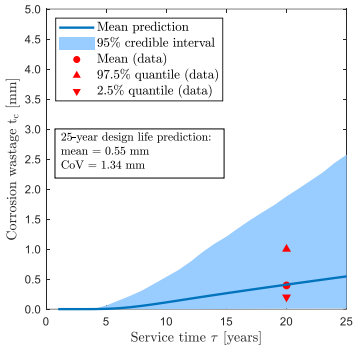
Mean prediction
95% credible interval
Mean (data)
97.5% quantile (data)
2.5% quantile (data)
25-year design life prediction:
mean = 0.55 mm
CoV = 1.34 mm
Corrosion wastage t_c [mm]
Service time τ [years]

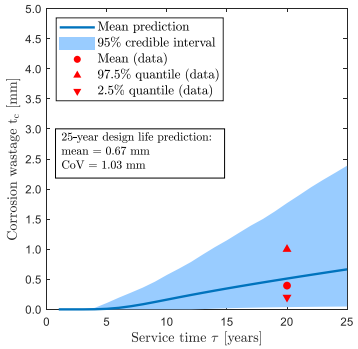
Mean prediction
95% credible interval
Mean (data)
97.5% quantile (data)
2.5% quantile (data)
25-year design life prediction:
mean = 0.67 mm
CoV = 1.03 mm
Corrosion wastage t_c [mm]
Service time τ [years]

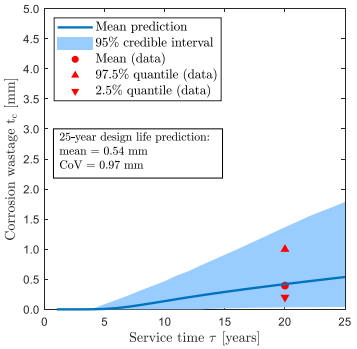
Mean prediction
95% credible interval
Mean (data)
97.5% quantile (data)
2.5% quantile (data)
25-year design life prediction:
mean = 0.54 mm
CoV = 0.97 mm
Corrosion wastage t_c [mm]
Service time τ [years]

LBLC (F)

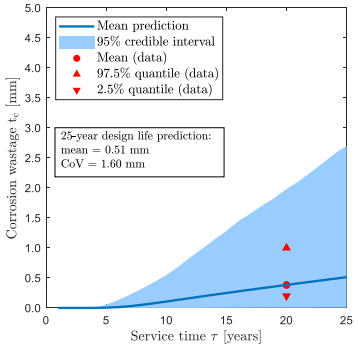
Mean prediction
95% credible interval
Mean (data)
97.5% quantile (data)
2.5% quantile (data)
25-year design life prediction:
mean = 0.51 mm
CoV = 1.60 mm
Corrosion wastage t_c [mm]
Service time τ [years]

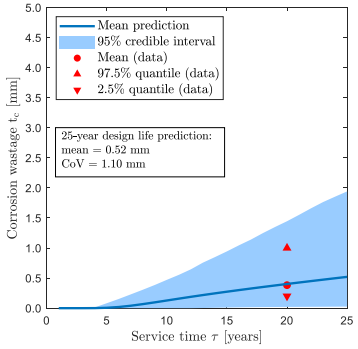
Mean prediction
95% credible interval
Mean (data)
97.5% quantile (data)
2.5% quantile (data)
25-year design life prediction:
mean = 0.52 mm
CoV = 1.10 mm
Corrosion wastage t_c [mm]
Service time τ [years]

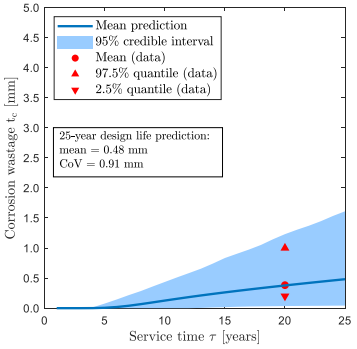
Mean prediction
95% credible interval
Mean (data)
97.5% quantile (data)
2.5% quantile (data)
25-year design life prediction:
mean = 0.48 mm
CoV = 0.91 mm
Corrosion wastage t_c [mm]
Service time τ [years]

Appendix I. Sensitivity analysis on Smith's model

A global sensitivity analysis is presented here in order to assess the relative influence of input random variables on the variance of the Smith's model output, that is, the ultimate bending moment in sagging. In particular, a graphical sensitivity analysis (through the form of scatterplots) is performed based on Monte Carlo simulation, as well a variance-based sensitivity analysis based on the first-order Sobol index, after Sobol (1993). The reader who is not familiar with the theory of global sensitivity analysis is referred to the book of Saltelli et al. (2008).

The total number of random variables considered in the problem is 25, including, one variable for Young's modulus E, one variable for yield strength of mild steel $\sigma_{y(mild)}$, one variable for the yield strength of high-tensile AH-32 type steel $\sigma_{y(AH-32)}$, and twenty-two variables representing the thickness loss t_c variability for each of the specified classified groups (see Figure 6.10). The distribution models of corrosion loss correspond to the 15th year of service life when the first inspection takes place.

I.1 Graphical sensitivity analysis

Graphical sensitivity analysis depicts the relationship between inputs and output values in a schematic way, through scatterplots. For the problem at hand, the samples generated for each random variable X_i with $i = 1, \dots, 25$ are depicted in a single plot against the corresponding samples of output Y. Using MCS in conjunction with Latin-Hypercube sampling technique, totally $K = 10^5$ samples have been generated. The results for the present analysis are illustrated in Figure I.2.

In general, scatterplots with more "shape" (or pattern) express an influential parameter X_i. On the contrary, a scatterplot with less shape, i.e., when a rather uniform cloud of points is observed over the range of parameter values x_i, indicate a non-influential parameter X_i.

The following can be noticed by visual inspection of Figure I.2:

- Yield strength of high-tensile grade has a pronounced effect on the variability of hull girder ultimate bending capacity. In particular, a strong positive correlation is observed.
- Young's modulus also seems to have a positive effect on the output strength.
- Thickness wastage parameters seem to have no influence. The only exception seems to be the deck plates of cargo tanks (group A/O-H) where a negative correlation is observed, i.e., for increasing values of corrosion loss, the ultimate strength is diminished.

I.2 Variance-based sensitivity analysis

A more quantitative way of defining the importance of input variables X_i is to look at their contribution to the variance of the output $\mathrm{Var}[Y]$. A common measure to implement this task is the so-called Sobol indices. The *first-order Sobol index* is defined as:

$$\mathrm{S}_i = \frac{V_i}{\mathrm{Var}[Y]} \tag{I.1}$$

where V_i denotes a first-order measure for the part of the variance $\mathrm{Var}[Y]$ that can be attributed to the uncertainty in X_i given by:

$$V_i = \mathrm{Var}_{X_i}\left\{\mathrm{E}_{\boldsymbol{X}_{-i}}[Y|X_i]\right\} \tag{I.2}$$

The term $\mathrm{E}_{\boldsymbol{X}_{-i}}[Y|X_i]$ is the expected value of the model output Y with respect to all input random variables $\boldsymbol{X}_{-i}$, except X_i which is fixed.

An intuitive description of Eq. (I.2) is provided with a demonstrative example in Figure I.1. Consider a model that consists of two input random variables X_1 and X_2. The scatterplots of X_1 and X_2 against model output Y are presented. The scatterplots are splitted into a number of vertical thin slices; each slice representing a subset that contains a fixed number of samples denoted by k_s. Now, an approximation of $\mathrm{E}_{\boldsymbol{X}_{-i}}[Y|X_i]$ can be obtained for each subset by computing the expected value of output Y with respect to all variables $\boldsymbol{X}_{-i}$, except X_i which is fixed. The variance of $\mathrm{E}_{\boldsymbol{X}_{-i}}[Y|X_i]$ over the subsets gives us the V_i. If X_i has no effect on Y, the expected value is constant with X_i, and hence, $V_i = 0$ (the case of parameter X_2). On the other hand, if X_i has an important effect on Y, then V_i approximates the full variance of the model output, $\mathrm{Var}[Y]$ (the case of parameter X_1).

A simple and intuitive Monte Carlo-based algorithm that can be used to estimate the first-order Sobol indices is given as follows:

1. Conduct a MCS of the model resulting in $k = 1, \dots, K$ samples of the model output. The use of variance reduction sampling techniques, such as Latin-Hypercube sampling technique is recommended in order to have a more stratified sampling of the inputs range.
2. Repeat the following steps for all input random variables X_i for $i = 1, \dots, n$:
    a. Set the sample pairs $\left[x_i^{(k)}, y^{(k)}\right]$ in ascending order according to x_i values.
    b. Divide the total K samples into $j = 1, \dots, n_s$ subsets of size k_s (e.g., k_s can be range from a few hundreds to a few thousands) and compute the mean value of Y for each subset, μ_{Y_j}. This mean provides an estimate of $\mathrm{E}_{\boldsymbol{X}_{-i}}[Y|X_i]$.

c. The variance of the subset means μ_{Y_j} is an estimate of V_i.

Sobol indices are computed for each of the 25 random variables presented above. The results are presented in Table I.1 for the 15th year of service life, where the distribution models of thickness loss before and after observing the measurements have been adopted. As it can be noticed, the only parameters that have an influence on the variance of the ultimate bending capacity are the yield strength of the high-tensile steel, the Young's modulus and the thickness of deck plates located in the cargo area. For all the other variables the Sobol index is approximately zero. This finding justifies the results of Table 7.3.

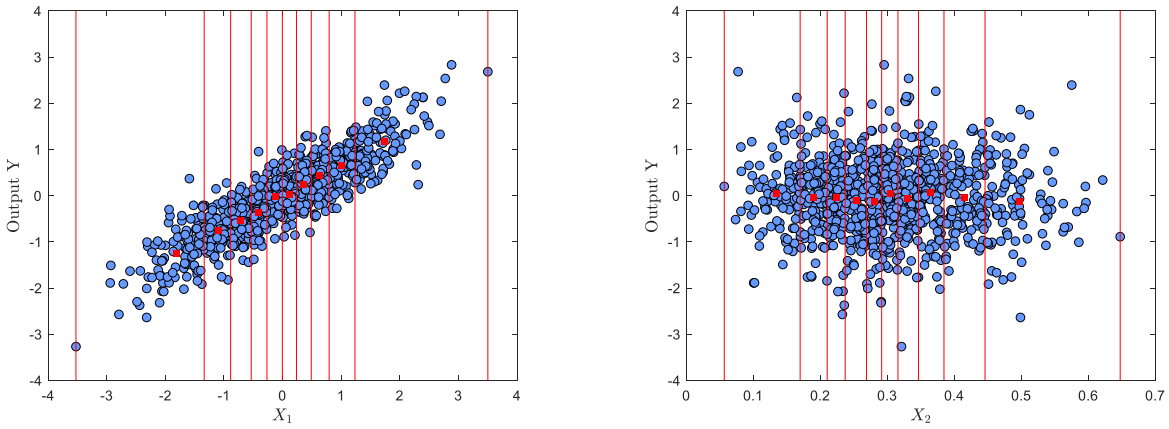

(a) (b)

Figure I.1. A demonstrative example. Graphical representation of input variable X_1, X_2 vs. model output Y. The scatter plot of figure (a) shows a clear pattern, indicating that the parameter X_1 has a strong influence on the variance of the model output. In figure (b), however, no obvious shape is observed which is an indication of a non-influential parameter. Alternatively, using Sobol first-order sensitivity measure: the sample space of X_1, X_2 has been splitted into $n_s = 10$ subsets, each containing $k_s = 100$ samples. An estimate of $\mathrm{E}_{\boldsymbol{X}_{-i}}[Y|X_i]$ has been depicted with a red square for each case. In figure (b), the variance of the values represented by the red squares is calculated close to zero (non-influential parameter), whereas in figure (a), the corresponding variance is close to the variance of the model output (influential parameter).

Table I.1. Sobol indices for the input parameters of Smith's model. Only the parameters that have a relative influence on the resulted variability of hull girder ultimate strength are listed.

Variable X_i	**Symbols**	**Sobol index** S_i	
		Prior $(\tau = 15 \text{ years})$	**Posterior** $(\tau = 15 \text{ years})$
Yield strength (AH-32 steel)	$\sigma_{y(AH-32)}$	0.69	0.70
Young's modulus	E	0.26	0.23
Yield strength (mild steel)	$\sigma_{y(mild)}$	0.01	0.01
Thickness loss (A/O-H)	t_c	0.01	0.06

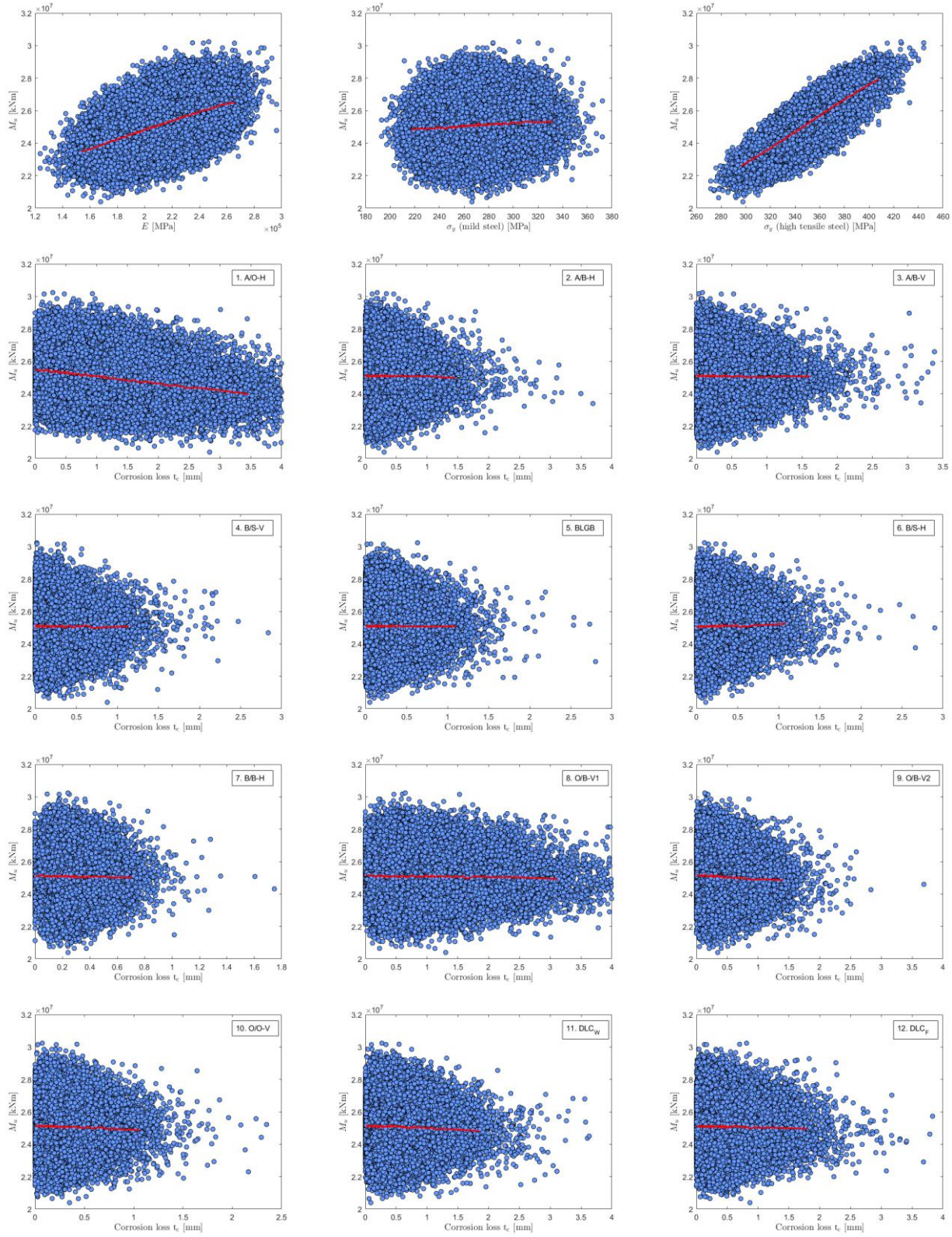
M_u [kNm]
E [MPa]
σ_y (mild steel) [MPa]
σ_y (high tensile steel) [MPa]
1. A/O-H
2. A/B-H
3. A/B-V
4. B/S-V
5. BLGB
6. B/S-H
7. B/B-H
8. O/B-V1
9. O/B-V2
10. O/O-V
11. DLC$_W$
12. DLC$_F$
Corrosion loss t_c [mm]

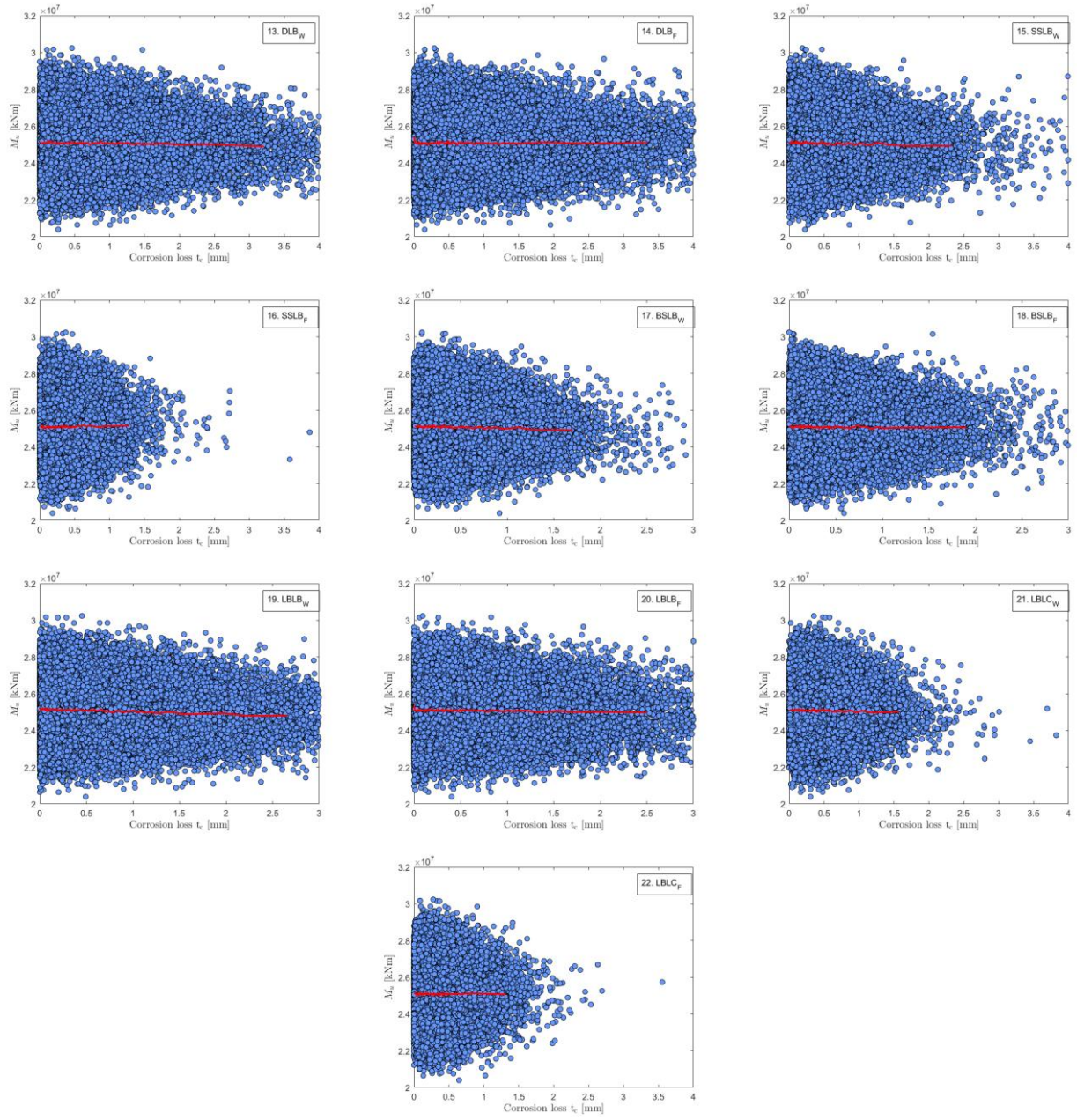

Figure I.2. Sensitivity analysis with MCS for hull girder ultimate strength prediction using IACS CSR Smith's model. The sensitivity analysis is performed for the 15th year of service and using the posterior generalized corrosion model after observing 10 measurements. The scatterplots of samples of the inputs against samples of the output are depicted. Red lines show the mean approximation of model output for given input.